

University College London

**Development of Small Molecule  
Iminodihydroquinolines as New  
Generation Pain Therapeutics**

by

Elena Yiannaki

Submitted in partial fulfilment of the requirements for the degree of

Doctor of Philosophy

---

# Declaration

I, Elena Yiannaki, confirm that the work presented in this thesis is my own. Where information has been derived from other sources, I confirm that this has been indicated in the thesis.

Elena Yiannaki

February 2016

---

## Acknowledgments

I would like to thank,

My supervisor, Prof. Erik Årstad for giving me the opportunity to work on this exciting project, for the trust that he has placed in my work, and for his constant support, motivation and guidance throughout my PhD. With his joy and enthusiasm for research, Erik will serve as a role model for the rest of my scientific career;

Prof. Martin Koltzenburg, for supervising the peripheral nerve study, introducing me to the exciting world of neurology and allowing me to challenge myself in a new field;

Dr. Carlos Pérez-Medina for the early synthetic work of this project as well as his invaluable guidance during the first months of my PhD;

Dr. Mona Alqatari for performing the peripheral nerve experiments at the early stages of the project, and importantly for the transfer of knowledge and her patience on training me in electrophysiological techniques;

Dr. Kerstin Sander and Dr. Thibault Gendron for their contribution to this work with the PET study, as well as for the motivating and fruitful discussions and the friendship throughout the years. Their perfectionism and immense knowledge has made me a better scientist and communicator.

My colleagues and friends Dr. Eva Galante, Dr. Ran Yan, Dr. Niral Patel, Dr. Bhavesh Premjee, Dr. Ahmed Akhbar, Dr. Atif Elahi and Dr. Ramiz Nathani for all the fun times in and out of the lab, the great philosophical discussions, and their encouragement in the last five years.

Lastly, I would like to dedicate this thesis to my parents and brother; none of this work would have been possible without their love and support. Thank you for your unshaken trust and belief in me.

---

## Abstract

Acute and chronic pain is a common symptom of many diseases. Therapy is often not effective or is associated with significant adverse effects; the development of novel analgesic drugs with high therapeutic index is an urgent unmet clinical need. Several lines of evidence converge to show that pain is mostly signalled by activity in peripheral unmyelinated (C) or thinly myelinated (A $\delta$ ) sensory fibres, called nociceptors. A drug selectively affecting the conduction of nociceptors without interfering with the function of other peripheral nerve fibres (A $\alpha$ , A $\beta$ , A $\gamma$ ) or cells in the central nervous system and heart would be an ideal pain therapeutic.

We recently discovered that WIN17317-3, a small molecule iminodihydroquinoline, previously reported as a high affinity, state-dependent sodium channel (Na<sub>v</sub>) blocker, can produce such a selective nociceptor block. Specifically, WIN17317-3 blocks the conduction of nociceptive C-fibers, leaving A-fibers, mainly involved in motor control and non-painful sensations, largely unaffected. To the best of our knowledge no other small molecule has been reported to exhibit such a selective blocking effect. This thesis describes the development of iminodihydroquinolines as novel analgesic candidate drugs with selective action on pain-signalling neurons.

Following the traditional “hit” to “lead” drug discovery approach, a library of WIN17317-3 derivatives was synthesized. The compounds were screened using state of the art electrophysiological assays to determine their effects on the human Na<sub>v</sub>1.7 isoform, and selected structures were further characterized in a functional assay using rodent peripheral sensory nerves. Voltage-gated sodium channels are responsible for the generation and propagation of action potentials in all electrically excitable cells; Na<sub>v</sub>1.7 channels are highly expressed in nociceptors, but are sparsely expressed or absent in non-nociceptive neurons. The iminodihydroquinolines described, were found to potently inhibit Na<sub>v</sub>1.7 channels and nociceptor conduction leaving non-nociceptive fibers largely unaffected. A selected lead preclinical drug candidate was subjected to *in vivo* pharmacokinetic profiling and toxicity studies in rodents. The results suggest that iminodihydroquinolines may be suitable analgesic drugs for topical, local, or regional administration with a wide safety margin.

To achieve selective blockade of nociceptors clinically without interfering with the action of motor neurons would be a major breakthrough for the treatment of pain disorders and anesthesia.

---

# Table of Contents

<b>Declaration</b> .....	<b>i</b>
<b>Aknowledgments</b> .....	<b>ii</b>
<b>Abstract</b> .....	<b>iii</b>
<b>Table of contents</b> .....	<b>iv</b>
<b>Abbreviations</b> .....	<b>vii</b>
<b>List of tables</b> .....	<b>xi</b>
<b>List of figures</b> .....	<b>xiii</b>
<b>1. Voltage-Gated Sodium Channels as Targets for Pain Therapy</b> .....	<b>1</b>
1.1. Pain, an unmet clinical challenge .....	1
1.2. The perception and modulation of pain: a brief overview .....	2
1.3. Peripheral mechanisms of pain .....	4
1.4. Neurochemistry of cutaneous nociceptors.....	5
1.4.1. Transduction .....	6
1.4.2. Action potential generation and axonal conduction.....	7
1.4.3. CNS terminal - synaptic transmission.....	8
1.5. Nociceptor sensitization .....	9
1.6. Pain pharmacology .....	10
1.7. The voltage-gated sodium channel (Na <sub>v</sub> ) as therapeutic target for pain....	13
1.7.1. Structure .....	13
1.7.2. Function .....	14
1.7.3. Na <sub>v</sub> subtypes, tissue distribution, and channelopathies .....	16
1.7.4. Localization of Na <sub>v</sub> isoforms in nociceptors and their biophysical characteristics .....	17
1.7.5. Implication of Na <sub>v</sub> isoforms in pain.....	19
1.7.6. Na <sub>v</sub> blockers as pain relief medicines .....	21
1.8. Previous studies related to this work: Iminodihydroquinolines as Na <sub>v</sub> blockers for pain therapy .....	27
1.9. Research aim and objectives .....	33

---

<b>2. The Design of an Iminodihydroquinoline Compound Library .....</b>	<b>34</b>
<b>3. Chemical Approaches and Reactions .....</b>	<b>38</b>
3.1. Synthesis of a WIN17317-3 Compound Library .....	38
3.1.1. <i>N</i> -substituted-4-imino-1,4-dihydroquinolines .....	38
3.1.1.1. Route A: From 4-chloroquinolines .....	39
3.1.1.2. Route B: From 4-quinolones .....	46
3.1.1.3. Route C: From substituted benzoic acids <i>via</i> ring annulation .....	49
3.1.2. <i>N</i> -substituted-4-imino-1,4-dihydro-naphthyridines .....	53
3.1.3. <i>N</i> 9-substitued-6-aminoaryl-purines and .....	
<i>N</i> -substituted-4-imino-1,4-dihydro-pyridines .....	57
3.2. Synthesis of an <sup>18</sup> F-labeled lead drug candidate .....	59
3.2.1. The choice of radionuclide .....	59
3.2.2. The triarylsulfonium salt method for <sup>18</sup> F-labeling of aromatic .....	
compounds .....	60
3.2.3. Synthesis of a triarylsulfonium salt precursor for aromatic .....	
<sup>18</sup> F-fluorination .....	61
3.2.4. Radiolabeling of [ <sup>18</sup> F] <b>22</b> .....	64
<b>4. Sodium Channel Blockade by WIN17317-3 Analogues (<i>in Vitro</i>) .....</b>	<b>65</b>
4.1. Electrophysiological assays, and their use, for measuring Na <sub>v</sub> activity .....	65
4.2. The IonWorks Quattro screening platform .....	67
4.3. Evaluation of a two concentration-response point approach for .....	
screening Na <sub>v</sub> activity using IonWorks Quattro .....	70
4.4. State- and use- dependency .....	75
4.5. Structure-Activity Relationships for Na <sub>v</sub> 1.7 .....	78
4.6. Na <sub>v</sub> isoform profiling .....	89
4.7. Summary .....	92
<b>5. Selective blockade of C-fiber action potential propagation by .....</b>	<b>94</b>
<b>iminodihydroquinolines in rodent peripheral sensory neurons .....</b>	<b>94</b>
<b><i>in vitro</i> .....</b>	<b>94</b>
5.1. The skin-nerve preparation as an assay to measure pharmacological .....	
activity in peripheral endings of sensory neurons .....	94
5.1.1. Experimental set-up .....	95
5.1.2. Recordings and data analysis .....	98

---

---

5.2.	Effects of iminodihydroquinolines on C- and A-fiber conduction .....	101
5.2.1.	SARs for C-fiber blockade .....	102
5.2.2.	Selectivity for C- over A-fiber blockade.....	107
5.3.	Lead identification and development .....	108
5.4.	Second generation iminodihydroquinoline analogues.....	111
5.4.1.	Effects on C- and A-fiber conduction .....	111
5.4.2.	Na <sub>v</sub> screening.....	114
5.5.	Nerve absorption and metabolism pharmacokinetics.....	115
5.6.	Comparative assessment towards local anesthetics .....	119
5.7.	Unraveling the molecular mechanism of iminodihydroquinoline action at nociceptors .....	123
5.7.1.	Relationship between Na <sub>v</sub> 1.7 inhibition and C-fiber conduction block.....	123
5.7.2.	Na <sub>v</sub> isoform selectivity and C- over A-fiber selectivity .....	125
5.8.	Summary.....	126
<b>6.</b>	<b><i>In vivo</i> characterization of a lead preclinical drug candidate .....</b>	
	<b>in rodents.....</b>	<b>128</b>
6.1.	Assays .....	130
6.1.1.	Positron emission tomography (PET) for pharmacokinetic profiling .....	130
6.1.2.	The “up-and-down” method for determining acute lethal toxicity.....	132
6.2.	Pharmacokinetic profile of [ <sup>18</sup> F] <b>22</b> .....	133
6.3.	Maximum tolerated dose of the lead <b>22</b> after iv administration in rats.....	134
6.4.	Summary.....	135
<b>7.</b>	<b>Conclusions.....</b>	<b>136</b>
<b>8.</b>	<b>Experimental.....</b>	<b>138</b>
8.1.	Experimental for Chapter 3.....	138
8.1.1.	Synthesis of <i>N</i> -substitued-4-imino-1,4-dihydroquinolines. ....	139
8.1.2.	Synthesis of <i>N</i> -substitued-4-imino-1,4-dihydro-naphthyridines .....	174
8.1.3.	Synthesis of <i>N</i> 9-substitued-6-aminoaryl-purines and <i>N</i> -substitued-4-imino-1,4-dihydro-pyridines .....	181
8.1.4.	Synthesis of sulfonium salt <b>100</b> .....	185
8.1.5.	Radiochemistry .....	189
8.2.	Experimental for Chapter 4.....	190
8.3.	Experimental for Chapter 5.....	191

---

---

<b>8.4.</b>	Experimental for Chapter 6.....	<b>192</b>
<b>9.</b>	<b>References</b> .....	<b>193</b>



---

## Abbreviations

ADME	absorption, distribution, metabolism and excretion
AP	action potential
ASIC	acid-sensing ion channels
BNZA	1,3,4,5-tetrahydro-2H-benzo[ <i>b</i> ]azepin-2-one
BTX	batrachotoxin
CAP	compound action potential
Ca <sub>v</sub>	voltage-gated calcium channels
CHO	Chinese hamster ovarian
CIP	Congenital indifference to pain
CNS	central nervous system
COX	cyclo-oxygenase
CVS	cardiovascular
DAST	diethylamino sulfur trifluoride
DCM	dichloromethane
DMF	dimethylformamide
DMSO	dimethyl sulfoxide
DRG	dorsal root ganglia
EWG	electron-withdrawing group
GABA	γ-aminobutyric acid
GI	gastro-intestinal
GPCR	G-protein coupled receptor
HPLC	high performance liquid chromatography
IEM	Erythermalgia
I <sub>NaP</sub>	persistent sodium current
I <sub>NaR</sub>	resurgent sodium current
ISAP	International Association for the Study of Pain
IUPAC	International Union of Pure and Applied Chemistry
iv	intravenous

---

IWB	IonWorks Barracuda™
IWQ	IonWorks Quattro™
K <sub>2P</sub>	two-pore potassium channel
K <sub>CA</sub>	calcium-activated potassium channel
K <sub>ir</sub>	inward rectifying potassium channel
K <sub>vS</sub>	voltage-gated potassium channels
LAs	local anesthetics
LBDD	ligand-based drug design
<i>m</i> CPBA	3-chloroperoxybenzoic acid
MRI	magnetic resonance imaging
NaChBac	bacterial voltage-gated sodium channel
Na <sub>vS</sub>	voltage-gated sodium channels
NSAID	non-steroidal anti-inflammatory drug
P2X	purinergic receptors
PEPD	Paroxysmal extreme pain disorder
PET	positron emission tomography
PG	prostaglandin
PK/PD	pharmacokinetic/pharmacodynamics
PNS	peripheral nervous system
RCY	radiochemical yield
RTK	receptor tyrosine kinase
SAR	structure-activity relationship
SBDD	structure-based drug design
SEM	standard error of the mean
SIF	simulated intestinal fluid
SNL	spinal nerve ligation
SPECT	single-photon emission computed tomography
THF	tetrahydrofuran
TNF-α	tumor necrosis factor-α
TP	test pulse
TRP	transient receptor potential channels

---

---

TRPA1	ankyrin-1 transient receptor potential channel
TRPM8	melastatin-8 transient receptor potential channel
TRPV1	vanilloid-1 transient receptor potential channel
TTX	tetrodotoxin
TTX-R	tetrodotoxin-resistant
TTX-S	tetrodotoxin-sensitive
WHO	World Health Organization
3D	three-dimensional

---

## List of tables

<b>Table 1.</b> Anatomical and functional characteristics of sensory neuronal fibers.....	4
<b>Table 2.</b> Cloned Na <sub>v</sub> $\alpha$ -subunit genes, their major expression sites and the effect of their mutation. <sup>78 79</sup> .....	16
<b>Table 3.</b> Na <sub>v</sub> channel modulators that have reached clinical development for the treatment of pain. <sup>122</sup> .....	24
<b>Table 4.</b> <i>hNav</i> isoform profiling of iminodihydroquinolines WIN17317-3 and 2.* .....	29
<b>Table 5.</b> Synthesis of (4-alkylamino)quinoline intermediates 3 - 11. ....	40
<b>Table 6.</b> <i>N</i> -benzylation of (4-alkylamino)quinolines 19 - 27.....	44
<b>Table 7.</b> <i>N</i> -alkylation of (4-alkylamino)quinolines 7-10.....	45
<b>Table 8.</b> <i>N</i> -alkylation of 4-quinolones. ....	47
<b>Table 9.</b> Synthesis of iminodihydroquinolines 1, and 36 - 38. ....	48
<b>Table 10.</b> Concentration-response relationships and characterization of WIN17317-3, 116* and 118* at <i>hNa<sub>v</sub>1.7</i> . ....	72
<b>Table 11.</b> IC <sub>50</sub> values of first generation iminodihydroquinoline analogues for <i>hNa<sub>v</sub>1.7</i> channels at tonic-, 10 Hz- and inactivated- voltage states. The structures of compounds exhibiting preference for a particular voltage state/s over other/s are illustrated to the right. ....	77
<b>Table 12.</b> Characterization of R <sup>1</sup> -series iminodihydroquinolines as <i>hNa<sub>v</sub>1.7</i> inhibitors.....	79
<b>Table 13.</b> Characterization of R <sup>2</sup> -series iminodihydroquinolines as <i>hNa<sub>v</sub>1.7</i> inhibitors.....	82
<b>Table 14.</b> Characterization of R <sup>3</sup> -series iminodihydroquinolines as <i>hNa<sub>v</sub>1.7</i> inhibitors.....	84
<b>Table 15.</b> Characterization of heterocyclic scaffold analogues (R <sup>4</sup> -series) as <i>hNa<sub>v</sub>1.7</i> inhibitors.....	85
<b>Table 16.</b> Functional characterization of iminodihydroquinolines as <i>hNa<sub>v</sub>1.7</i> inhibitors.....	86
<b>Table 17.</b> Blocking potencies of ten selected iminodihydroquinolines against <i>hNa<sub>v</sub></i> isoforms.....	89

---

<b>Table 18.</b> Selectivity of iminodihydroquinolines for blocking $hNa_v1.7$ over other $hNa_v$ s.....	91
<b>Table 19.</b> Example of data recording and analysis of WIN17317-3 effects in the saphenous skin-nerve preparation.....	100
<b>Table 20.</b> Summary of half-maximal and maximal concentrations ( $EC_{50}$ and $EC_{90}$ ) for C-CAP blockade as a result of modifications at the $R^2$ substituent.....	105
<b>Table 21.</b> Summary of half maximal and maximal effective concentrations ( $EC_{50}$ and $EC_{90}$ ) for C-fiber blockade in rat saphenous nerve as a result of modifications at the $R^3$ substituent. ....	106
<b>Table 22.</b> Summary of half-maximal and maximal effective concentrations ( $EC_{50}$ and $EC_{90}$ ) for C-fiber blockade in rat saphenous nerve by second generation analogues. ....	112
<b>Table 23:</b> $IC_{50}$ values of second generation iminodihydroquinolines for $hNa_v$ inhibition. ....	114
<b>Table 24.</b> Physicochemical properties and functional characterization of 22, WIN17317-3 and the marketed drug lidocaine.....	126
<b>Table 25.</b> “Up-and-down” test series to determine the CNS, cardiovascular toxicity and lethality in rats after iv administration of 22. ....	134

---

## List of figures

- Figure 1.** Gate control theory of pain. This model proposed that inhibitory interneurons located in the substantia gelatinosa (yellow, GS) determine whether nociceptive input from the periphery is relayed through the spinal transmission system (pink, T) to the higher CNS for pain to be consciously received.<sup>19</sup> .....3
- Figure 2.** Schematic representation of pain signaling mechanisms showing ascending and descending modulatory pathways. Adapted from reference 1.<sup>1</sup> .....3
- Figure 3.** Anatomy of nociceptors. The central projections of nociceptors are highly organized with different types of fiber terminating within specific dorsal horn laminae. (A) Unmyelinated C-fibers project to superficial laminae I and II. (B) Myelinated A-fibers project to superficial laminae I and V. Adapted from reference 26.<sup>26</sup> .....5
- Figure 4.** Potential mediators for nociceptor stimulation and the corresponding transducer receptors and ion channels in the peripheral free nerve ending. Adapted from reference 23.<sup>23</sup> .....6
- Figure 5.** Contribution of voltage-gated ion channels in neuronal action potential firing. ....7
- Figure 6.** Subcellular localization of potassium channel isoforms in unmyelinated and myelinated murine DRG neurons. Adapted from reference 42.<sup>42</sup> .....8
- Figure 7.** Release of neurotransmitters and neuromodulators, upon AP arrival at the pre-synaptic nociceptive terminal, in the superficial dorsal horn of the spinal cord or the brainstem. Adapted from reference 2.<sup>2</sup> .....9
- Figure 8.** The adapted WHO analgesic ladder. The classic 1986 version of the WHO analgesic ladder, originally applied to management of cancer pain, proposed the treatment should begin with non-opioid medication, followed by the use of weak and strong opioids if pain is not controlled. The updated bidirectional version of the ladder (*vide supra*) is applicable for the treatment of both acute and chronic (including cancer) pain conditions, and it integrates a fourth step with invasive analgesic techniques.<sup>52</sup> .....10
- Figure 9.** Non-selective NSAIDs and their molecular mechanism of action at the arachidonic acid metabolic pathway. ....10
- Figure 10.** Schematic representation of the generic structure of the mammalian Na<sub>v</sub> α-subunit. The α-subunit is composed of four pseudo homologous domains (I to IV), each comprised by six transmembrane segments (1 to 6) presented as cylinders. The S4 segments serve as the voltage sensor (+). Pink circles indicate the positions of amino acids important for ion conductance and selectivity. Green circles indicate the positions of hydrophobic amino acids part of the inactivation gate, which is

---

thought to fold into and block the ion-conducting pore. Side view (left) and top view (right). Adapted from references 67, 68.<sup>66, 67</sup> ..... 13

**Figure 11.** Classic Na<sub>v</sub> channel current profile. When the membrane is at resting potential, -90 mV, the channel is at its closed (resting state). Upon depolarization (shift of membrane potential to +30 mV), the channel becomes activated and sodium ions enter the cell through the Na<sub>v</sub> channel pore. Within a few ms the inactivation loop “enters” the pore and the channel inactivates. When the membrane is repolarized to -50 mV, the channel partially recovers from inactivation, yet no current flows. Upon further repolarization to -90 mV the channel returns to its resting (closed) state. Adapted from reference 77.<sup>76</sup> ..... 15

**Figure 12.** Na<sub>v</sub> channel homology model illustrating the postulated toxin binding sites (1-6) and the LAs binding site; side view (left) and top view (right). (1) TTX (2) batrachotoxin (BTX) (3) scorpion α-toxin (4) scorpion β-toxin (5) brevetoxins (6) δ-conotoxin (7) pyrethroids.<sup>122</sup> ..... 23

**Figure 13.** Na<sub>v</sub> channel modulators in clinical development for the treatment of pain. .... 24

**Figure 14.** Structures of the TRPV1 agonist, capsaicin, and the tertiary lidocaine derivative, QX-313 (left). TRPV1 agonist–Na<sub>v</sub> antagonist effects at nociceptors. Activation of TRPV1 by capsaicin allows QX314 internalization and binding to the Na<sub>v</sub> LA site blocking Na<sub>v</sub> current passage (right).<sup>128</sup> ..... 25

**Figure 15.** Chemical structure of WIN177317-3. .... 27

**Figure 16.** Autoradiographic localization of [<sup>3</sup>H]WIN17317-3 binding sites in rat brain. Brain sections were incubated with the tracer (2-3 nM) in the absence (A) and the presence (B) of non-radiolabeled WIN17317-3.<sup>132</sup> ..... 27

**Figure 17.** Biological evaluation of [<sup>125</sup>I]2 after iv administration in mice. (A) Tissue distribution expressed as % ID/g ± SD (n≥3) (B) SPECT/CT summation image from 15-35 min after injection.<sup>3</sup> ..... 28

**Figure 18.** WIN17317-3 evaluation in the rat skin-nerve assay. Saphenous nerve A- (■) and C-fiber (●) CAP blockade as a function of WIN17317-3 concentration. Data points are shown as mean ± S.E.M (n = 9), fitted dose-response curves are presented as solid lines. (Koltzenburg group, unpublished data). .... 30

**Figure 19.** (A) Aminoacid sequence of the tarantula *T. Pruriens* peptide, ProTx-II. (B) 3D-structure model of ProTx-II, constructed using the optimal docking area method by homology modeling with ICM-PRO (Molsoft) based on the NMR structure of GsMTx2 (PDB:1lup). Blue, green, yellow, red and purple represent positively charged, aromatic, hydrophobic, negatively charged and polar residues respectively. The locations of aminoacid residues important for Na<sub>v</sub>1.5 binding as revealed by mutation experiments are indicated.<sup>136</sup> (C) ProTx-II effects on the isolated nerve preparation. Saphenous nerve Aβ- (●) and C-fiber (■) CAP blockade as a function ProTx-II concentration. Data points are shown as mean ± S.E.M (n = 9). (D) Block of

---

<i>h</i> Na <sub>v</sub> 1 subtypes by ProTx-II examined by whole-cell voltage clamp. IC <sub>50</sub> values: Na <sub>v</sub> 1.2, 41 nM; Na <sub>v</sub> 1.3, 102 nM; Na <sub>v</sub> 1.4, 41 nM; Na <sub>v</sub> 1.5, 79 nM; Na <sub>v</sub> 1.6, 26 nM; Na <sub>v</sub> 1.7, 0.3 nM; Na <sub>v</sub> 1.8, 146 nM. <sup>123</sup> .....	31
<b>Figure 20.</b> WIN17317-3 effects on (A) TRPV1- and (B) TRPA1-transfected HEK293 cells examined using live cell ratiometric calcium imaging. A control agonist was administered prior to and after WIN17317-3 administration to confirm the expression of functional channels. Koltzenburg group, unpublished data. ....	32
<b>Figure 21.</b> Characterization of the WIN17317-3 pharmacophore. ....	35
<b>Figure 22.</b> The chemical structure of TTX. ....	35
<b>Figure 23.</b> LogP and LogD equations.....	36
<b>Figure 24.</b> The heterocyclic compounds composing the WIN17317-3 library, for which the chemical synthesis is described in this chapter. From left to right: quinolines, naphthyridines, purines and pyridines and an [ <sup>18</sup> F]labelled selected lead compound.....	38
<b>Figure 25.</b> General structure of <i>N</i> -substituted-4-imino-1,4-dihydroquinolines and the three building blocks used for their synthesis.....	39
<b>Figure 26.</b> Key NOESY interactions (↔) .....	47
<b>Figure 27.</b> Structures of marketed 4-quinolone drugs.....	50
<b>Figure 28.</b> The chemical family of diazanaphthalenes.....	53
<b>Figure 29.</b> Structures of purine-containing biomolecules and drugs. ....	57
<b>Figure 30.</b> Lead structure 22 and the corresponding [ <sup>18</sup> F]radiotracer. ....	59
<b>Figure 31.</b> <sup>18</sup> F-Labeling of dimethylsulfonium salts. ....	60
<b>Figure 32.</b> Timeline of sulfonium salt development as leaving groups for aromatic [ <sup>18</sup> F]fluorination. ....	61
<b>Figure 33.</b> HPLC chromatogram of the isolated compound [ <sup>18</sup> F]22, co-injected with the non-labelled reference 22. ....	64
<b>Figure 34.</b> Schematic representation of the general features of a conventional patch clamp chip (A) and a planar patch clamp chip (B). (C) Illustration of a 16 well planar patch clamp configuration allowing parallel patch clamping. Adapted from reference 189. <sup>189</sup> .....	66
<b>Figure 35.</b> Voltage protocol for measuring <i>h</i> Nav1.x blockade. The test pulse (TP) pattern was repeated twice: before (-control) and 5 minutes after compound (cpd) addition. The peak current amplitudes at TP <sub>1</sub> , TP <sub>11</sub> and TP <sub>12</sub> were measured and used for calculating the percentage inhibitions at resting and inactivate states, and use-dependency respectively. Four replicates were performed for each compound	

---



---

concentration tested. Lidocaine (3 mM) and DMSO (0.3%) were included in each plate as positive and negative control, respectively.....68

**Figure 36.** Concentration-response relationships for lidocaine and TTX at *hNa<sub>v</sub>1.7* measured using the IWQ platform operated at the voltage protocol of Fig. 35. IC<sub>50</sub> values for lidocaine were 548 μM, 49 μM and 8 μM for the tonic, frequency-dependent and inactivated states respectively. Data are presented as mean ± SD (*n* = 3–5). TTX produced similar concentration-response curves at all three voltage states.....69

**Figure 37.** Screening results of 400 known drugs for blocking activity against *hNa<sub>v</sub>1.3* at 10 μM using E-VIPR. Each plate contained four negative (DMSO, red) and four positive (100 mM tetracaine, blue) controls. Drug-blocking activity was calculated according to the two controls, with hits defined as compounds producing more than 60% of the tetracaine block. Adapted from reference 194.<sup>194</sup> .....70

**Figure 38.** (A) Percentage inhibition of *hNa<sub>v</sub>1.7* channels by ~12,000 compounds (grey dots) tested at 10 μM in duplicate (Obs1 and Obs2) (Pearson *r* correlation coefficient = 0.66, *r*<sup>2</sup> = 0.44, *P* < 0.0001). (B) Compounds producing greater than 80% inhibition (square with dashed border) were re-evaluated at 10 μM in duplicate (Pearson *r* correlation coefficient = 0.86, *r*<sup>2</sup> = 0.75, *P* < 0.0001). (C) Plot of IC<sub>50</sub>s, calculated from 8-point concentration-response curves, versus the percentage inhibition produced at 10 μM as determined from B. Compounds producing >50% inhibition at 10 μM in study B are depicted in black circles whilst those producing <50% are illustrated with open squares. Adapted from reference 189.<sup>189</sup> .....71

**Figure 39.** Screening of 41 first generation iminodihydroquinoline analogues against *hNa<sub>v</sub>1.7*. Plot of %tonic inhibitions obtained at 1 μM and 10 μM concentrations. According to the pre-defined set of criteria compounds were classified as highly potent (green, 13 cpds), as moderately potent (blue, 14 cpds) as inactive (red, 12 cpds) or as outliers (grey, 2 cpds).....73

**Figure 40.** 3D Plot of *hNa<sub>v</sub>1.7* IC<sub>50</sub>s versus %tonic inhibitions measured at 1 μM and 10 μM concentrations. (A) Side view and (B) top view. Compounds are classified as potent (●), moderately potent (●) or inactive (●) according to the results of the screening at 1 and 10 μM and the predefined set of criteria. The % inhibitions at 1 μM and 10 μM shown, were part of the 8 point concentration-response curves used for determining the compounds' IC<sub>50</sub>s.....74

**Figure 41.** Plots of tonic (A), use-dependent (B) and inactivation blocks (C) of first generation analogues against *hNa<sub>v</sub>1.7* at 1 μM and 10 μM concentrations. According to the defined set of criteria compounds were classified as highly potent (green), as moderately potent (blue), as inactive (red), or as outliers (⊥). (D) Superposition of the data from all three blocking states showed no apparent differences amongst them.....75

**Figure 42.** The WIN17317-3 pharmacophore.....78

<b>Figure 43.</b> Plot of <i>t</i> PSA - activity relationship. High potency (●), moderate potency (●), inactive (●). .....	80
<b>Figure 44.</b> <i>t</i> PSA – Na <sub>v</sub> 1.7 inhibition relationship for first generation iminodihydroquinoline analogues. Compounds are classified as highly potent (●), as moderately potent (●) Na <sub>v</sub> 1.7 blockers or as inactive (●).....	87
<b>Figure 45.</b> Structure-activity relationships of small molecule iminodihydroquinolines for <i>h</i> Na <sub>v</sub> 1.7. (high potency inhibition: ↑, low potency inhibition: ↓, abolished activity: x).....	88
<b>Figure 46.</b> Iminodihydroquinolines' selectivity for blocking <i>h</i> Na <sub>v</sub> 1.7 over other Na <sub>v</sub> isoforms. The radar charts' axes represent the compounds' selectivity for Na <sub>v</sub> 1.7 as the ratio of IC <sub>50</sub> (Na <sub>v</sub> 1.7) over IC <sub>50</sub> (Na <sub>v</sub> 1.x). (A) Selectivity for Na <sub>v</sub> 1.7 over Na <sub>v</sub> 1.2, Na <sub>v</sub> 1.4, Na <sub>v</sub> 1.5, Na <sub>v</sub> 1.6, and Na <sub>v</sub> 1.8. (B) Focus in the three isoforms, Na <sub>v</sub> 1.2, Na <sub>v</sub> 1.6 and Na <sub>v</sub> 1.8, that showed the highest Na <sub>v</sub> 1.7 blocking selectivity.....	92
<b>Figure 47.</b> Example of six CAP signal overlays evoked by electrical stimulation (time 0) of the sciatic-tibial nerve of a mouse <i>in vivo</i> . Dashed lines indicate conduction velocity cutoffs for differentiation of the three major fiber types present (Aβ, Aδ, C). Note difference in vertical scales for A and C fibers. Aβ-Aδ fibers were evoked by a 100 μA stimulus and C fibers were evoked by 6 mA stimulus. Adapted from reference 209. <sup>209</sup> .....	95
<b>Figure 48.</b> Anatomical context of the rat saphenous nerve (lower right leg). The saphenous nerve (yellow) is a terminal sensory branch of the femoral nerve, arising from the third lumbar root. At the level of the thigh it separates from the femoral nerve and descends on the lateral side of the femoral vessels (arteries: red, veins: blue) to lie on the medial side of the leg. It supplies the skin of the medial side and front of the knee. At the ankle, it passes anterior to the medial malleolus to innervate skin on the medial and dorsal aspects of the foot. <sup>215</sup> Its superficial anatomical path, allows <i>in vivo</i> electrophysiological studies. Adapted from reference 215.....	96
<b>Figure 49.</b> The experimental set up for the skin-nerve preparation. (A) Schematic representation of the skin-nerve chamber illustrating fluid circulation. Adapted from reference 215. (B) Top view of the skin-nerve chamber. The skin is placed in the stimulation chamber dermis side up (1), and the proximal end of the attached nerve is extended through a hole to the adjacent recording chamber (2).....	97
<b>Figure 50.</b> Schematic representation of the skin-nerve assay data capture. Electrical stimulation is administered to the receptive field. The recorded signal is fed into an AC-coupled differential preamplifier that is connected in series with a second single ended 10 <sup>4</sup> –gain amplifier and a band-pass filter (between 1 Hz and 1 kHz).The signal is subsequently fed to audio speakers and oscilloscope and processed through a DAP board, where the action potentials above set amplitudes are discriminated and fed into the computer. Adapted from reference 215. <sup>215</sup> .....	97
<b>Figure 51.</b> Schematic representation (A) and view (B) of the skin-nerve preparation with the metal ring. An application system's tip is positioned within the ring to	

---

superfuse the isolated receptive field with the drug solution of interest. Labels: (1) pair of stimulation electrodes; (2) pair of wire electrodes used for recording the signal; (3) metal ring used to isolate the receptive field.....98

**Figure 52.** Typical CAP traces evoked by electrical stimulation of the saphenous nerve at time 0 as indicated by the open point arrows. (A) Shows all the components of the saphenous CAP while (B) and (C) focus in at specific settings for measuring A $\beta$  and C-CAPs respectively. Dotted lines denote the peak responses recorded....99

**Figure 53.** Data analysis of WIN17317-3 effects in the saphenous skin-nerve preparation. The %CAP blocks produced by ascending drug concentrations were calculated as % current reduction relative to baseline as depicted by the equation to the right. The data points are plotted on a concentration - %block semi-logarithmic plot, as means of nine recordings  $\pm$  SEM. Dose-response curves were fitted and EC<sub>50</sub>, EC<sub>90</sub> parameters were calculated using the Origin Pro9.0<sup>®</sup> software in DoseResp fitting mode. .... 100

**Figure 54.** The WIN17317-3 pharmacophore..... 101

**Figure 55.** Effects of R<sup>2</sup>-series analogues in the skin-nerve preparation. Saphenous nerve A $\beta$  (■) and C (●) fiber CAP blockade as a function of iminodihydroquinoline concentration. Data shown as mean  $\pm$  S.E.M ( $n = \geq 4$ , (a)  $n = 2$ ), fitted dose-response curves presented as solid lines..... 104

**Figure 56.** Effects of R<sup>3</sup>-series analogues in the skin-nerve preparation. Block of saphenous nerve A $\beta$  (■) and C (●) fiber CAP as a function of drug concentration. Data are shown as mean  $\pm$  S.E.M ( $n = \geq 4$ ). Fitted dose-response curves are presented as solid lines. .... 106

**Figure 57.** C- over A-fiber selectivity for R<sup>2</sup>- and R<sup>3</sup>-series analogues. 90% C-CAP block for each compound is plotted alongside the simultaneously recorded value for % A-CAP. The C-over A-fiber selectivity was calculated as the ratio between the two at the bottom of the chart..... 107

**Figure 58.** Hit to lead development. Optimal R<sup>2</sup> and R<sup>3</sup> substituents were combined for the design of the lead compound 22. .... 109

**Figure 59.** Effects of Hit (WIN17317-3) and Lead (22) molecules in the skin-nerve preparation. Block of saphenous nerve A $\beta$  (■) and C (●) fiber CAP as a function of drug concentration. Data are shown as mean  $\pm$  S.E.M ( $n = \geq 4$ ). Fitted dose-response curves are presented as solid lines. .... 110

**Figure 60.** Effects of second generation analogues in the skin-nerve preparation. Block of saphenous nerve A $\beta$  (■) and C (●) fiber CAP as a function of drug concentration. Data are shown as mean  $\pm$  S.E.M ( $n = \geq 4$ , <sup>a</sup> $n = 3$ ). Fitted dose-response curves are presented as solid lines. .... 111

**Figure 61.** Effects of second generation analogues on C- and A-fiber conduction as measured in the skin-nerve preparation. 90% C-CAP block for each compound is plotted alongside the simultaneously recorded value for % A-CAP block at this

---

concentration. C/A-CAP block ratios, at the bottom of the chart, were calculated as a measure of the C/A-fiber selectivity. .... 113

**Figure 62.** Half maximal effective concentrations ( $EC_{50} \pm S.E.$ ,  $n \geq 3$ ) of second generation analogues for C- and A-CAP blockade as measured in the skin-nerve preparation. .... 113

**Figure 63.** Cross sectional aspects of the rat saphenous nerve. A. Schematic representation of the nerve illustrating fascicles and individual nerve fibers. Components in an orderly fashion from the outermost layer to the inner most include the epineurium, perineurium, endoneurium and Swann cells surrounding the axon. B. Light micrograph of a monofasciculated nerve, enveloped by a well-defined perineurium (arrows), showing myelinated fibers and capillary blood vessels (\*) in the endoneural space.<sup>214</sup> .... 115

**Figure 64.** Effects of the lead compound 22 in intact (left) and desheathed (right) saphenous nerves. Block of  $A\beta$  (■) and C (●) fiber CAP as a function of drug concentration. Data are shown as mean  $\pm$  S.E.M ( $n = 9$  intact,  $n = 2$  desheathed). Fitted dose-response curves are presented as solid lines. .... 117

**Figure 65.** Effects of lead compound 22, applied at a single concentration, 130  $\mu$ M, at the intact saphenous nerve for 1.5 h. Block of  $A\beta$  (■) and C (●) fiber CAP as a function of time. Data are shown as mean  $\pm$  S.E.M ( $n = 4$ ). .... 118

**Figure 66.** Effects of lidocaine in the rat sciatic nerve. (A) Tonic block of individual nerve fiber axons *in vivo*. All categories ( $A\beta$ ,  $A\delta$ , C) are blocked over a range of concentrations from 0.2 to 0.8 mM yet nociceptive C-fibers are evidently significantly less susceptible.<sup>220</sup> (B) Time course of impulse blockade as a response to a non-equilibrium percutaneous bolus injection of 0.5% lidocaine around the nerve.<sup>223</sup> The differential rate and maximum degree of block exhibited by nerve fibers are consistent amongst the two studies. Adapted from references 220 and 223. .... 119

**Figure 67.** Effects of lead 22 and local anesthetics lidocaine, butamben and dibucaine, in the skin-nerve preparation. Block of saphenous nerve  $A\beta$  (■) and C (●) fiber CAP as a function of drug concentration. Data are shown as mean  $\pm$  S.E.M ( $n = \geq 4$ , <sup>a</sup> $n = 3$ ). Fitted dose-response curves are presented as solid lines. .... 120

**Figure 68.** Half-maximal effective concentrations of lead 22 and local anesthetics lidocaine butamben and dibucaine ( $EC_{50} \pm S.E.$ ,  $n \geq 3$ ) for C- and A-CAP blockade in the skin-nerve preparation. Asterisks (\*) indicate the significance level of A and C-CAP  $EC_{50}$  difference, as calculated by the unpaired Students *t*-test (\*  $P \leq 0.05$ , \*\*\*  $P \leq 0.001$ , \*\*\*\*  $P \leq 0.0001$ ). .... 121

**Figure 69.** Effects of 'lead' 22 and local anesthetics on C- and A-fiber conduction in the skin-nerve preparation. 90% C-CAP block for each compound is plotted alongside the simultaneously recorded value for % A-CAP. C/A ratios, at the bottom of the chart, were calculated as a measure of the C/A-fiber selectivity for each compound. .... 121

---

<b>Figure 70.</b> Logarithmic relationship between IC <sub>50</sub> of hNa <sub>v</sub> 1.7 at resting state, and EC <sub>50</sub> of C-fiber blockade as determined by the automated patch clamp and the skin-nerve assays respectively. Standard deviations and standard errors are plotted as relative log error bars. <sup>231</sup> .....	123
<b>Figure 71.</b> Linear regression models for describing the activity of iminodihydroquinolines at Na <sub>v</sub> 1.7 and at sensory C-fibers. (A) The linear model characterizing the relationship between all data points, adj. R <sup>2</sup> = 0.40 (B) Two linear models, applied at two group subsets, display increased R <sup>2</sup> values (0.91, 0.68) and are therefore more appropriate predictors of the log(IC <sub>50</sub> )/ log(EC <sub>50</sub> ) relationship. Models and adjusted R <sup>2</sup> values were calculated using the OriginPro software at linear fitting mode with no weighting. ....	124
<b>Figure 72.</b> Selectivity for Na <sub>v</sub> 1.7 over Na <sub>v</sub> 1.6 isoform blockade, as calculated from the relative potencies at tonic state in automated patch clamp assays, plotted alongside the selectivity for C- over A-fiber blockade for each compound, calculated as the ratio of 90% C-CAP blockade over the corresponding A-CAP block in the skin nerve preparation. ....	125
<b>Figure 73.</b> A conceptual model depicting the fate of local drugs injected perineurally indicating potential sites for toxicity effects (*). ....	129
<b>Figure 74.</b> Relationship of plasma concentration and signs and symptoms of toxicity for lidocaine. Adapted from reference 219. <sup>219</sup> .....	129
<b>Figure 75.</b> Principles of PET. A. A positron (e <sup>+</sup> ) and a neutrino (ν) are ejected from an atom that undergoes positron decay. Two 511 keV photons are produced when the positron annihilates with an electron (e <sup>-</sup> ). B. If both photons are detected within a set timing window, as determined by the PET scanner coincidence timing processor, then a line of response is registered. ....	131
<b>Figure 76.</b> Representative PET/CT images illustrating the biodistribution of [ <sup>18</sup> F]22 in wild-type albino (Balb/C) mouse after iv administration. The radiotracer retention is presented as a percentage of the injected dose per unit tissue volume (%ID/ml). ....	133
<b>Figure 77.</b> Biodistribution of [ <sup>18</sup> F]22. Summed PET/CT image, 2 hours. ....	134

# 1. Voltage-Gated Sodium Channels as Targets for Pain Therapy

## 1.1. Pain, an unmet clinical challenge

Pain is one of the most important human experiences, and one of the most complex. It is defined as the “unpleasant sensory and emotional experience associated with actual or potential tissue damage” (International Association for the Study of Pain- ISAP).<sup>4</sup> The definition recognizes pain as a multidimensional phenomenon involving sensory, affective and cognitive components, which are not necessarily correlated to tissue damage.

Conventionally, pain is broadly categorized into two classes mainly on the basis of the arbitrary time interval from onset: acute and chronic pain.<sup>5</sup> Acute pain is typically the result of soft tissue injury or inflammation notifying the presence of physical insult, is of sudden onset, and usually lasts for a short period of time (less than three months). It subsides when the underlying cause resolves. Acute pain can be successfully managed for the majority of patients with non-steroidal anti-inflammatory drugs (NSAIDs), opioids, local anesthetics (LAs) and anticonvulsants. Chronic pain, by contrast, long outlasts the initial insult to tissues, lasts greater than six months and rarely serves any biological function.<sup>6</sup> Although improvement maybe observed, for many patients complete cure can be rarely achieved using the current analgesic treatments.<sup>7</sup>

Additionally, pain is classified as of three types according to its etiology: nociceptive, neuropathic and psychogenic.<sup>8,9</sup> Nociceptive pain arises due to noxious external or inflammatory stimuli activating free peripheral nerve endings, nociceptors, which transmit the signal to the central nervous system (CNS).<sup>10</sup> Neuropathic pain, which is also known as dysfunctional pain, is indicative of dysfunction or damage to the nervous system with some of the probable causes including mechanical factors (e.g. nerve compression), toxicity (e.g. from chemotherapeutic drugs), metabolic diseases (e.g diabetes), post-inflammatory changes or idiopathic causes. Its mechanisms are entirely different from that of normal - nociceptive pain as apart from the detection of inflammatory mediators by nociceptors, it also involves peripheral and central sensitization.<sup>11</sup> Psychogenic pain most often has a physical origin (tissue damage or nerve damage) however in this

case the pain caused by the actual damage is increased or prolonged by psychological factors such as fear, depression, stress, or anxiety; it can also originate from purely psychological conditions.

By any measure, pain is an enormous global health problem.<sup>12</sup> The overall annual prevalence of chronic pain in Europe has been estimated to around 20% of the general population, significantly affecting the patients' social and working lives.<sup>13</sup> Very few (2%) are managed by pain specialists and only half report receiving adequate pain treatment. Pain is the leading cause for absenteeism from work with nearly 500 million working days lost per annum costing the European economy at least €34 billion. Approximately 10% of the population use analgesic medications on a regular basis leading to substantial direct and indirect (because of the plethora of adverse events of these compounds) costs. This is highlighted by the fact that the fatality associated with the use of NSAIDs exceeds 5 per 100,000, number higher than that for cervical cancer or malignant melanoma.<sup>14</sup> According to the official data of the American Academy of Pain Medicine, pain affects more Americans than diabetes, heart disease and cancer combined, and the annual cost of pain (\$560-\$635 billion) is nearly 30% higher than the combined cost of cancer and diabetes.<sup>15</sup> Evidently, pain management remains to date largely ineffective and the currently available pharmacological treatments are associated with significant adverse events. Development of novel, efficacious, analgesics with less serious adverse events is evidently an urgent unmet clinical need.

## **1.2. The perception and modulation of pain: a brief overview**

The word "pain" comes from the Latin *poena* meaning penalty. Physiologists distinguish between the terms pain and nociception. Nociception refers to the signals arriving in the CNS as a result of activation of specialized sensory neurons, nociceptors, providing information about tissue damage. Pain is the unpleasant emotional experience that usually accompanies nociception.<sup>16</sup>

The gate control theory of pain, proposed by Ronald Melzack and Patrick David Wall in 1965, was the first model explaining the variability between the input and output in the sensory system of pain, describing the relationship between nociceptive and non-nociceptive afferents in the dorsal horn as an electronic switch (Fig. 1).<sup>17,18</sup> Despite flaws in the presentation of neural architecture, the model was the first to account for the physical and psychological aspects of pain perception; whilst more recent detailed mechanisms have been added to the model, the general framework remains intact to date.

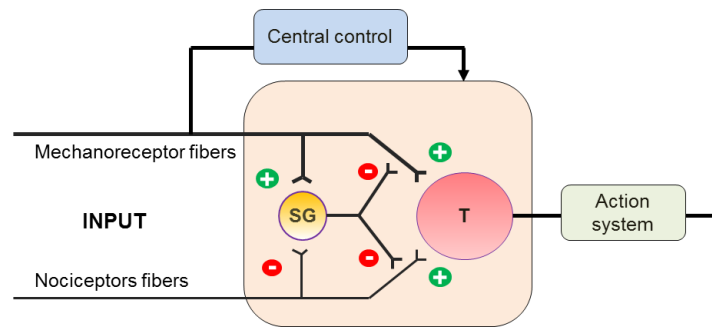


**Figure 1.** Gate control theory of pain. This model proposed that inhibitory interneurons located in the substantia gelatinosa (yellow, GS) determine whether nociceptive input from the periphery is relayed through the spinal transmission system (pink, T) to the higher CNS for pain to be consciously received.<sup>19</sup>

The sequence of events by which a painful stimulus is perceived involves four key processes: (a) transduction, (b) transmission, (c) modulation, and (d) perception (Fig. 2). Transduction occurs in the peripheral terminals of primary afferents where different forms of stimuli (mechanical, heat, chemical) are converted to electrical signals (action potential, AP).<sup>20, 1</sup> The generated AP is transmitted through the nervous system *via* three major components. The peripheral sensory neurons will first transfer the impulse from the transduction site to the spinal cord, where their central terminals synapse with second-order neurons. The latter will subsequently send projections to the thalamus and various brainstem and diencephalic structures where neurons will finally project to various cortical sites. Modulation is the process by which neural activity can be altered along the pain transmission pathway.<sup>21</sup> The major site for modulation is the dorsal horn. The process involves a multitude of neurotransmitter systems and can have both inhibitory and facilitator effects. Perception is the final stage of the pain signaling process. It is presumed to be the result of concerted activation of primary and secondary somatosensory and limbic cortices leading to the subjective sensation of pain.

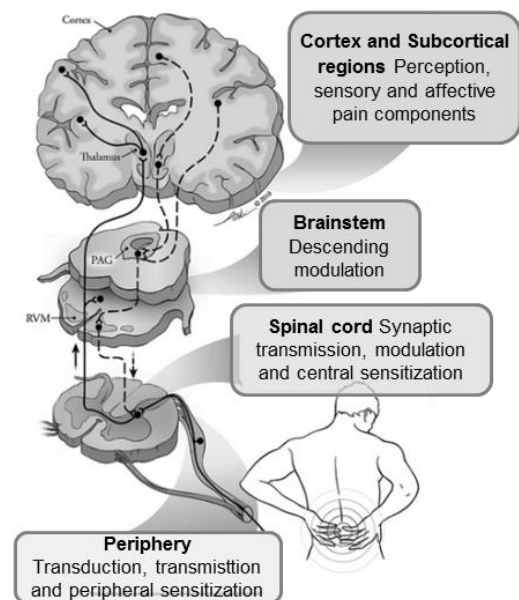


**Figure 2.** Schematic representation of pain signaling mechanisms showing ascending and descending modulatory pathways. Adapted from reference 1.<sup>1</sup>






In the following sections the peripheral pain nervous system is discussed in more detail. Further information for the central mechanisms of pain and other general aspects of pain can be found in all fundamental pain textbooks.<sup>1, 22, 23</sup>

### 1.3. Peripheral mechanisms of pain

Afferent neurons of the somatosensory system continuously “taste their environment”.<sup>24</sup> They convey information about the external environment and the state of the organism itself to the CNS. Primary sensory neurons are classified into two main groups based on anatomical and functional criteria: (a) the myelinated A-fibers which are subdivided into A $\beta$ - and A $\delta$ -fibers, and (b) the non-myelinated C-fibers (Table 1). Each fiber class is responsible for transmitting a specific type of sensory information.

**Table 1.** Anatomical and functional characteristics of sensory neuronal fibers.

	<b>A<math>\beta</math>-fibers</b>	<b>A<math>\delta</math>-fibers</b>	<b>C-fibers</b>
<b>Schematic</b>			
<b>Threshold</b>	low	medium	High
<b>Axon diameter</b>	6-14 $\mu\text{m}$	1-6 $\mu\text{m}$	0.1-1 $\mu\text{m}$
<b>Myelination</b>	yes	Yes, thin	No
<b>Velocity</b>	36-90 $\text{ms}^{-1}$	5-36 $\text{ms}^{-1}$	0.1-1 $\text{ms}^{-1}$
<b>Receptor type</b>	mechanoreceptor*	mechanoreceptor nociceptor	nociceptor
<b>Receptive field</b>	small	Small	small
<b>Quality</b>	touch*	sharp “first” pain	dull “second” pain

\*for the majority of fibers

The two major types of afferents transmitting nociceptive information, named nociceptors, are the medium diameter myelinated A $\delta$ -fibers which convey what is called “fast” pain (the initial component of acute pain) and the small diameter unmyelinated C-fibers, that mediate “slow” pain. In their vast majority A $\beta$  fibers detect innocuous stimuli applied to skin, muscle and joints and thus do not contribute to pain.<sup>25</sup>

Like all primary sensory neurons, the cell bodies of nociceptors are located in the dorsal root ganglia (DRG) or the trigeminal ganglia for the innervation of the face. They have a peripheral axonal branch that innervates the target tissue (free nerve ending) and a central axon branch that enters the spinal cord to synapse with the CNS second order neurons (Fig. 3).<sup>26</sup>

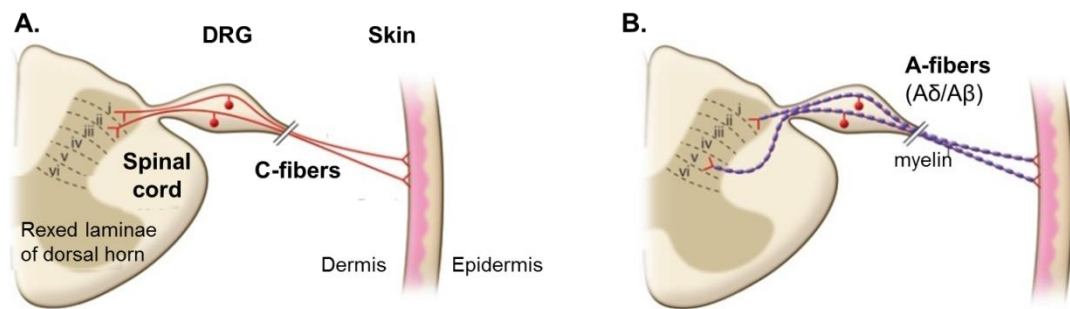


**Figure 3.** Anatomy of nociceptors. The central projections of nociceptors are highly organized with different types of fiber terminating within specific dorsal horn laminae. (A) Unmyelinated C-fibers project to superficial laminae I and II. (B) Myelinated A-fibers project to superficial laminae I and V. Adapted from reference 26.<sup>26</sup>

Nociceptors can be found in any area of the body capable of sensing pain, either externally or internally, such as the skin, muscles, joints (somatic pain)<sup>27</sup> and the internal organs (visceral pain).<sup>28, 29</sup> Depending on the tissue they innervate they feature distinct anatomical and functional characteristics. Skin nociceptors, also known as cutaneous nociceptors, are the most thoroughly studied class of nociceptors. The neurophysiology of cutaneous nociceptors is discussed in more detail below.

#### 1.4. Neurochemistry of cutaneous nociceptors

Peripheral nociceptors have four key operational components:

- The free nerve ending, which is the peripheral terminal responsible for transducing external stimuli into APs
- The axon responsible for transmitting APs
- The cell body that controls the identity and the integrity of the neuron and
- The central terminal which is the presynaptic elements of the first synapse, responsible for transmitting the information to the CNS.

### 1.4.1. Transduction

Cutaneous nociceptor transduction is the process of detection of painful stimuli (hot and cold thermal stimuli, intense noxious mechanical stimuli, harmful chemical stimuli) by the nociceptive free nerve ending.<sup>30</sup> The peripheral terminal sensitivity to the various stimulus modalities is mediated by multiple specialized receptors which upon activation lead to membrane depolarization and in effect to AP generation (Fig. 4).

Briefly, thermal sensitivity is mostly mediated by transient receptor potential (TRP) channels, large ligand-gated cationic channels ( $\text{Ca}^{2+}$ ), that open in response to thermal fluctuations and certain chemical modulators.<sup>31</sup> The vanilloid-1 (TRPV1)<sup>32</sup> subtype senses heat ( $> 43\text{ }^{\circ}\text{C}$ ) and can also be stimulated by capsaicin (the pungent ingredient of chili peppers) and protons. The ankyrin-1 (TRPA1)<sup>33, 34</sup> and melastatin-8 (TRPM8)<sup>35</sup> subtypes sense cold as well as mustard oil and menthol respectively.

Mechanotransduction is the least understood of the stimulus modalities, with different lines of evidence providing conflicting data.<sup>36, 37</sup> The acid-sensing ion channels (ASIC),<sup>38</sup> the Piezo 1 and 2 channels,<sup>39</sup> and the TRPA1<sup>40</sup> are some of the transducers that appear to be implicated in the process. Lastly nociceptors can be stimulated by a wide range of chemicals that are either released as part of the inflammatory response or are external irritants (e.g. plant or insect stings).

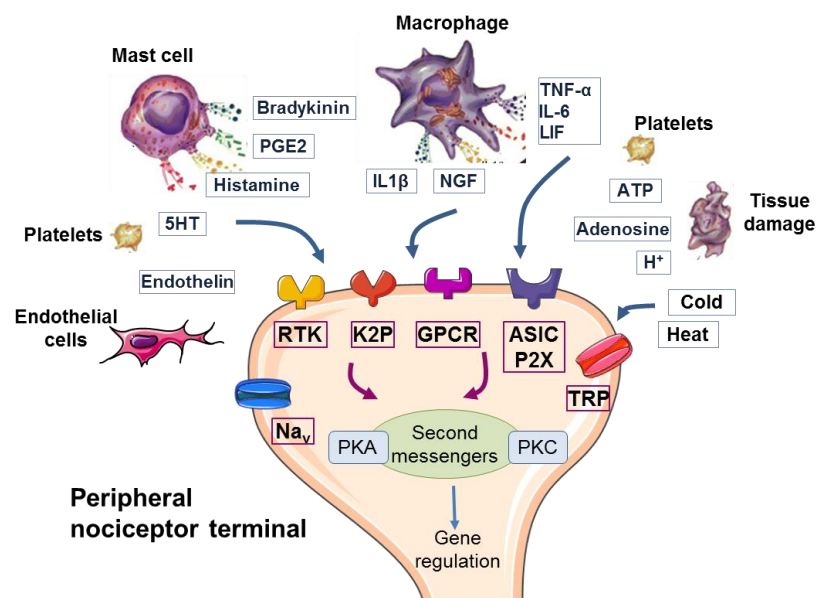


**Figure 4.** Potential mediators for nociceptor stimulation and the corresponding transducer receptors and ion channels in the peripheral free nerve ending. Adapted from reference 23.<sup>23</sup>

These mediators can act directly to alter the sensitivity of peripheral nociceptors or indirectly *via* coupling to one or more membrane bound receptors (TRP, ASICs, purinergic receptors (P2X), G-protein coupled receptors (GPCR), two-pore potassium channels ( $K_{2P}$ ), and receptor tyrosine kinase (RTK)). Binding of ligands to their corresponding receptors can initiate a cascade of events that includes activation of second-messenger systems and alteration of gene regulation.

Many, if not most, of the transducer receptors and ion channels can respond to more than one stimulus modality and are therefore named polymodal. The relative expression of transducer elements in specific subset of nociceptor sensory neurons defines their modality sensitivity. Nociceptors capable of detecting a wide range of stimulus modalities are defined as polymodal.<sup>26</sup>

### 1.4.2. Action potential generation and axonal conduction

Nociceptor stimulation at the free nerve ending and transducer activation as described above leads to local membrane depolarization, in graded response to the strength of the applied stimulus, named as the generator potential. This generator potential is passively propagated to a site with a high density of voltage-gated sodium channels ( $Na_v$ ) known as the AP initiation site. Depending on the size of the generator potential and the electrophysiological properties of the nociceptor terminal, an AP can be generated at the AP initiation site which will be subsequently propagated along the peripheral axon towards the CNS.

Voltage-gated sodium channels ( $Na_v$ s) and potassium channels are the key players for the generation and transmission of neuronal APs (Fig. 5).  $Na_v$ s are responsible for the rising phase of the AP. The role of  $Na_v$ s in nociception is described extensively in section 1.7, these being the precise pharmacological targets of this study.

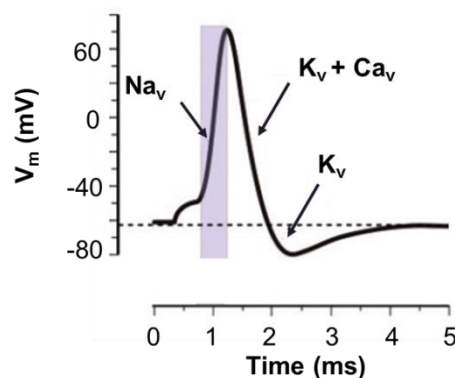


**Figure 5.** Contribution of voltage-gated ion channels in neuronal action potential firing.

Potassium channels are responsible for the falling phase of the AP leading to cell membrane repolarization and hyperpolarization, which limits AP generation and the AP firing rate. Certain potassium channels do not inactivate at resting membrane potential, thereby a steady voltage-dependent outward current is generated, responsible for the stabilization of the membrane potential in the presence of small depolarizing currents. Potassium channels are classified into four groups: voltage-gated ( $K_v$ ), two-pore ( $K_{2P}$ ), calcium-activated ( $K_{CA}$ ), and inward rectifying ( $K_{ir}$ ).<sup>41</sup> Their most prominent expression patterns in peripheral neurons, as reported in literature, are depicted in Figure 6.

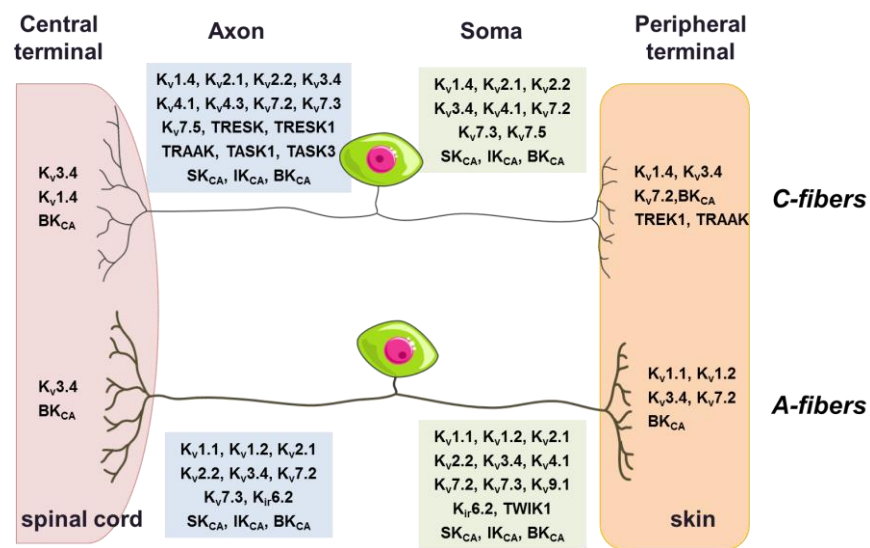


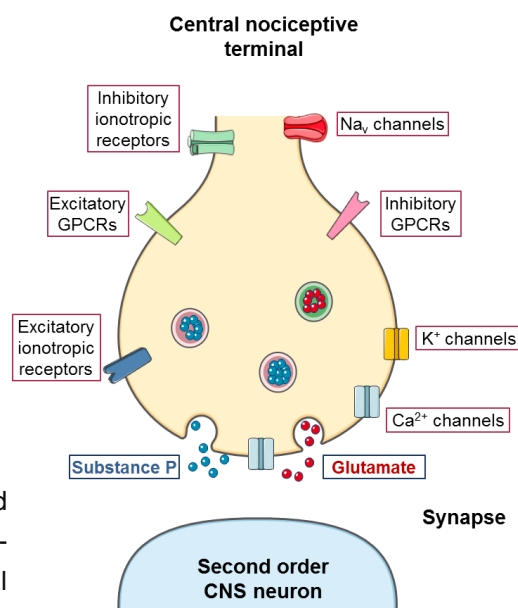
**Figure 6.** Subcellular localization of potassium channel isoforms in unmyelinated and myelinated murine DRG neurons. Adapted from reference 42.<sup>42</sup>

### 1.4.3. CNS terminal - synaptic transmission

Voltage-gated calcium channels ( $Ca_v$ ), amongst their other crucial physiological roles, are the key mediators of synaptic transmission responsible for the initial influx of calcium into the nerve terminal that is required for neurotransmitter release.<sup>43</sup> When an AP reaches the nociceptive central terminal, the membrane is depolarized, activating  $Ca_v$ s; calcium flux initiates a cascade of events leading to neurotransmitter release *via* synaptic vesicle exocytose (glutamate,<sup>44</sup> substance P<sup>45</sup>).  $Ca_v$ s are classified into two groups based on their electrophysiological properties: low-voltage (T-type) and high-voltage (L, N, P/Q and R-type) activation threshold  $Ca_v$ s.<sup>43</sup>

All  $Ca_v$  types are found in the dorsal horn, yet evidence suggests that the high-threshold N and P/Q type  $Ca_v$ s are the ones predominantly expressed on the central terminals of presynaptic afferents.<sup>46</sup> A number of excitatory ionotropic receptors as well as excitatory and inhibitory GPCRs appear to modulate (facilitate or inhibit) the neurotransmitter release (Fig. 7).

**Figure 7.** Release of neurotransmitters and neuromodulators, upon AP arrival at the pre-synaptic nociceptive terminal, in the superficial dorsal horn of the spinal cord or the brainstem. Adapted from reference 2.<sup>2</sup>



## 1.5. Nociceptor sensitization

Sensitization -increased excitability- is a characterizing and important property of nociceptors. It typically develops as a consequence of tissue insult and inflammation and can be expressed and defined as a reduction in the threshold of nociceptor activation or/and an increase in the magnitude of a response to noxious stimulation (hyperalgesia).<sup>47</sup> Naturally ineffective stimuli may become effective (allodynia) and can also be accompanied by the development of ongoing, spontaneous activity. Furthermore, nociceptor sensitization may include a decrease in the response adaptation something that is commonly observed when a certain stimulus is applied for a prolonged period of time. Peripheral nociceptor sensitization can also trigger increased excitability of central neurons in the nociceptive pathway, an event termed “central sensitization”.<sup>48</sup> This is found to contribute both in acute chemogenic but also neuropathic chronic pain.<sup>49</sup>

Mechanistically, sensitization is a reflection of changes in the behavior of voltage-gated and/or ligand-gated ion channels, resulting from the release of endogenous substances that are either synthesized or attracted at the site of tissue insult.<sup>2</sup> Endogenous substances typically contributing to nociceptor sensitization include the inflammatory mediators described in section 1.4.1. Arachidonic acids, prostanoids,<sup>50</sup> and the tumor necrosis factor- $\alpha$  (TNF- $\alpha$ ), appear to play a particularly important role in nociceptor sensitization.<sup>51</sup>

## 1.6. Pain pharmacology

Several classes of pharmacological agents are currently used for pain management. The most commonly used system for classifying analgesic drugs is the world health organization (WHO) ladder which separates them into three groups based on increasing strength of analgesic properties: non-opioid drugs, weak opioids and strong opioids (Fig. 8).

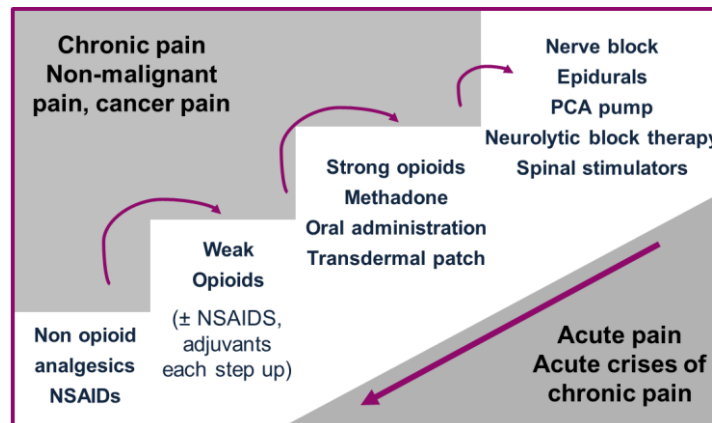


**Figure 8.** The adapted WHO analgesic ladder. The classic 1986 version of the WHO analgesic ladder, originally applied to management of cancer pain, proposed the treatment should begin with non-opioid medication, followed by the use of weak and strong opioids if pain is not controlled. The updated bidirectional version of the ladder (*vide supra*) is applicable for the treatment of both acute and chronic (including cancer) pain conditions, and it integrates a fourth step with invasive analgesic techniques.<sup>52</sup>

The most widely prescribed drugs in the world are the non-opioid analgesics NSAIDs and acetaminophen (paracetamol), valuable in the management of both acute and chronic painful and inflammatory conditions, administered both systemically and locally. NSAIDs act *via* inhibition of cyclo-oxygenase (COX), a key enzyme of the arachidonic acid metabolic pathway (Fig. 9). There are two COX isoforms, COX-1 and COX-2. COX-1 is constitutively expressed and has a homeostatic role (blood fluidity and blood pressure) and a protective role in the gastro-intestinal (GI) mucosa. COX-2 expression is inducible in inflamed tissues and leads to prostaglandin E<sub>2</sub> (PGE<sub>2</sub>) production, which is known to

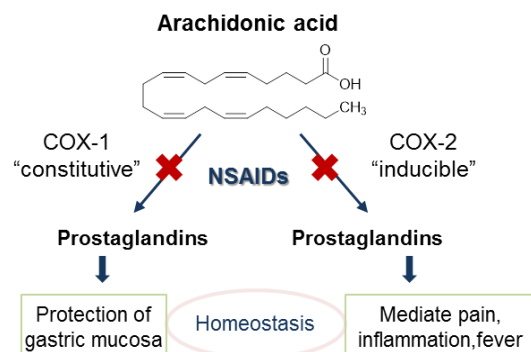


**Figure 9.** Non-selective NSAIDs and their molecular mechanism of action at the arachidonic acid metabolic pathway.

sensitize the peripheral terminals of sensory afferents. NSAIDs mediate their analgesic, antipyretic and anti-inflammatory effects via COX-2 blockade.<sup>53</sup> Early NSAIDs (such as aspirin) are non-selective for the two enzymes, and are associated with serious GI side effects; in the last decade, COX-2 selective NSAIDs (e.g. rofecoxib) have been introduced as a safer alternative in terms of GI effects,<sup>54</sup> however at the expense of cardiovascular safety.<sup>55</sup> Acetaminophen is a *para*-aminophenol derivative with analgesic and antipyretic properties like NSAIDs. Its mechanism of action is largely unknown with recent reports suggesting that the analgesic effects may be mediated *via* the serotonergic pathway.<sup>56</sup> It has no effect on peripheral PG synthetase inhibition hence lacks the useful peripheral anti-inflammatory activity of NSAIDs, however it is much better tolerated.

Opioids are the most effective treatment for patients with moderate and severe pain. Opioids bind to specific GPCRs, the opioid receptors, which are found in the periphery, at pre- and post-synaptic sites in the dorsal horn, in the brain stem, thalamus and cortex (ascending pain pathways) and in structures of the descending inhibitory pain system.<sup>57</sup> Opioid receptors are divided in three principle classes:  $\mu$ ,  $\kappa$  and  $\delta$ . Clinically used opioids (e.g. morphine, codeine, tramadol) are predominantly  $\mu$ -receptor agonists. At cellular level, opioid receptor activation inhibits  $Ca_v$ s reducing neurotransmitter release, and also certain  $K_v$ s leading to hyperpolarization of postsynaptic neurons. A third mechanism of opioid action is the activation of descending inhibitory pain transmission, *via* inhibition of  $\gamma$ -aminobutyric acid (GABA) modulatory interneurons.<sup>58</sup> Given their ubiquitous expression in the nervous system, opioid receptors influence numerous physiological functions such as reward, stress, respiration, and GI motility; opioid use is therefore associated with multiple adverse effects.

Several other pharmacological classes are used in pain management, mainly in efforts to alleviate chronic conditions such as neuropathic and cancer pain.<sup>59</sup> The antidepressants,<sup>60</sup> the anticonvulsants,<sup>61, 62</sup> the muscle relaxants and the LAs are frequently employed for pain relief; as their primary indication is other than pain relief, these are often referred to as adjuvant analgesics. The analgesic effects of these drugs are mediated, for the vast majority of cases, *via*  $Na_v$  inhibition or  $Ca_v$  modulation. Clinically used  $Na_v$  blockers are discussed in detail in section 1.7.6. Analgesic drugs with different molecular mechanisms of action are often administered together, aiming at superior efficacy and safety compared to the drugs acting alone.

The insufficient effectiveness for the treatment of several types of pain and the adverse effects associated with currently marketed analgesic drugs are the two



driving forces for the development of novel pain therapeutics.<sup>63</sup> A large number of potential pain targets have emerged in the last decade and extensive efforts are being made for exploiting those as novel strategies for treating pain.<sup>64</sup> However, their probability of success cannot be determined until these are evaluated in Phase 2 (efficacy) clinical trials.

Analgesic drugs currently in development (already in or very close to entering clinical studies) include drugs that have arisen as a result of improvements in drugs/targets that are already used clinically (e.g. variations on the theme of NSAIDs, COX-2 and opioid inhibitors), as well as chemical entities targeting novel pain targets (e.g. voltage-gated ion channels and TRP channels). The use of biologics for the treatment of pain is also being evaluated. This topic is extensively described in the Wall and Melzack's, Textbook of pain.<sup>23</sup>

## 1.7. The voltage-gated sodium channel ( $\text{Na}_v$ ) as therapeutic target for pain

Voltage gated sodium channels ( $\text{Na}_v$ s) play a key role in the neuronal network, by initiating and propagating APs rapidly throughout neurons and other electrically excitable cells.  $\text{Na}_v$ s in multicellular organisms are responsible for the communication and the coordination of higher processes, such as cognition and locomotion, where fast signal transmission is of essence. Variation in the expression of  $\text{Na}_v$ s has been linked with multiple diseases like epilepsy, cancer, multiple sclerosis, stroke and pain.<sup>65</sup> Recent clinical and experimental data validate the  $\text{Na}_v1.7$  isoform as a potential therapeutic target for pain.

### 1.7.1. Structure

$\text{Na}_v$ s are dynamic transmembrane proteins present in all eukaryotic cells, as well as certain types of prokaryotes, though their exact role in the latter is still to be understood. They consist of a principal  $\alpha$ -subunit (~260 kDa) which folds to shape the ion-conducting pore, and one or more smaller auxiliary  $\beta$ -subunits (~39 kDa) which assist in the integration of the  $\alpha$ -subunit into the membrane and modulate the biophysical properties of the channel.

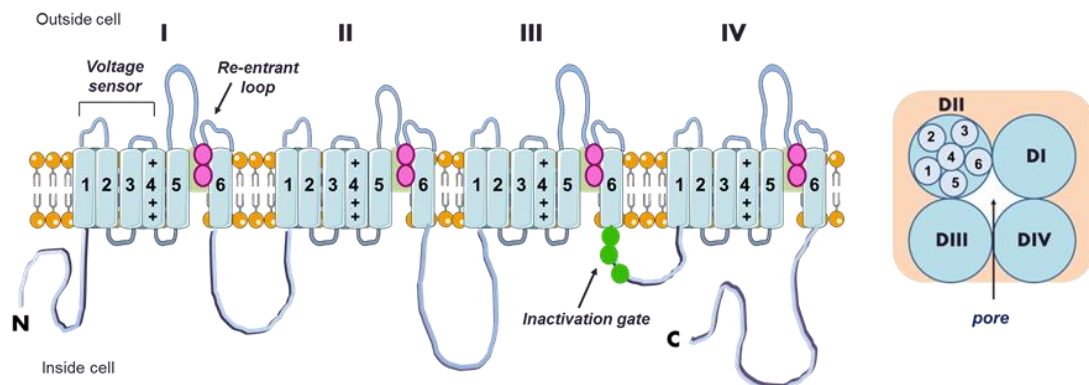


**Figure 10.** Schematic representation of the generic structure of the mammalian  $\text{Na}_v$   $\alpha$ -subunit. The  $\alpha$ -subunit is composed of four pseudo homologous domains (I to IV), each comprised by six transmembrane segments (1 to 6) presented as cylinders. The S4 segments serve as the voltage sensor (+). Pink circles indicate the positions of amino acids important for ion conductance and selectivity. Green circles indicate the positions of hydrophobic amino acids part of the inactivation gate, which is thought to fold into and block the ion-conducting pore. Side view (left) and top view (right). Adapted from references 66, 67.<sup>66, 67</sup>

The  $\alpha$ -subunit comprises of four pseudo homologous domains (I-IV) sharing approximately 90% sequence identity. Each of the four domains corresponds to six segments (S1-S6) which traverse the membrane in the form of  $\alpha$ -helices (Fig. 10). The S1-S4 segments comprise the voltage-sensing region whereas S5-S6 segments and the re-entrant loop, consist the pore forming region. Residues in the S5-S6 unit determine the channel's selectivity and ion permeation properties.<sup>66, 68, 69</sup>

The mammalian  $\text{Na}_v$  channel, being a large amphipathic membrane, is exceptionally difficult to crystalize therefore no direct three-dimensional (3D) structural information is available to date. The molecular model currently available for the  $\alpha$ -subunit relies largely on information provided by the crystal structure of the structurally related  $\text{K}_v$  channel, by studies using mammalian  $\text{Na}_v$  chimeras and point mutation experiments. The crystal structure of a bacterial voltage-gated sodium channel (NaChBac) from *Arcobacter butzleri*, a homotetramer with similar pharmacological profile to the mammalian  $\text{Na}_v$  channel, was solved in 2011 (2.7 Å resolution) with the channel being in a pre-open conformation.<sup>70</sup> Later work revealed structures of the channel in two inactivated states.<sup>71</sup> Since then, two additional NaChBacs crystal structures became available, altogether providing significant new information about the architecture of the pore, the selectivity filter, and probable interaction sites with channel modulators.<sup>72, 73</sup>

### 1.7.2. Function

The opening and closing of  $\text{Na}_v$ s requires their transit between different conformational states depending on the voltage gradient across the membrane, a model first proposed by Hodgins and Huxley in 1952 termed as voltage-gating.<sup>74</sup> At resting membrane potential ( $\sim -70$  mV), the channels exist in a resting, closed, non-conducting state (Fig. 11). In response to an electrical stimulus that depolarizes sufficiently the membrane ( $> -50$  mV), positively charged residues in the S4 voltage-sensor region (in particular arginines), induce changes to the tertiary structure of the protein, allowing the opening of the pore and the selective passage of sodium ions inside the cell; this constitutes the upstroke of the AP. On sustained depolarization ( $\sim +35$  mV) the channel enters an inactivated closed state, which leaves the channel refractory, i.e, unable to open again for a period of time. Two types of inactivation processes exist, the "classical" fast inactivation (in the ms range) and a slow inactivation that can last much longer (up to seconds).<sup>75</sup> The two types of inactivation have different underlying mechanisms, located in different parts of the channel and consequently respond differently to bio/chemical agents. Subsequent to

inactivation and membrane depolarization, the channel re-enters the closed resting state. Changes in the activation/inactivation properties of the channel have profound effects on the onset, frequency and duration of APs and hence on neuronal signaling.

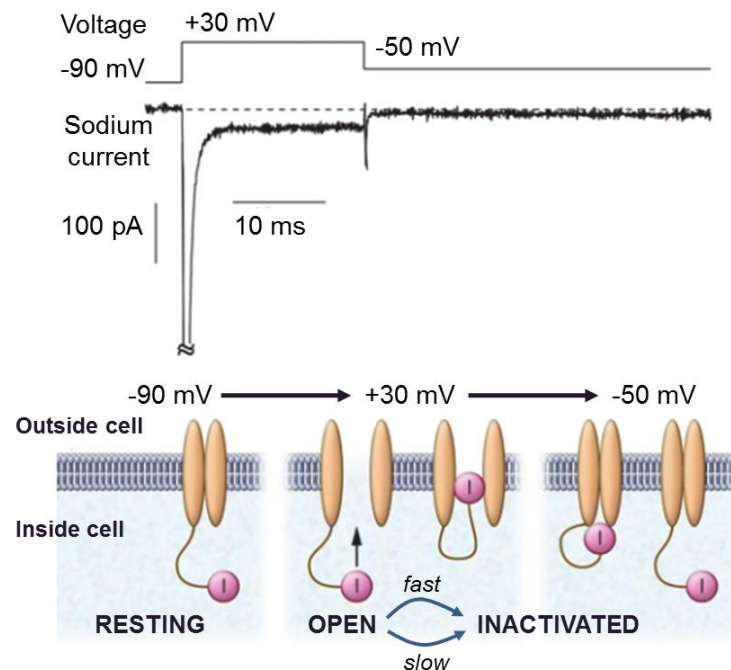


**Figure 11.** Classic Na<sub>v</sub> channel current profile. When the membrane is at resting potential, -90 mV, the channel is at its closed (resting state). Upon depolarization (shift of membrane potential to +30 mV), the channel becomes activated and sodium ions enter the cell through the Na<sub>v</sub> channel pore. Within a few ms the inactivation loop “enters” the pore and the channel inactivates. When the membrane is repolarized to -50 mV, the channel partially recovers from inactivation, yet no current flows. Upon further repolarization to -90 mV the channel returns to its resting (closed) state. Adapted from reference 76.<sup>76</sup>

### 1.7.3. Na<sub>v</sub> subtypes, tissue distribution, and channelopathies

Since the cloning of the first  $\alpha$ -subunit in 1984, ten mammalian Na<sub>v</sub> subtypes have been identified, sharing 50% sequence identity within their transmembrane and extracellular domains.<sup>77</sup> Na<sub>v</sub> isoforms are conventionally classified in two groups: those that are sensitive to block by the pufferfish toxin tetrodotoxin (TTX), exhibiting nanomolar potencies (Na<sub>v</sub>1.1, 1.2, 1.3, 1.4, 1.6, 1.7), and those that are resistant (Na<sub>v</sub>1.5, 1.8, 1.9). The ten Na<sub>v</sub> isoforms vary in terms of their pharmacology, their biophysical properties and their tissue distributions (Table 2).

**Table 2.** Cloned Na<sub>v</sub>  $\alpha$ -subunit genes, their major expression sites and the effect of their mutation.<sup>78 79</sup>

Subunit	Gene	TTX sensitivity	Major expression	Effects of mutation (human)
Na <sub>v</sub> 1.1	SCN1A	✓	CNS, PNS	epilepsy, migraine, autism, episodic ataxia
Na <sub>v</sub> 1.2	SCN2A	✓	CNS, PNS	epilepsy, autism
Na <sub>v</sub> 1.3	SCN3A	✓	CNS, PNS	epilepsy
Na <sub>v</sub> 1.4	SCN4A	✓	skeletal muscle	hyperkalaemic periodic paralysis, paramyotonia congenita
Na <sub>v</sub> 1.5	SCN5A	×	cardiac muscle	brugada syndrome, long QT syndrome 3, atrial fibrillation
Na <sub>v</sub> 1.6	SCN8A	✓	CNS, PNS, smooth muscle	mental retardation, pancerebellar atrophy, ataxia, infantile experimental encephalopathy
Na <sub>v</sub> 1.7	SCN9A	✓	PNS	congenital indifference in pain, erythromalgia, paroxysmal extreme pain disorder, anosmia
Na <sub>v</sub> 1.8	SCN10A	×	PNS, heart	idiopathic painful small-fiber neuropathy.
Na <sub>v</sub> 1.9	SNC11A	×	PNS	painful peripheral neuropathy
Na <sub>x</sub>	SNC6/7A	non functional	circumventricular organs	Unknown

#### 1.7.4. Localization of Na<sub>v</sub> isoforms in nociceptors and their biophysical characteristics

Each Na<sub>v</sub> channel subtype has distinct electrophysiological properties, exhibiting specific voltage thresholds and transition kinetics for channel opening, inactivation, and recovery from inactivation, that determine the AP firing pattern of the cell type in which they are expressed. The precise anatomical distribution of Na<sub>v</sub> isoforms in sensory afferents is far from clear; channels are differentially distributed within a given afferent and between subpopulations of afferents.<sup>80</sup> Out of the ten cloned Na<sub>v</sub> isoforms, five have been linked to nociceptor responses: Na<sub>v</sub>1.3, Na<sub>v</sub>1.6, Na<sub>v</sub>1.7, Na<sub>v</sub>1.8, and Na<sub>v</sub>1.9. Out of these, isoforms Na<sub>v</sub>1.7, Na<sub>v</sub>1.8, and Na<sub>v</sub>1.9, are almost exclusively expressed in nociceptors and hence their selective blockade is currently one of the most prominent novel strategies for the development of new analgesic drugs. The localization of Na<sub>v</sub> isoforms in nociceptors, as reported in literature, is discussed below alongside the isoforms' salient characteristics.

The Na<sub>v</sub>1.3 isoform is highly expressed in developing neurons, yet is not detectable in the adult nervous system. It has however been shown to be upregulated in DRG neurons following peripheral nerve injury.<sup>81</sup> It exhibits fast activation and inactivation kinetics, characteristic of TTX-sensitive (TTX-S) channels, and recovers rapidly from inactivation thereby supporting repetitive neuronal firing. It is known to mediate a persistent current ( $I_{NaP}$ ), a steady-state sodium current that is involved in AP initiation at membrane voltages near the threshold of firing.<sup>82</sup> It responds to small depolarizations, close to the resting membrane potential, thus amplifying small current inputs.<sup>83</sup>

The Na<sub>v</sub>1.6 isoform also exhibits fast kinetics and recovers rapidly from inactivation therefore sustaining high firing frequencies. It has the unique property of mediating resurgent currents ( $I_{NaR}$ ), currents that occur during membrane repolarization due to unusual channel reopening, also contributing to high-frequency firing. Na<sub>v</sub>1.6 is the predominant Na<sub>v</sub> isoform in the nodes of Ranvier in both PNS and CNS myelinated neurons, supporting saltatory conduction. It has recently been demonstrated to also be a significant component of non-myelinated nociceptive neurons, contributing to AP propagation.<sup>84</sup>

The Na<sub>v</sub>1.7 isoform is present along the entire trajectory of nociceptive DRG neurons, highly expressed in the cell body as well as in the peripheral and centrally directed axons and terminals.<sup>85</sup> It exhibits fast kinetics but slow recovery from inactivation thus preventing high frequency firing. This is consistent with studies showing that the maximal firing rate of C-fibers is significantly lower than that of A-

fibers. It exhibits slow onset of closed state-inactivation (negative membrane potential), which leads to the generation of large currents during slow ramp depolarizations. Overall the biophysical properties of Na<sub>v</sub>1.7 channels closely resemble those of the predominant TTX-S current in small diameter DRG sensory neurons. Na<sub>v</sub>1.7 channels have an important role both in setting the threshold for the generation of APs but also in AP conduction.<sup>86</sup>

Na<sub>v</sub>1.8 is one of the two isoforms generating the TTX-resistant (TTX-R) current recorded from DRG nociceptors, the other one being Na<sub>v</sub>1.9. Na<sub>v</sub>1.8 currents exhibit ~10-fold slower rates of activation and fast inactivation than TTX-S currents and their voltage-dependence of activation and inactivation is typically 30-40 mV more depolarized. Na<sub>v</sub>1.8 channels are therefore likely to be activated subsequent to Na<sub>v</sub>1.7 in response to stimuli, and are hence less likely to contribute to setting the threshold for the generation of action potentials. Na<sub>v</sub>1.8 produces most of the inward current responsible for the AP upstroke and supports repetitive firing in depolarized DRG neurons.<sup>87</sup> Na<sub>v</sub>1.8 is predominately localized in the cell body and the peripheral terminal of nociceptors.<sup>88</sup>

Na<sub>v</sub>1.9, the second neuronal TTX-R channel, has been cloned almost 20 years ago yet it has been proven extremely difficult to express and study in heterologous expression systems. Na<sub>v</sub>1.9 is distributed throughout the nociceptive afferents. It activates at hyperpolarized potentials close to the resting membrane potential (-60 to -70 mV). It does not contribute to the action potential upstroke but rather depolarizes the neurons and prolongs and enhances small depolarizations, thus setting the resting membrane potential and increasing excitability.<sup>83, 89, 90</sup>

Changes in the biophysical properties or the expression levels of these channels have been associated with a number of pathological pain conditions. Evidence for the contribution of each of the above isoforms in pain is provided below.

### 1.7.5. Implication of Na<sub>v</sub> isoforms in pain

“A Holy Grail of pain research has been the discovery of ‘peripheral’ sodium channels.”

*Prof. Stephen Waxman*

Consideration of Na<sub>v</sub>1.3 as a potential pain target was triggered by the demonstration that the channel is undetectable in the healthy adult rodent nervous system, yet it is upregulated in DRG neurons following peripheral nerve injury and is highly expressed in secondary and third order CNS neurons of the pain signaling pathway.<sup>91</sup> Studies using antisense Na<sub>v</sub>1.3 knockout models gave controversial results: whilst a certain construct led to amelioration of pain behavior in an animal model of peripheral nerve injury,<sup>91</sup> the use of a different construct showed no pain attenuation.<sup>92</sup> The use of a different, virus mediated, knockout strategy in a rodent neuropathic model led to pain behavior improvement.<sup>93</sup> The development of Na<sub>v</sub>1.3 selective blockers is important from a scientific point of view, for evaluating the isoform’s contribution in pain however it is not as yet clear whether these will be clinically useful.<sup>94</sup>

Despite the low Na<sub>v</sub>1.6 abundance in nociceptors, recent studies pinpoint this isoform as the underlying cause of multiple painful conditions. It has been shown to mediate chemotherapy induced pain,<sup>95</sup> and RNA-mediated knockout of the channel *in vivo* has been demonstrated to prevent localized inflammation of the lumbar DRG.<sup>96</sup> Furthermore, local knockdown of Na<sub>v</sub>1.6 in a rodent model of neuropathic pain was found to reduce pain behaviors, neuronal excitability and sympathetic sprouting.<sup>97</sup> These studies suggest that Na<sub>v</sub>1.6 may have a value as a therapeutic target for pain, yet its abundant expression in large myelinated fibers may compromise the therapeutic window.

A large body of preclinical data identify Na<sub>v</sub>1.7 as the major isoform implicated in the pathophysiology of pain.<sup>86</sup> Brief exposure of rat pheochromocytoma cells to an inflammatory stimulus (nerve growth factor), leads to increased expression levels of Na<sub>v</sub>1.7.<sup>98</sup> Global Na<sub>v</sub>1.7 gene deletion in mice is lethal, yet nociceptor-specific Na<sub>v</sub>1.7 gene deletion leads to viable mice, exhibiting reduced or completely abolished responses to inflammatory induced pain and thermal hyperalgesia induced by burn injury.<sup>99, 100</sup>

Recent genetic studies and functional profiling of mutant channels in individuals with rare hereditary pain disorders has validated the Na<sub>v</sub>1.7 isoform as a target for pain therapy and led to the big urge by the scientific community and the



pharmaceutical industries for the discovery of Na<sub>v</sub>1.7 selective inhibitors as the next generation pain therapeutics.<sup>101</sup> Erythralgia (IEM) is a rare autosomal dominant disorder in which the patient experiences episodes of very painful burning sensation and red hot skin, usually in the extremities. IEM is attributed to a gain-of-function mutation which hyperpolarizes the Na<sub>v</sub>1.7 activation threshold, increasing the response of the channel to depolarizing stimuli.<sup>102</sup> Paroxysmal extreme pain disorder (PEPD) is another Na<sub>v</sub>1.7 gain-of-function attributed hereditary disease, characterized by episodes of burning pain in the rectum, ocular and mandibular regions. PEPD has been linked to slow channel inactivation (hundreds of ms) in some cases, to complete failure of inactivation in others, and in some to more negative activation thresholds.<sup>103</sup> On the other end of the spectrum, Na<sub>v</sub>1.7 loss-of-function mutations lead to disorders where individuals are unable to perceive or interpret the intensity of painful stimuli. Congenital indifference to pain (CIP) is one such autosomal recessive disorder result of non-sense or frame-shift mutations in the SCN9A gene which make the Na<sub>v</sub>1.7 channel completely dysfunctional and unable to pass a current.<sup>104</sup>

Despite the compelling evidence for Na<sub>v</sub>1.7's crucial role in acute inflammatory and chronic pain conditions associated with channelopathies, it is still not clear whether the isoform is necessary for the presentation of other forms of pain e.g. neuropathic pain. Nociceptor specific deletion of Na<sub>v</sub>1.7, for example, revealed the isoform is not implicated in oxaliplatin-induced neuropathic pain.<sup>105, 106</sup> On a similar note, a different study showed that spinal nerve ligation (SNL)-induced pain can still be perceived after Na<sub>v</sub>1.7 deletion from sensory neurons.<sup>106</sup> The above data suggest that Na<sub>v</sub>1.7 inhibition could potentially provide effective analgesia clinically, for a number of painful conditions, yet given the numerous Na<sub>v</sub> isoforms involved in the pathophysiology of pain, Na<sub>v</sub>1.7 selective blockers are unlikely to be the one-treats-all pain medicines that many seem to propose.

Na<sub>v</sub>1.8 is the second Na<sub>v</sub> isoform that received much attention as a potential pain target. The expression and biophysical properties of Na<sub>v</sub>1.8 channels have been shown to be largely modulated by nociceptive inputs. Intraplantar administration of complete Freund's adjuvant,<sup>107</sup> or carrageenan,<sup>108</sup> resulted in increased Na<sub>v</sub>1.8 expression in the rat digital nerve and DRG respectively. Additional evidence for the role of Na<sub>v</sub>1.8 in normal pain function and inflammatory pain is derived from knockout<sup>109</sup> and knockdown studies in rodents using small-molecule blockers<sup>110</sup> and antisense oligonucleotides.<sup>111</sup> The recent functional profiling of patients with small fiber neuropathies, revealed gain-of-function mutations in Na<sub>v</sub>1.8 which produced hyper-excitability and inappropriate

spontaneous firing in DRG neurons; the study provided a strong link between  $\text{Na}_v1.8$  and painful neuropathy.<sup>112</sup>

The contribution of  $\text{Na}_v1.8$  currents to neuropathic pain conditions however, like for  $\text{Na}_v1.7$ , remains controversial. Antisense mediated knockdown of  $\text{Na}_v1.8$  was found to reverse neuropathic pain behavior after L5/L6 SNL, and direct L5/L6 SNL nerve injury led to immunocytochemical and electrophysiological changes in  $\text{Na}_v1.8$ .<sup>113</sup> On the contrary studies using  $\text{Na}_v1.8$ -null mice have concluded that  $\text{Na}_v1.8$  is not involved in neuropathic pain.<sup>105</sup> In one study  $\text{Na}_v1.8$  mRNA, protein and current were found to be substantially decreased in axotomized DRG neurons.<sup>114</sup>

The role of the  $\text{Na}_v1.9$  isoform in the pathophysiology of pain has been less explored mainly due to difficulties in expressing and studying the channel in heterologous expression systems. Inflammatory mediators have been shown to cause an increase in  $\text{Na}_v1.9$  mediated current and  $\text{Na}_v1.9$  knockout mice display attenuated responses in inflammatory pain.<sup>115, 116</sup> In addition,  $\text{Na}_v1.9$  has been demonstrated to be implicated in the perception of noxious cold-induced pain with  $\text{Na}_v1.9$  null mice and knockdown rats exhibiting increased cold pain thresholds.<sup>117</sup> Strong evidence for the role of  $\text{Na}_v1.9$  in neuropathic pain comes from the recent discovery that  $\text{Na}_v1.9$  gain-of-function mutations cause painful peripheral neuropathy by increasing the resting membrane potential and reducing in the current threshold required to trigger an AP.<sup>118</sup>

### **1.7.6. $\text{Na}_v$ blockers as pain relief medicines**

$\text{Na}_v$  blockers have been used in pain medicine for over a century now. Drugs like cocaine and procaine have been used for analgesia long before their actual pharmacological properties were defined; whilst widely known for their serotonin-norepinephrine-dopamine reuptake inhibition properties, they also act as  $\text{Na}_v$  blockers.<sup>119</sup> Over the years, more specific  $\text{Na}_v$  blockers have dominated the field of pain therapeutics. The local anesthetics (e.g. lidocaine, bupivacaine and ropivacaine) and the anticonvulsants (e.g. carbamazepine, phenytoin, lamotrigine), are nowadays regularly used for the treatment of several acute and chronic pain conditions.

Both LAs and the anticonvulsants are low potency  $\text{Na}_v$  blockers, that exhibit no particular selectivity between the different  $\text{Na}_v$  isoforms yet they are reasonably tolerated for use in certain clinical settings. They share overlapping binding sites localized at the inner vestibule of the pore on the S6 helix of the  $\text{Na}_v$  domain IV (Fig.

12), yet they exhibit different pharmacological properties.<sup>120, 121</sup> The key for their relatively safe therapeutic profile and distinct pharmacology lies in their preferential binding to specific Na<sub>v</sub> conformational states, with different kinetics, altering the channels' biophysical properties.

As described above, Na<sub>v</sub>s transit between different conformational states in response to changes in the membrane potential (resting, activated, inactivated). Drugs that bind to Na<sub>v</sub> with affinity independent to the conformational state, or to a site that is accessible in any channel conformation are known as tonic blockers. State-dependent blockers on the other hand bind preferentially to one or more conformational states.

The LAs and the anticonvulsants are state-dependent blockers exhibiting preferential binding to the inactivated state; this is either due to higher affinity of the blocker for this particular state (anticonvulsants) or to higher accessibility of the binding site when at this state (LAs). As a consequence, the channel is stabilized at a non-conducting state which slows down its repriming time (return to the resting state). Hyper-excitability in chronic pain diseases is characterized by neuronal membrane depolarization (that increases with the frequency of firing), which means more channels enter the inactivated state; in effect, state-dependent blockers lead to a greater block in such diseased rather than normal firing neurons.

The functional consequences of state-dependent binding are the voltage-dependent block (amount of block versus voltage) and the use-dependent block (amount of block versus frequency of stimulation/firing). Anticonvulsants exhibit high voltage-dependence, but only moderate use-dependence due to their fast drug dissociation after repolarization. Therefore, anticonvulsants are best at inhibiting high-frequency firing, allowing normal action potential firing in the presence of the drug. LAs on the other hand, dissociate with a slower time constant than they associate to the binding site leading to accumulation of inhibition, making potency dependent on the opening frequency (use-dependence). In effect, LAs tend to be more effective in blocking low-frequency firing.

The development of state-dependent Na<sub>v</sub> blockers remains to date one of the most pursued strategies for the discovery of novel analgesic drugs.

A more recent strategy, currently pursued by numerous pharmaceutical companies, is the development of subtype-selective blockers specifically targeting the Na<sub>v</sub> isoforms of the periphery (Na<sub>v</sub>1.3, Na<sub>v</sub>1.7, Na<sub>v</sub>1.8, and Na<sub>v</sub>1.9).

A combination of site-directed mutagenesis, binding and electrophysiological studies have identified at least seven distinct binding sites in addition to the LA binding site, located in and around the pore region of the  $\alpha$ -subunit (Fig. 12).<sup>78</sup>

These were identified using toxins and alkaloids as pharmacological probes, several of which exhibit high  $\text{Na}_v$  isoform selectivity. The clinical usefulness of such toxins is often limited by their large molecular weight however they are invaluable pharmacological tools, used as therapeutic leads in many drug discovery programs.

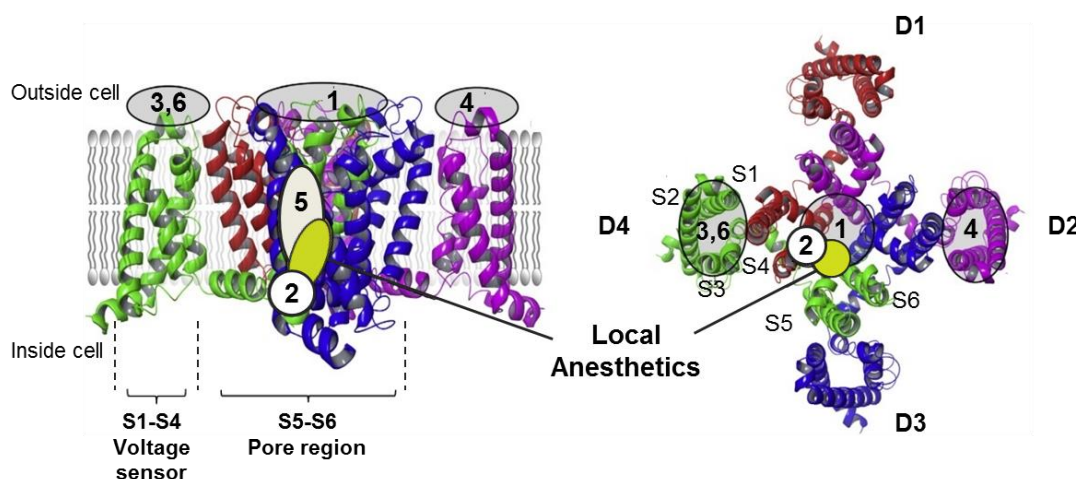


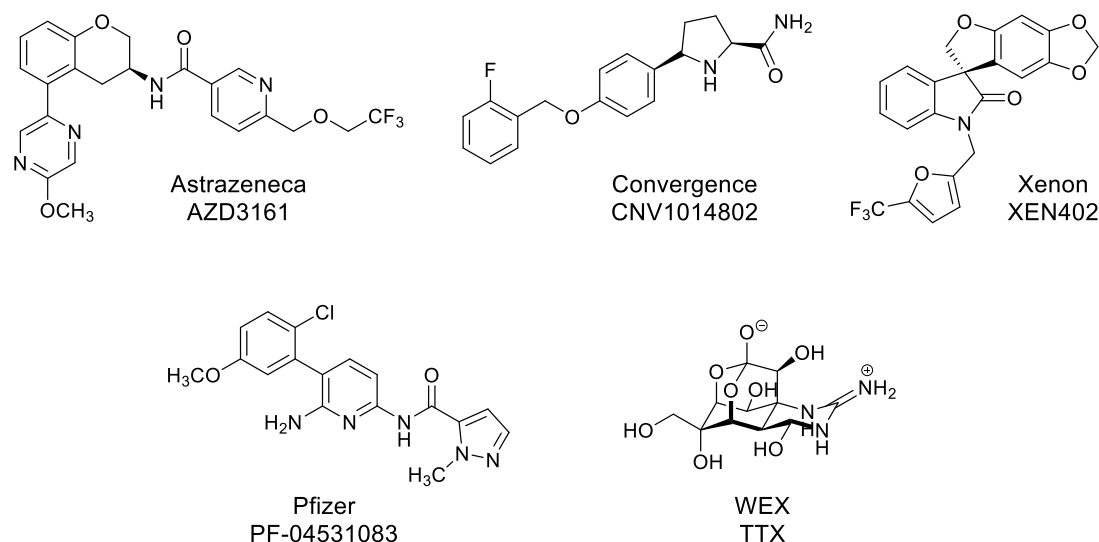
**Figure 12.**  $\text{Na}_v$  channel homology model illustrating the postulated toxin binding sites (1-6) and the LAs binding site; side view (left) and top view (right). (1) TTX (2) batrachotoxin (BTX) (3) scorpion  $\alpha$ -toxin (4) scorpion  $\beta$ -toxin (5) brevetoxins (6)  $\delta$ -conotoxin (7) pyrethroids.<sup>122</sup>

Several studies examining the analgesic properties of toxins that selectively block peripheral  $\text{Na}_v$  isoforms have been published. ProTx II, a selective  $\text{Na}_v1.7$  blocker derived from the tarantula venom (site 4), completely blocks AP propagation in nociceptors at concentrations that have little effect on other sensory fibers when applied to desheathed cutaneous nerves.<sup>123</sup> Sadly, it has no activity when applied to intact nerves as it is connective-tissue impermeant. More recently,  $\mu$ -SLPTX-Ssm6a, another  $\text{Na}_v1.7$  selective inhibitor isolated from centipede venom, was found more potent than morphine in a rodent model of chemical-induced pain and it was equipotent with morphine in rodent models of thermal and acid-induced pain.<sup>124</sup>

In the past decade, a very large number of studies/patents have been published reporting small molecule  $\text{Na}_v1.7$  and  $\text{Na}_v1.8$  specific inhibitors, with efficacy in animal models of pain; however, in the vast majority, the compounds' activity against other  $\text{Na}_v$  isoforms is not being reported in a native neuronal environment and the results should therefore be interpreted with care. Table 3 describes compounds targeting  $\text{Na}_v$ s for pain relief currently in clinical development.

**Table 3.** Na<sub>v</sub> channel modulators that have reached clinical development for the treatment of pain.<sup>122</sup>

Compound	Company	Pharmacology	Phase	Therapeutic indication
AZD3161	AstraZeneca	Na <sub>v</sub> 1.7	I	Neuropathic/inflammatory pain (IV, intradermal)
CNV1014802	Convergence	Na <sub>v</sub> 1.7	II	Neuropathic pain, Trigeminal neuralgia (oral)
DSP-2230	Dainippon Sumitoto	Na <sub>v</sub> 1.7/1.8	I	Neuropathic pain (oral)
NKTR-171	Nektar	Broad Na <sub>v</sub>	I	Neuropathic pain (oral)
PF-04531083	Pfizer	Na <sub>v</sub> 1.8	I	Neuropathic/inflammatory pain (oral)
PF-05089771	Pfizer	Na <sub>v</sub> 1.7	II	Neuropathic/inflammatory pain erythralgia (oral)
TTX	WEX	TTX-S Na <sub>v</sub>	III	Neuropathic/inflammatory cancer pain (IV)
XEN402	Xenon/Teva	Na <sub>v</sub> 1.7	II	Neuropathic/inflammatory pain erythralgia (topical)
XEN403	Xenon	Na <sub>v</sub> 1.7	I	Neuropathic/inflammatory pain erythralgia (oral)

**Figure 13.** Na<sub>v</sub> channel modulators in clinical development for the treatment of pain.

A third, currently less exploited strategy, for improving the side effect profile of non-selective  $\text{Na}_v$  inhibitors, is to restrict their action to the desired target tissue i.e. in the periphery, aiming to increase tolerability by reducing action on the CNS.<sup>125</sup> Two different approaches have been explored to date: (a) a passive approach where compounds are prevented from penetrating the blood-brain barrier and (b) a more active approach where compounds are specifically delivered to nociceptors.

One example of the first approach is the development of BZP;<sup>126</sup> BZP is a small molecule  $\text{Na}_v1.7$  blocker developed by Merck, producing substantial reversal of inflammatory hyperalgesia and mechanical allodynia on rat models of inflammatory and neuropathic pain, comparable to that of clinically used drugs; due to its poor brain-penetrance it confers fewer sedative, and motor-coordination impairments. Limitations of this approach remain the plausible adverse effects from cross activity at cardiac  $\text{Na}_v$ s and the unsuited use of such compounds in conditions which compromise the blood-brain or the blood-spinal cord barrier.<sup>127</sup>

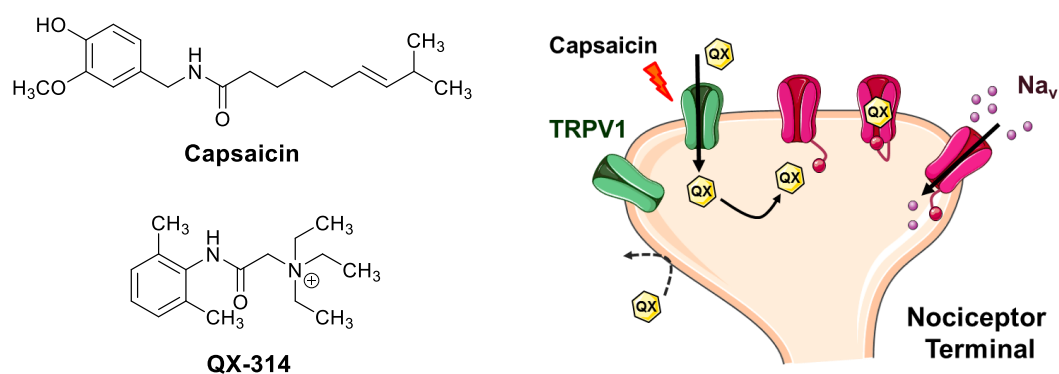


**Figure 14.** Structures of the TRPV1 agonist, capsaicin, and the tertiary lidocaine derivative, QX-313 (left). TRPV1 agonist– $\text{Na}_v$  antagonist effects at nociceptors. Activation of TRPV1 by capsaicin allows QX314 internalization and binding to the  $\text{Na}_v$  LA site blocking  $\text{Na}_v$  current passage (right).<sup>128</sup>

The concept of the second approach is well described by the cell-specific targeting of QX-314, a quaternary lidocaine derivative, into nociceptors.<sup>129</sup> QX-314 is a charged molecule, hence cannot access its intracellular LA binding site by passive diffusion. Its neuronal internalization has been made possible *via* TRPV1 receptors which upon prolonged activation and pore dilation allow the passage of large cations such as QX-314 into the cell. TRPV1 activation allows QX-314 to reach its active site and mediate its  $\text{Na}_v$  blocking effects (Fig. 14). Indeed, co-administration of a TRPV1 agonist (e.g. capsaicin, lidocaine) and QX-314 in rodents has been shown to produce long lasting inhibition to painful mechanical and thermal stimuli. TRPV1 is

selectively expressed in nociceptive neurons therefore QX-314 pain-signalling blockade proceeds without the motor deficits normally associated with the use of LA drugs.

Unfortunately, several limitations have been associated with the development of TRPV1 agonists- $\text{Na}_v$  antagonists as pain therapeutics. Intrathecal application of QX-314 caused serious irritation and death in mice,<sup>130</sup> something not observed after subcutaneous, or perineural administration even at high doses. Systematically, it is twice as toxic as lidocaine.<sup>131</sup> In addition, the initial activation of TRPV1 is accompanied by an intense pain sensation which lasts until the onset of the  $\text{Na}_v$ -mediated analgesic effect. It therefore does not appear as the most appealing strategy for producing analgesia however, it provides proof-of-concept evidence for the significant therapeutic advantages of selective nociceptor blockade.

## 1.8. Previous studies related to this work: Iminodihydroquinolines as $\text{Na}_v$ blockers for pain therapy

The small molecule iminodihydroquinoline WIN17317-3 (**1**, Fig. 15) was the first, high affinity, tissue selective  $\text{Na}_v$  inhibitor to be reported.<sup>132</sup> The compound was initially described as a selective  $\text{K}_v1.3$  and  $\text{K}_v1.4$  blocker,<sup>133</sup> when however, in a subsequent study a radiolabeled analogue of WIN17317-3 ( $[^3\text{H}]$ WIN17317-3, Merck) was employed to probe

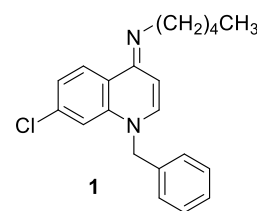


**Figure 15.** Chemical structure of WIN17317-3.

neuronal  $\text{K}_v1$  channels in rat brain synaptic membranes, its binding interactions were found insensitive to any of the well-characterized potassium channel ligands. Instead,  $[^3\text{H}]$ WIN17317-3 binding was blocked by a number of  $\text{Na}_v$  modulators, such as the neurotoxins (TTX, BTX), the LAs (lidocaine) and the antiarrhythmics; it was found to bind saturably and reversibly to a single neuronal binding site ( $K_d$   $2.2 \pm 0.3$  nM;  $B_{\text{max}}$   $5.4 \pm 0.2$  pmol/mg of protein) that corresponded pharmacologically to the  $\text{Na}_v1.2$ . Importantly, autoradiography of rat brain sections incubated with  $[^3\text{H}]$ WIN17317-3 revealed high specific binding to sites that correspond with the known distribution of  $\text{Na}_v$ s in the CNS (Fig. 16). Similar experiments, in rabbit skeletal muscle microsomal membranes revealed that WIN17317-3 also interacts with skeletal muscle  $\text{Na}_v$ s *via* an analogous allosteric interaction, but interacts much more weakly with the cardiac  $\text{Na}_v$ s. This suggested that WIN17317-3 possesses selectivity for neuronal and skeletal muscle  $\text{Na}_v$  isoforms over isoforms expressed in the heart. WIN17317-3 was found to block the binding of  $[^3\text{H}]$ BTX-B *via* an allosteric mechanism of action.

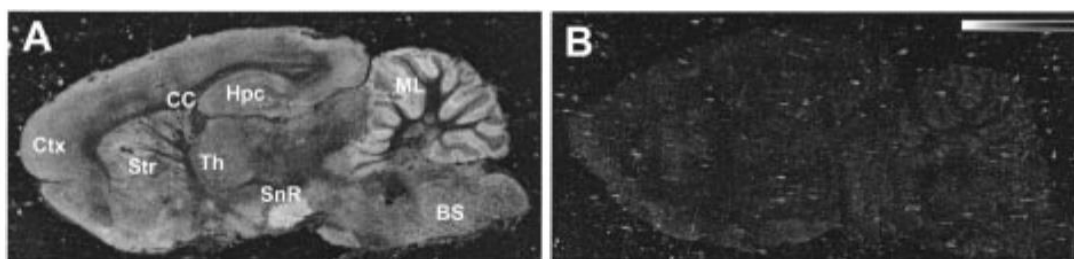
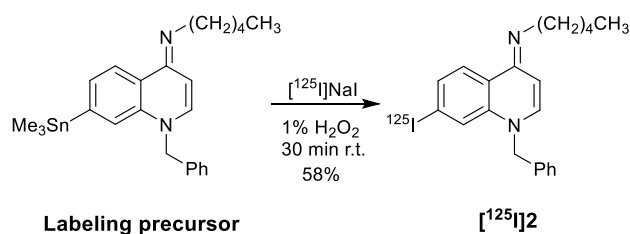


**Figure 16.** Autoradiographic localization of  $[^3\text{H}]$ WIN17317-3 binding sites in rat brain. Brain sections were incubated with the tracer (2-3 nM) in the absence (A) and the presence (B) of non-radiolabeled WIN17317-3.<sup>132</sup>



In the following years, Merck laboratories have evaluated a diverse spectrum of chemical structures as  $\text{Na}_v$  inhibitors for various clinical indications, yet no further studies were reported exploiting the structural class of iminodihydroquinolines.<sup>134, 135</sup> The favorable physicochemical properties of WIN17317-3, and its ability to depict the  $\text{Na}_v$  distribution *in vitro* led our group to pursue a  $^{125}\text{I}$ -labeled iminodihydroquinoline, **2**, as tracer for imaging  $\text{Na}_v$ s in the brain.<sup>3</sup> *In vivo* imaging of  $\text{Na}_v$ s can potentially provide insights to the activation of neuronal pathways and aid the diagnosis of a number of neurological diseases.



**Scheme 1.** Radiosynthesis of  $^{125}\text{I}$ 2.<sup>3</sup>

To evaluate the suitability of  $^{125}\text{I}$ 2 for imaging  $\text{Na}_v$ s *in vivo*, its pharmacokinetic profile and tissue distribution were examined after iv administration in mice (Fig. 17). Unfortunately, both biodistribution studies and whole body SPECT/CT imaging showed very low brain uptake ( $0.48 \pm 0.04\%$  ID/g) with no sign of retention, and quick clearance from the liver and kidneys, paralleled by an increased uptake in the intestines, consistent with hepatobiliary excretion. The  $^{125}\text{I}$ -labeled tracer also suffered from rapid metabolism, with less than 5.5% of the intact tracer remaining in the circulation 30 minutes post injection, with the rest of the activity observed as a highly polar metabolite. The results suggested that iminodihydroquinolines are poorly suited for tracer development.

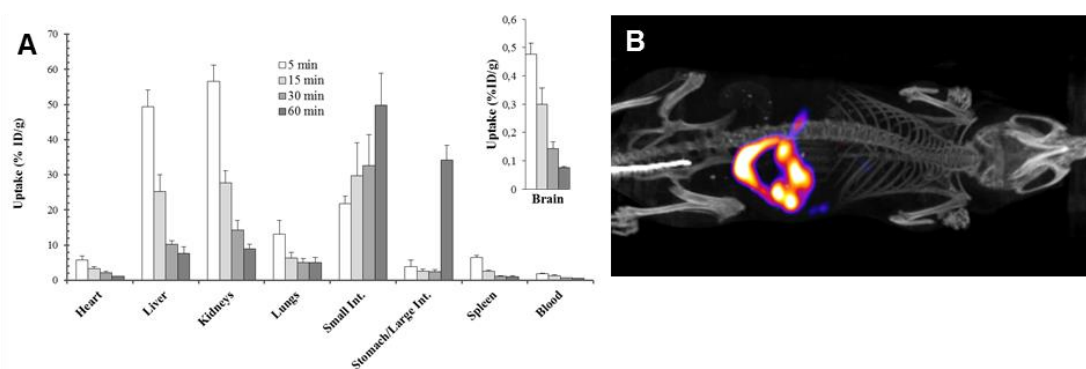


**Figure 17.** Biological evaluation of  $^{125}\text{I}$ 2 after iv administration in mice. (A) Tissue distribution expressed as % ID/g  $\pm$  SD ( $n \geq 3$ ) (B) SPECT/CT summation image from 15-35 min after injection.<sup>3</sup>

As part of the same study, WIN17317-3 and **2** were evaluated in an automated patch clamp electrophysiology assay for their activity at the panel of human Na<sub>v</sub> isoforms. Comparison of the two suggested that the Na<sub>v</sub> blocking potency of WIN17317-3 is fully retained by the newly developed iodinated analogue. Based on the previously reported data, suggesting preferential binding of WIN17317-3 at the neuronal and skeletal muscle tissues over the cardiac tissue, higher potency was anticipated for the Na<sub>v</sub>1.2 and Na<sub>v</sub>1.4 isoforms over Na<sub>v</sub>1.5; unexpectedly, both compounds showed higher affinity binding to the Na<sub>v</sub>1.4, Na<sub>v</sub>1.5 and Na<sub>v</sub>1.7 isoforms over the Na<sub>v</sub>1.2 (10-fold), Na<sub>v</sub>1.6 (10-fold) and Na<sub>v</sub>1.8 (80-fold) isoforms (Table 4).

**Table 4.** *h*Nav isoform profiling of iminodihydroquinolines WIN17317-3 and **2**.\*

Isoform Cpd	<i>h</i> Na <sub>v</sub> IC <sub>50</sub> (μM)					
	1.2 <sup>3</sup> CNS	1.4 <i>Skeletal muscle</i>	1.5 <i>Heart</i>	1.6 <i>PNS</i>	1.7 <i>PNS</i>	1.8 <i>PNS</i>
WIN17317-3	2.2 ± 1.2	0.2 ± 0.2	0.3 ± 0.1	1.9 ± 0.7	0.2 ± 0.1	15.0 ± 5.8
<b>2</b>	1.5 ± 0.5	0.1 ± 0.1	0.2 ± 0.1	0.6 ± 0.2	0.2 ± 0.1	5.5 ± 4.1

\*Årstad group, unpublished data.

The most powerful known method of blocking pain while retaining consciousness, is to inject LAs, like lidocaine, regionally into areas of the body generating pain. However, as previously discussed, LAs are non-selective Na<sub>v</sub> blockers, causing apart from Na<sub>v</sub> blockade in nociceptors also blockade of Na<sub>v</sub>s in the heart, brain as well as non-nociceptive sensory, sympathetic and motor fibers leading to adverse side effects.

Re-evaluating the results obtained from the iodinated iminodihydroquinoline study, we envisioned that iminodihydroquinolines could potentially be clinically useful as locally administered pain therapeutics with reduced side effect burden compared to the currently available analgesic treatments. The high affinity Na<sub>v</sub>1.7 inhibition could lead to effective pain-signaling blockade (C-fibers), with less prominent effects on other sensory and motor fibers (A-fibers), as suggested by the lower potency exhibited for their predominately expressed isoform, Na<sub>v</sub>1.6. In addition, the low brain uptake and the restriction of [<sup>125</sup>I]**2** in the periphery, as well as the 10-fold selectivity over the brain isoform Na<sub>v</sub>1.2 suggest iminodihydroquinolines are less likely to exhibit serious CNS side effects. The quick blood metabolism is anticipated to minimize the drug concentration in circulation thereby reducing the probability for cardiovascular toxicity.

The first step towards validating the above hypothesis was to examine the iminodihydroquinolines efficacy in blocking pain signaling. In collaboration with the Koltzenburg group, UCL Neurology, WIN17317-3 was evaluated in the rodent skin-nerve assay for its *in vitro* effects on peripheral sensory neurons. The skin-nerve assay is one of the most powerful methods for investigating pain-signaling as it allows direct recording of AP conduction from the several types of neuronal fibers independently, as well as provides a quantifiable measure of their responses upon pharmacological intervention. The rodent skin-nerve assay is described in depth in chapter 5.1.

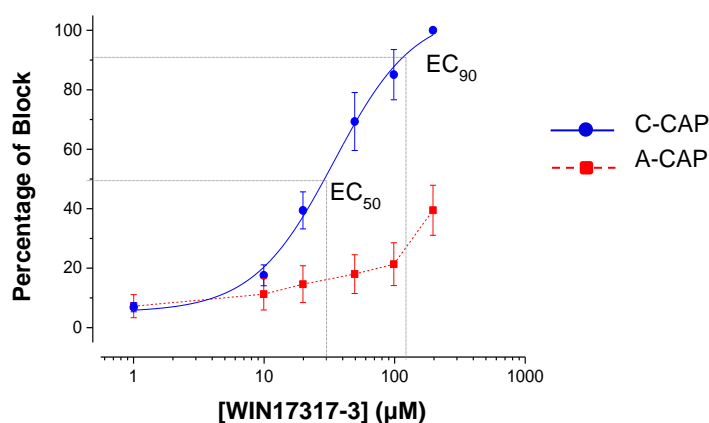


**Figure 18.** WIN17317-3 evaluation in the rat skin-nerve assay. Saphenous nerve A- (■) and C-fiber (●) CAP blockade as a function of WIN17317-3 concentration. Data points are shown as mean  $\pm$  S.E.M ( $n = 9$ ), fitted dose-response curves are presented as solid lines. (Koltzenburg group, unpublished data).

The results of the assay were overwhelming (Fig. 18). WIN17317-3 blocked nociceptive C-fibers with moderate potency ( $EC_{50} = 34.6 \mu\text{M}$ ) yet with remarkable selectivity over the non-nociceptive A-fibers; less than 40% of the A-CAP signal was blocked at the  $EC_{90}$  for C-fibers ( $149.2 \mu\text{M}$ ). To the best of our knowledge, only two examples of such differential fiber block have been reported in literature, by proTx-II or co-administration of QX-314 with a TRPV1 agonist. The effects of the tarantula toxin ProTx-II, a highly potent and selective  $\text{Na}_v1.7$  blocker, were evaluated on the exact same skin-nerve assay by the Koltzenburg group; selective C-CAP blockade was obtained however only when applied to the desheathed nerve (Fig. 19).<sup>123</sup> Due to its large molecular weight proTx-II is not connective tissue penetrant and hence is of limited therapeutic potential.

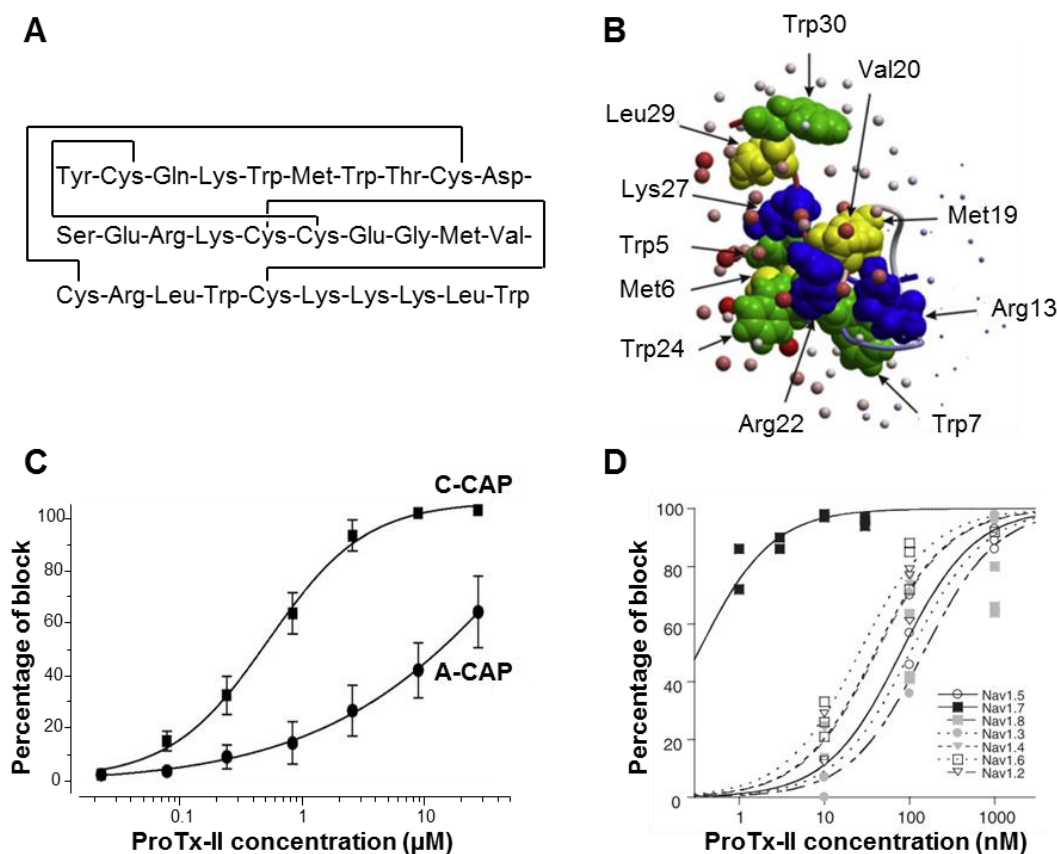


**Figure 19.** (A) Amino acid sequence of the tarantula *T. Prurien* peptide, ProTx-II. (B) 3D-structure model of ProTx-II, constructed using the optimal docking area method by homology modeling with ICM-PRO (Molsoft) based on the NMR structure of GsMTx2 (PDB:1lup). Blue, green, yellow, red and purple represent positively charged, aromatic, hydrophobic, negatively charged and polar residues respectively. The locations of amino acid residues important for  $\text{Na}_v1.5$  binding as revealed by mutation experiments are indicated.<sup>136</sup> (C) ProTx-II effects on the isolated nerve preparation. Saphenous nerve A $\beta$ - (●) and C-fiber (■) CAP blockade as a function ProTx-II concentration. Data points are shown as mean  $\pm$  S.E.M ( $n = 9$ ). (D) Block of  $h\text{Na}_v1$  subtypes by ProTx-II examined by whole-cell voltage clamp. IC<sub>50</sub> values:  $\text{Na}_v1.2$ , 41 nM;  $\text{Na}_v1.3$ , 102 nM;  $\text{Na}_v1.4$ , 41 nM;  $\text{Na}_v1.5$ , 79 nM;  $\text{Na}_v1.6$ , 26 nM;  $\text{Na}_v1.7$ , 0.3 nM;  $\text{Na}_v1.8$ , 146 nM.<sup>123</sup>

Internalization of the permanently charged lidocaine derivative QX-314 through activation of ion channels selectively expressed in nociceptors (TRPV1, TRPA1), as previously discussed in section 1.7.6, was also shown to produce selective and prolonged conduction block of C-fibers.<sup>137</sup> The Koltzenburg group investigated the possibility of WIN17317-3 eliciting its nociceptive effects *via* an analogous mechanism of action: acting as a TRPV1/TRPA1 agonist, resulting in the opening of the channel(s) and to its internalization in the nociceptor terminal, where action at  $\text{Na}_v$ s would mediate C-CAP conduction blockade. Calcium imaging experiments<sup>138</sup> performed on HEK293 cells transfected with the TRPV1 and TRPA1

channels of interest, showed no increase in  $\text{Ca}^{2+}$  flux upon WIN17317-3 application at the concentration range this causes C-CAP blockade (Fig. 20). This suggested the two TRP channels are not activated by WIN17317-3 therefore the proposed mechanistic hypothesis was disapproved.

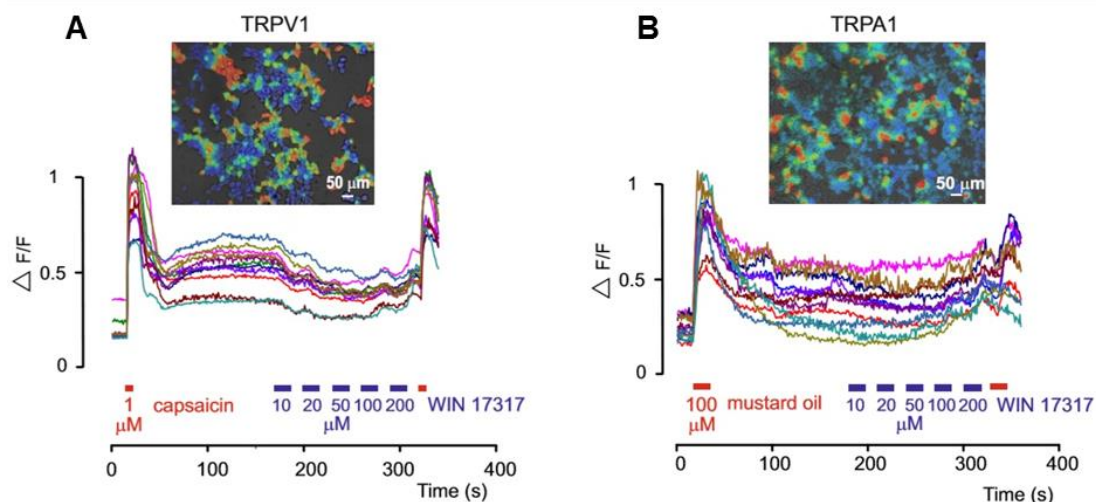


**Figure 20.** WIN17317-3 effects on (A) TRPV1- and (B) TRPA1-transfected HEK293 cells examined using live cell ratiometric calcium imaging. A control agonist was administered prior to and after WIN17317-3 administration to confirm the expression of functional channels. Koltzenburg group, unpublished data.

The selective action of WIN17317-3 on nerve conduction was therefore considered to be mediated most likely *via* the selective blockade of  $\text{Na}_v$  isoforms, in particular  $\text{Na}_v1.7$ , or by another unknown mechanism.

## 1.9. Research aim and objectives

The aim of this work was to develop small molecule iminodihydroquinolines as novel local analgesic drug candidates with high therapeutic index for progression into clinical development. To achieve this, the traditional medicinal chemistry approach of 'hit' to 'lead' development, commonly used in drug discovery programs for optimizing newly identified chemical entities for their activity against a certain biological/therapeutic target, was employed. According to this, the following objectives were set:

- (a) *Design and synthesis of a compound library* based on the structure of the 'hit' molecule WIN17317-3. Synthetic routes were to be developed for accessing structurally-diverse analogues of WIN17317-3.
- (b) *Pharmacological characterization* of compounds using a combination of  $\text{Na}_v$  screening assays and evaluation at peripheral sensory neurons.
- (c) *Development of a pharmacophore model*. Understanding the compounds' SARs for the binding site is essential for optimizing activity at the target.
- (d) *Mechanistic investigation of the molecular mode of action*. Diverse pharmacological characterization and analysis was endeavoring to unravel the relationship between  $\text{Na}_v$  inhibition and nociceptor blockade and explain the underlying mechanism for the observed preferential nociceptor block.
- (e) *Characterization of a lead compound in early preclinical safety studies*, including pharmacokinetic profiling and evaluation of toxicity. The lead compound was to be selected on the basis of its efficacy towards potently blocking nociceptors without interfering with other neuronal fibers or blocking off-target  $\text{Na}_v$  isoforms.

---

## 2. The Design of an Iminodihydroquinoline Compound Library

The underlying principle of the compound library design, part of this work, was the effective exploration of the structure-activity relationships (SARs) of the iminodihydroquinoline class for Na<sub>v</sub> isoform blockade, in particular Na<sub>v</sub>1.7, and the description of the respective pharmacophore, with the minimum required number of ligands. A pharmacophore, as defined by the International Union of Pure and Applied Chemistry (IUPAC), is the ensemble of steric and electronic features that is necessary to ensure the optimal supramolecular interactions with a specific biological target structure, and to trigger or block its biological response.<sup>139</sup>

Drug design is conventionally characterized as being of two types:<sup>140</sup>

- a. Structure-based drug design (SBDD)<sup>141, 142</sup> which exploits the three-dimensional (3D) structure of a biomolecular target (X-ray crystallography, NMR spectroscopy) for the design of complementary ligands according to the electronic and steric requirements of the active site, and
- b. Ligand-based drug design (LBDD) which uses the relationship between the structure of ligands and their paired activity at the target, for building a pharmacophore model identifying the optimal physicochemical properties for binding.<sup>143, 144</sup>

Despite the continuing efforts of the scientific community, the crystal structure for the mammalian Na<sub>v</sub> channel has not as yet been characterized; consequently, the design of Na<sub>v</sub> ligands has traditionally followed the LBDD approach. Accordingly, in this study, efforts were concentrated on generating new ligands based on the structure of the hit molecule, WIN17317-3. By systematically altering molecular features and measuring the impact of these on Na<sub>v</sub>1.7 activity, we aimed to create a pharmacophore model defining those structural characteristics leading to high affinity binding.

Structural modifications were methodically introduced in four areas of the parent WIN17317-3 molecule: the 4-imino substituent (R<sup>1</sup>), the *N*-1 substituent (R<sup>2</sup>), the 7-chloro substituent (R<sup>3</sup>) and the core heterocyclic scaffold (Fig. 21). Only one molecular feature was altered at a time in order for results to be conclusive regarding the specific parameter varied.

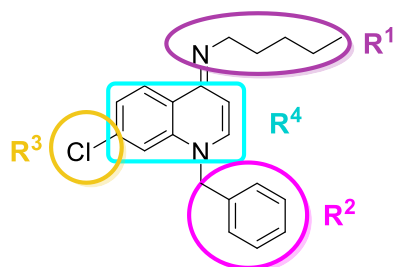


**Figure 21.** Characterization of the WIN17317-3 pharmacophore.

Multiple molecular characteristics can contribute to the SAR of a compound class, like the size and shape, the stereochemical arrangement and distribution of functional groups, and the chemical reactivity and electronic effects. Substituents were introduced at the four pharmacophoric areas defined above, with the aim to collectively investigate activity trends implied by the following descriptors:

a. *Molecular weight, size and shape*

Both parameters are of high importance for the discovery of novel ion channel ligands. The mechanism of action of several  $\text{Na}_v$  toxins largely relies on their bulky structure. The TTX binding site for example is located in short proximity from the opening of the channels pore so as when bound it physically obstructs the passage of sodium ions.<sup>145</sup> In contrast, the LA binding site is situated in the lumen of the channel hence the introduction of large/bulky groups could be in this case detrimental for activity, since ligands could be prevented from reaching their active site.<sup>120</sup> The shape of the drug should be in general complementary to the active site (key and lock relationship) for optimum activity to be achieved.

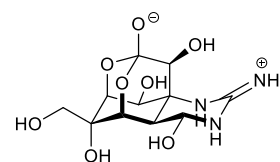


**Figure 22.** The chemical structure of TTX.

b. *Lipophilicity*

This parameter refers to a compound's ability to dissolve in oils, lipids, and non-polar solvents versus polar, aqueous, environments. It reflects molecular desolvation in transfer from aqueous phases to cell membranes and binding sites, hence plays an important role to the pharmacokinetics/pharmacodynamics (PK/PD) and toxicity profile of a drug.<sup>146</sup> The partition coefficient (logP) is the most widely used measure of lipophilicity and it can be either measured experimentally or predicted using algorithms (cLogP). For charged molecules, the distribution coefficient (logD) at a set pH, is rather measured, reflecting the net result of all intermolecular forces involved between the solute (ionized plus unionized forms) and the two phases between which it partitions.



$$\log P_{oct/wat} = \log \left( \frac{[solute]_{octanol}^{unionised}}{[solute]_{water}^{unionised}} \right) \quad \log D_{oct/wat} = \log \left( \frac{[solute]_{octanol}^{ionised} + [solute]_{octanol}^{unionised}}{[solute]_{water}^{ionised} + [solute]_{water}^{unionised}} \right)$$

**Figure 23.** LogP and LogD equations.

c. *Acidity/Basicity*

The presence of ionizable functional groups in a drug can serve two principal functions: it can lead to direct specific interactions/bonds with the biomolecular target, and/or can increase the molecule's overall polarity thereby influencing other key physicochemical properties such as solubility and lipophilicity.<sup>147</sup> The prerequisite of two basic centers at the pharmacophore, these being the quinoline and imine functionalities of the hit WIN17317-3, was to be examined, by tuning the acid-base dissociation constants ( $pK_a$ ) of the two, using different substitution patterns.

d. *Topological polar surface area (tPSA)*

tPSA is defined as the sum of the contributions to the molecular (usually van der Waals) surface area of all the polar atoms in a molecule such as oxygen, nitrogen and their attached hydrogens. It is a convenient measure of the polarity of a ligand, as it avoids the need for 3D structure calculations, or determination of the biologically relevant conformations of ligands. A recently published study by Prasanna *et al.*, demonstrates that tPSA and pharmacological activity are correlated (positively or negatively) in many of the drug classes examined.<sup>148</sup>

e. *Hydrogen-bond donors and acceptors*

The hydrogen bond interactions between a ligand and its target protein are known to play a critical role in the overall affinity between the two. In addition, the number of hydrogen bonds in a molecule is known to affect pharmacokinetic properties such as tissue absorption and penetration across the blood-brain barrier; according to the Lipinski's rule of five a compound is more likely to be membrane permeable, by passive diffusion, if it contains less than five hydrogen bond donors and less than ten hydrogen bond acceptors.<sup>149</sup> Hydrogen bond donors and acceptors of variable strengths were to be incorporated in all four pharmacophoric areas under investigation.

The molecular descriptors described above were used to guide the Na<sub>v</sub> ligand design in this study. In many cases, a single structural modification induced changes in more than one molecular descriptor hence a careful assessment of all plausible properties altered was performed for every new compound examined.

Of particular interest was the introduction of fluorine-containing ligands in the library. *Fluorine substitution* is routinely used in medicinal chemistry as depicted by

the large number of fluorine-containing drugs currently in the pharmaceutical pipeline (>20%).<sup>150</sup> Fluorine, due to its small size (van der Waals radius 1.47 Å), can serve as a hydrogen bioisostere (van der Waals radius 1.20 Å), yet as the most electronegative element in the periodic table (3.98 Pauling scale) it can have profound effects on a compound's biological activity. In multiple real-life examples, the introduction of fluorine substitution in pharmaceutical entities has led to enhanced binding affinity (direct interaction of fluorine with the target), improved physicochemical properties (lipophilicity and basicity), and increased metabolic stability.<sup>151</sup> In addition, radioactive <sup>18</sup>F-tags are increasingly introduced as pharmacological tools for characterizing the pharmacokinetic profile of drug candidates using positron emission tomography (PET) imaging in the early stages of clinical development.<sup>152</sup> In this study, fluorine substitution was used as a tool for (a) probing the SARs of the class, (b) optimizing the properties of a lead drug candidate and (c) identifying sites suitable for potential <sup>18</sup>F-fluorination.

### 3. Chemical Approaches and Reactions

In this chapter the synthetic methods and chemical transformations employed for the synthesis of a library of 25 novel structural analogues of WIN17317-3 are described. For convenience of representation, the data are classified in three sections according to the nature of the heterocyclic scaffold incorporated (quinolines, naphthyridines, purines and pyridines) and subcategorized according to the synthetic building blocks and chemical routes used. The rationale behind compound design and the biological activity of compounds are discussed in separate chapters. The second part of this chapter describes the radiosynthesis of a selected lead compound labeled with fluorine-18 for pharmacokinetic profiling *in vivo*.

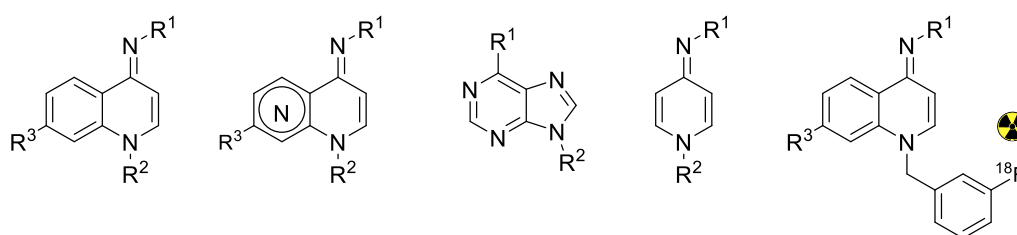


**Figure 24.** The heterocyclic compounds composing the WIN17317-3 library, for which the chemical synthesis is described in this chapter. From left to right: quinolines, naphthyridines, purines and pyridines and an [ $^{18}\text{F}$ ]labelled selected lead compound.

#### 3.1. Synthesis of a WIN17317-3 Compound Library

##### 3.1.1. N-substituted-4-imino-1,4-dihydroquinolines

Based on the structure of 'hit' WIN17317-3 (**1**), 22 novel iminodihydroquinoline analogues were designed bearing diverse substitution patterns (Fig. 25). To access these, three synthetic routes were developed; *Route A* starting from 4-chloroquinolines, *route B* starting from 4-quinolones and *route C* starting from benzoic acids. The route employed for each compound was selected based on the commercial availability of building blocks and the reactivity of those with the desired  $\text{R}^1$ - and  $\text{R}^2$ -containing functionalities.

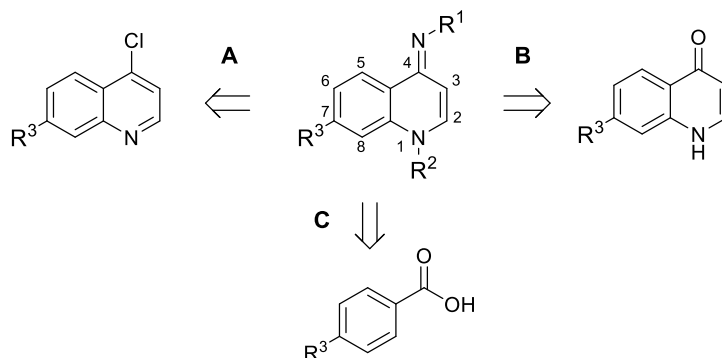
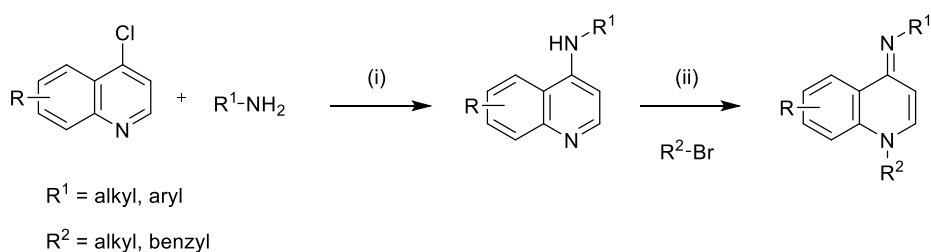


**Figure 25.** General structure of *N*-substituted-4-imino-1,4-dihydroquinolines and the three building blocks used for their synthesis.

### 3.1.1.1. Route A: From 4-chloroquinolines

The first synthetic approach involved a two-step reaction sequence using commercially available 4-chloroquinoline building blocks and was adapted from previously described literature methods (Scheme 2).<sup>133,132</sup> According to these, 4-chloroquinoline is heated with an alkyl or aryl amine to install the 4-alkylamino group of a 4-(alkylamino)-quinoline intermediate; the quinolone nitrogen is subsequently substituted by treatment with an alkyl or benzyl halide to afford the target iminodihydroquinoline system.

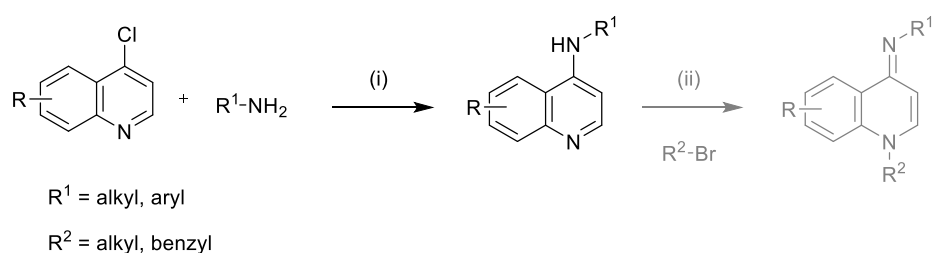


**Scheme 2.** Literature route to iminodihydroquinolines.

Reagents and conditions: (i) EtOH, reflux, 18-24 h (ii) NaI, acetone, reflux, 18-24 h

The first step of the above procedure was optimized by altering the reagent stoichiometry and the reaction conditions (Scheme 3). In the optimized procedure, 4-chloroquinolines were heated with 5.5 equivalents of the neat amines. The higher effective concentration of amines, in combination with the use of higher reaction temperatures, led to higher reaction rates and improved reaction times. In addition, the excess of amine used, quenched the hydrogen chloride released as reaction by product; this significantly simplified the work-up procedure, avoiding alkaline washes

and allowing for the majority of cases pure product isolation through precipitation from ice-cold water.

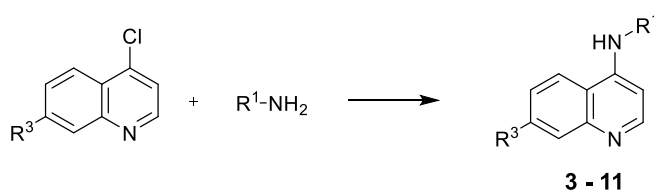


**Scheme 3.** Optimized synthesis to 4-alkylaminoquinoline intermediates.

Reagents and conditions: (i) No solvent, reflux, 18-24 h

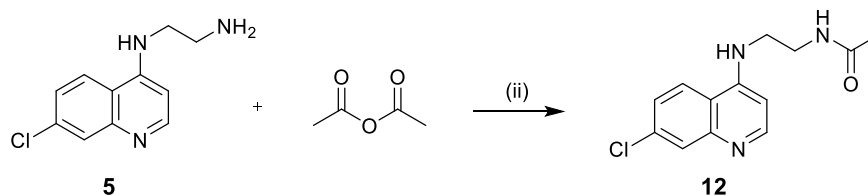
Table 5 summarizes the reaction of 7-substituted 4-chloroquinolines with various aliphatic and aromatic amines. The 4-alkylaminoquinoline intermediates (**3 - 11**) were obtained in excellent yields, exceeding 90% for the majority of cases.

**Table 5.** Synthesis of (4-alkylamino)quinoline intermediates **3 - 11**.



Product	-R <sup>1</sup>	-R <sup>3</sup>	Time (h)	Temp. (°C)	Yield (%)
<b>3</b>		Cl	18	120	96
<b>4</b>		Cl	5	120	99
<b>5</b>		Cl	5	110	90
<b>6</b>		Cl	3	120	91
<b>7</b>		Cl	24	90	35
<b>8</b>		Cl	1.5	110	60
<b>9</b>		H	24	110	88
<b>10</b>		H	24	110	90
<b>11</b>		OMe	48	110	81

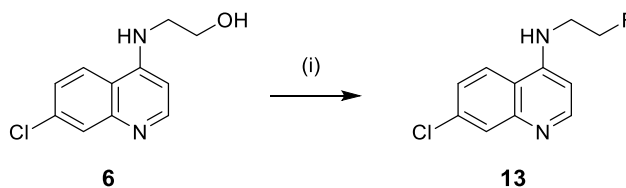
Two intermediates, **5** and **6**, were further functionalized to attain the desired R<sup>1</sup> motifs of the target iminodihydroquinolines. The primary amine in quinoline **5** was treated with acetic anhydride, to afford amide **12** in 85% yield (Scheme 4).



**Scheme 4.** Synthesis of amide **12**.

Reagents and conditions: (i) DCM, 0 °C → rt, 3 h, 85%

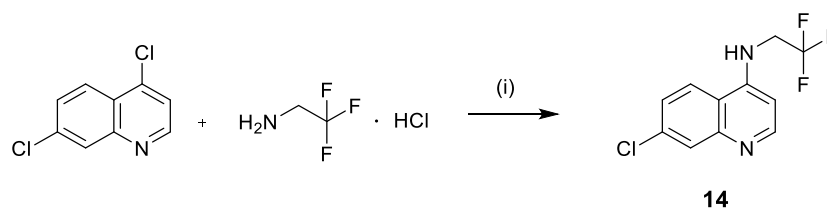
The primary alcohol of **6** was converted to the corresponding monofluoride in **13** using diethylamino sulfur trifluoride (DAST) (Scheme 5). DAST is an organosulfur fluorinating reagent developed in the early 70s, widely used for the nucleophilic fluorination of oxidized organic compounds.<sup>153</sup>



**Scheme 5.** Synthesis of intermediate **13**.

Reagents and conditions: (i) DAST, DCM, 0 °C → rt, 48 h, 63%

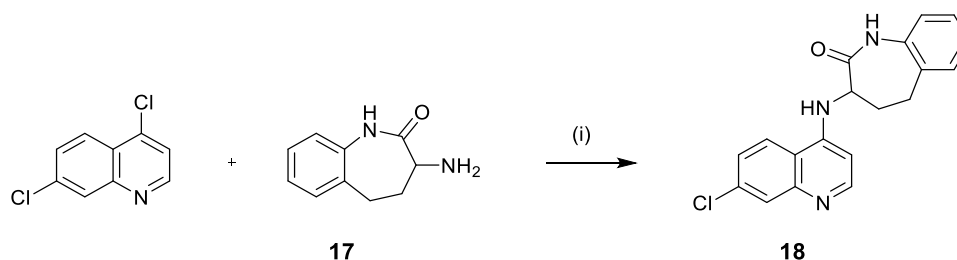
The synthesis of two 4-(alkylamino)quinoline intermediates, **14** and **18** (*vide infra*), deviated from the established optimised reaction conditions (Schemes 6, 7). Stoichiometric amounts of quinolines and amines were used and reaction solvents were introduced in the mixture. The first case involved installation of the 4-(2,2,2-trifluoroethyl)amino substituent in **14** (Scheme 6). 2,2,2-trifluoroethylamine, was purchased as the hydrochloride salt therefore a base, excess triethylamine, in DMF was added to release the corresponding reactive free amine *in situ*.



**Scheme 6.** Synthesis of intermediate **14**.

Reagents and conditions: (i)  $\text{NEt}_3$ , DMF, 110 °C, 4 h, 92%

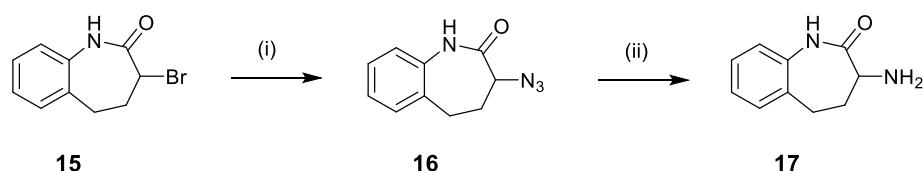
The second case involved the reaction of 4,7-dichloroquinoline with 3-amino-1,3,4,5-tetrahydro-2H-benzo[*b*]azepin-2-one, **17** (Scheme 7). Both reagents were solids therefore DMF was introduced to solubilize the reaction mixture. Furthermore, with a limited amount of **17** available, only one equivalent of the amine was used and triethylamine was added to quench the hydrogen chloride released as reaction by product.



**Scheme 7.** Synthesis of 1,3,4,5-tetrahydro-2H-benzo[*b*]azepin-2-one (bnza) intermediate **18**.

Reagents and conditions: (i)  $\text{NEt}_3$ , DMF, 150 °C, 18 h, 26%

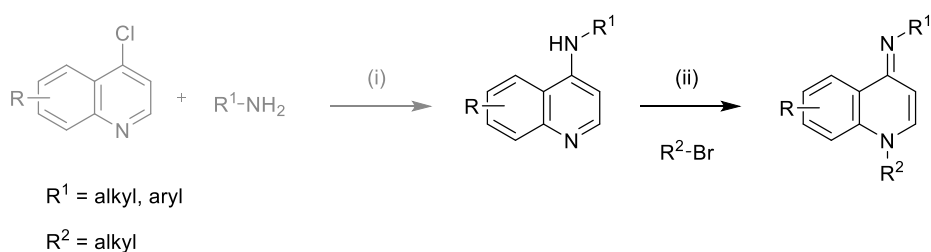
Amine **17** was synthesized according to literature procedures from racemic 3-bromo-1,3,4,5-tetrahydro-benzo[*b*]azepin-2-one (**15**) in two steps (Scheme 8). According to these, **15** was reacted with sodium azide in the presence of sodium iodide to afford azide **16** in 93% yield.<sup>154</sup> **18** was subsequently reduced to amine **17**, following a facile method using a mixture of zinc and ammonium chloride as the reducing agent and mild reaction conditions.<sup>155</sup>



**Scheme 8.** Synthesis of benzazepine-containing amine **17**.

Reagents and conditions: (i)  $\text{NaN}_3$ ,  $\text{NaI}$ ,  $\text{DMF}$ ,  $\text{rt}$ , 24 h, 93% (ii)  $\text{Zn}$  powder,  $\text{NH}_4\text{Cl}$ ,  $\text{EtOH}/\text{H}_2\text{O}$  (3:2),  $80\text{ }^\circ\text{C}$ , 20 min, 61%

Following the synthesis for all (4-alkylamino)quinoline intermediates, the final step of this route involved alkylation of the quinoline nitrogen to furnish the target iminodihydroquinolines (Scheme 9).

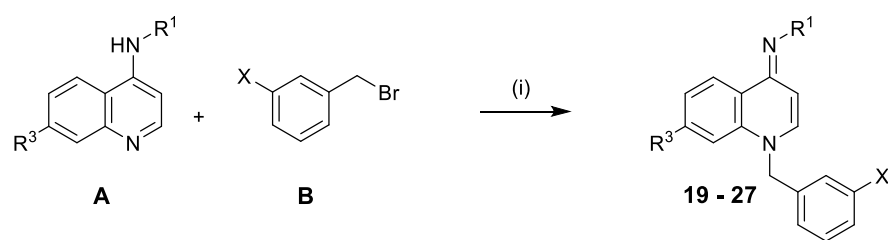


**Scheme 9.** Second step of iminodihydroquinoline synthesis.

Reagents and conditions: (ii)  $\text{NaI}$ ,  $\text{acetone}$ ,  $\text{reflux}$ , 18-24 h

4-(alkylamino)quinoline intermediates were heated to reflux with the selected alkyl or aryl bromides in the presence of sodium iodide in acetone to improve the leaving group character (Finkelstein ion exchange)<sup>132</sup> (Table 6). All reactions proceeded to completion. 4-(alkylamino)-quinolines **12** and **15**, exhibited poor solubility in acetone therefore the two reactions were performed in DMSO and DMF respectively. The target iminodihydroquinolines were recrystallized and isolated in high purity (>98%) for submission to pharmacological assays. The reaction yields reflect the compounds ability to crystallize from the selected solvent system rather than the efficiency of the reaction. Given the low amount of material required for biological testing, enough material was obtained with the first crystal crop, therefore recrystallization from the mother liquor for yield improvement purposes was not attempted, to avoid compromising purity.

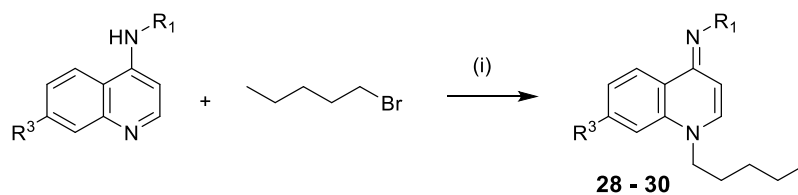


**Table 6.** *N*-benzylation of (4-alkylamino)quinolines **19** - **27**.

Starting material A	Product	R <sup>1</sup>	R <sup>3</sup>	X	Yield (%)
<b>4</b>	<b>19</b>		Cl	H	17
<b>8</b>	<b>20</b>		Cl	H	98
<b>9</b>	<b>21</b>		H	H	86
	<b>22</b>			F	71
	<b>23</b>			I	79
<b>11</b>	<b>24</b>		OMe	H	42
<b>12</b>	<b>25</b>		Cl	H	25 <sup>a</sup>
<b>14</b>	<b>26</b>		Cl	H	73
<b>18</b>	<b>27</b>		Cl	H	49 <sup>b</sup>

(i) NaI, acetone, reflux, 3-18 h (a) DMSO, NEt<sub>3</sub>, 110 °C, 24 h (b) DMF, 100 °C, 24 h

The same method was applied for the installation of alkyl groups as *N*-1 substituents (Table 7). The reactivity of (4-alkylamino)quinolines with benzylic halides was markedly higher than with alkyl halides, fact mirrored in the longer reaction times for the latter.

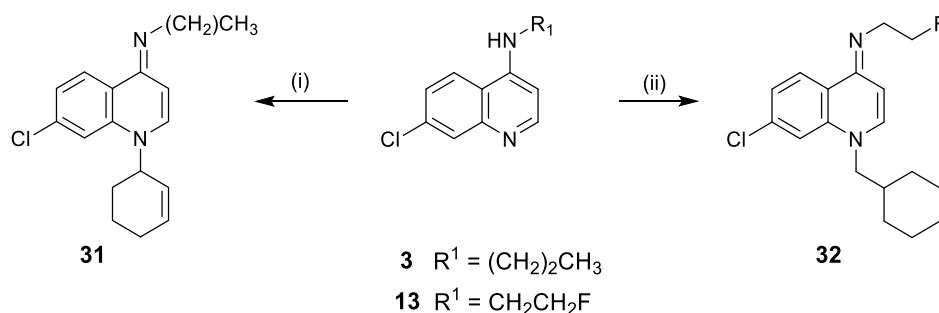
**Table 7.** *N*-alkylation of (4-alkylamino)quinolines **7-10**.

Starting material	Product	-R <sup>1</sup>	-R <sup>3</sup>	Yield (%)
<b>7</b>	<b>28</b>		Cl	24 <sup>a</sup>
<b>8</b>	<b>29</b>		Cl	92
<b>10</b>	<b>30</b>		H	51

(i) NaI, acetone, reflux, 32 h (a) NaH, THF, 0 °C, 0.5 h → 65 °C, 72 h

The reaction of (4-aminophenyl)quinoline, **7**, with 1-bromopentane did not proceed under the established reaction conditions. The decreased reactivity was attributed to conjugation of the quinoline's nitrogen electron lone pair to the R<sup>1</sup> aniline ring. To compensate for this, the amine was deprotonated with NaH prior to alkylation; the increased nucleophilicity allowed alkylation to proceed with the target compound **28** obtained in 24% yield.

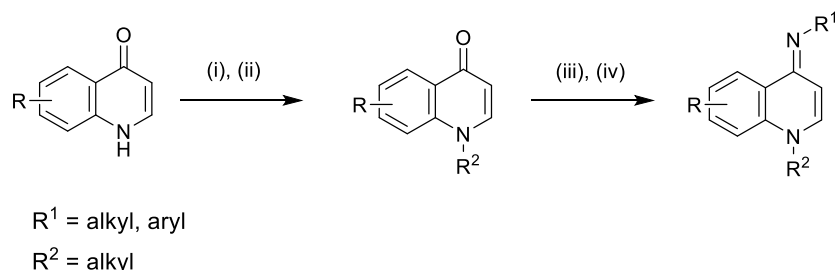
Apart from alkyl chains, cycloalkyl rings were also introduced as *N*-1 substituents (Scheme 10). Reaction of **3** with 3-bromocyclohexene afforded compound **31** in 28% yield. Similarly **13** was reacted with (bromomethyl)cyclohexane to afford compound **32** in 27% yield.

**Scheme 10.** Synthesis of iminodihydroquinolines **31** and **32**.

Reagents and conditions: (i) 3-Bromocyclohexene, NaI, DMF, 80 °C, 4 days, 28% (ii) (Bromomethyl)cyclohexane, NaI, DMF, 120 °C, 4 days, 27%.

### 3.1.1.2. Route B: From 4-quinolones

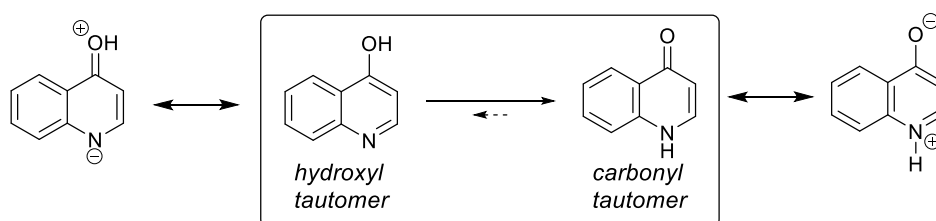
The second synthetic approach to iminodihydroquinolines relied on commercially available 4-quinolones as building blocks, which were assembled in a two-step reaction sequence (Scheme 11).



**Scheme 11.** Second route to iminodihydroquinolines starting from 4-quinolones.

Reagents and conditions: (i) NaH, 0 °C, 15 min (ii) R<sup>2</sup>-Br, DMF, 80 -110 °C, 18-24 h (iii) POCl<sub>3</sub>, 110 °C, 3 h (iv) R<sup>1</sup>-NH<sub>2</sub>, MeOH, rt, 5-18h

The first step involved the R<sup>2</sup> alkylation of 4-quinolones to afford *N*-substituted quinolone intermediates. 4-quinolones exist exclusively in their carbonyl tautomeric form (Scheme 12). N-H deprotonation generates ambident anions that can react at either oxygen or nitrogen depending on the exact reaction conditions. Selective *N*-alkylation/benzylation has been previously reported by means of N-H deprotonation using a strong base such as sodium hydride or potassium hydroxide prior to reaction with alkyl/benzyl halides;<sup>156</sup> O-alkylation has been reported for reactions performed in the presence of silver carbonate.<sup>157</sup>



**Scheme 12.** 4-Quinolone tautomerization. Equilibrium lies heavily in the carbonyl form as the hydroxyl tautomer lacks a favorable polarized resonance state.<sup>158</sup>

Reaction of 4-quinolones with sodium hydride, followed by treatment with benzyl bromide or *n*-pentyl bromide, afforded *N*-substituted quinolones **33**, **34** and **35** (Table 8). Alkylation at the nitrogen atom was verified by analysis of the NOESY spectra of the three compounds. Hydrogen correlation was observed between the benzylic protons and the quinolone protons at positions 2 and 8 suggesting these nuclei are spatially close (Fig. 26).

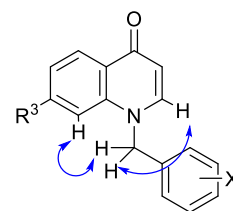
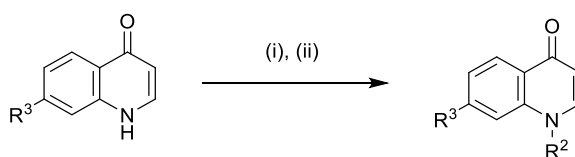


**Figure 26.** Key NOESY interactions ( $\leftrightarrow$ )

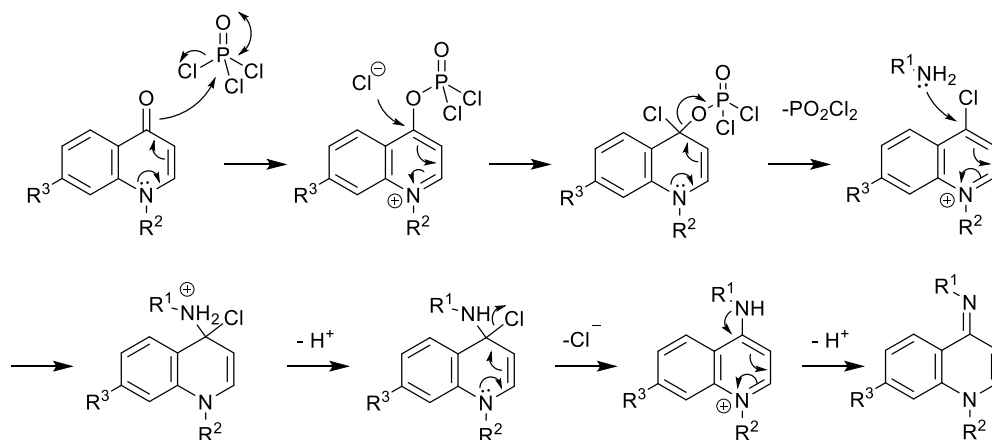
**Table 8.** *N*-alkylation of 4-quinolones.



Starting material	Product	R <sup>3</sup>	R <sup>2</sup>	Yield (%)
7-chloro-4-quinolone	<b>33</b>	Cl		57
7-chloro-4-quinolone	<b>34</b>	Cl		31
4-quinolone	<b>35</b>	H		68

(i) NaH, 0 °C, 15 min (ii) Benzyl/alkyl bromide, DMF, 80-110 °C, 18-24 h

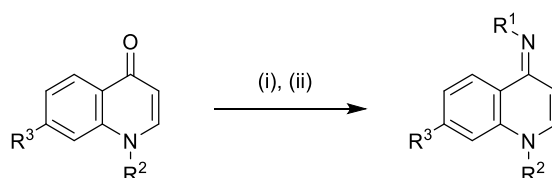
The second and final step of this route involved installation of the R<sup>1</sup> 4-iminoalkyl group. The *N*-substituted quinolones were reacted with phosphorous oxychloride in a Vilsmeier-type reaction to afford highly reactive haloquinolinium ions. These were subsequently treated with the selected amine to furnish the target iminodihydroquinolines (Scheme 13).<sup>159</sup>



**Scheme 13.** Proposed mechanism for carbonyl to imine transformation *via* a chloroquinolinium intermediate.

This second synthetic approach was applied for the synthesis of six iminodihydroquinolines, **1** and **36** - **40** (Table 9, Scheme 14). It was considered advantageous over the 4-chloroquinoline route for a number of cases. Firstly, the use of a highly reactive chloroquinolinium intermediate allowed the incorporation of low nucleophilicity amines as R<sup>1</sup>-imino substituents; *N*-benzyl-4-quinolone (**33**) was treated with *O*-phenylhydroxylamine ( $pK_a=1.96$ )<sup>160</sup> at ambient temperature, yielding compound **36** in an excellent 74% yield. In addition, installation of the 4-imino substituent in the last step of the reaction sequence allowed the synthesis of a series of iminodihydroquinolines with the same R<sup>2</sup> substituents *via* a common *N*-substituted-4-quinolone intermediate; for example compounds **37** and **38** were both accessed *via* quinolone **35**. This effectively translates to a more labor-, time- and cost-efficient library synthesis.

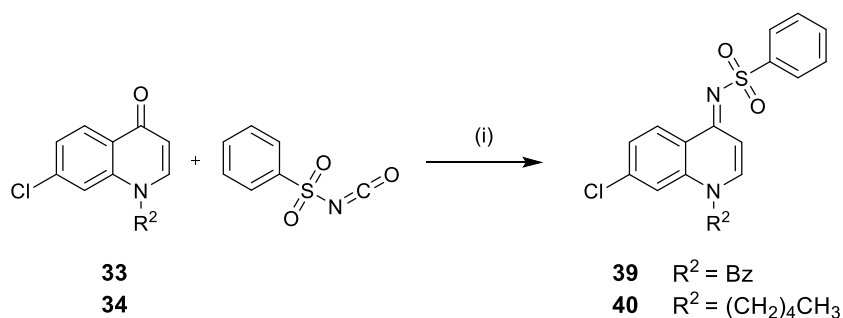
**Table 9.** Synthesis of iminodihydroquinolines **1**, and **36** - **38**.



4-Quinolone	Product	R <sup>1</sup>	R <sup>2</sup>	R <sup>3</sup>	Yield (%)
<b>33</b>	<b>1</b>			Cl	51
	<b>36</b>			Cl	74
<b>35</b>	<b>37</b>			H	57
	<b>38</b>			H	88

(i) POCl<sub>3</sub>, 110 °C, 3 h (ii) R<sup>2</sup>-NH<sub>2</sub>, MeOH, rt, 5-18h

Furthermore, the reaction sequence was used for the installation of benzylsulfonyls as R<sup>1</sup> substituents (Scheme 14). According to a previously described procedure, quinolones **33** and **34** were reacted with benzylsulfonyl isocyanate to afford the target iminodihydroquinolines **39** and **40**, in 70% and 85% yield respectively.<sup>161</sup>



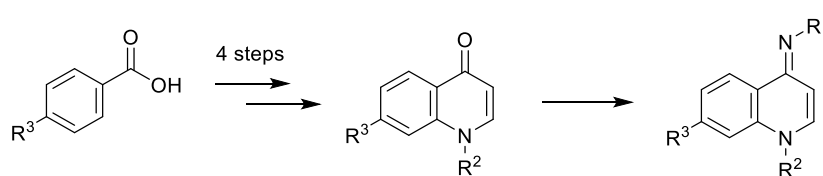
**Scheme 14.** Synthesis of iminodihydroquinolines **39** and **40**.

Reagents and conditions: (i)  $\text{CH}_3\text{CN}$ ,  $70^\circ\text{C}$ , 24 h, **39**  $\rightarrow$  70%, **40**  $\rightarrow$  85%.

### 3.1.1.3. Route C: From substituted benzoic acids *via* ring annulation

The third synthetic approach, as the previously described route B, also involved substituted 4-quinolones as synthetic intermediates; however, in this case, the quinolone biaryl scaffold had to be constructed from single aryl units in multistage reactions (Scheme 15). Two reasons led us pursue this otherwise time- and labor- intensive synthetic route:

- Limited availability of building blocks for use in routes A and B: in certain cases the building blocks with the desired  $\text{R}^3$  substitution pattern were not commercially available or were too expensive for practical applications (for example where  $\text{R}^3 = \text{F}$ ).
- The need to access compounds bearing cycloalkyl or aryl  $\text{R}^2$  groups: direct nucleophilic addition at the quinoline or quinolone nitrogen using aryl halides or secondary alkyl halides was not feasible *via* the previously described routes.



**Scheme 15.** Third route to iminodihydroquinolines from substituted benzoic acids denoting the key 4-quinolone intermediate.

4-Quinolones are particularly interesting scaffolds from a biological point of view, dominating the class of antibacterial agents for more than four decades (ciprofloxacin).<sup>162</sup> Recent studies have demonstrated they are multi-faceted drugs also exhibiting antiischaemic (flusequinan), antiviral (elvitegravir) and antitumor properties (Fig. 27).<sup>163</sup>

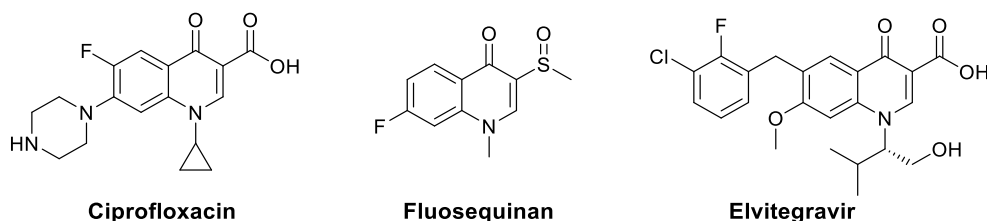
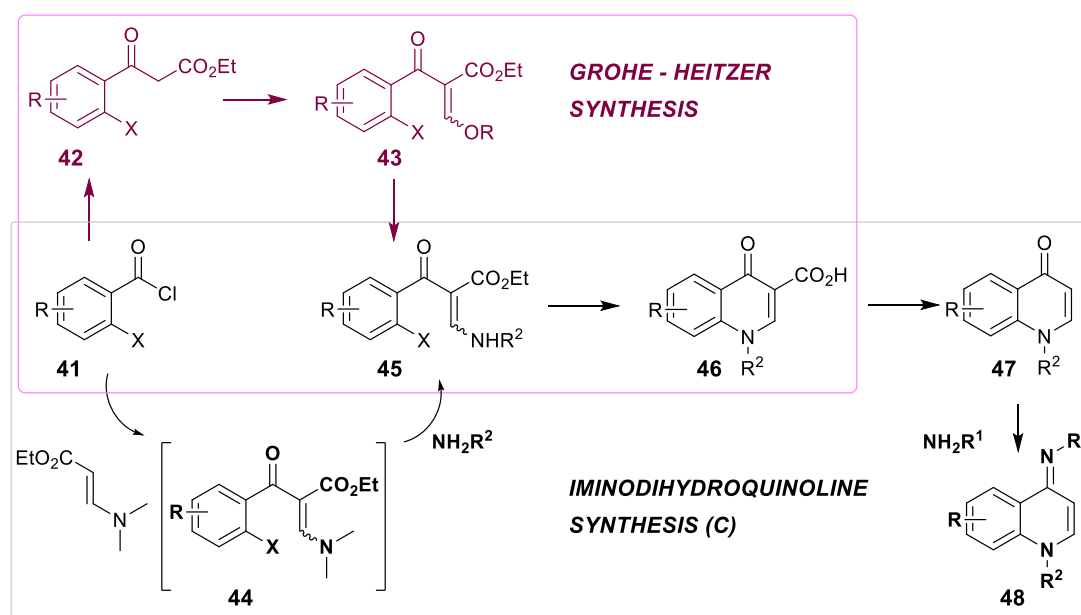


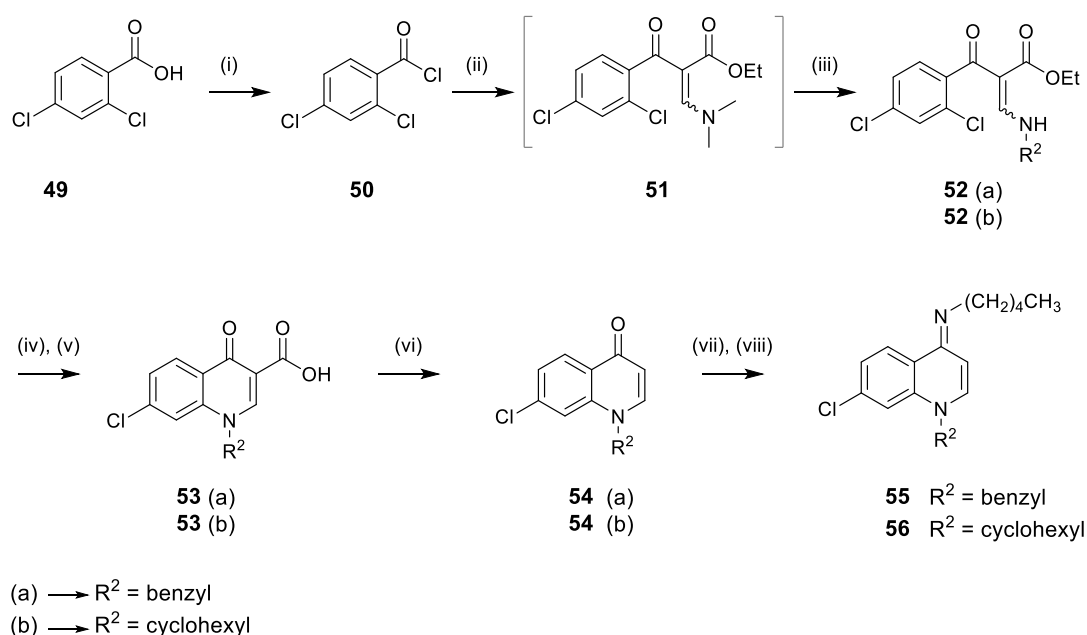
**Figure 27.** Structures of marketed 4-quinolone drugs.

Their synthesis has therefore been the subject of extensive research with flexible routes developed, allowing access to highly substituted and diverse quinolone libraries. The recent review by Boteva and Krasny, provides an excellent summary of preceding methods to substituted 4-quinolones.<sup>164</sup> The selected synthetic approach to 4-quinolones was based on the Grohe-Heitzer synthesis of 4-quinolone-3-carboxylic acids (**46**) (Scheme 16).<sup>165</sup>



**Scheme 16.** The Grohe-Heitzer synthesis (pink) and the modified Grohe-Heitzer synthesis employed as part of the third synthetic route (C) to 4-iminodihydroquinolines (black).

According to this, an acid chloride, **41**, is initially condensed with the active methylene of ethyl 3-(*N,N*-dimethylamino)acrylate to form enamine **44** (Scheme 16). This is subjected *in situ* to an addition-elimination reaction by the action of primary amines making it possible to introduce diverse R<sup>2</sup> substituents at the N-1 position.<sup>166</sup> Enamine **45** is cyclized, through intramolecular nucleophilic aromatic substitution with the *ortho* halogen leaving group with respect to the activating carbonyl group, to afford after ester hydrolysis, the quinolone carboxylic acid **46**. Having furnished the biaryl core, the final steps of the sequence involve acid decarboxylation to generate the *N*-1 substituted quinolone **47** which can be successively transformed to the target 4-iminodihydroquinoline.



**Scheme 17.** Synthesis of iminodihydroquinolines **55** and **56**.

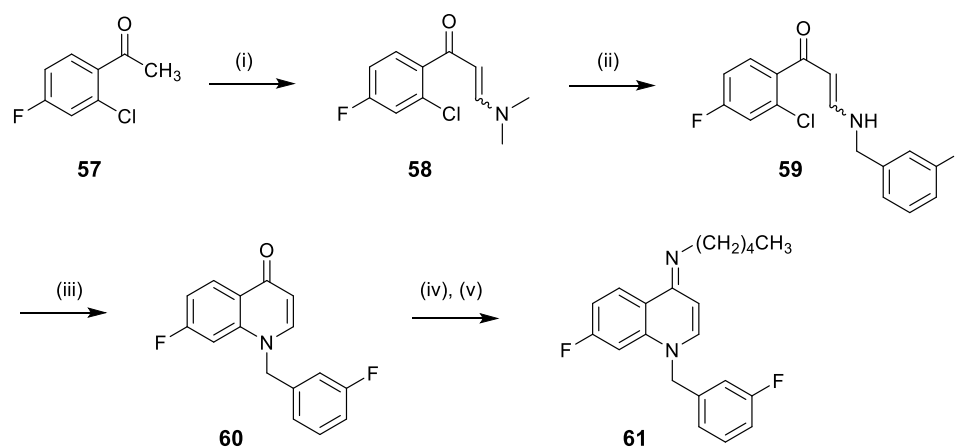
Reagents and conditions: (i) (COCl)<sub>2</sub>, DMF (cat.), DCM, rt, 2h, quant. (ii) ethyl 3-(*N,N*-dimethylamino)acrylate, NEt<sub>3</sub>, CH<sub>3</sub>CN, 70 °C, 3-5 h (iii) NH<sub>2</sub>-R<sup>2</sup>, 70 °C, 18 h, **52(a)**  $\rightarrow$  31%, **52(b)**  $\rightarrow$  61% (iv) NaH, THF, reflux, 4-6.5 h (v) NaOH, THF/EtOH (6:1), 50-60 °C, 6 h, **53(a)**  $\rightarrow$  58%, **53(b)**  $\rightarrow$  43% (vi) HCl (aq.), biphenyl ether, 260 °C, 7 h, **54(a)**  $\rightarrow$  18%, **54(b)**  $\rightarrow$  24% (vii) POCl<sub>3</sub>, 100 °C, 2 h (viii) *n*-pentylamine, rt, 2-3 h, **55**  $\rightarrow$  68%, **56**  $\rightarrow$  96%

The route was successfully applied for the synthesis of iminodihydroquinolines **55** and **56** (Scheme 14). Commercially available 2,6-dichlorobenzoic acid (**49**) was treated with oxalyl chloride in the presence of a catalytic amount of DMF to form acid chloride **50** in quantitative yield. **50** was reacted with ethyl 3-(*N,N*-dimethylamino)acrylate to afford enamine **51**. Transamination using aniline or cyclohexylamine resulted in formation of enamines **52(a)** and **52(b)** in 31% and 61% yield respectively. The enamines were obtained as



racemic mixtures of the *E* and *Z* isomers, in 77:23 ratio for **52(a)** and in 83:17 ratio for **52(b)**, as determined by the  $^1\text{H}$  NMR spectra. The results are in agreement with a previously published study by Kędzia, J. *et al.* which demonstrated that in similar systems the *E* isomer is preferentially formed, due to the *Z* isomer being destabilized by steric interactions between the diethoxycarbonyl and the amino alkyl/aryl groups.<sup>167</sup> Ring cyclisation in the presence of NaH, followed by ester hydrolysis under basic conditions furnished the biaryl core generating carboxylic acids **53(a)** and **53(b)**. These were subsequently decarboxylated *via* harsh heating in acidic pH to afford 4-quinolones **54(a)** and **54(b)** in 18% and 24% yield. The final steps involved installation of the 4-imino substituent, *via* reaction of a chloroquinolinium ion intermediate with *n*-pentylamine as previously described for route B. The target compounds **55** and **56** were obtained in overall yields of 2% and 6% respectively.

The lowest yielding step in the above reaction sequence was the thermal decarboxylation of the quinolone-3-carboxylic acids. In an attempt to improve the overall yield, the synthesis of iminodihydroquinoline **61**, was modified to circumvent this step (Scheme 18).



**Scheme 18.** Synthesis of iminodihydroquinoline **61**.

Reagents and conditions: (i) *N,N*-dimethylformamide dimethyl acetal, toluene, reflux, 24 h, 61% (ii) 3-fluorobenzyl amine, acetic acid, 60 °C, 8 h, 48% (iii) NaH, DMF, 0 → 80 °C, 3 h, 14% (iv) POCl<sub>3</sub>, 100 °C, 2.5 h (v) *n*-pentylamine, MeOH, rt, 5 h, 50%

The first step of the sequence, involved condensation of commercially available 2-chloro-4-fluoroacetophenone with *N,N*-dimethyl formamide dimethyl acetal at 110°C, to afford intermediate enamine **58** in 61% yield. *N,N*-dimethylamino group substitution of **58** using 3-fluorobenzylamine in acetic acid provided intermediate **59** as a single isomer in 48% yield. This was subsequently treated with

NaH to furnish the biaryl quinolone core in **60** in 14% yield. It is worth noting that the reaction yield was significantly lower compared to the ones previously obtained for the ester-containing compounds **52(a)** and **52(b)** (Scheme 17). The ease of cyclization is known to be dependent on the nature of the substituent at the enamine nitrogen. Reaction of **60** sequentially with phosphorous oxychloride and *n*-pentylamine, afforded the target iminodihydroquinoline **61** in 50% yield. The overall reaction yield was 2%. The sequence was eventually proven to be as low yielding as the one initially described (Scheme 17); it is however by one synthetic step shorter.

### 3.1.2. *N*-substituted-4-imino-1,4-dihydro-naphthyridines

The naphthyridines are aromatic heterocyclic compounds members of the chemical class of diazanaphthalenes, increasingly applied in medicinal chemistry as quinoline bioisosteres.<sup>168</sup> Their framework consists of a naphthalene ring at which one carbon per ring has been replaced with a nitrogen atom (Fig. 27).

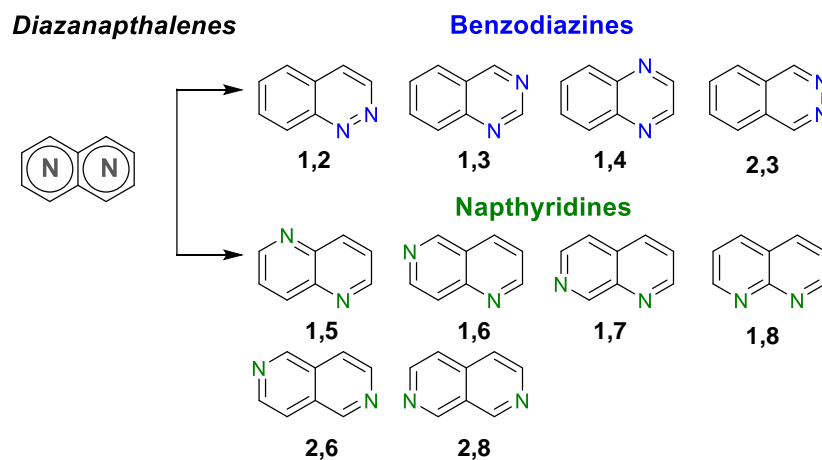
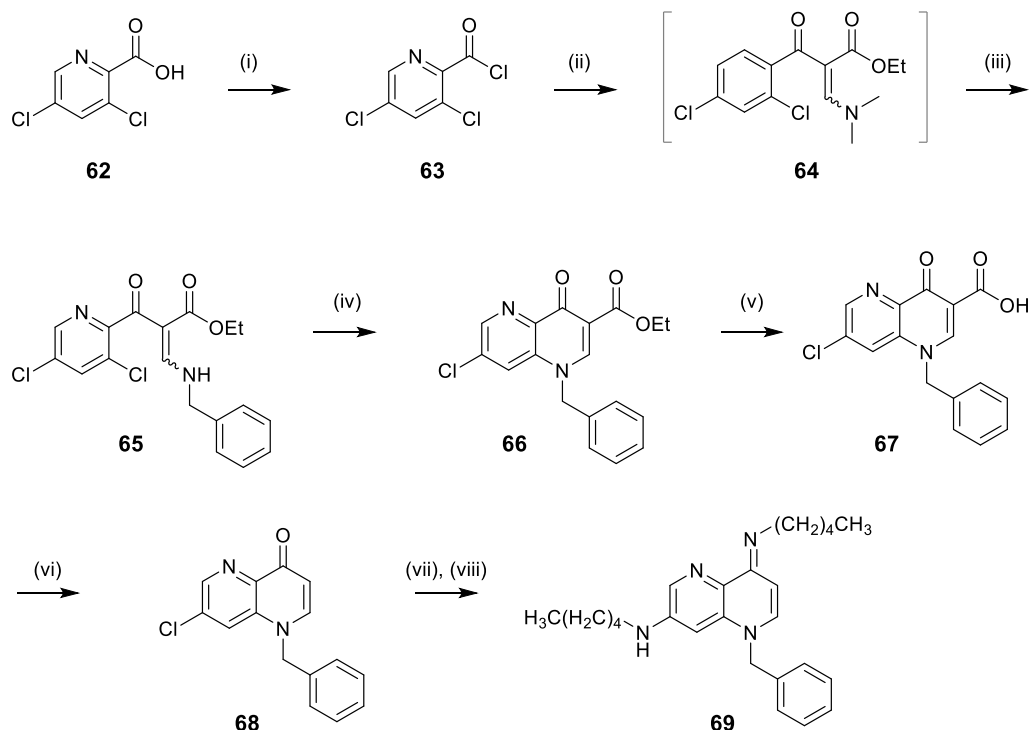


**Figure 28.** The chemical family of diazanaphthalenes.

Traditionally, synthetic approaches to naphthyridines involved extension of established routes to quinolines with the benzyl building blocks of the latter being replaced with appropriately substituted pyridines. Two out of the six possible naphthyridine isomeric scaffolds, and in particular the 1,5- and 1,8-isomers, were introduced giving rise to two novel structural analogues in the library, **69** and **82**. The *N*-1, 4-imino substitution pattern met in the parent WIN17317-3 and the synthesized iminodihydroquinoline series was retained.

The modified Grohe-Heitzer iminodihydroquinoline synthesis (route C, *vide supra*), was adapted for the synthesis of the 4-imino-1,5-naphthyridine analogue **69** (Scheme 19).



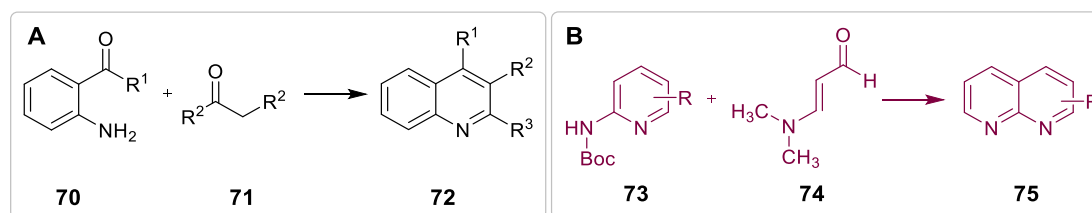
**Scheme 19.** Synthesis of the substituted naphthyridine **69**.

Reagents and conditions: (i)  $(\text{COCl})_2$ , DMF (cat.), DCM, rt, 2 h, quant. (ii) Ethyl 3-(*N,N*-dimethylamino)acrylate,  $\text{NEt}_3$ ,  $\text{CH}_3\text{CN}$ , 65 °C, 3.5 h (iii) Benzylamine, 70 °C, 18 h, 45% (d) NaH, THF, 50 °C, 4 h, 94% (iv) NaOH, THF, 60 °C, 3 h, 90% (v) HCl (aq.), biphenyl ether, 280 °C, 7 h, 74% (vi)  $\text{POCl}_3$ , 110 °C, 2 h (vii) *n*-pentylamine, rt → 18 h, 80 °C → 6 h, 59%

Commercially available picolinic acid (**62**) was the utilized building block. The acid chloride derivative **63** was reacted with ethyl 3-(*N,N*-dimethylamino)acrylate, and the resulting enamine **64** was transaminated with benzylamine to afford a mixture of **65** isomers (83:17 ratio). **65** was cyclized following treatment with NaH, to furnish the 1,5-naphthyridine scaffold in **66** in an excellent 94% yield. Ester hydrolysis and decarboxylation afforded intermediate **68** in 74% yield. Reaction with  $\text{POCl}_3$  followed by treatment with an excess of *n*-pentylamine led to the doubly alkylated analogue **69**. This was not surprising as naphthyridine rings are  $\pi$ -electron deficient and hence highly susceptible to nucleophilic attack, particularly at the *ortho* and *para* positions.<sup>169</sup>

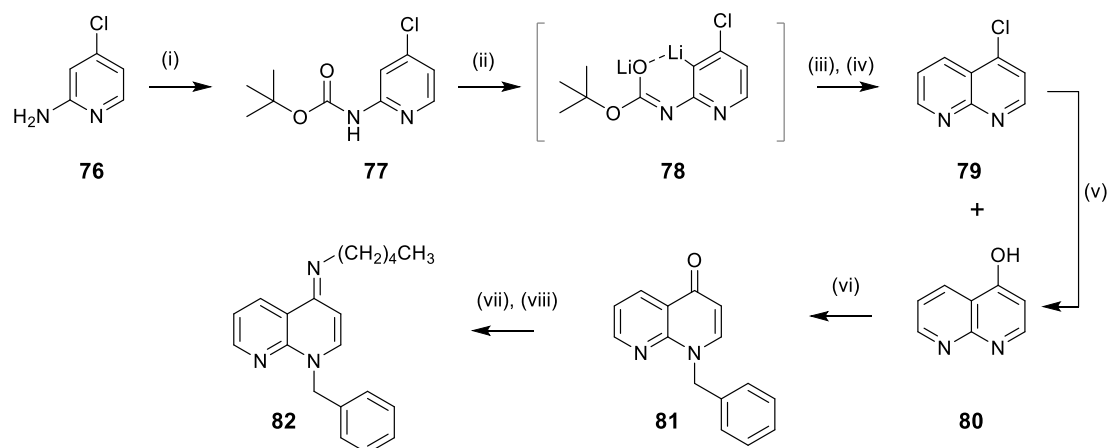
A different approach was employed for the synthesis of the 4-imino-1,8-naphthyridine analogue **82**. The synthesis was based on a recent report of a one-pot

method to naphthyridines *via* a modified Friedländer reaction.<sup>170</sup> The archetypal Friedländer quinoline synthesis involves condensation of an aromatic *o*-amino aldehyde or ketone (**70**) with an aldehyde or a ketone containing an active methylene group (**71**), followed by acid catalyzed cyclisation to furnish the quinoline core (**72**, Scheme 20.A).<sup>171</sup> The advanced method uses more accessible 2-pyridyl pivalamides or *tert*-butylcarbamates (**73**) as building blocks that are subjected to *ortho*-metalation before being reacted with the active methylene of a  $\beta$ -dimethylamino or  $\beta$ -alkoxy acrolein derivative (**74**) (Scheme 20.B). Acid mediated cyclisation gives access to the naphthyridine core (**75**).



**Scheme 20.** The archetypal Friedländer quinoline synthesis (A) and the adopted 1,8-naphthyridine synthesis (B).

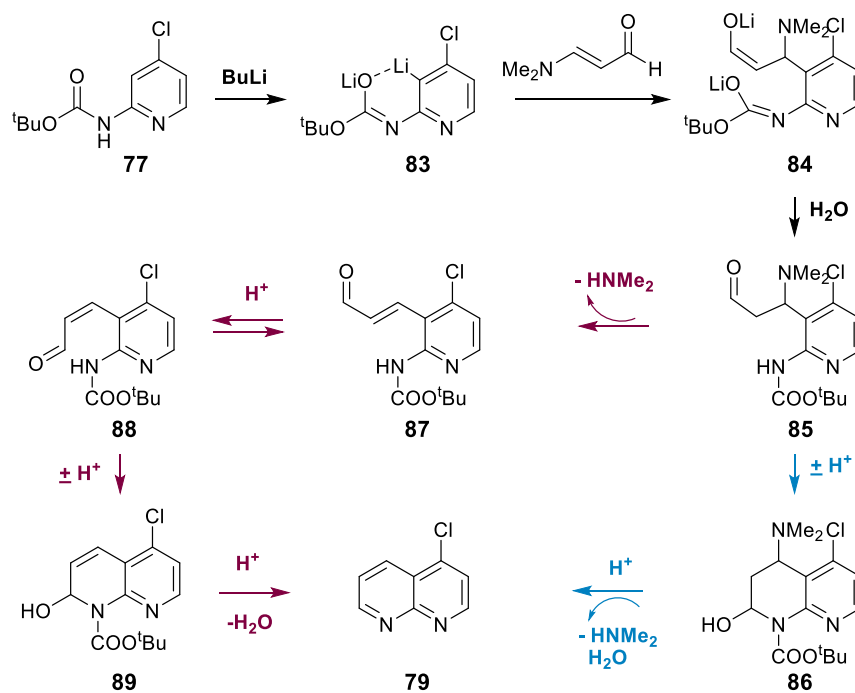
An efficient four-step route to the target 4-iminonaphthyridine **82** was designed integrating the advanced Friedländer method (Scheme 21). The required *tert*-butylcarbamate starting material **77** was synthesized from commercially available 4-chloro-2-aminopyridine (**76**). In a one-pot procedure, **77** was treated with *n*-butyllithium to form the dilithiated intermediate **78** which was subsequently reacted with  $\beta$ -dimethylaminoacrolein and heated in refluxing aqueous hydrochloric acid to furnish the 1,8-naphthyridine scaffold. Two products, **79** and **80**, were isolated in 39% and 17% yields respectively, the latter being the hydrolysis product of **79**. The final steps in the sequence involved *N*-1 benzylation of **80** to afford compound **81** which was subsequently reacted with POCl<sub>3</sub> and *n*-pentylamine to afford the target compound **82** in 90% yield.



**Scheme 21.** Synthesis of the substituted naphthyridine **82**.

Reagents and conditions: (i) Di-*tert*-butyl dicarbonate, LiHMDS, THF,  $-5-0\text{ }^{\circ}\text{C}$ , 2 h, 77% (ii) *n*-BuLi, HMPA, THF,  $-78\text{ }^{\circ}\text{C}$ , 1 h (iii)  $\beta$ -dimethylaminoacrolein,  $-78\text{ }^{\circ}\text{C}$ , 1.5 h (iv) HCl (aq.),  $100\text{ }^{\circ}\text{C}$ , 3 h, **79**  $\rightarrow$  39%, **80**  $\rightarrow$  17% (v)  $\text{CH}_3\text{COOH}$ ,  $125\text{ }^{\circ}\text{C}$ , 1.5 h, 92% (vi) Benzyl bromide,  $\text{K}_2\text{CO}_3$ , DMF,  $80\text{ }^{\circ}\text{C}$ , 3 h, 80% (vii)  $\text{POCl}_3$ ,  $110\text{ }^{\circ}\text{C}$ , 1.5 h (viii) *n*-pentylamine, MeOH, rt, 18 h, 90%

Mechanistic insights to the one-pot transformation of carbamate **77** to 4-chloronaphthyridine **79** are given in Scheme 22. The suggested mechanism is based on the findings of Cho *et al.* who investigated similar transformations of *ortho*-lithiated *N*-acylanilines to quinolines.<sup>172</sup> According to these, the reaction of dilithiated *tert*-butylcarbamate **83** with dimethylaminoacrolein leads to the formation of a primary adduct **84** which upon hydrolysis generates aldehyde **85**. **85** can form 4-chloronaphthyridine **79** via two plausible pathways. The first (blue pathway) involves cyclisation to hemiamidal **86**, followed by loss of a dimethylamine molecule, aromatization, and Boc-deprotection under acidic conditions, to yield the target naphthyridine **79**. The second viable pathway (purple) involves elimination of dimethylamine from **85** generating the  $\alpha,\beta$ -unsaturated *E*-aldehyde **87**. **87** isomerizes to the corresponding *Z* aldehyde **88**, which sets all substituents in place for intramolecular cyclisation to hemiamidal **89**. **89** undergoes aromatization by the loss of a water molecule, and Boc-deprotection under acidic conditions, to form 4-chloroquinoline **79**.



**Scheme 22.** Proposed mechanisms for the one-pot transformation of *tert*-butylcarbamates to 1,8-naphthyridines.<sup>172</sup>

### 3.1.3. **N9**-substitued-6-aminoaryl-purines and **N**-substitued-4-imino-1,4-dihydro-pyridines

With the aim to introduce more structurally diverse scaffolds as part of the library, two more heterocyclic ring systems - purine and pyridine - were incorporated, giving rise to three additional structural analogues of WIN17317-3.

Purines consist of a pyrimidine ring fused to an imidazole ring; they are the most widely occurring nitrogen-containing heterocycles in nature, ubiquitous motifs of significant biomolecules such as adenine, guanine (nucleic acid bases), adenosine (neuromodulator) and adenosine triphosphate (ATP) (coenzyme-energy transfer) (Fig. 29).<sup>173</sup> The purine framework is found in drugs with various pharmacological activities such as caffeine (CNS stimulant, adjuvant analgesic), fludarabine and thioguanine (chemotherapeutics).

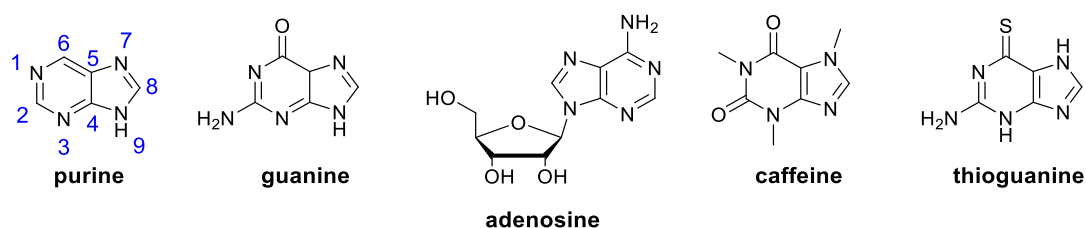
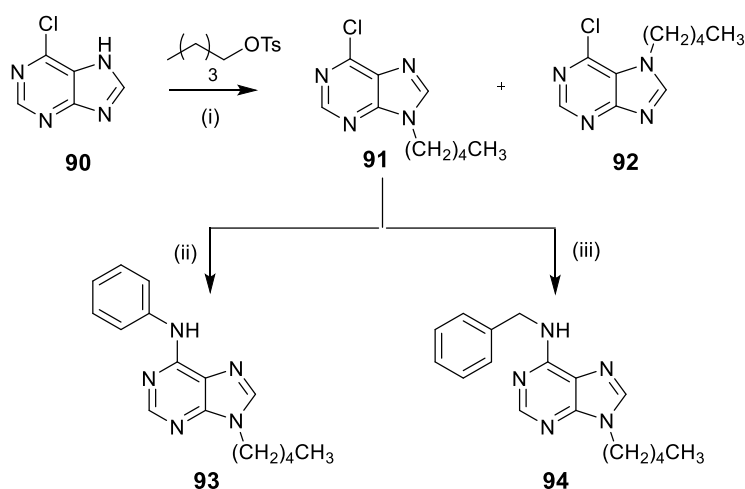


**Figure 29.** Structures of purine-containing biomolecules and drugs.

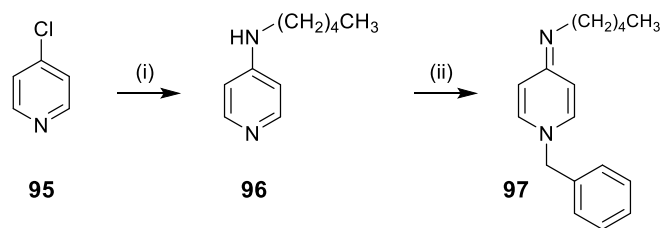
Two purine analogues **93** and **94** were synthesized *via* a two-step reaction sequence using commercially available 6-chloropurine (**90**) as the starting material (Scheme 23). Base promoted *N*-alkylation of purine **90**, as previously described in literature, afforded a mixture of two products: the *N7*-isomer **92** isolated in 13% yield, and the desired *N9*-isomer (**91**) constituting the major product isolated in 48% yield.<sup>174</sup> The increased polarity of the *N7*-isomer relative to its *N9* alkylated counterpart allowed separation of the two by standard flash chromatography on silica gel. Nucleophilic aromatic substitution in **91** by aniline and benzylamine afforded the final compounds **93** and **94** in 75% and 90% yields respectively.



**Scheme 23.** Synthesis of substituted purines **93** and **94**.

Reagents and conditions: (i) NaH, DMF, rt, 24 h, **91** → 48%, **92** → 13% (ii) Aniline, NEt<sub>3</sub>, *n*-pentanol, 110 °C, 24 h, 75% (iii) Benzylamine, EtOH, reflux, 3 h, 90%

Shifting away from a fused bicyclic core, analogue **97** featuring a 1,4-dihydropyridine scaffold was synthesized (Scheme 24). The halogen substitution - *N*-alkylation reaction sequence applied for the synthesis of iminodihydroquinolines (route A) was used (see Section 3.1.1.1). 4-chloroquinoline (**95**) was treated with *n*-pentylamine to afford 4-aminoalkylpyridine intermediate **96**, which was subsequently reacted with benzyl bromide under Finkelstein reaction conditions to afford the target compound **97** in an overall 32% yield.



**Scheme 24.** Synthesis of substituted pyridine **97**.

Reagents and conditions: (i) *n*-Pentylamine, 110 °C, 48 h, 51% (ii) Benzyl bromide, NaI, acetone, reflux, 8 h, 62%

### 3.2. Synthesis of an $^{18}\text{F}$ -labeled lead drug candidate

The synthesized compounds were submitted to pharmacological assays to determine their activity as  $\text{Na}_v$  inhibitors and as nociceptor blockers, with several members of the library found efficacious in blocking pain signaling (see Chapters 4 and 5). Appreciating the importance of an integrated PK/PD strategy in the drug development process, a selected compound from the library, **22**, designated as the 'lead,' was to be submitted in early pharmacokinetic profiling and safety pharmacology studies *in vivo* in rodents (Fig. 30).

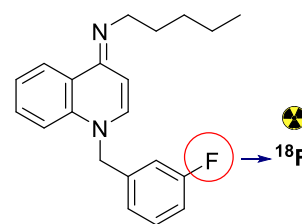


**Figure 30.** Lead structure **22** and the corresponding [ $^{18}\text{F}$ ]radiotracer.

Nuclear imaging methods, explicitly positron emission tomography (PET) and single-photon emission computed tomography (SPECT) are increasingly applied for the determination of the PK/PD properties of novel drug candidates.<sup>175</sup> Briefly portraying the methods' principles, a radioactive tag is inserted into the selected drug candidate; the radiolabeled molecule is subsequently administered to a living subject and is detected *in vivo* as a function of time, with high sensitivity and specificity by the appropriate nuclear imaging modality. The two modalities, PET and SPECT, vary on the type of radionuclides they can accommodate.

#### 3.2.1. The choice of radionuclide

In this event, the synthesis of an isotopically labeled version of lead compound **22** was pursued. Isotopically labeled tracers are labeled by replacement of the stable isotope of an element in the compound with the corresponding radionuclide; they thus retain all chemical and biological properties of the non-labeled molecule. The nature of the radionuclide incorporated, and hence the

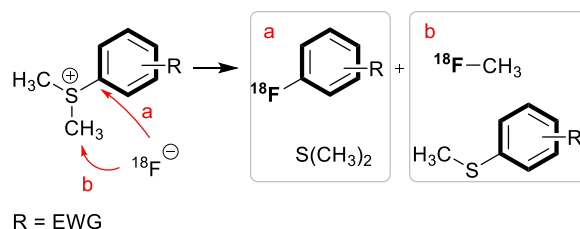


imaging modality employed, were therefore dictated by the chemical composition of **22**. Out of all possible isotopic substitutions (H, C, N, F), fluoride replacement by positron emitting fluoride-18 was selected for [ $^{18}\text{F}$ ]**22** imaging with PET. Fluoride-18, with a half-life of 110 min, offers a reasonable time frame for radiosynthesis, administration and visualization of the distribution and metabolism profile of the radiolabeled drug candidate *in vivo*, limiting unnecessary radiation burden.

### 3.2.2. The triarylsulfonium salt method for $^{18}\text{F}$ -labeling of aromatic compounds

Historically, direct [ $^{18}\text{F}$ ]fluorination of activated aromatic rings (containing electron-withdrawing groups, EWG), has been achieved by nucleophilic aromatic substitution ( $\text{S}_{\text{N}}\text{Ar}$ ) of one of the following leaving groups: trimethylammonium ( $-\text{NMe}^{3+}$ ), nitro ( $-\text{NO}_2$ ), halogen ( $-\text{F}$ ,  $-\text{Cl}$ ,  $-\text{Br}$ ), and sulfonium salts ( $-\text{SAr}_2^+$ ).<sup>176</sup> [ $^{18}\text{F}$ ]fluorination of electron neutral or non-activated aromatic rings, like the benzylic moiety of interest, has been diachronically challenging; the few methods reported require the use of palladium, nickel, and copper or hypervalent iodine complexes in procedures posing a number of practical difficulties and harsh reaction conditions.<sup>177</sup> The practical utility of such reactions for the preparation of biologically relevant  $^{18}\text{F}$ -labeled molecules remains to be demonstrated.

Sulfonium salts were first proposed as leaving groups for [ $^{18}\text{F}$ ] nucleophilic aromatic fluorination in the late 1980s; dimethylsulfonium ions were employed for the labelling



of strongly activated aromatic rings (Fig. 31).<sup>178</sup> Difficulties however in

synthesizing dimethylsulfonium derivatives of complex aromatic compounds, their high reactivity, and the formation of [ $^{18}\text{F}$ ]fluorination side products during labeling (methyl fluoride), made this a poor general method for the labeling of aromatic compounds with fluorine-18.

Two decades later, the method was reassessed, this time using diarylsulfonium leaving groups (Figure 32.B).<sup>179</sup> Triarylsulfonium salts exhibit high thermal and chemical stability and allow highly efficient labeling of activated aromatic rings. [ $^{18}\text{F}$ ]fluoride preferentially reacts at the most electron poor of the three sulfonium-substituted carbons. Our group exploited this reactivity trend further,

engineering novel electron rich sulfonium leaving groups bearing electron-donating spectator ligands (OMe, CH<sub>3</sub>) aiming to direct fluorination at non-activated, electron-neutral aromatic rings (Figure 32.C). The applicability of such sulfonium salts for the highly efficient and regioselective aromatic [<sup>18</sup>F]fluorination of non-activated aromatic scaffolds bearing drug-like functionalities has been demonstrated.<sup>180</sup>

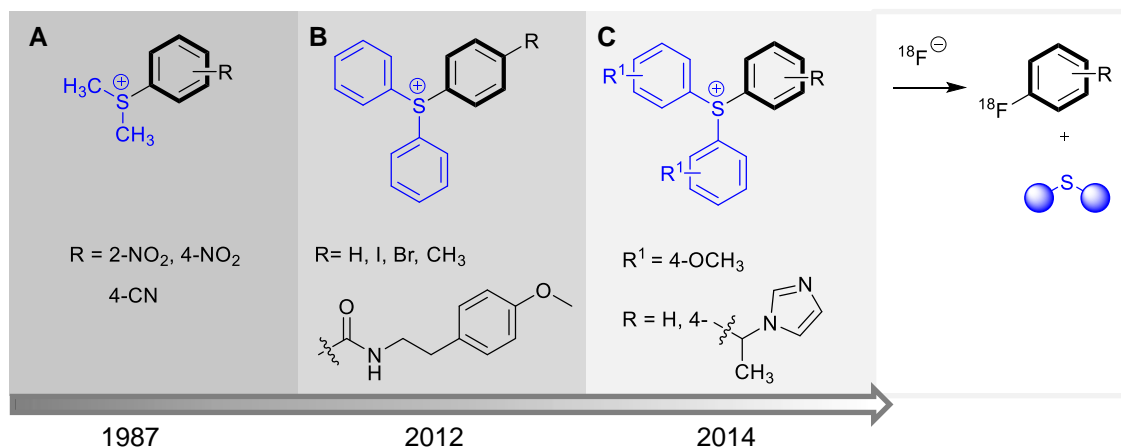
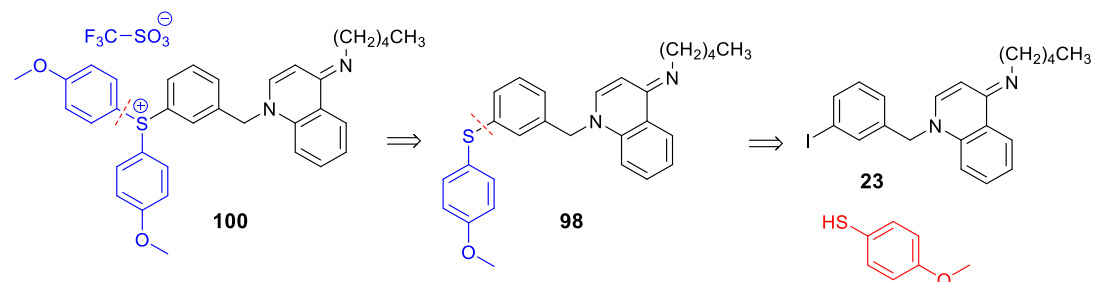


**Figure 32.** Timeline of sulfonium salt development as leaving groups for aromatic [<sup>18</sup>F]fluorination.

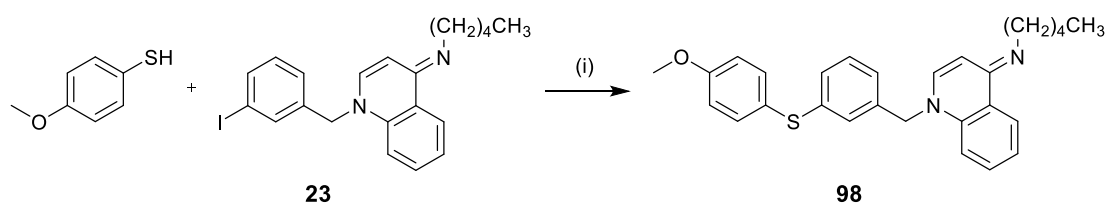
### 3.2.3. Synthesis of a triarylsulfonium salt precursor for aromatic <sup>18</sup>F-fluorination

Based on the above principle, triarylsulfonium salt **100** bearing a di(4-methoxyphenyl)sulfonium leaving group, was designed as the precursor for the <sup>18</sup>F-labeling of **22**. The retrosynthetic approach to **100** is illustrated in Scheme 25. According to this, sulfonium salt **100** could potentially be accessed *via* arylation of thioether **98**, which could in turn be obtained from the reaction of a suitably substituted aryl halide with 4-methoxythiophenol.



**Scheme 25.** Retrosynthetic analysis of triarylsulfonium salt **100**.

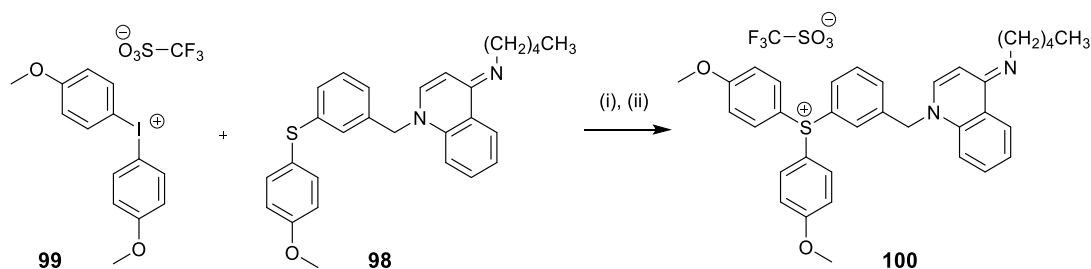
The first step in the sequence involved the preparation of thioether **98**. Amongst multiple routes explored,<sup>181</sup> palladium-catalysed cross coupling of aryl iodide **23** with (4-methoxy)thiophenol was proved to be the most efficient and reliable route to **98** (Scheme 26).<sup>182</sup> Full conversion of starting materials to product was essential as **23** and **98** exhibited similar retention factors meaning the two were inseparable by standard chromatographic means. The iodinated iminodihydroquinoline **23** was synthesized *via* *N*-alkylation of 4-pentylaminoquinoline (**9**) as described in section 3.1.1.1 (page 43).



**Scheme 26.** Synthesis of thioether **98**.

Reagents and conditions: (i) Pd<sub>2</sub>dba<sub>3</sub> (cat., 1%), bis[(2-diphenylphosphino)phenyl] ether, *t*BuOK, toluene, reflux, 3 h, 63%

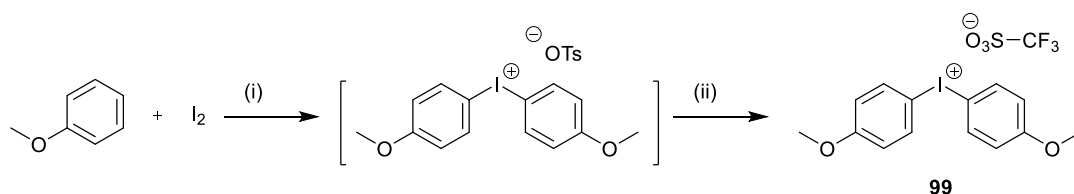
A highly versatile method recently developed by the group was employed for the synthesis of triarylsulfonium salt **100** (Scheme 27).<sup>183</sup> The functionalized thioether **98** was reacted with a diaryliodonium triflate salt under copper(II) catalysis, an approach first introduced by Crivello *et al.*<sup>184</sup> According to our group's advanced method, the imine functionality was masked prior to reaction by protonation using triflic acid, avoiding coordination with the copper(II) hence allowing the reaction to proceed. Gratifyingly, the corresponding triflate salt of **98** reacted cleanly with bis(4-methoxyphenyl)iodonium triflate affording the desired sulfonium salt **100** in 32% yield. **100** was isolated by column chromatography on silica gel in high purity. To enable labeling, the free base was liberated after purification using aqueous sodium hydroxide.



**Scheme 27.** Synthesis of triarylsulfonium salt **100**.

Reagents and conditions: (i) TFSA, Cu(II)benzoate, chlorobenzene, reflux, 2 h (ii) NaOH (2M), basic workup, 32%

The diaryliodonium salt reagent **99** used in the reaction above, was synthesized according to a previously described procedure (Scheme 28).<sup>185</sup> The one-pot synthesis involved reaction of anisole with elemental iodine and 3-chloroperoxybenzoic acid (*m*CPBA) and tosic acid as the oxidizing agent to afford an iodonium tosylate intermediate; this which was subsequently treated with triflic acid, to afford by *in situ* anion exchange, the desired iodonium triflate **99** in 80% yield.

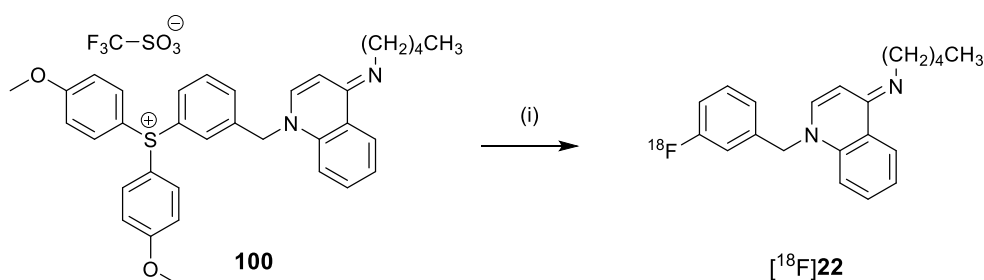


**Scheme 28.** Synthesis of di(methoxyphenyl)iodonium triflate, **99**.

Reagents and conditions: (i) *m*CPBA, TsOH, DCM, 40 °C, 15 min (ii) TfOH, rt, 1 h, 80%

### 3.2.4. Radiolabeling of [ $^{18}\text{F}$ ]22

Screening of bases and solvents commonly used for nucleophilic [ $^{18}\text{F}$ ]fluoride substitution reactions, revealed potassium bicarbonate and dimethyl sulfoxide (DMSO) to be optimal for triarylsulfonium salt labeling, in a study performed by Dr. Kerstin Sander.<sup>180</sup> [ $^{18}\text{F}$ ]fluorination of **100** was performed under these optimized established reaction conditions (Scheme 29).<sup>180</sup> According to these (5 mg precursor, 0.5 ml DMSO, 120 °C, 15 min), sulfonium salt **100** was reacted with dried [ $^{18}\text{F}$ ]fluoride to give [ $^{18}\text{F}$ ]22 in 47% analytical radiochemical yield (RCY) and 30% decay-corrected isolated RCY.



**Scheme 29.** Labeling of [ $^{18}\text{F}$ ]22.

Reagents and conditions: (i) [ $^{18}\text{F}$ ]F<sup>-</sup>, KHCO<sub>3</sub>, K<sub>222</sub>, DMSO, 15 min, 120 °C, analytical RCY: 47 ±6%, decay-corrected isolated RCY: 30 ±6%, (±SD) (*n* = 6).

The identity of the radiochemical product [ $^{18}\text{F}$ ]22 was confirmed by co-elution with the non-radioactive analogue **22** (Fig. 33).

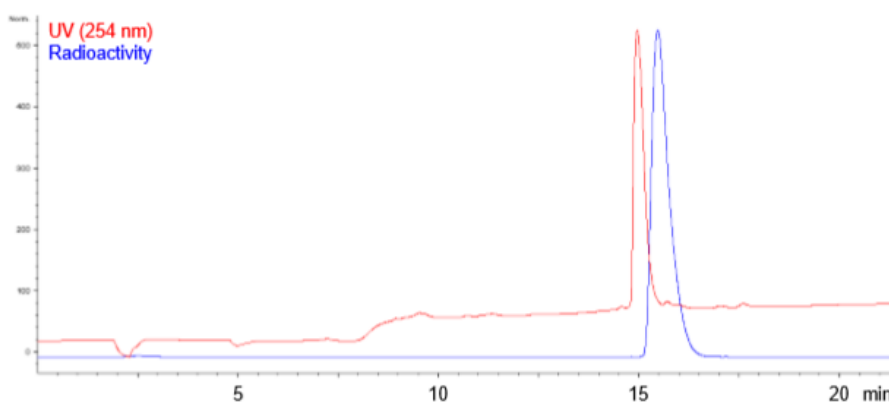


**Figure 33.** HPLC chromatogram of the isolated compound [ $^{18}\text{F}$ ]22, co-injected with the non-labelled reference **22**.

## 4. Sodium Channel Blockade by WIN17317-3 Analogues (*in Vitro*)

One of the key objectives of this study, as discussed in chapter 1 (page 32), was the elucidation of the structure-activity requirements of 4-iminodihydroquinolines for blocking Na<sub>v</sub> isoforms, in particular Na<sub>v</sub>1.7. In this chapter, the human Na<sub>v</sub> blocking efficiencies of iminodihydroquinolines, as measured in automated patch clamp electrophysiology assays, are described. The first ever pharmacophore model for the iminodihydroquinoline class at Na<sub>v</sub>s is defined.

### 4.1. Electrophysiological assays, and their use, for measuring Na<sub>v</sub> activity

Multiple functional assays have been developed for studying the function and pharmacology of Na<sub>v</sub> channels (ion flux, fluorescent dyes, radioligand binding, patch clamp) exploiting either the actual Na<sup>+</sup> ion flux across the cell membrane or the concomitant transient changes in membrane potential.<sup>186</sup> Out of these, the electrophysiological patch clamp technique has progressively stood out as the gold standard.<sup>187</sup> The technique is a refinement of the traditional voltage clamp method, developed by Erwin Neher and Bert Sakmann in 1976, for which they were awarded the Nobel Prize in Physiology or Medicine in 1991.

In a simplified description of the method's principles, a patch of membrane is electrically isolated from the external solution by pressing a glass pipette, filled with an electrolyte solution, against the surface of the cell (Fig. 34.A). By applying light suction, a seal is formed (electrical resistance >10 GΩ), with the glass pipette and the cell membrane being less than 1 nm apart. Currents fluxing through the channel(s) in this patch flow into the pipette and are recorded by an electrode connected to a highly sensitive differential amplifier. To prevent alterations in the membrane potential, a compensating current that resembles the current flowing through the membrane is generated by the amplifier as a negative feedback mechanism and injected into the cell. The current is recorded, allowing conclusions to be drawn regarding the membrane conductance. The advantage of this method is that the membrane potential can be precisely controlled independent of the fluxing

ionic currents. Patch clamp is the only available method suitable for investigating the function of channels at specific voltage states (resting, open inactivated).

Despite its ubiquitous use in academic research for drug discovery, the technique holds significant drawbacks. It has low throughput, it is labor intensive and requires highly skilled operators, all factors making it not amenable to screening large compound libraries. The recent development of automated patch electrophysiology technologies in the last decade has resolved these issues and has since revolutionized the field of ion channel research allowing the screening of hundreds of compounds per day.<sup>188</sup>

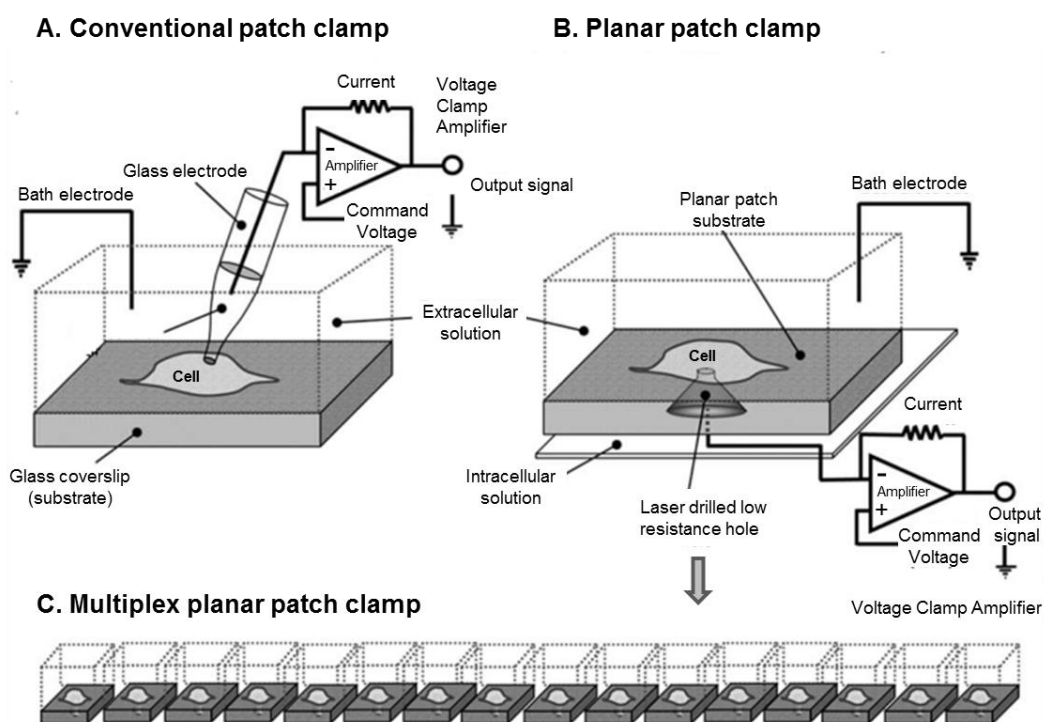


**Figure 34.** Schematic representation of the general features of a conventional patch clamp chip (A) and a planar patch clamp chip (B). (C) Illustration of a 16 well planar patch clamp configuration allowing parallel patch clamping. Adapted from reference 189.<sup>189</sup>

Automated patch clamp assays share the principles of the manual method, yet the experimental set up was adapted to allow automation. The traditional glass pipette has been replaced by a planar plastic substrate in what are named as planar patch screening platforms. The planar substrate is perforated with small micron-sized holes mimicking the tip of the glass electrode (Fig. 34.B). An automated liquid handling device is used to deliver both cells and test compounds into the planar patch clamp chip and a mobile electronic head stage is automatically positioned into the wells to establish the voltage-clamp and record fluxing currents.

Five planar system platforms have been commercialized to date; QPatch (Sophion Bioscience), PatchXpress (Molecular Devices), IonWorks -HT, -Quattro, -Barracuda (Molecular devices), Patchliner (Nanon Technologies), and Cytospatch (Cytocentrics), with divergent chip constructions and technologies resulting in differences in the compound throughput capacity and the quality of data obtained from each one. An in depth description of the available automated planar-array electrophysiology platforms can be found in the review by Dunlop *et al.*, as well as a comparison of those to the conventional patch clamp method.<sup>190</sup>

In this study, the Na<sub>v</sub> screening assay employed was selected on the basis of the following considerations: (a) cost- and (b) time-efficiency, given the large number of compounds to be screened, and (c) consistency/reproducibility as subsets of the compound library would be tested sequentially in different runs/time periods. After examining all possible options, the assay was decided to be outsourced to Cambridge Bioscience<sup>®</sup>, in collaboration with a U.S. company, ChanTest<sup>®</sup> Corporation. In consultation with one of Chan Test's<sup>®</sup> ion channel expert scientists, the IonWorks Quattro<sup>™</sup> planar electrophysiology platform was selected.

## 4.2. The IonWorks Quattro screening platform

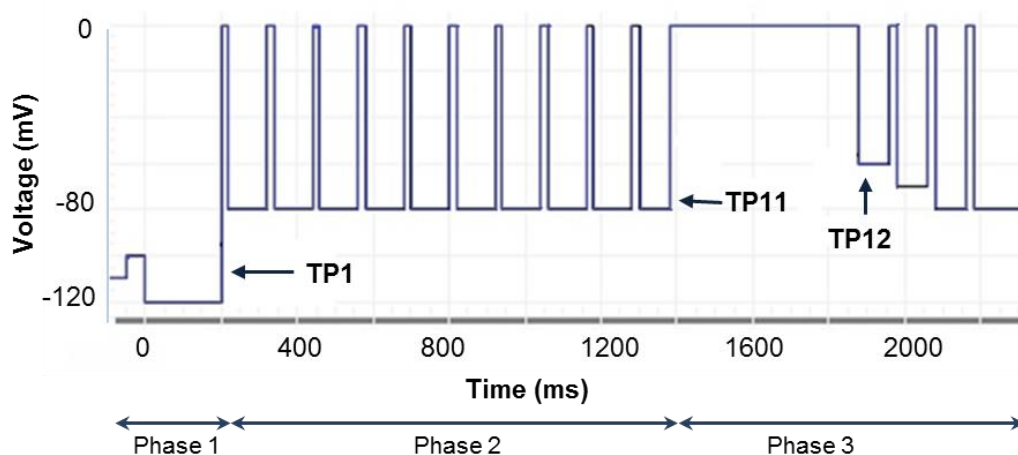
IonWorks Quattro<sup>™</sup> (IWQ) is the screening platform with the highest compound throughput (up to 10,000 data points per day), each plate being a multiplex of 384 individual chips.<sup>191</sup> Each chip has 64 engraved cavities (population patch chip, PPC) meaning up to 64 cells can be simultaneously sealed and voltage clamped. This statistically increases the probability of forming a viable seal and hence successfully recording a data point from a chip. Indeed, more than 95% success rate is associated with IWQ in terms of data point collection. Furthermore, the PCC chip allows averaging of cell-to-cell variations in current amplitude and therefore accounts for cell variability factors in the current measurement.<sup>192</sup> The use of the IWQ platform for studying the pharmacology of Na<sub>v</sub> channels has been validated.

Despite the high throughput and high success rate, the IWQ platform holds certain limitations. It is the only one of the newly automated systems incapable of GΩ seals, although the measurements show good consistency with manual patch clamp data. It is incapable of performing ligand application with simultaneous voltage clamping, a significant drawback in particular for slowly desensitizing ligand-gated channels. Lastly, in certain studies examining the effects of highly lipophilic



compounds right-shifting of activities has been observed (higher  $IC_{50}$ s), which was attributed to compounds adhering to the plastic surface of the plate.<sup>193</sup>

For the purpose of this study, the IWQ platform was operated at a voltage protocol validated for evaluating the state-dependent interactions of pharmacological agents with human  $Na_v1.7$  channels cloned in Chinese hamster ovarian (CHO) cells (Fig. 35). The protocol consists of a series of depolarizing pulses delivered at precise time intervals.



$$\%Block = (1 - I_{TPX, CPD} / I_{TPX, Control}) \times 100\%$$

**Figure 35.** Voltage protocol for measuring  $hNav1.x$  blockade. The test pulse (TP) pattern was repeated twice: before (-control) and 5 minutes after compound (cpd) addition. The peak current amplitudes at  $TP_1$ ,  $TP_{11}$  and  $TP_{12}$  were measured and used for calculating the percentage inhibitions at resting and inactivate states, and use-dependency respectively. Four replicates were performed for each compound concentration tested. Lidocaine (3 mM) and DMSO (0.3%) were included in each plate as positive and negative control, respectively.

The voltage protocol consists of three phases of stimulation. During phase 1, the membrane is hyperpolarized from -80 mV (holding potential) to -120 mV, at which potential the  $Na_v1.7$  isoform is known to completely recover from inactivation. A single pulse ( $TP_1$ ) is subsequently applied, allowing the measurement of tonic block, mainly reflecting the effect of drug binding to channels in the resting state. The maximum depolarization-evoked current for  $Na_v1.7$  occurs at  $\sim 0$  mV. During phase 2, a train of short pulses ( $TP_1 - TP_{10}$ ) is applied at 10 Hz frequency serving as the conditioning step for assessing use-dependent inhibition at  $TP_{11}$ . At the same time,  $TP_{11}$  serves as the long inactivating conditioning pulse for assessing inactivation-dependent inhibition at phase 3. After a brief stop at -60 mV which is the

midpoint of  $\text{Na}_v1.7$  steady-state inactivation, to allow partial recovery of unblocked channels from inactivation, inactivation-dependent inhibition is measured at TP12.

The test pulse protocol of Figure 35 was successful in determining the state- and use-dependent block induced by lidocaine at  $h\text{Na}_v1.7$  (Fig. 36). In addition, the pufferfish toxin TTX produced similar levels of block at all three phases consistent with previous findings demonstrating that this is insensitive to changes in membrane potential or channel gating.

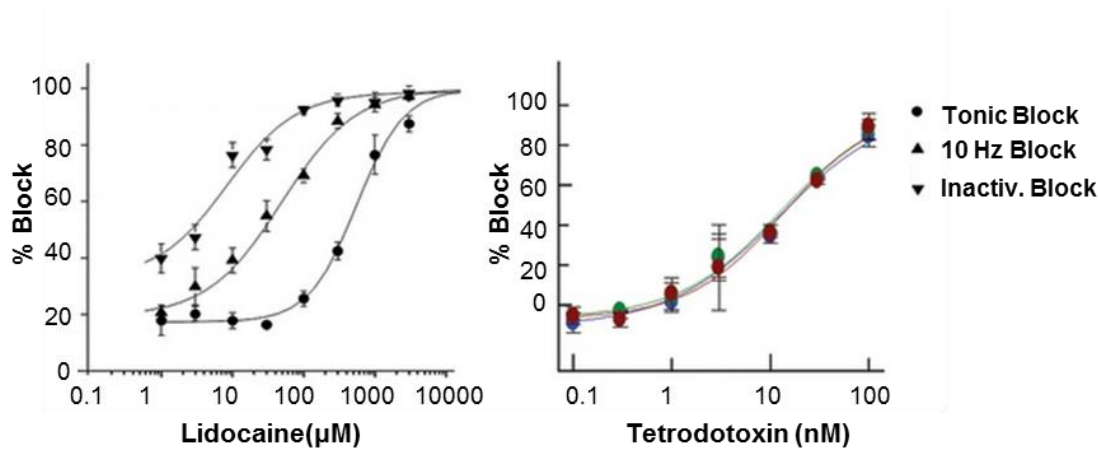
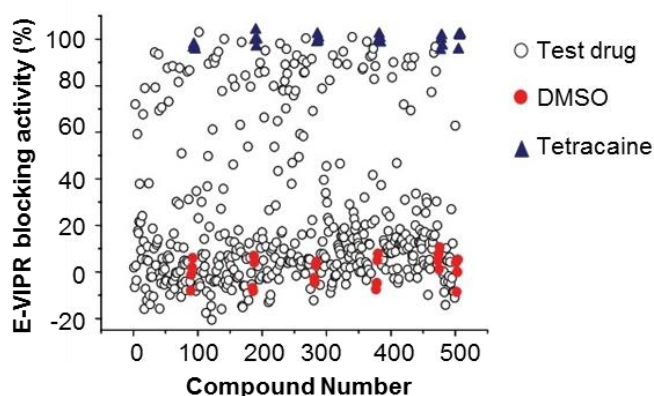


**Figure 36.** Concentration-response relationships for lidocaine and TTX at  $h\text{Na}_v1.7$  measured using the IWQ platform operated at the voltage protocol of Fig. 35.  $\text{IC}_{50}$  values for lidocaine were 548  $\mu\text{M}$ , 49  $\mu\text{M}$  and 8  $\mu\text{M}$  for the tonic, frequency-dependent and inactivated states respectively. Data are presented as mean  $\pm$  SD ( $n = 3-5$ ). TTX produced similar concentration-response curves at all three voltage states.

The  $\text{Na}_v$  screening of all first generation iminodihydroquinoline analogues, described in this chapter, was performed at the IWQ platform. From September 2013, ChanTest<sup>®</sup> replaced IWQ with a higher efficiency second generation IonWorks instrument, the IonWorks<sup>™</sup> Barracuda (IWB). Whilst IWQ records from 48 recording wells at a time, the IWB allows recordings from all 384 wells at once. Furthermore IWB supports recordings during compound addition, but does not allow wash out of ligands, which reduces the efficiency for investigating ligand-gated ion channels since only one concentration per recording well can be obtained.<sup>191</sup> The second generation iminodihydroquinoline analogues, the  $\text{Na}_v$  characterization of which is described in chapter 5.4, were tested at the IWB platform.

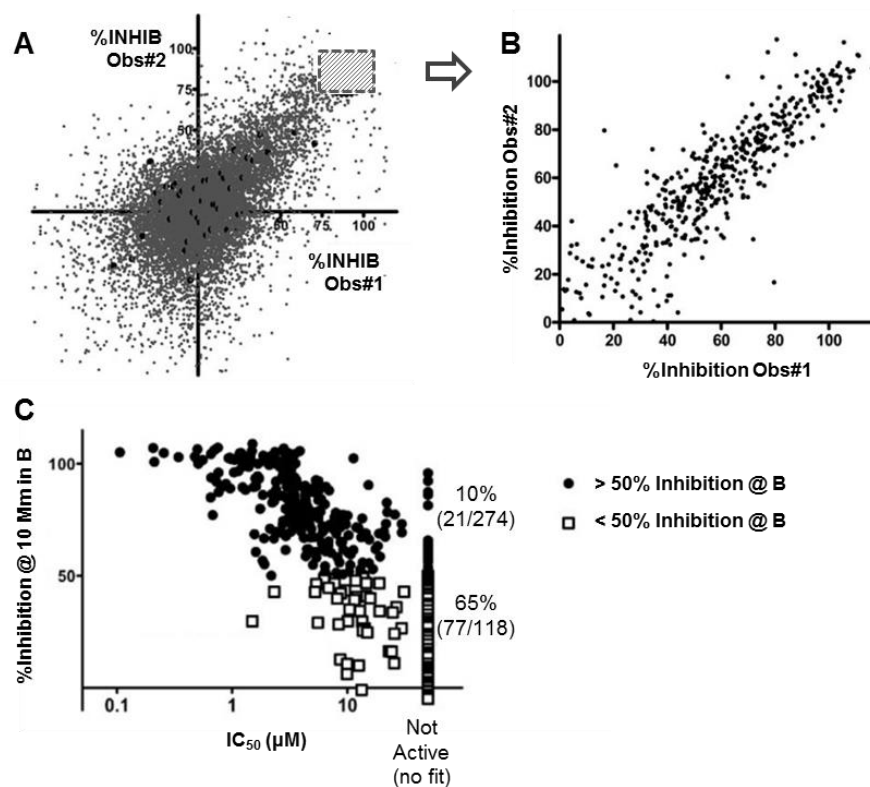
### 4.3. Evaluation of a two concentration-response point approach for screening $\text{Na}_v$ activity using IonWorks Quattro

Given the high cost of automated patch clamp electrophysiology assays (3900 GBP per IonWorks plate), a cost-efficient yet meaningful approach for screening our compound library with the minimum possible number of plates was required. After a search in literature, several studies were identified which used only one concentration-response point per compound for characterizing the  $\text{Na}_v$  activity of large compound libraries. One such example is the study by Huang *et al.* where 400 known drugs were screened at 10  $\mu\text{M}$  concentration against  $h\text{Na}_v1.3$  using a novel technology platform called the electrical stimulation voltage ion probe reader (E-VIPR); based on the percentage of  $h\text{Na}_v1.3$  inhibition produced, compounds were classified as  $h\text{Na}_v1.3$  blockers or not (Fig. 37).



**Figure 37.** Screening results of 400 known drugs for blocking activity against  $h\text{Na}_v1.3$  at 10  $\mu\text{M}$  using E-VIPR. Each plate contained four negative (DMSO, red) and four positive (100 mM tetracaine, blue) controls. Drug-blocking activity was calculated according to the two controls, with hits defined as compounds producing more than 60% of the tetracaine block. Adapted from reference 194.<sup>194</sup>

The applicability of a similar screening approach using the IWQ platform has recently been assessed, as part of a study evaluating the use of automated patch clamp electrophysiology assays in  $\text{Na}_v$  channel drug discovery.<sup>189</sup> 12,000 compounds were screened for their blocking activity against  $h\text{Na}_v1.7$  at 10  $\mu\text{M}$  concentration, with hits defined as compounds producing greater than 80% inhibition in two consecutive experiments (Fig. 38.A).

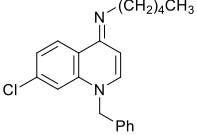
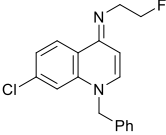
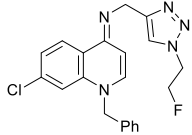


**Figure 38.** (A) Percentage inhibition of  $hNa_v1.7$  channels by ~12,000 compounds (grey dots) tested at 10  $\mu\text{M}$  in duplicate (Obs1 and Obs2) (Pearson  $r$  correlation coefficient = 0.66,  $r^2 = 0.44$ ,  $P < 0.0001$ ). (B) Compounds producing greater than 80% inhibition (square with dashed border) were re-evaluated at 10  $\mu\text{M}$  in duplicate (Pearson  $r$  correlation coefficient = 0.86,  $r^2 = 0.75$ ,  $P < 0.0001$ ). (C) Plot of  $IC_{50}$ s, calculated from 8-point concentration-response curves, versus the percentage inhibition produced at 10  $\mu\text{M}$  as determined from B. Compounds producing >50% inhibition at 10  $\mu\text{M}$  in study B are depicted in black circles whilst those producing <50% are illustrated with open squares. Adapted from reference 189.<sup>189</sup>

Unfortunately, when re-submitting the selected hits to the same assay for confirmation purposes, although correlation between duplicate observations was largely improved compared to the primary screen, there was an unexpected change in the compounds' levels of inhibitions ranging from 5-80% (Fig. 38.B). Interestingly, the %inhibitions at 10  $\mu\text{M}$  at this follow up study were found to correlate well with subsequently measured  $IC_{50}$ s for the compounds (Fig. 38.C). The most potent compounds,  $IC_{50}$ s less than 1  $\mu\text{M}$ , exhibited more than 80% inhibition at 10  $\mu\text{M}$ . In contrast, more than 90% of the compounds showing less than 50% inhibition at 10  $\mu\text{M}$  were either inactive or had  $IC_{50}$ s greater than 10  $\mu\text{M}$ . This led us to conclude, that provided there is high confidence in the accuracy of the single concentration measurement, this can indeed be predictive of the relative blocking activity ( $IC_{50}$ ) of a compound.

Inspired by the findings of the study described above, a novel screening approach was designed for evaluating the  $\text{Na}_v$  activity of WIN17317-3 analogues. The concentration-response relationships of WIN17317-3 and two of its structural analogues, **116\*** and **118\***, were previously described using IWQ, as part of a study conducted by the Årstad group investigating novel  $\text{Na}_v$  blockers as tracers for imaging fast neurotransmission. All compounds in this thesis given a star annotation were synthesised by PDRA Dr. Carlos Medina-Perez.  $\text{IC}_{50}$  values for the three compounds were calculated from 8-point concentration response curves (4 replicates per data point) as shown in Table 10.

**Table 10.** Concentration-response relationships and characterization of **WIN17317-3**, **116\*** and **118\*** at  $h\text{Na}_v1.7$ .

Compound	WIN17317-3	116*	118*
Structure			
Concentration ( $\mu\text{M}$ )	% Channel block $\pm$ SD* (n=2-4)		
0.03	7.5 $\pm$ 1.5	-0.2 $\pm$ 14.6	-9.2 $\pm$ 5.0
0.1	31.3 $\pm$ 12.1	6.8 $\pm$ 3.6	-6.0 $\pm$ 4.2
0.3	65.7 $\pm$ 6.9	13.0 $\pm$ 4.6	-12.0 $\pm$ 12.5
1	74.6 $\pm$ 16.4	42.2 $\pm$ 11.3	8.9 $\pm$ 1.4
3	76.8 $\pm$ 4.7	36.8 $\pm$ 3.5	-1.2 $\pm$ 8.2
10	92.9 $\pm$ 2.9	60.7 $\pm$ 2.2	14.4 $\pm$ 3.1
30	100.1 $\pm$ 6.4	80.0 $\pm$ 13.0	29.6 $\pm$ 11.6
100	106 $\pm$ 2.6	88.9 $\pm$ 9.4	63.0 $\pm$ 12.2
$\text{IC}_{50}$ ( $\mu\text{M}$ )	0.21 $\pm$ 0.05	3.6 $\pm$ 0.98	54.8 $\pm$ 6.2
Potency	High	Moderate	Low
Potency score	II	I	0

\*Peak current at tonic state

On examining the dose-response data for the three iminodihydroquinolines, (*vide supra*) as well as the data of the Castle *et al.* study (Fig. 38), specific correlation trends became apparent between the percentage inhibitions produced at two concentrations, 1  $\mu\text{M}$  and 10  $\mu\text{M}$ , and the compounds'  $\text{IC}_{50}$ s. Based on this, it was decided for test compounds to be screened only at 1  $\mu\text{M}$  and 10  $\mu\text{M}$  concentrations and according to the %inhibitions produced, to estimate their  $\text{Na}_v$  blocking potency.

More specifically, guided by the above findings, the classification criteria for predicting the potency of compounds based on the %Na<sub>v</sub> block at 1 and 10 μM were set as:

- i) > 50% block at 1 μM, and >80% at 10 μM → Highly potent
- ii) 15-50% block at 1 μM and >50% at 10 μM → Moderately potent
- iii) < 15% block at 1 μM, and <50% at 10 μM → Inactive
- iv) Compounds failing to fulfil any of the above → Outliers

By measuring two points at the concentration-response curve, each being an average of four experiments, and by setting the double set of criteria for potency classification, compound misassignment due to experimental errors could be effectively reduced. Along these lines, the synthesised iminodihydroquinoline analogues were screened against *h*Na<sub>v</sub>1.7, at 1 μM and 10 μM concentrations, and were classified as highly or moderately potent *h*Na<sub>v</sub>1.7 blockers, as inactive or as outliers (Fig. 39).

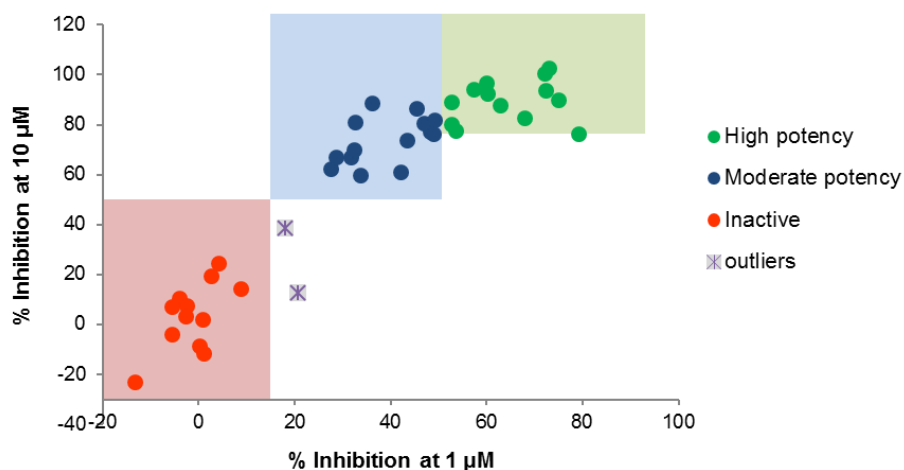


**Figure 39.** Screening of 41 first generation iminodihydroquinoline analogues against *h*Na<sub>v</sub>1.7. Plot of %tonic inhibitions obtained at 1 μM and 10 μM concentrations. According to the pre-defined set of criteria compounds were classified as highly potent (green, 13 cpds), as moderately potent (blue, 14 cpds) as inactive (red, 12 cpds) or as outliers (grey, 2 cpds).

The IC<sub>50</sub> values for 20 of the iminodihydroquinoline analogues screened were subsequently measured in order to (a) evaluate the validity of the two-point screening method for predicting the Na<sub>v</sub> activity of test compounds and (b) define the range of IC<sub>50</sub>s anticipated for each of the activity categories set above. IC<sub>50</sub> values were calculated from 8-point concentration-response curves, measured at the IWQ using the same cell line and voltage protocol as for the screening study.

$IC_{50}$ s for compounds from all three potency categories were measured. These were plotted alongside the %inhibitions produced at 1  $\mu$ M and 10  $\mu$ M as illustrated in Figure 40. Two out of the four compounds examined from the 'inactive' category exhibited  $IC_{50}$ s higher than 100  $\mu$ M and are therefore not included in the graph. Gratifyingly, linear correlation was observed between the three variables suggesting that the inhibitions at the two concentrations are indeed predictive of the  $IC_{50}$  values of compounds.

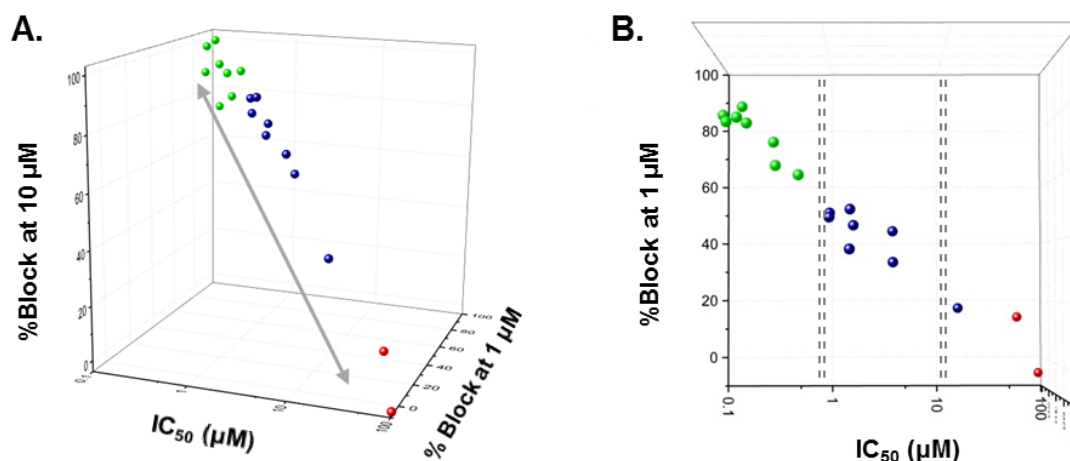


**Figure 40.** 3D Plot of  $hNa_v1.7$   $IC_{50}$ s versus %tonic inhibitions measured at 1  $\mu$ M and 10  $\mu$ M concentrations. (A) Side view and (B) top view. Compounds are classified as potent (●), moderately potent (●) or inactive (●) according to the results of the screening at 1 and 10  $\mu$ M and the predefined set of criteria. The % inhibitions at 1  $\mu$ M and 10  $\mu$ M shown, were part of the 8 point concentration-response curves used for determining the compounds'  $IC_{50}$ s.

As clearly illustrated above, the  $IC_{50}$  values for the three activity categories can be divided in three concentration ranges, each being one order of magnitude apart. More specifically, the defined activity categories were found to correspond to the following  $IC_{50}$  values:

- a) highly potent  $\rightarrow IC_{50} < 1 \mu$ M
- b) moderately potent  $\rightarrow 1 \mu$ M  $< IC_{50} < 10 \mu$ M
- c) inactive  $\rightarrow IC_{50} > 10 \mu$ M.

The results of the study demonstrate that the suggested two concentration screening approach can successfully predict the relative blocking activity of iminodihydroquinoline analogues at  $Na_v$ s. The method is particularly useful in the context of this work where a new pharmacophore model is being built and qualitative information is initially sought for defining the acceptable substitution patterns at the active site.

#### 4.4. Investigation for state- and use- dependency

In the paper by Wanner *et al.*, first describing the effects of WIN17317-3 at  $\text{Na}_v$ s, WIN17317-3 was reported as a highly potent state-dependent  $\text{Na}_v$  blocker; in electrophysiological experiments using CHO cells transfected with rat brain  $\text{Na}_v$ s, WIN17317-3 exhibited higher affinity for inactivated channels ( $K_D = 9.3$  nM) compared to channels in the resting state ( $K_D = 310$  nM).<sup>132</sup>

The iminodihydroquinoline analogues were submitted to the voltage pulse protocol of section 4.2 (page 68) aiming to access information regarding their state and use-dependency at  $h\text{Na}_v1.7$ . Higher levels of inhibition were anticipated for the 10 Hz and inactivation states than for the tonic state. The data obtained for each of the three voltage-states were analyzed separately as plotted in Figure 41. For each state, compounds were classified as potent, moderately potent, inactive, or outliers according to the previously defined set of criteria.

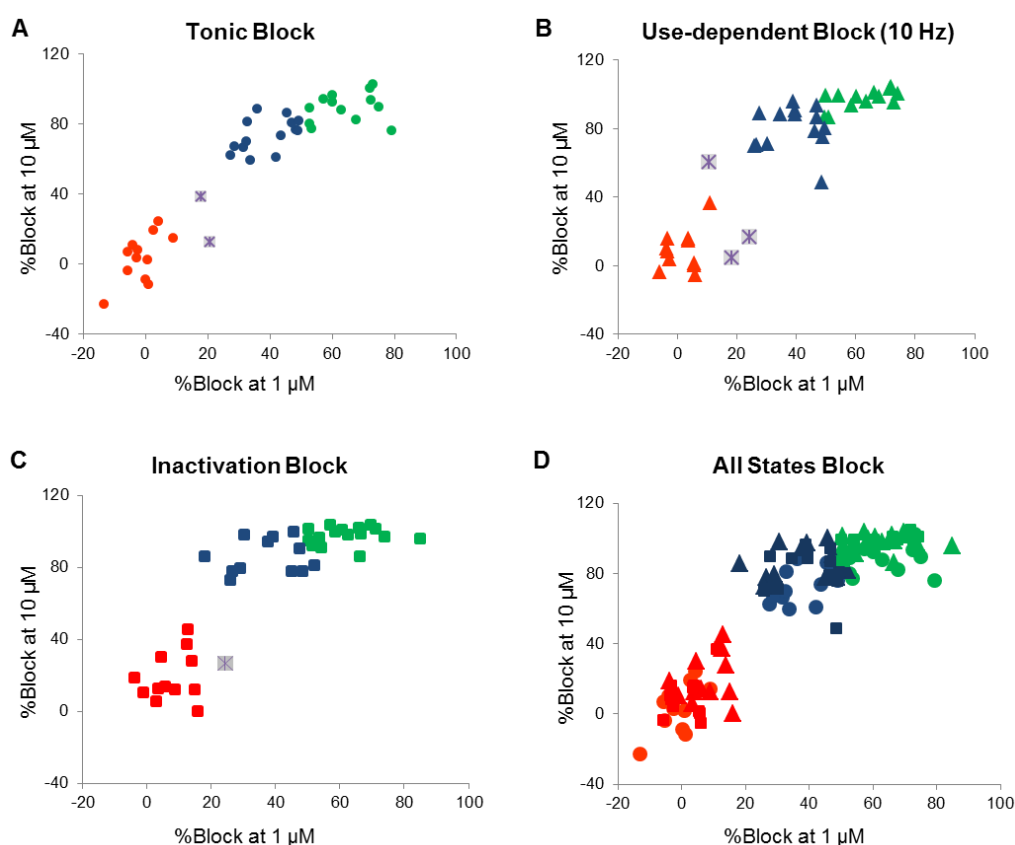


**Figure 41.** Plots of tonic (A), use-dependent (B) and inactivation blocks (C) of first generation analogues against  $h\text{Na}_v1.7$  at 1  $\mu\text{M}$  and 10  $\mu\text{M}$  concentrations. According to the defined set of criteria compounds were classified as highly potent (green), as moderately potent (blue), as inactive (red), or as outliers ( $\boxplus$ ). (D) Superposition of the data from all three blocking states showed no apparent differences amongst them.

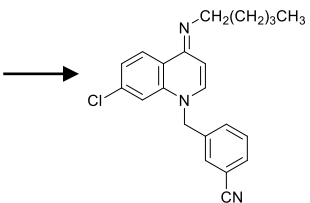
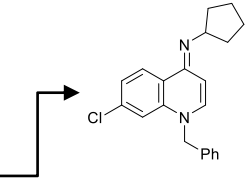
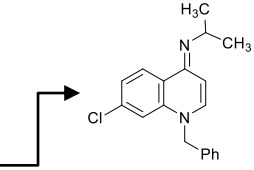
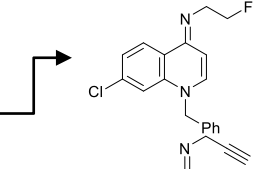
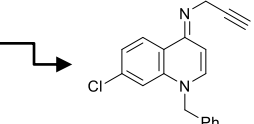


Unexpectedly, no apparent differences were observed between the relative levels of inhibition exerted by compounds amongst the three states (Fig. 41). Although compounds showed a tendency for higher potency blockade (shift towards the right top corner) when subjected to the use-dependent and inactivation voltage pulses relative to tonic block, superposition of the three graphs revealed no clear differences amongst them. All compounds classified as inactive or outliers, with the exception of one, failed to produce activity at all three investigational states. Likewise, the vast majority of compounds exhibiting moderate or high potency showed similar levels of inhibition in the three states hence had identical activity classification at all three voltage states.

The  $IC_{50}$  values for 20 iminodihydroquinoline analogues, as measured from 8-point concentration-response curves, were also examined at the voltage states under investigation (Table 11). A two-fold difference between  $IC_{50}$ s was set as the minimum requirement for classifying a compound as having a preference for any particular state. Disappointingly, in agreement with the findings of the screening study, WIN17317-3 (**1**) was found to exhibit equal blocking potencies in all three states and so did most of the iminodihydroquinoline analogues explored. Only four compounds, **111\***, **114\***, **116\***, and **117\***, appeared to show a preference for the inactivated state and use-dependency. Notably, all four have small and compact *N*-1 imino substituents ( $R^1$ ). One compound, **102\***, was found to exhibit higher potency blockade for resting channels than channels in the other two states.

Given the previously published manual patch clamp data for WIN17317-7's effects at  $Na_v$ s, it was considered highly unlikely for this to lack state- and use-dependency. It was instead considered plausible that the absence of selectivity amongst the three voltage states observed in this study could be related to an experimental limitation of the assay used; for example, the voltage-potential and test pulse protocol employed could be poorly suited for measuring the state-dependent interactions of this compound class with  $Na_v$ s. Further manual patch clamp experiments are required to clarify this result.

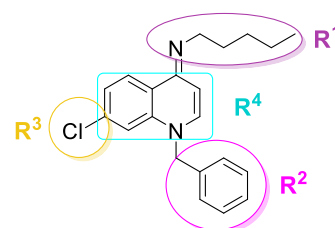
**Table 11.** IC<sub>50</sub> values of first generation iminodihydroquinoline analogues for *h*Na<sub>v</sub>1.7 channels at tonic-, 10 Hz- and inactivated- voltage states. The structures of compounds exhibiting preference for a particular voltage state/s over other/s are illustrated to the right.

Compound	IC <sub>50</sub> ±SE (μM)			Structure
	Tonic	10 Hz	Inactivated	
1	0.21 ± 0.05	0.22 ± 0.03	0.23 ± 0.04	
2	0.22 ± 0.04	0.27 ± 0.04	0.34 ± 0.05	
101*	0.42 ± 0.06	0.62 ± 0.10	0.74 ± 0.14	
102*	0.64 ± 0.08	1.2 ± 0.19	1.2 ± 0.29	
103*	1.6 ± 0.20	1.4 ± 0.22	1.2 ± 0.29	
104*	0.18 ± 0.03	0.22 ± 0.04	0.24 ± 0.05	
105*	0.16 ± 0.03	0.20 ± 0.03	0.21 ± 0.04	
106*	1.6 ± 0.40	1.9 ± 0.60	1.6 ± 0.74	
107*	94.4 ± 9042*	38.1 ± 471*	21.4 ± 10.6	
108*	0.25 ± 0.04	0.34 ± 0.05	0.40 ± 0.08	
109*	1.1 ± 0.19	1.3 ± 0.28	1.5 ± 0.48	
110*	13.8 ± 3.9	16.4 ± 4.5	18.5 ± 4.9	
111*	1.7 ± 0.26	0.36 ± 0.05	0.43 ± 0.06	
112*	>100	>100	>100	
113*	>100	91.3 ± 16.3	85.9 ± 9.6	
114*	3.6 ± 0.78	2.0 ± 0.40	1.9 ± 0.47	
115*	0.39 ± 0.10	0.41 ± 0.08	0.42 ± 0.10	
116*	3.6 ± 0.98	1.8 ± 0.48	1.6 ± 0.62	
117*	1.1 ± 0.16	0.63 ± 0.09	0.47 ± 0.09	
118*	54.8 ± 6.2	51.2 ± 6.7	44.6 ± 8.9	

\*IC<sub>50</sub> value determined based only one concentration

## 4.5. Structure-Activity Relationships for Na<sub>v</sub>1.7

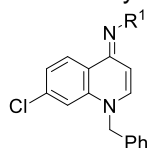
A series of 41 structural analogues of WIN17317-3 were designed and synthesized by systematically introducing substituents in the four defined pharmacophore regions of WIN17317-3 (Fig. 42). The compounds' activity at *h*Na<sub>v</sub>1.7 was evaluated at 1 μM and 10 μM concentrations and according to the %inhibitions produced these were classified as of high or moderate potency or as inactive. The deduced SARs for each of the pharmacophoric areas are sequentially described below, followed by an assessment of the effects of overall molecular properties such as lipophilicity and *t*PSA. The Na<sub>v</sub> activity data provided in this section represent the blocking efficiencies obtained for channels at the tonic state; however, since similar levels of inhibition were recorded for compounds at all voltage states explored, the deduced SARs can be considered as applicable to all. The IC<sub>50</sub> values reported were calculated from 8-point dose-response curves, whereas estimated IC<sub>50</sub> values refer to predicted values based on the %Na<sub>v</sub> block at 1 μM and 10 μM.



**Figure 42.** The WIN17317-3 pharmacophore.

The first pharmacophore region to be described is the R<sup>1</sup> substituent (Table 12). The spatial requirements of the R<sup>1</sup> substituent were initially investigated using a series of analogues bearing straight and branched aliphatic chains, as well as aliphatic and aromatic rings. The progressive shortening of the alkyl chain length, from five carbons in **1**, to three carbons in **117\***, and to two carbons in **114\***, led to a systematic drop in potency. The introduction of the branched isopropyl group in analogue **114\*** was found to be well tolerated with the noted decrease in potency most likely attributed to the concurrent shortening of the chain length. The conformationally restrained analogue **111\*** bearing a cyclopentyl ring, showed a ten-fold drop in potency relative to its linear chain equivalent **1**. On the contrary, the more flexible planar benzyl group in **20** produced equipotent inhibition to **1**.

As described in chapter 2, investigating the effects of fluoride containing derivatives was of particular interest in this study. Three fluorinated R<sup>1</sup> analogues, **115\***, **116\*** and **26** were examined. The 5-fluoropentyl analogue **115\*** was found equipotent to the parent **1**; likewise, β-fluorination at **116\*** produced similar levels of inhibition as the same chain length analogue **114\***. The two positions were identified as plausible sites for [<sup>18</sup>F]fluorination.

**Table 12.** Characterization of R<sup>1</sup>-series iminodihydroquinolines as hNa<sub>v</sub>1.7 inhibitors.

Compound	R <sup>1</sup>	%Inhibition ± SD 1 μM, 10μM	Na <sub>v</sub> 1.7 Activity	
			IC <sub>50</sub> (μM)	Potency score
WIN17317-3 (1)		79.2 ± 4.6	0.21	II
		76.0 ± 6.6		
117*		45.5 ± 4.9	1.10	I
		86.3 ± 6.9		
114*		32.5 ± 2.9	3.60	I
		69.9 ± 7.4		
111*		43.6 ± 30.2	1.70	I
		73.6 ± 26.2		
20		60.0 ± 6.9	N/A	II
		96.7 ± 4.7		
115*		67.9 ± 2.1	0.39	II
		82.4 ± 4.1		
116*		42.2 ± 11.3	3.60	I
		60.7 ± 2.2		
26		4.2 ± 10.3	N/A	0
		24.5 ± 19.6		
113*		-5.6 ± 1.9	>100	0
		7.0 ± 6.9		
19		27.5 ± 9.6	N/A	I
		62.3 ± 4.8		
25		20.8 ± 8.3	N/A	0
		12.5 ± 6.4		
39		-2.5 ± 7.1	N/A	0
		7.6 ± 0.8		
118*		8.9 ± 1.4	54.8	0
		14.4 ± 3.1		
27		2.7 ± 6.3	N/A	0
		19.4 ± 5.1		

\*Potency score: 0= Inactive, I= moderately potent, II= highly potent

Interestingly, replacement of the terminal CH<sub>2</sub>F group in **116\*** with a CF<sub>3</sub> group in **26** was found detrimental for activity. The van der Waals volume of the CF<sub>3</sub> group is comparable to that of an ethyl group<sup>195</sup> hence the observed loss of activity is unlikely to be attributed to steric effects. The CF<sub>3</sub> group is only inductively electron withdrawing, meaning the effect cannot be attributed to altered electron density of the imine nitrogen either; the methylene group between the CF<sub>3</sub> and the imine nitrogen should diminish the effect leaving the  $\sigma$ -bonding of the imine nitrogen unaffected. Fluorine, with strong C-F and C-CF<sub>3</sub> bond dipoles and three sets of lone pairs can also be involved in weak intra- or inter- molecular dipolar and hydrogen bond interactions.<sup>196</sup> These however, were also regarded as an unlikely reason for the observed loss of activity for **26**; the RCH<sub>2</sub>F group of **116\*** which is known to be a superior hydrogen-bond acceptor compared to the RCF<sub>3</sub> moiety led to high potency inhibition.<sup>197</sup>

The electronic requirements of the R<sup>1</sup> pharmacophore region were investigated next. Various analogues bearing polar alkyl chain functionalities were examined. The incorporation of the amide and hydroxyl functionalities in compounds **25** and **113\***, respectively, was proved detrimental for activity. Hydroxyl group masking and conversion to the less polar ether functionality in **19** was found to restore activity. The *t*PSA of all R<sup>1</sup>-series analogues of table 13 were calculated, and paired with the corresponding Na<sub>v</sub> activity for each compound (Fig. 43). Notably all R<sup>1</sup> series compounds exhibiting high Na<sub>v</sub> potency had *t*PSAs lower than 20 Å<sup>2</sup> and all inactive compounds, with the exception of one, had *t*PSAs higher than 38 Å<sup>2</sup>. These findings led us conclude that polar groups are not tolerated at the R<sup>1</sup> pharmacophore region. This could be attributed to a number of reasons, such as electrostatic repulsion with groups at the active site, or hydrogen bonding of the molecule with either the channel preventing optimal compound binding at the active site, or with water molecules altering the compound's solvation thermodynamics.

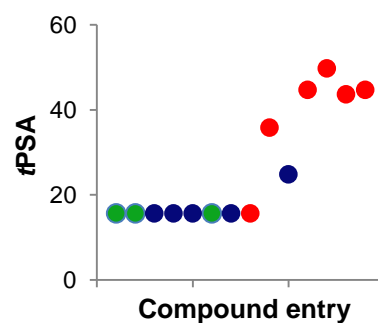


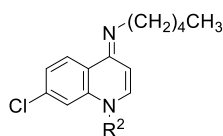
**Figure 43.** Plot of *t*PSA - activity relationship. High potency (●), moderate potency (●), inactive (●).

Expanding on the classical approach of systematically altering molecular properties for characterizing the pharmacophore, a more unconventional fragment-based drug design approach was also employed.<sup>144</sup> Small fragments from well-established structurally diverse Na<sub>v</sub> inhibitors were incorporated as R<sup>1</sup> substituents aiming to identify common or overlapping pharmacophore regions between WIN17317-3 and the scaffolds from which the respective fragments originated. The

benzene sulfonamide moiety<sup>198</sup> of compound **39**, the triazole ring<sup>199</sup> of compound **118\*** and the bnza<sup>200</sup> moiety of compound **27** are all structures encountered in potent Na<sub>v</sub> blockers described in literature. Unfortunately, when part of the R<sup>1</sup> chain, all three fragments abolished activity.

The second pharmacophore region to be explored was the *N*-1 benzyl substituent denoted as R<sup>2</sup> (Table 13). The effects of introducing substituents at the various positions of the benzyl ring, such as electron withdrawing groups (-CN and -F), were initially examined. The nitrile group is commonly introduced as a substituent on aromatic rings, and is present in numerous pharmaceutical compounds. It can inductively polarize aromatic rings thereby altering benzylic π-π interactions. In addition, nitriles can engage in polar interactions through hydrogen bonding. They are commonly used as ketone bioisosteres and in several cases they were demonstrated to increase metabolic stability towards oxidation.<sup>201</sup> *Ortho* and *meta* nitrile group incorporation in analogues **101\*** and **102\***, respectively, was found to be well tolerated, producing potent Na<sub>v</sub> inhibition. A nearly ten-fold drop in potency was observed with a nitrile substituent in the *para* position, as for **103\***. Interestingly, the similarly π-deficient 4-pyridyl analogue **106\*** (large permanent pyridine dipole moment)<sup>202</sup> also showed low Na<sub>v</sub> blocking efficiency suggesting that the *para* position of the phenyl ring cannot tolerate electron withdrawing groups. The *meta* fluoride substituent in analogue **104\*** was well tolerated and **104\*** was in fact one of the most potent compounds of the series.

As part of a broader exploration of the R<sup>2</sup> pharmacophore region, a variety of alkyl, heteroalkyl, aryl and heteroaryl groups with diverse physicochemical properties were introduced as R<sup>2</sup> substituents. The introduction of a branched phenylethyl group led to the chiral analogue **108\*** which upon testing as a racemic mixture, produced equipotent inhibition to the parent compound **1**. On the contrary, removal of the phenyl ring as for the methyl analogue **107\***, abolished activity. Moving from aromatic to aliphatic substituents, benzyl ring replacement by the bulkier cyclohexyl ring in **105\*** was found to retain activity (IC<sub>50</sub>=0.16 μM). Incorporation of a polar heteroatom in the cyclohexyl ring as in **109\*** led to a nearly ten-fold drop in potency (IC<sub>50</sub>=1.1 μM). Decreasing the ring size by one carbon to the 5-membered THF group in **110\***, led to a further drop in potency by one order of magnitude (IC<sub>50</sub>=13.8 μM). Finally, incorporation of the highly polar triazole ring, in analogue **112\***, was proved detrimental for activity. These findings highlight the requirement for a large hydrophobic substituent at the R<sup>2</sup> pharmacophore region.

**Table 13.** Characterization of R<sup>2</sup>-series iminodihydroquinolines as hNa<sub>v</sub>1.7 inhibitors.

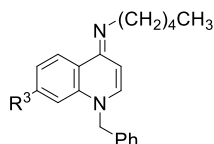
Compound	R <sup>2</sup>	%Inhibition ± SD 1 μM, 10μM	Na <sub>v</sub> 1.7 Activity	
			IC <sub>50</sub> (μM)	Potency score
WIN17317-3 (1)		79.2 ± 4.6	0.21	II
		76.0 ± 6.6		
101*		60.2 ± 6.5	0.42	II
		92.4 ± 3.2		
102*		57.4 ± 10.0	0.64	II
		94.0 ± 1.6		
103*		36.1 ± 5.7	1.60	I
		88.6 ± 0.1		
106*		48.3 ± 2.1	1.60	I
		77.0 ± 1.8		
104*		72.1 ± 5.1	0.18	II
		100.2 ± 3.2		
107*		-5.5 ± 17.1	94.4	0
		-3.9 ± 6.9		
108*		72.4 ± 7.3	0.25	II
		93.6 ± 6.5		
105*		75.1 ± 9.4	0.16	II
		89.7 ± 9.8		
109*		47.0 ± 2.9	1.10	I
		80.6 ± 5.0		
110*		18.0 ± 4.2	13.8	0
		38.2 ± 6.3		
112*		-4.0 ± 4.9	>100	0
		10.5 ± 3.1		
55		32.7 ± 2.3	N/A	I
		81.0 ± 5.4		
56		49.3 ± 7.4	N/A	II
		81.8 ± 2.4		
31		31.7 ± 8.0	N/A	I
		66.7 ± 5.6		

\*Potency score: 0= Inactive, I= moderately potent, II= highly potent

It is widely accepted that the binding conformation of a pharmaceutical compound with many rotational degrees of freedom is not necessarily the lowest energy conformation of the molecule but rather the one that allows the highest number of stabilizing interactions with the active site. In order to investigate the active conformation of WIN17317-3, the methylene linker of the benzyl group was removed aiming to restrict molecular flexibility. Three analogues, **55**, **56** and **31** (table 14) were examined. All three analogues were found to maintain activity; analogue **56** bearing a cyclohexyl group produced high Na<sub>v</sub> inhibition (<1 μM) whilst analogues **55** and **31** bearing phenyl and cyclohexene substituents respectively, showed reduced activity with IC<sub>50</sub> values estimated in the range of 1 and 10 μM.

The third pharmacophore region to be explored was the R<sup>3</sup> substituent at the seven position of the quinoline scaffold; this is a chloride substituent for the parent WIN17317-3 (Table 14). Chlorine and the heavier halogens have unique electronic properties when bound to aryl rings; apart from the electron withdrawing effects they exert, they can also form interactions (halogen bonds) with adjacent electrophiles, nucleophiles and other halogens at the binding pocket. Halogen bonds are weaker than hydrogen bonds yet their strength increases with the size of the halogen atom and is dependent on the electronegativity of the other carbon substituents and the density of the binding partner.<sup>203</sup> Chlorine for iodine substitution in analogue **2** was found to be well tolerated with comparable IC<sub>50</sub>s obtained for the two compounds. Chlorine for hydrogen substitution in analogue **21** led to a considerable drop in potency, with an estimated IC<sub>50</sub> value in the range of 1 - 10 μM. Interestingly, incorporation of the electron-donating methoxy group in **24** appears to lead to only a small drop in inhibition potency relative to the halogenated analogues **1** and **2**, yet more experiments are required to verify this result. The small size of the library precludes the deduction of firm conclusions regarding the requirements for the R<sup>3</sup> pharmacophore region, yet the results suggest that the electronic nature of substituents at this position has limited effect on binding, and that the binding pocket tolerates substituents with a range of steric requirements.



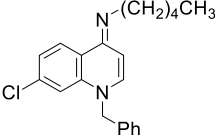
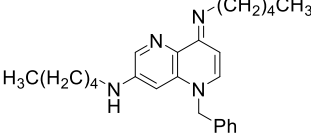
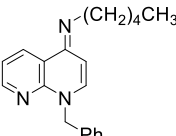
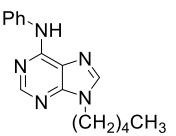
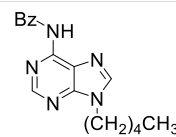
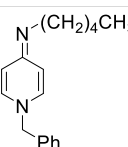
**Table 14.** Characterization of R<sup>3</sup>-series iminodihydroquinolines as hNa<sub>v</sub>1.7 inhibitors.

Compound	R <sup>3</sup>	%Inhibition ± SD 1 μM, 10μM	Na <sub>v</sub> 1.7 Activity	
			IC <sub>50</sub> (μM)	Potency score
WIN17317-3 (1)	-Cl	79.2 ± 4.6	0.21	II
		76.0 ± 6.6		
2	-I	73.1 ± 8.3	0.22	II
		102.6 ± 2.9		
21	-H	33.8 ± 8.1	N/A	I
		59.5 ± 5.4		
24	-OCH <sub>3</sub>	52.7 ± N/A	N/A	II
		89.1 ± 14.0		

\*Potency score: 0= Inactive, I= moderately potent, II= highly potent

The 1,4-iminodihydroquinoline heterocyclic scaffold was the fourth pharmacophore region to be investigated using analogues containing other, structurally diverse, nitrogen-containing heterocycles (Table 15). The effect of introducing additional nitrogen atoms to the quinoline scaffold was initially examined. Two naphthyridine analogues **69** and **82** were synthesized. The nitrogen at the 8<sup>th</sup> position of analogue **82** led to a drop in potency and to an estimated IC<sub>50</sub> in the range of 1-10 μM. Interestingly, the 1,5-naphthyridine **69**, bearing an additional *n*-pentyl alkyl chain at the 7 position maintained potency for Na<sub>v</sub>1.7 inhibition. This suggested that the nitrogen at the 5<sup>th</sup> position is well tolerated, and also that bulkier substituents than those previously explored for the R<sup>3</sup> region, *vide supra*, can be accommodated at the site. The effects of a 5,6-biaryl system, were also examined through two purine analogues, **93** and **94**. Purines are frequently referred to as privileged structures due to their profound ability to bind to multiple receptors hence having applications across a wide range of therapeutic areas. The structural similarities of purines and quinolines have been extensively exploited by recent medicinal chemistry studies; in several examples quinolines have been successfully employed as viable purine isosteres maintaining biological activity.<sup>204</sup> Unfortunately, both purine analogues **93** and **94**, although bearing similar substitution patterns to the parent WIN17317-3, failed to produce inhibition at Na<sub>v</sub>1.7. Quinoline substitution by pyridine in analogue **97** also led to abolished activity.

**Table 15.** Characterization of heterocyclic scaffold analogues (R<sup>4</sup>-series) as hNa<sub>v</sub>1.7 inhibitors.

Compound	Structure	%Inhibition ± SD 1 μM, 10μM	Na <sub>v</sub> 1.7 Activity	
			IC <sub>50</sub> (μM)	Potency score
WIN17317-3 (1)		79.2 ± 4.6	0.21	II
		76.0 ± 6.6		
69		48.9 ± 13.8	N/A	I
		76.2 ± 5.0		
82		28.8 ± 5.0	N/A	I
		66.9 ± 13.8		
93		-2.5 ± 7.1	N/A	0
		7.6 ± 0.8		
94		-13.2 ± 9.8	N/A	0
		23.0 ± 2.3		
97		0.9 ± 9.9	N/A	0
		2.0 ± 5.9		

\*Potency score: 0= Inactive, I= moderately potent, II= highly potent

Examining the deduced SARs for the R<sup>1</sup> and R<sup>2</sup> pharmacophore regions it became apparent that the two areas share similar structural characteristics: both require large, hydrophobic substituents to achieve potent Na<sub>v</sub>1.7 blockade. Based on this, it was hypothesized that the molecule could potentially behave as a dimer allowing binding at the active site *via* two orientations. The use of homodimers/symmetrical ligands is a common practice in medicinal chemistry and usually aims at the production of more potent and/or more selective drugs compared to the single entity.<sup>205</sup> The previously described analogue **20** presenting benzyl rings as both R<sup>1</sup> and R<sup>2</sup> substituents exhibited comparable levels of inhibition to the parent WIN17317-3 providing support to the suggested dual binding hypothesis (Table 16). Five analogues, bearing *n*-pentyl chains as R<sup>2</sup> substituents were synthesized aiming to investigate this hypothesis further. The “reversed” substituent

analogue **29** produced highly potent inhibition similar to that of the parent WIN17317-3. Three highly conjugated analogues **28**, **36**, and **40** were additionally examined. Interestingly, the aniline analogue **28** produced high affinity inhibition whereas analogues **36** and **40** lacked activity at Na<sub>v</sub>1.7. The selected imino-oxyphenyl ether and -phenyl sulfonamide moieties in analogues **36** and **40** respectively, are motifs encountered in potent Na<sub>v</sub> blockers previously described in literature.<sup>198, 206</sup> Possible explanations for the observed lack of efficacy for analogues **36** and **40** are: (a) their high polarity, given the hydrophobic requirements of the R<sup>1</sup> pocket as established above, and/or (b) the altered pK<sub>s</sub> of the imine and quinoline nitrogen atoms due to the electron-withdrawing nature of the substituents.

**Table 16.** Functional characterization of iminodihydroquinolines as hNa<sub>v</sub>1.7 inhibitors.

Compound	Structure	%Inhibition ± SD 1 μM, 10μM	Na <sub>v</sub> 1.7 Activity	
			IC <sub>50</sub> (μM)	Potency score
WIN17317-3 (1)		79.2 ± 4.6	0.21	II
		76.0 ± 6.6		
<b>20</b>		60.0 ± 6.9	N/A	II
		96.7 ± 4.7		
<b>28</b>		53.6 ± 5.6	N/A	I
		77.4 ± 13.9		
<b>29</b>		62.9 ± 9.1	N/A	II
		87.8 ± 14.1		
<b>36</b>		-2.7 ± 4.5	N/A	0
		3.2 ± 5.8		
<b>40</b>		0.2 ± 10.5	N/A	0
		-8.9 ± 4.9		

In an effort to obtain further information to support the development of a pharmacophore model, the effects of overall physical properties such as  $pK_a$ ,  $tPSA$  and  $\log D$  on  $Na_v1.7$  inhibition were also to be examined. The  $pK_a$  and  $\log D$  values for iminodihydroquinolines were calculated using the Accelrys Accord for Excel software and  $tPSA$  values were calculated using ChemBioDraw Ultra 14.0.

The published  $pK_a$  value for WIN17317-3 is 11.5.<sup>133</sup> The  $pK_a$  values calculated by the Accelrys software for WIN17317-3 were 5.38 for the imino nitrogen and 3.10 for the quinoline nitrogen. Given our experimental observations regarding the polarity and basicity of WIN17317-3 and the class of iminodihydroquinolines in general, the calculated  $pK_a$  values were believed to be incorrect. The  $\log D_{7.4}$  value of the iodinated iminodihydroquinoline analogue **2** has been measured by a previous member of the group using the traditional *n*-octanol flask method to be  $2.98 \pm 0.08$  ( $n = 3$ ).<sup>3</sup> The calculated  $\log D_{7.4}$  value for the same compound was 5.60. Given that the  $\log D$  calculation requires the concentration of ionized species in solution, and since the calculated  $pK_a$  value predicted by the software was false, calculated  $\log D$  values were also considered to be inaccurate. The effects of  $pK_a$  and  $\log D$  parameters on  $Na_v1.7$  inhibition could therefore not be assessed.

The effects of the polar surface area on  $Na_v1.7$  activity were however examined (Fig. 44). Compounds acting as highly or moderately potent  $Na_v1.7$  inhibitors were found to exhibit  $tPSA < 25 \text{ \AA}^2$ ; whereas inactive compounds were evidently far more polar with the majority (8/10) exhibiting  $tPSA > 25 \text{ \AA}^2$ .

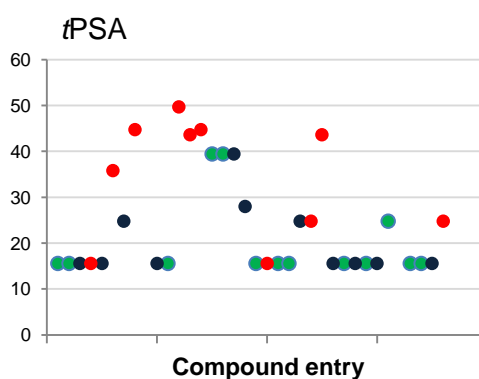


**Figure 44.**  $tPSA$  –  $Na_v1.7$  inhibition relationship for first generation iminodihydroquinoline analogues. Compounds are classified as highly potent (●), as moderately potent (●)  $Na_v1.7$  blockers or as inactive (●).

Overall, summarizing the results of the SAR study, the following are concluded regarding the WIN17317-3 pharmacophore:

- The  $R^1$  region can accommodate non-polar aliphatic or aromatic substituents. A noticeable decrease in potency is observed when the aliphatic chain is shortened and loss of biological activity is observed in the presence of polar functionalities.
- Similar to  $R^1$ , the  $R^2$  region can also accommodate hydrophobic aliphatic and aromatic substituents. Substituents conjugated to the quinoline ring lead to a drop in potency and the introduction of polar substituents results in complete loss of biological activity.
- Despite the small number of  $R^3$  substituents investigated, the  $R^3$  region appears to tolerate both electron withdrawing and electron donating substituents, both yielding high potency  $Na_v1.7$  inhibition. Hydrogen, the halogens, and the larger aminopentyl chain are all well tolerated suggesting the presence of a large pocket with weak binding interactions.
- The  $R^4$  pharmacophore region requires the presence of a fused, 6+4 nitrogen containing heterocyclic scaffold, like the quinolines and naphthyridines.

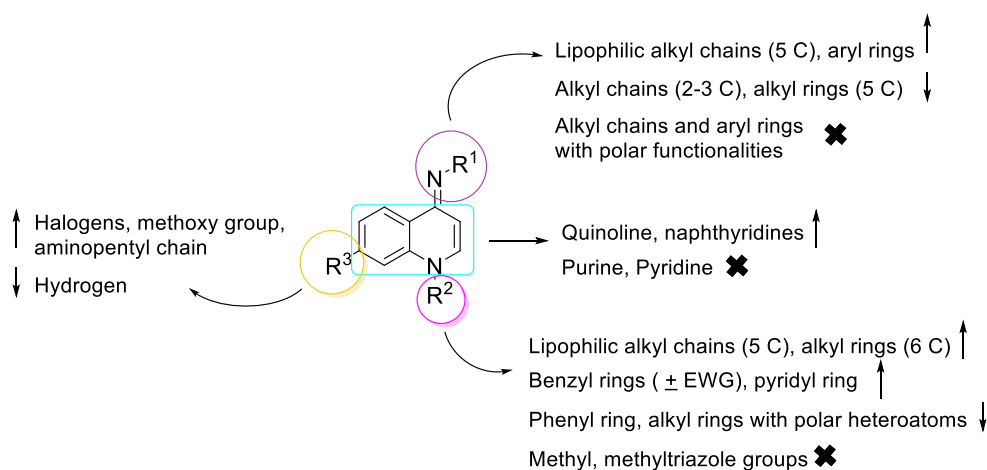


**Figure 45.** Structure-activity relationships of small molecule iminodihydroquinolines for  $hNa_v1.7$ . (high potency inhibition:  $\uparrow$ , low potency inhibition:  $\downarrow$ , abolished activity:  $\times$ ).

## 4.6. Na<sub>v</sub> isoform profiling

One of the key objectives of this study was to investigate the underlying mechanism for the observed selectivity of WIN17317-3 in blocking C-fibres with higher potency than A-fibres. As previously discussed, it was speculated that such selectivity could originate from WIN17317-3 inhibiting Na<sub>v</sub> isoforms expressed at C-fibres (Na<sub>v</sub>1.7, Na<sub>v</sub>1.8, Na<sub>v</sub>1.9) with higher potency than the ones expressed at A-fibres (Na<sub>v</sub>1.6). Our approach was based on developing pharmacophore hypotheses for the distinct Na<sub>v</sub> channels; divergent SARs for Na<sub>v</sub>1.7 and Na<sub>v</sub>1.8 from Na<sub>v</sub>1.6, would support an Na<sub>v</sub> isoform-based mechanism. Additionally, the screening of compounds against the wider range of Na<sub>v</sub>s would provide information regarding potential off-target toxicity. The Na<sub>v</sub>1.2, Na<sub>v</sub>1.4, and Na<sub>v</sub>1.5 isoforms are expressed in the CNS, the muscles and the heart, respectively, hence their blockade *in vivo* could lead to serious adverse effects.<sup>207</sup>

Ten selected iminodihydroquinolines from the library, with varying R<sup>1</sup>, R<sup>2</sup> and R<sup>3</sup> substituents, were screened for their blocking potency against the human Na<sub>v</sub>1.2, Na<sub>v</sub>1.4, Na<sub>v</sub>1.5, Na<sub>v</sub>1.6, Na<sub>v</sub>1.7 and Na<sub>v</sub>1.8 isoforms (Table 17).

**Table 17.** Blocking potencies of ten selected iminodihydroquinolines against *hNa<sub>v</sub>* isoforms.

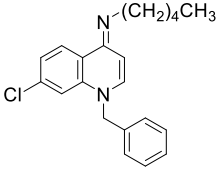
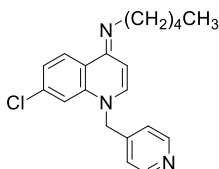
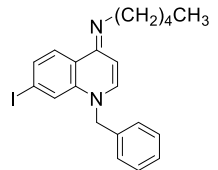
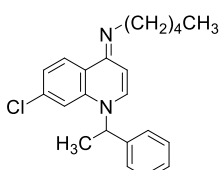
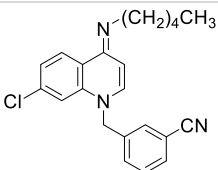
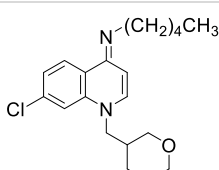
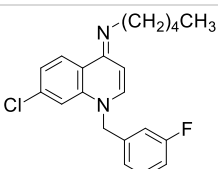
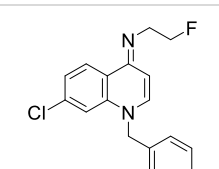
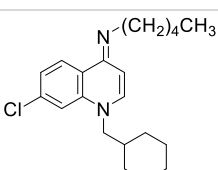
Cpd	IC <sub>50</sub> (μM)					
	1.2	1.4	1.5	1.6	1.7	1.8
<b>1</b>	2.2 ± 1.2	0.19 ± 0.08	0.33 ± 0.10	1.92 ± 0.72	0.21±0.05	15.03± 5.76
<b>2</b>	1.5 ± 0.5	0.14 ± 0.06	0.23 ± 0.05	0.64 ± 0.21	0.22±0.04	5.47±4.05
<b>102*</b>	4.8 ± 1.2	0.67 ± 0.26	1.51 ± 0.15	2.95 ± 0.85	0.64±0.08	3.98±1.21
<b>104*</b>	2.8 ± 1.0	0.20 ± 0.26	0.46 ± 0.15	1.46 ± 0.85	0.18±0.03	14.26±1.21
<b>105*</b>	4.3 ± 1.0	0.20 ± 0.07	0.45 ± 0.09	0.81 ± 0.38	0.16±0.03	12.62±5.74
<b>106*</b>	17.9 ± 5.0	0.72 ± 0.22	4.38 ± 1.30	12.53± 2.87	1.6 ± 0.40	36.14±7.01
<b>107*</b>	>100	58.34 ±12.8	>100	98.43	94.4	>100
<b>108*</b>	2.5 ± 0.4	0.25 ± 0.13	0.72 ± 0.16	0.99 ± 0.31	0.25±0.04	3.92±1.17
<b>109*</b>	10.7 ± 2.1	0.89 ± 0.34	1.98 ± 0.33	4.48 ± 0.87	1.1 ± 0.19	12.18±1.86
<b>116*</b>	53.4 ± 26.2	3.93 ± 1.57	4.72 ± 1.17	18.77 ±3.62	3.6 ± 0.98	41.31±3.95

Given the high cost associated with automated patch clamp electrophysiology assays the least relevant Na<sub>v</sub>1.1 and Na<sub>v</sub>1.3 isoforms were excluded at this stage from the screen. The Na<sub>v</sub>1.9 isoform, although of particular interest due to its selective expression in nociceptors,<sup>118</sup> is not part of commercially available Na<sub>v</sub> screening portfolios due to difficulties in expressing, maintaining and recording from stable Na<sub>v</sub>1.9 cell lines; it was therefore also excluded from the screen.

For comparison purposes, the selectivity of each compound towards blocking *h*Na<sub>v</sub>1.7, the isoform of interest, over other *h*Na<sub>v</sub>s, was calculated and is provided alongside the compounds' structures in Table 18. Selectivity was measured as the ratio between the IC<sub>50</sub> values for the respective isoforms:

$$\text{Selectivity for } h\text{Na}_v1.7 \text{ over } h\text{Na}_v1.x = \frac{\text{IC}_{50}(\text{Na}_v 1.x)}{\text{IC}_{50}(\text{Na}_v 1.7)}$$

**Table 18.** Selectivity of iminodihydroquinolines for blocking  $hNa_v1.7$  over other  $hNa_v$ s.

Compound	Na <sub>v</sub> 1.7 Selectivity					Compound	Na <sub>v</sub> 1.7 Selectivity				
	1.2	1.4	1.5	1.6	1.8		1.2	1.4	1.5	1.6	1.8
 <b>1</b>	10	1	2	9	72	 <b>106*</b>	11	0	3	8	23
 <b>2</b>	7	1	1	3	25	 <b>108*</b>	10	1	3	4	16
 <b>102*</b>	8	1	2	5	6	 <b>109*</b>	10	1	2	4	11
 <b>104*</b>	16	1	3	8	79	 <b>116*</b>	15	1	1	5	11
 <b>105*</b>	27	1	3	5	79						

Interestingly, several iminodihydroquinolines were found to exhibit higher blocking potency for Na<sub>v</sub>1.7 over three particular Na<sub>v</sub> isoforms: the Na<sub>v</sub>1.2, Na<sub>v</sub>1.6 and Na<sub>v</sub>1.8 isoforms (Fig. 46). Examining the highest selectivity achieved for Na<sub>v</sub>1.7 over each of these isoforms, with respect to Na<sub>v</sub>1.2, up to 27-fold selectivity was observed for **105\***, with the next most selective compounds **104\*** and **116\*** exhibiting 15-fold selectivity. The remaining iminodihydroquinolines showed ~10 fold selectivity over Na<sub>v</sub>1.2. With respect to Na<sub>v</sub>1.6, WIN17317-3 and analogues **104\*** and **106\*** were the most selective (~10 fold), with the remaining compounds exhibiting 5-fold or lower selectivity. Three compounds stand out for their selectivity over Na<sub>v</sub>1.8: **1**



(72-fold), **104\*** and **105\*** (~80 fold). The next most selective compounds were **2** and **106\***. All iminodihydroquinolines were essentially equipotent towards blocking  $Na_v1.7$  and the  $Na_v1.4$  and  $Na_v1.5$  isoforms.

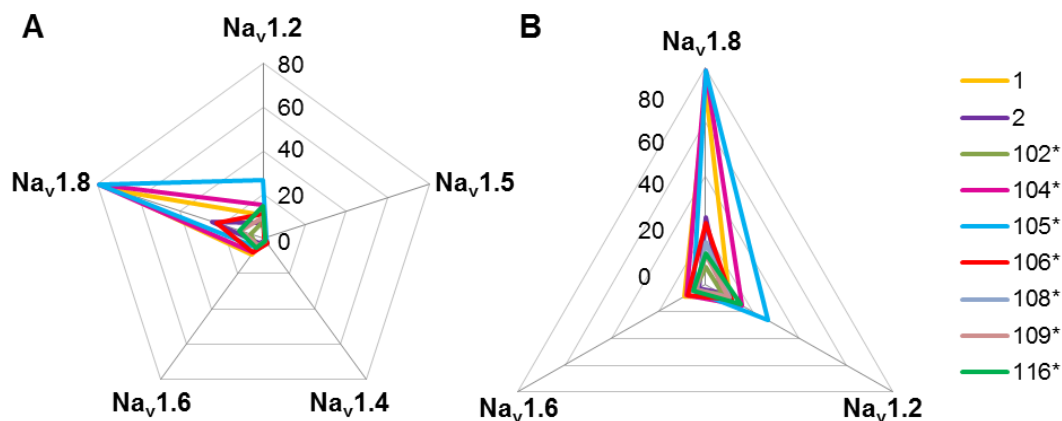


**Figure 46.** Iminodihydroquinolines' selectivity for blocking  $hNa_v1.7$  over other  $Na_v$  isoforms. The radar charts' axes represent the compounds' selectivity for  $Na_v1.7$  as the ratio of  $IC_{50}(Na_v1.7)$  over  $IC_{50}(Na_v1.x)$ . (A) Selectivity for  $Na_v1.7$  over  $Na_v1.2$ ,  $Na_v1.4$ ,  $Na_v1.5$ ,  $Na_v1.6$ , and  $Na_v1.8$ . (B) Focus in the three isoforms,  $Na_v1.2$ ,  $Na_v1.6$  and  $Na_v1.8$ , that showed the highest  $Na_v1.7$  blocking selectivity.

Despite the relatively small differences in the  $IC_{50}$  values of iminodihydroquinolines for the various  $Na_v$  isoforms, the results of this study suggest the presence of structural variations between the binding sites at the  $Na_v1.7$  and the  $Na_v1.2$ ,  $Na_v1.6$ , and  $Na_v1.8$  isoforms. Intriguingly, **104\***, **105\*** and **116\*** were the three compounds that exhibited markedly higher selectivity for blocking  $Na_v1.7$  over the three other isoforms. Unfortunately, given the small number of compounds investigated, there is insufficient data to draw any conclusions regarding the structural origin of this selectivity.

#### 4.7. Summary

To conclude, the blocking activities of iminodihydroquinolines at  $Na_v$ s have been described in this chapter. A cost- and time- effective screening approach was validated and used for predicting the *in vitro* potency of compounds at  $Na_v$ s by measuring only two concentration-response points, using the IonWorks Quattro automated patch clamp electrophysiology platform. The first ever SAR of the

iminodihydroquinoline class for the human Na<sub>v</sub>1.7 isoform has been defined using a 4-region WIN17317-3 pharmacophore model. Compounds with varying Na<sub>v</sub>1.7 potencies were identified, ranging in the low micromolar range for some compounds to others being completely inactive. Several members of the library were found to exhibit equipotent inhibition of all Na<sub>v</sub> isoforms explored, whilst certain compounds showed significantly higher potency for Na<sub>v</sub>1.7 relative to the Na<sub>v</sub>1.2, Na<sub>v</sub>1.6 and Na<sub>v</sub>1.8 isoforms. This diversity in the compound library provides suitable candidates-tools for investigating (a) the relationship between Na<sub>v</sub>1.7 potency and pain signaling blockade and (b) the hypothesis that selective Na<sub>v</sub> isoform blockade is the underlying mechanism for the observed C/A-fiber selectivity exhibited by WIN17317-3.

## **5. Selective blockade of C-fiber action potential propagation by iminodihydroquinolines in rodent peripheral sensory neurons *in vitro***

The effects of iminodihydroquinolines at peripheral sensory neurons *in vitro* are described in this chapter. The potency of iminodihydroquinolines for blocking nociceptors, as well as their selectivity over non-nociceptive fiber blockade, as measured in the skin-nerve assay, are described herein; the role of Na<sub>v</sub> isoforms in the process is also examined. A 'lead' preclinical drug candidate with profound selectivity for nociceptor block has been selected from a second generation compound library, for further characterization *in vivo*.

### **5.1. The skin-nerve preparation as an assay to measure pharmacological activity in peripheral endings of sensory neurons**

The rodent skin-nerve preparation is an increasingly used technique in the field of experimental pain medicine. It is a method for directly recording APs extracellularly from peripheral sensory nerve endings *in vitro*. It enables recording of propagated APs from single nerve fibers but also from groups of nerve fibers known as compound action potentials (CAP).<sup>208</sup> Several studies have demonstrated that the responses are comparable to those obtained *in vivo* for the same species of rodent.<sup>209, 210</sup>

As previously described in section 1.3, peripheral sensory nerves consist of a large number of sensory fibers, of different types, each type being responsible for transmitting a particular type of information. Each of the nerve fiber categories (A $\beta$ , A $\delta$ , C) has unique morphology (axonal diameter, level of myelination) and therefore conducts electrical signals, APs, at a specific unique speed. This neurophysiological principle is exploited by the skin-nerve assay; a peripheral nerve is stimulated at its distal end, the generated CAP is propagated along the nerve and the CAP signal is recorded at a defined proximal end. The CAP train signal is recorded, and then separated and assigned, according to the times electrical activity is reaching the recorder, as the CAPs of individual nerve fiber classes (Fig. 47). Precise

pharmacological manipulation at the preparation allows the examination of the modulatory effects of drugs on individual nerve fiber(s) classes.<sup>211, 212</sup>

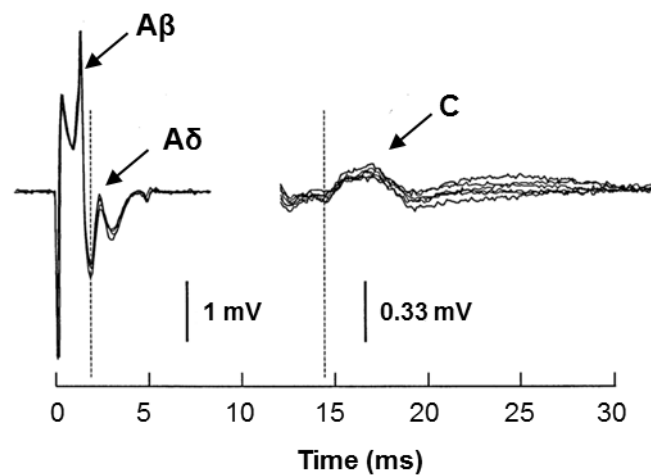


**Figure 47.** Example of six CAP signal overlays evoked by electrical stimulation (time 0) of the sciatic-tibial nerve of a mouse *in vivo*. Dashed lines indicate conduction velocity cutoffs for differentiation of the three major fiber types present ( $A\beta$ ,  $A\delta$ , C). Note difference in vertical scales for A and C fibers.  $A\beta$ - $A\delta$  fibers were evoked by a 100  $\mu$ A stimulus and C fibers were evoked by 6 mA stimulus. Adapted from reference 209.<sup>209</sup>

CAPs rather than individual neuronal fiber action potentials were recorded at this study; this allowed the simultaneous examination of the responses of several fiber categories within the nerve since the response of the peripheral nerve as a whole was of interest.

### 5.1.1. Experimental set-up

The saphenous nerve is the most commonly used tissue in the rodent skin-nerve preparation; being a purely sensory nerve it provides a large sample of the somato-sensory neuronal fibers to be investigated.<sup>213, 214</sup> The rat rather than mouse saphenous nerve was used in this study as it is easier to handle tissues of larger size. One of the advantages of the assay is that the nerve can be kept functional for many hours after dissection, under superfusion, meaning that both left and right nerves of an animal can be used and that a considerable number of recordings can be obtained from each nerve.

**Figure 48.** Anatomical context of the rat saphenous nerve (lower right leg). The saphenous nerve (yellow) is a terminal sensory branch of the femoral nerve, arising from the third lumbar root. At the level of the thigh it separates from the femoral nerve and descends on the lateral side of the femoral vessels (arteries: red, veins: blue) to lie on the medial side of the leg. It supplies the skin of the medial side and front of the knee. At the ankle, it passes anterior to the medial malleolus to innervate skin on the medial and dorsal aspects of the foot.<sup>215</sup> Its superficial anatomical path, allows *in vivo* electrophysiological studies. Adapted from reference 215.



In brief, the saphenous nerve is dissected in continuity with the skin of the lower hind limb and is placed with the corium side facing up into a superfused skin-nerve chamber (Fig. 49). The skin-nerve chamber consists of two compartments: the recording chamber accommodating the proximal end of the nerve, and the stimulation chamber accommodating the distal end of the nerve and the attached skin.

The nerve is electrically stimulated at the distal end, by delivering a supramaximal stimulus (110% of the stimulus exerting the maximal response). The propagated electrical potentials are recorded at the proximal end using a pair of gold wire electrodes. These potentials are in the  $\mu\text{V}$  range and are therefore passed through two types of amplification before being measured at a commercially available system (Fig. 50). The stimulation protocol, as well as the materials and methods used in this assay are provided as experimental details in chapter 8. The components of the equipment and the set-up of the skin-nerve recording station are described in detail in the recently published *Nature protocol* by Reeh *et al.*<sup>215</sup>

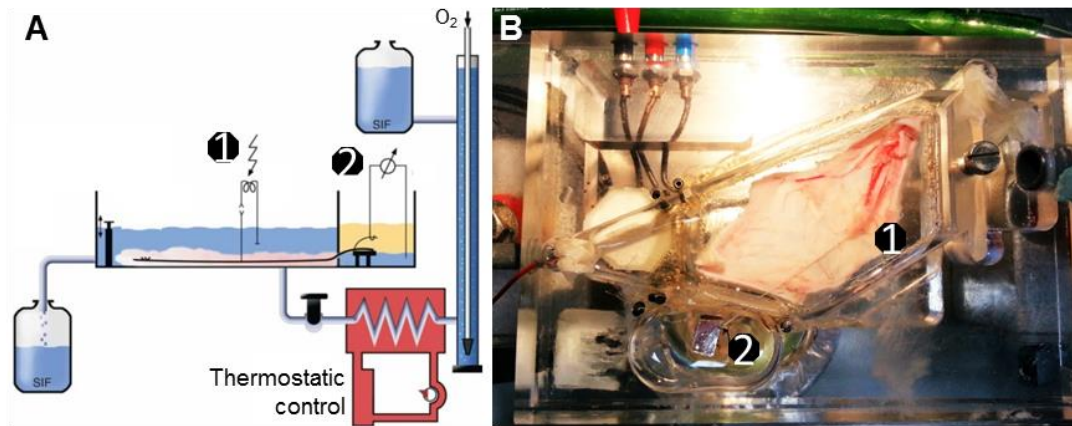


**Figure 49.** The experimental set up for the skin-nerve preparation. (A) Schematic representation of the skin-nerve chamber illustrating fluid circulation. Adapted from reference 215. (B) Top view of the skin-nerve chamber. The skin is placed in the stimulation chamber dermis side up (1), and the proximal end of the attached nerve is extended through a hole to the adjacent recording chamber (2).

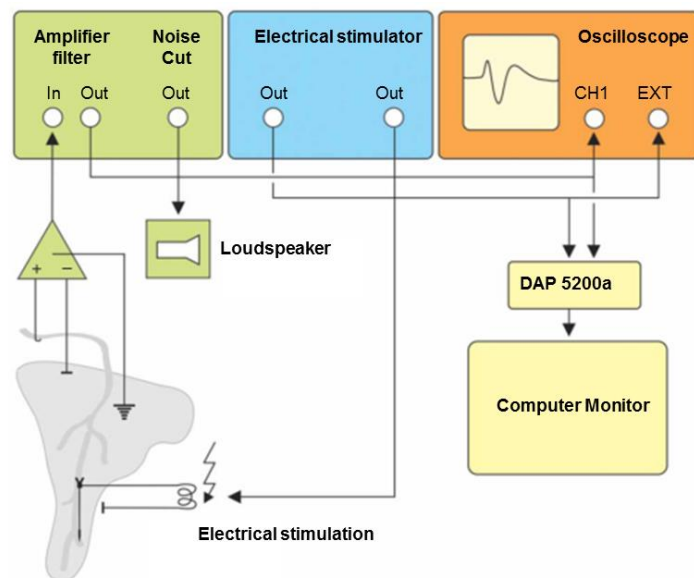


**Figure 50.** Schematic representation of the skin-nerve assay data capture. Electrical stimulation is administered to the receptive field. The recorded signal is fed into an AC-coupled differential preamplifier that is connected in series with a second single ended  $10^4$ –gain amplifier and a band-pass filter (between 1 Hz and 1 kHz). The signal is subsequently fed to audio speakers and oscilloscope and processed through a DAP board, where the action potentials above set amplitudes are discriminated and fed into the computer. Adapted from reference 215.<sup>215</sup>

In experiments where the effects of pharmacological agents at the nerve are to be investigated, a metal ring is used to isolate the area of the nerve to be treated with the drug, from the fluid in the rest of the chamber (Fig. 51). An application system is used to deliver the drug solutions in the ring for the selected time periods.

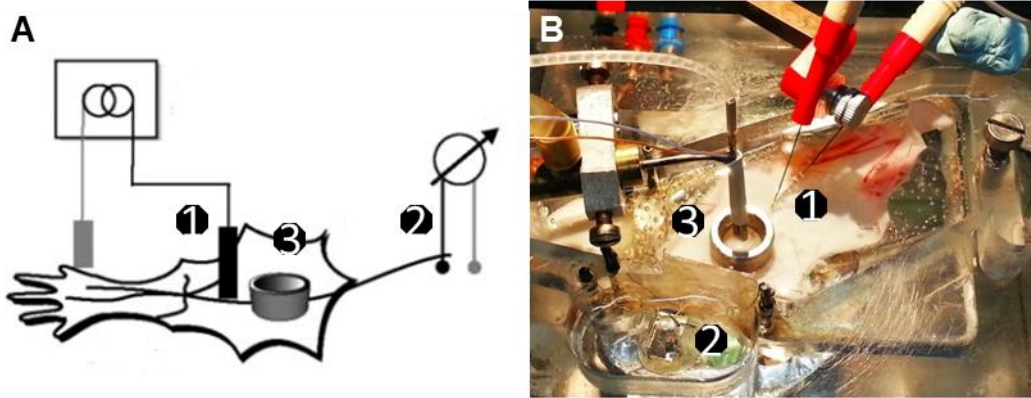


**Figure 51.** Schematic representation (A) and view (B) of the skin-nerve preparation with the metal ring. An application system's tip is positioned within the ring to superfuse the isolated receptive field with the drug solution of interest. Labels: (1) pair of stimulation electrodes; (2) pair of wire electrodes used for recording the signal; (3) metal ring used to isolate the receptive field.

### 5.1.2. Recordings and data analysis

The recorded CAP traces in this study typically comprised of two waves arriving at latencies of  $\sim 2$  ms and  $\sim 33$  ms, with conducting velocities higher than  $5 \text{ ms}^{-1}$  (fast conducting) and lower than  $1 \text{ ms}^{-1}$  (slow-conducting) respectively; these were assigned as the A- and C-fiber waves respectively (Fig. 52). This allocation was in accordance to literature reported CAP measurements from rats of similar age and weights in the same preparation.<sup>216, 216b, 217</sup> The  $A\delta$  wave coincided with the falling phase of the  $A\beta$  wave, hence it was difficult to determine the amplitude of each in isolation. Recorded CAP signals were therefore analyzed as originating collectively from groups of A- and C-fibers. The CAP peak response was used as a measure of the CAP amplitude (Fig. 52 dotted lines). This was considered as a more accurate measurement of axonal activity compared to the area under the curve as it is formed by the spatio-temporal summation of many single unit action potentials fired by individual axons.

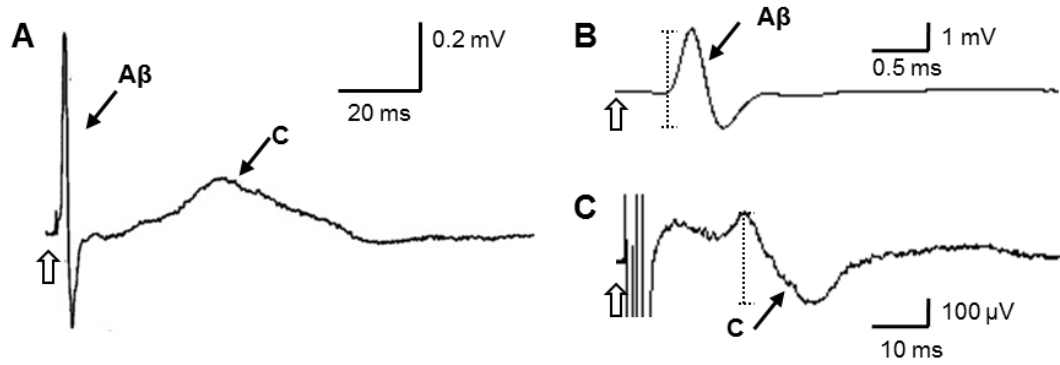


**Figure 52.** Typical CAP traces evoked by electrical stimulation of the saphenous nerve at time 0 as indicated by the open point arrows. (A) Shows all the components of the saphenous CAP while (B) and (C) focus in at specific settings for measuring A $\beta$  and C-CAPs respectively. Dotted lines denote the peak responses recorded.

The use of DMSO as vehicle for compound delivery at the skin-nerve preparation has been previously validated by the Koltzenburg group. The magnitude of CAPs remained stable over treatment with six ascending concentrations of DMSO (0.01, 0.1, 0.2, 0.5, 1, and 2% v/v), each circulated for 15 minutes, over the span of the recordings for 2-2.5 h. Changes in CAP magnitude did not exceed 10% of the initial values for up to 2.5 h of monitoring. Baseline control recordings of at least 20 minutes were performed prior to each experiment to verify the stability of the recording and served as the normalizing control for quantitative evaluation of the action of the respective drug.

Drug solutions were diluted in simulated intestinal fluid (SIF) from 10 mM or 100 mM stock solutions in DMSO, with the maximum concentration of vehicle never exceeding 2% v/v. The experimental protocol of a single recording session involved the successive circulation of six ascending concentrations of the drug solution of interest, from 1  $\mu$ M to 200  $\mu$ M or from 100  $\mu$ M to 1 mM, for 15 minutes intervals each. The amplitude of CAP block at each concentration was calculated as the percentage decrease in CAP relative to the initial measurement at baseline recording (Fig. 53). Each compound was tested on a minimum of three nerves and results are presented as mean CAP block  $\pm$  standard error of the mean (SEM) in semi logarithmic plots. Wherever appropriate, dose-response curves were fitted using the Origin Pro9.0<sup>®</sup> software in DoseResp fitting mode. The EC<sub>50</sub> for each compound was determined from the corresponding dose-response curve, as a summary measure of potency. Since no data are available to date regarding the percentage of C-fiber blockade in a sensory nerve required to produce pain relief,



EC<sub>90</sub>s were also determined, as a more cautious estimate of the drug concentration required for achieving effective analgesia.

**Table 19.** Example of data recording and analysis of WIN17317-3 effects in the saphenous skin-nerve preparation.

Conc. (µM)	A-CAP				C-CAP			
	I <sub>PR</sub> (mV)	%Block	Average %block from 9 expts	SEM	I <sub>PR</sub> (µV)	%Block	Average %block from 9 expts	SEM
0 Baseline	4.96	0	0	0	76.3	0	0	0
1	4.88	1.61	7.21	3.9	69.4	9.0	6.88	1.5
10	4.96	0.00	11.24	5.3	68.8	9.8	17.60	3.5
20	4.88	1.61	14.61	6.2	64.2	15.8	39.43	6.2
50	4.88	1.61	18.00	6.5	56.9	25.4	69.33	9.8
100	4.80	3.23	21.35	7.2	41.5	45.6	85.09	8.4
200	4.72	4.84	39.48	8.4	0	100	100	0.0

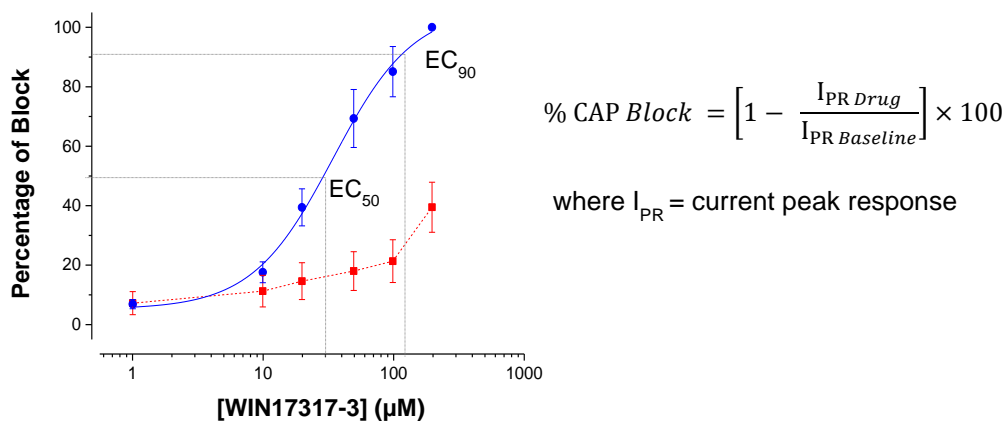


**Figure 53.** Data analysis of WIN17317-3 effects in the saphenous skin-nerve preparation. The %CAP blocks produced by ascending drug concentrations were calculated as % current reduction relative to baseline as depicted by the equation to the right. The data points are plotted on a concentration - %block semi-logarithmic plot, as means of nine recordings ± SEM. Dose-response curves were fitted and EC<sub>50</sub>, EC<sub>90</sub> parameters were calculated using the Origin Pro9.0<sup>®</sup> software in DoseResp fitting mode.

## 5.2. Effects of iminodihydroquinolines on C- and A-fiber conduction

The skin-nerve preparation was used to elucidate the SAR of the iminodihydroquinoline class for C-fiber blockade; the identification of structural features contributing to the selective blockade of C- over A-fibers was of particular interest. Fourteen compounds from the library were initially screened using the skin-nerve preparation and the effects of modifications in the R<sup>2</sup> and R<sup>3</sup> pharmacophore regions of WIN17317-3 were examined (Fig. 54).

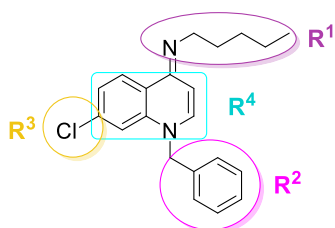


**Figure 54.** The WIN17317-3 pharmacophore.

### 5.2.1. SARs for C-fiber blockade

Focusing at modifications in the R<sup>2</sup> pharmacophore region first, the effects of nine compounds with various aryl, heteroaryl and alkyl R<sup>2</sup> substituents, of diverse physicochemical properties, were examined (Fig. 55). The compounds were applied at six ascending concentrations, 1 μM, 10 μM, 20 μM, 50 μM, 100 μM and 200 μM, the same concentration range previously used for characterizing the dose-response relationship of WIN17317-3. Each concentration was applied for a period of 15 minutes. 7 compounds from this series were tested by Dr. Mona Alqatari (PDRA, Koltzenburg group).

The dose-response curves are plotted alongside the structure of the compounds in Figure 55. All compounds, with the exception of **107\***, were found effective in largely blocking C-CAP conduction at the concentration range tested. The 1 μM concentration appeared to have no significant effect on C-CAP amplitude; for the majority of compounds 10 μM was the lowest concentration causing a decrease in the C-CAP current. Whilst for many compounds, full C-CAP blockade was achieved at the highest concentration investigated, that is 200 μM, some compounds (such as **101\***, **102\***, and **103\***), did not produce full C-CAP block at this concentration. The top asymptote of the dose-response curves for the latter could therefore not be defined. Parameters determined from such incomplete dose-response curves are usually associated with larger error values. EC<sub>50</sub> values calculated from such data sets are clearly marked in potency tables, to highlight the increased error likely associated with the values.

The R<sup>2</sup> series analogues investigated, exhibited a range of C-CAP EC<sub>50</sub>s between 26-160 μM and EC<sub>90</sub>s in the range of 107-337 μM (Table 20). Interpreting the observed SAR for this series, introduction of substituents at the benzyl ring (nitrile and fluoride) was found to be well tolerated; the C-CAP blocking activity was maintained independent of the electronic nature and the position of the substituent at the ring. Nitrile containing compounds **101\***, **102\***, and **103\*** caused more than 70% C-CAP block at the highest 200 μM concentration. Based on EC<sub>50</sub>s, the rank of potencies for nitrile containing analogues was *ortho*>*meta*>*para* (Table 20). The *meta* fluoro benzyl analogue **104\***, was the second most potent compound in the R<sup>2</sup> series with a C-CAP EC<sub>50</sub> of 39.5 (± 6.5) μM. The most potent compound of the series was the branched methyl benzyl analogue **108\***, tested as a racemic mixture, with an EC<sub>50</sub> of 26.2 ± 08 μM and EC<sub>90</sub> of 106.8 ± 9.2 μM. Compound **106\***, bearing a 2-pyridinyl ring as the R<sup>2</sup> substituent proved particularly interesting; its dose-response curve, unlike all other compounds explored, resembled the profile of a

partial rather than a full antagonist. The fitted dose-response curve appeared to reach a plateau at  $65 (\pm 4)\%$  of C-CAP block, suggesting that this is the maximal response that can be elicited by the drug. More experiments at a higher dose range are required to validate and investigate this result further.

Moving from aryl to alkyl  $R^2$  substituents, the methyl analogue **107\*** was the least active compound in the series, producing less than 40% C-CAP block at the 200  $\mu\text{M}$  concentration. Introduction of the bulkier methylcyclohexyl and cyclohexyl substituents in compounds **105\*** and **56**, respectively, restored blocking activity which implies that lipophilicity and energetic interactions play an important role at the binding site, and that this region of the pharmacophore tolerates sterically demanding groups. Compound **105\*** exhibited essentially the same dose-response profile as the 'hit' WIN17317-3. This suggested that both alkyl and aryl groups could potentially be introduced as the  $R^2$  substituent of an investigational therapeutic agent. Having a pool of active compounds can be beneficial for a drug development program as other important molecular properties of a drug such as solubility and metabolic stability could be optimized by exploring different substituents whilst retaining the desired biological effect.

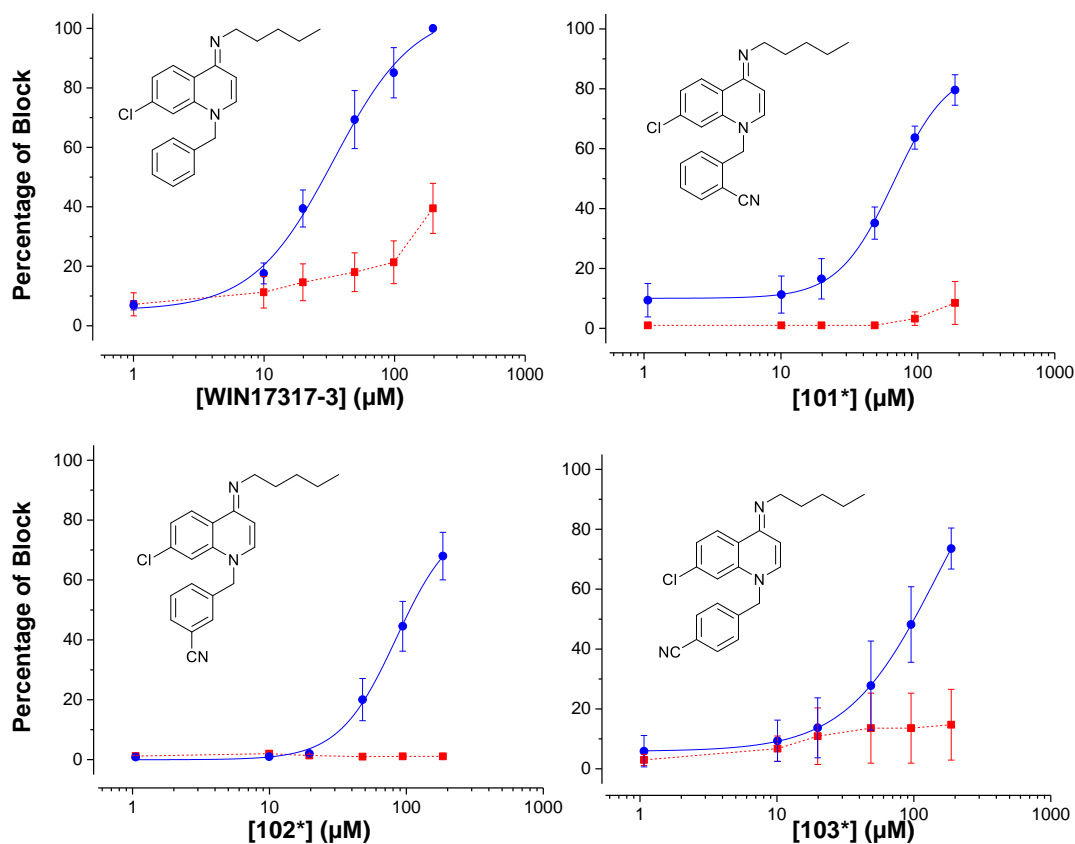
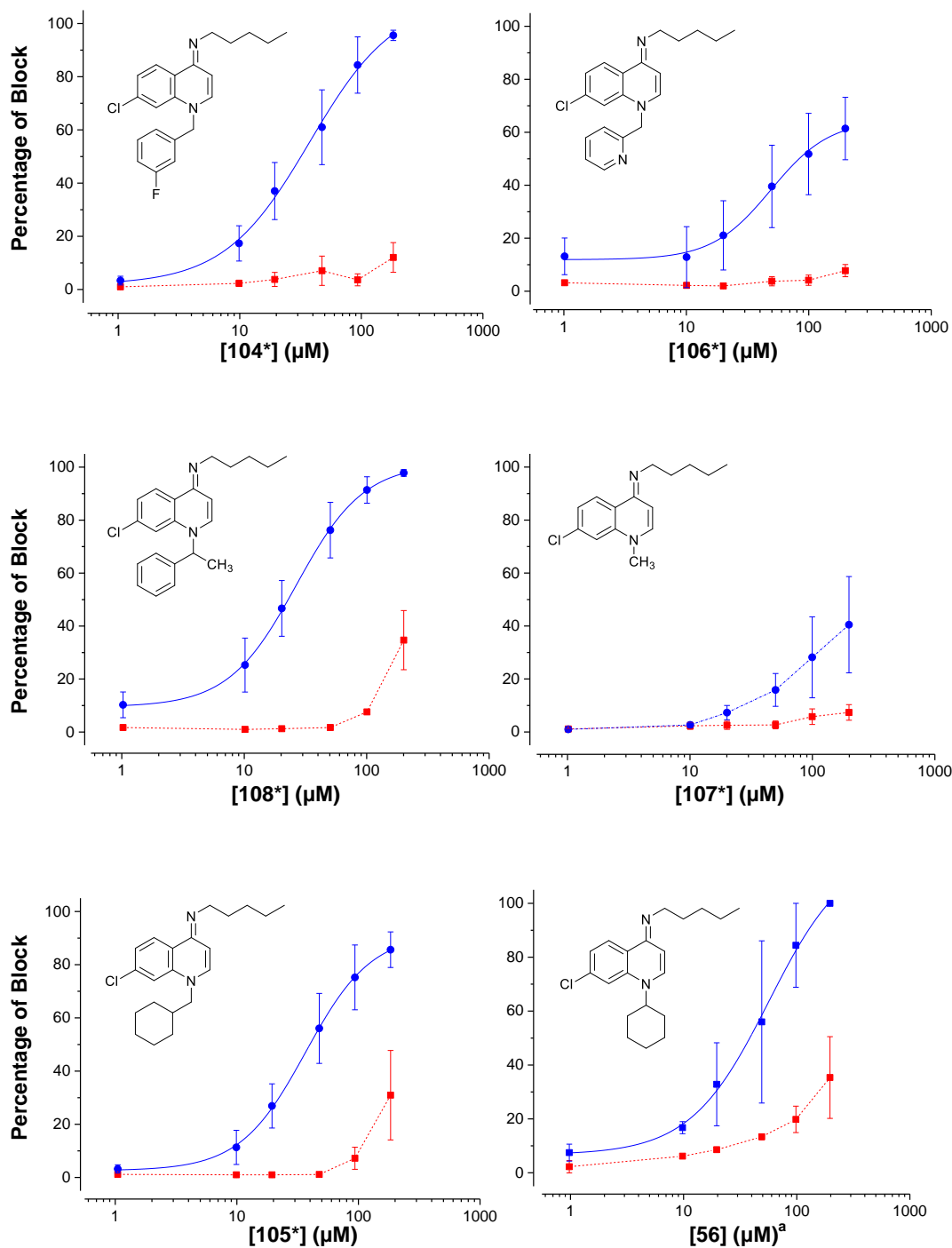


Figure 55. (continued).



**Figure 55.** Effects of R<sup>2</sup>-series analogues in the skin-nerve preparation. Saphenous nerve Aβ (■) and C (●) fiber CAP blockade as a function of iminodihydroquinoline concentration. Data shown as mean ± S.E.M ( $n \geq 4$ , (a)  $n = 2$ ), fitted dose-response curves presented as solid lines.

**Table 20.** Summary of half-maximal and maximal concentrations ( $EC_{50}$  and  $EC_{90}$ ) for C-CAP blockade as a result of modifications at the  $R^2$  substituent.

Entry	Cpd	$EC_{50}$ ( $\mu$ M)	S.E.	$EC_{90}$ ( $\mu$ M)	S.E.	N
1	1	34.6	5.1	149.2	49.7	9
2	101*	69.1 <sup>a</sup>	3.8	-	-	4
3	102*	89.4 <sup>a</sup>	8.6	-	-	5
4	103*	156.3 <sup>a</sup>	7.2	-	-	4
5	104*	39.5	6.5	243.4	99.6	4
6	106*	49.1 <sup>a</sup>	6.3	-	-	4
7	108*	26.2	0.8	106.8	9.2	4
8	107*	-	-	-	-	4
9	105*	38.4 <sup>a</sup>	1.5	-	-	5
10	56	57.6	11.6	331.4	156.2	2

<sup>a</sup>Dose-response relationship fitted with a non-defined top asymptote.

The SARs of  $R^3$  substituents were investigated next. Examining the dose-response curves of the  $R^2$ -series analogues (*vide supra*) it became apparent that the concentration range used was not sufficient to produce complete C-fiber block in the majority of examples. The experimental method was therefore modified to include a concentration scouting run for each new compound tested. This involved an experiment run at a concentration range of 20  $\mu$ M to 1 mM (20  $\mu$ M, 50  $\mu$ M, 100  $\mu$ M, 200  $\mu$ M, 500  $\mu$ M, 1 mM). Based on the outcome, the most appropriate out of two concentrations ranges was selected for evaluating the dose-response profile of the compound: (a) low: 1-200  $\mu$ M or (b) high: 20-1000  $\mu$ M.

Three analogues from the  $R^3$ -series, **2**, **21** and **24** were initially examined (Fig. 56). Chlorine substitution at the parent WIN17317-3 with the bulkier and more lipophilic iodine in **2** led to a two-fold drop in C-CAP  $EC_{50}$ . Halogen substitution with hydrogen in **21** led to a further drop in potency and a C-CAP  $EC_{50}$  of 120.7  $\mu$ M. Interestingly, incorporation of the electron-donating methoxy group in **24** led to equipotent C-CAP inhibition to the electron neutral hydrogen substituted compound **21**.

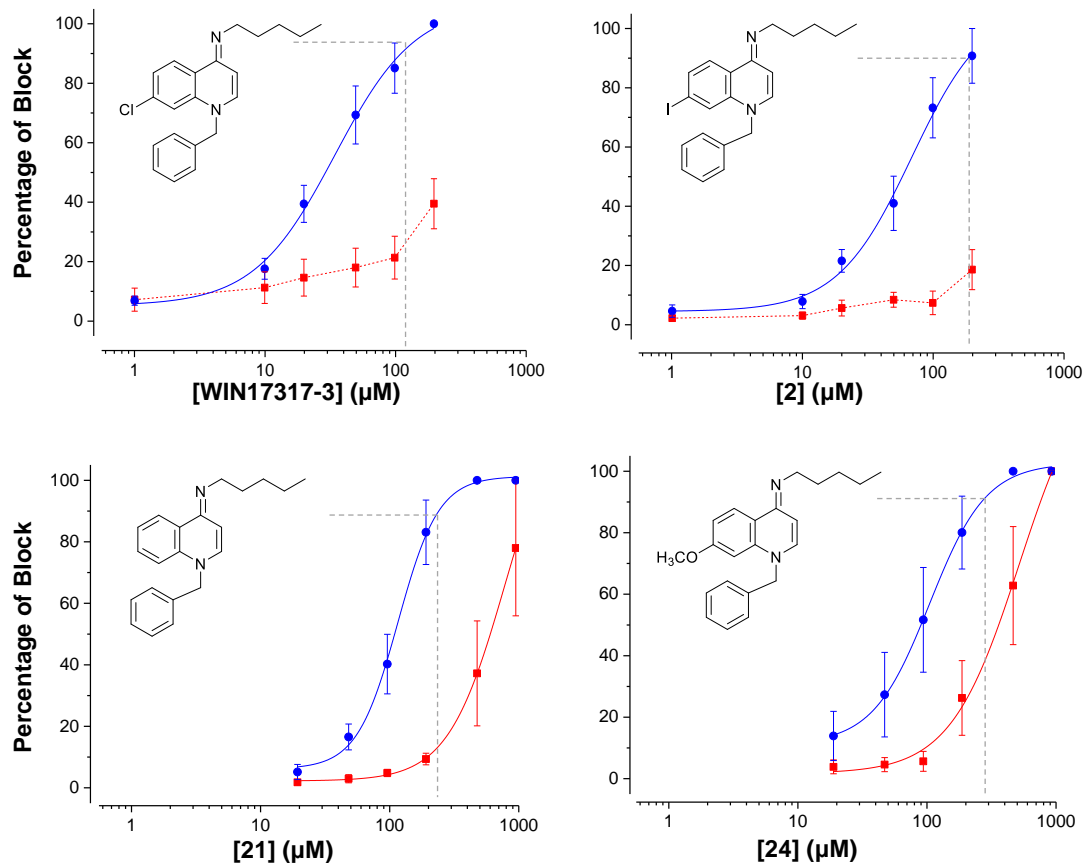


**Figure 56.** Effects of R<sup>3</sup>-series analogues in the skin-nerve preparation. Block of saphenous nerve Aβ (■) and C (●) fiber CAP as a function of drug concentration. Data are shown as mean ± S.E.M ( $n \geq 4$ ). Fitted dose-response curves are presented as solid lines.

**Table 21.** Summary of half maximal and maximal effective concentrations (EC<sub>50</sub> and EC<sub>90</sub>) for C-fiber blockade in rat saphenous nerve as a result of modifications at the R<sup>3</sup> substituent.

Entry	Cpd	EC <sub>50</sub> (μM)	S.E.	EC <sub>90</sub> (μM)	S.E.	N
1	1	34.6	5.1	149.2	49.7	9
2	2	68.9	15.7	290.7	157.7	4
3	21	120.7	5.8	269.6	28.2	4
4	24	112.0	5.5	341.9	38.1	4

### 5.2.2. Selectivity for C- over A-fiber blockade

In order to assess the compounds' selectivity for blocking C-fibers over A-fibers, the %A-CAP block produced at the concentration point where C-CAP reached maximal blockade ( $EC_{90}$ ) was measured. The selectivity for C- over A-fiber block was defined as the ratio between the %C-CAP and %A-CAP blocks at the  $EC_{90}$  concentration for C-CAP. The results are illustrated in Figure 57. The C- over A-fiber selectivity of compounds with incomplete C-CAP dose-response curves could not be quantified at this point.

From the  $R^2$  series, two compounds, **104\*** and **108\***, were found to exhibit superior C- over A-fiber selectivity relative to the hit WIN17317-3. The *meta*-fluoro substituted benzyl analogue **104\*** exhibited less than 15% A-CAP block at the C-CAP  $EC_{90}$ , 243.4  $\mu$ M, translating to a nearly 8-fold selectivity for C- over A-fibers. Similarly the branched methyl benzyl analogue **105\*** exhibited a 9-fold C-over A-fiber selectivity. The cyclohexyl analogue **56** was the least selective compound of the series with almost 50% of the A-CAP blocked at C-CAP  $EC_{90}$ .

**21** was the most selective compound of the  $R^3$  series with less than 20% A-CAP block at C-CAP  $EC_{90}$ . The iodinated analogue **2** was the next most selective with 22% block whilst the methoxy analogue **24** was the least selective compound of the  $R^3$  series with more than 50% of A-CAP blocked.

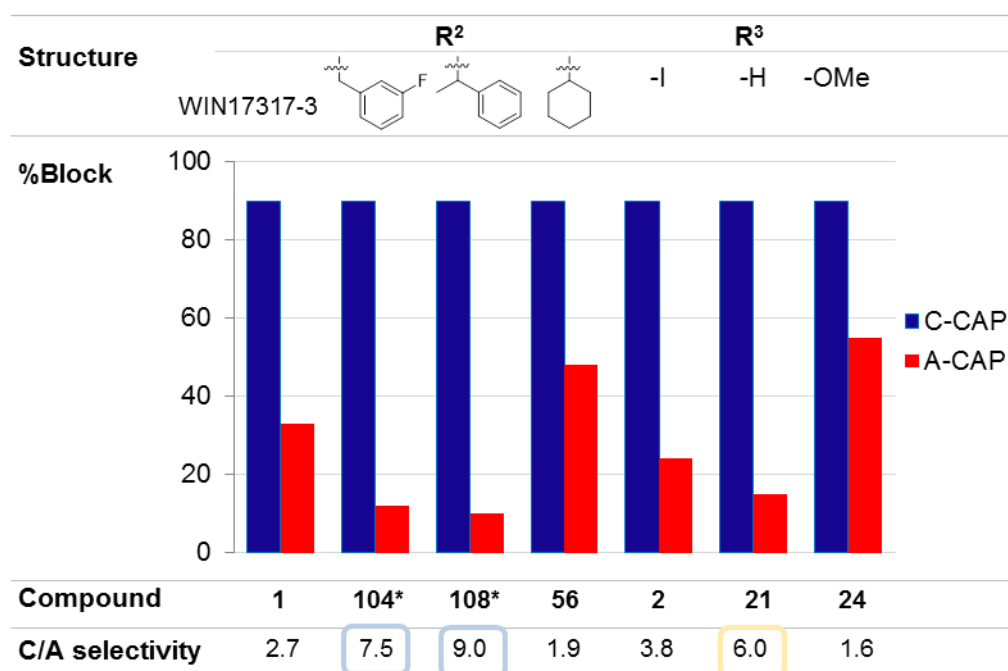


**Figure 57.** C- over A-fiber selectivity for  $R^2$ - and  $R^3$ -series analogues. 90% C-CAP block for each compound is plotted alongside the simultaneously recorded value for % A-CAP. The C- over A-fiber selectivity was calculated as the ratio between the two at the bottom of the chart.



After screening 14 compounds in total, it became apparent that iminodihydroquinolines are potent, selective blockers of C-fibers whilst leave the A-fibers largely unaffected. All attempted modifications at the R<sup>2</sup> and R<sup>3</sup> positions, with the exception of one (R<sup>2</sup> = CH<sub>3</sub>), were found to cause potent C-CAP inhibition. Several compounds with C- over A-fiber selectivity superior to that of WIN17317-3 were identified. Given the laborious nature of skin-nerve experiments, a lead compound from the first two series was selected and used as the basis for further investigations of the R<sup>1</sup> pharmacophore region.

### 5.3. Lead identification and development

Prior to selecting a lead from a compound series, it is important to define the potential roles that this would be required to fulfill; these will in turn determine the molecular properties the lead should possess and hence dictate the selection process. The lead compound in this study was to be used (a) as an experimental tool for investigating the mechanistic origin of the C- over A-fiber selectivity and (b) as a lead drug candidate that upon further optimization would enter *in vivo* pharmacokinetic and toxicity studies in rodents and potentially human *ex-vivo* nerve conduction studies for future development as a local analgesic drug.

As such, the most important property the lead should possess in terms of biological activity was maximal selectivity for blocking C- over A-fibers. This would facilitate the elucidation of its molecular mechanism of action at peripheral nerves, and at the same time minimize side effects and idiosyncratic toxicities when applied as a drug candidate at a therapeutic dose. The lead should exhibit high potency for its physiological target, the C-fibers, and in addition retain “drug-like” physicochemical properties. Accordingly, the optimal substituents from the R<sup>2</sup> and R<sup>3</sup> series were selected and combined in a molecule to afford a new lead compound (Fig. 58).

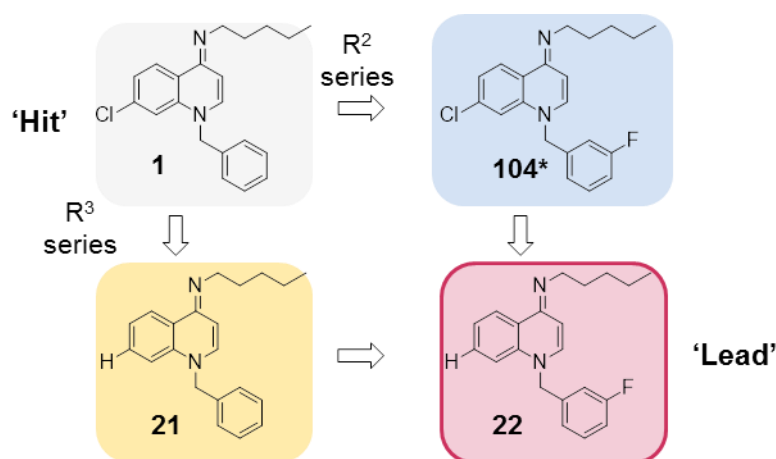


**Figure 58.** Hit to lead development. Optimal  $R^2$  and  $R^3$  substituents were combined for the design of the lead compound **22**.

The *meta*-fluorobenzyl substituent of compound **104\***, was selected as the optimal  $R^2$  substituent, on the basis of the high C- over A-fiber selectivity (8-fold) and also the high potency for C-fiber blockade ( $EC_{50} = 39.6 \pm 6.5 \mu\text{M}$ ) exhibited by **104\***. In addition, the fluoride substituent provides a potential site for [ $^{18}\text{F}$ ]fluorination, which would facilitate pharmacokinetic profiling studies. From the  $R^3$  series, the compound demonstrating the highest C-over A-fiber selectivity was **21** bearing hydrogen as the  $R^3$  substituent. **21** was less potent ( $EC_{50} = 120.7 \pm 5.8 \mu\text{M}$ ) than WIN17317-3 ( $EC_{50} = 34.6 \pm 5.1 \mu\text{M}$ ) towards blocking C-fibers, however it exhibited favorable “drug-like” physicochemical characteristics such as low melting point known to contribute to higher aqueous solubility. Hydrogen was therefore selected as the optimal  $R^3$  substituent.

The proposed new lead compound, **22**, bearing the optimal  $R^2$  and  $R^3$  substituents described above, was synthesized and tested for its effects in the skin-nerve preparation (Fig. 59). Gratifyingly, **22** was found to be the most selective of all compounds screened up to this point, with the C- over A-fiber selectivity exceeding those of both the hit WIN17317-3 and the “parent” molecules **104\*** and **21**. Less than 5% of A-CAP block was observed at the C-CAP  $EC_{90}$   $301 \pm 45 \mu\text{M}$ . This translates to a 30-fold selectivity for C- over A-fibers at the anticipated therapeutic dose range. In terms of potency, **22** with an  $EC_{50}$  value of  $160.4 \pm 9.6 \mu\text{M}$  was an order of magnitude less potent than WIN17317-3.

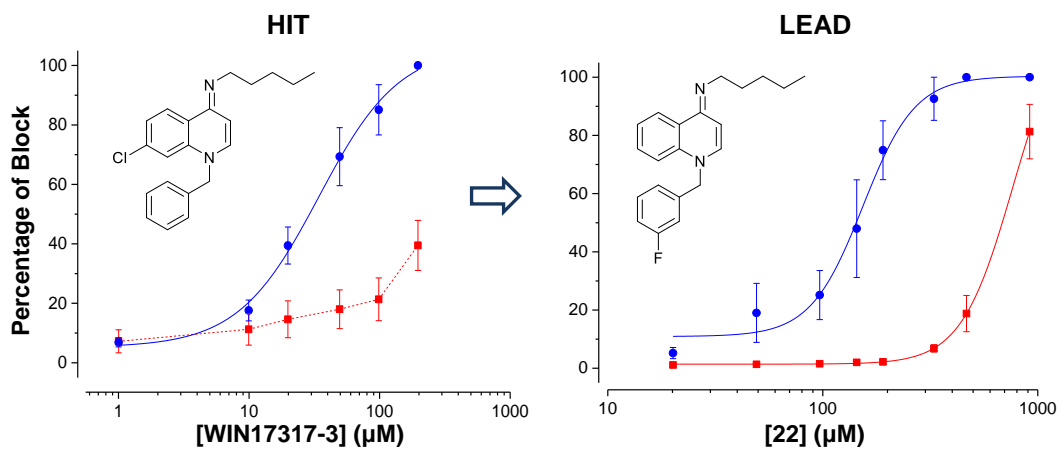


**Figure 59.** Effects of Hit (WIN17317-3) and Lead (**22**) molecules in the skin-nerve preparation. Block of saphenous nerve A $\beta$  ( $\blacksquare$ ) and C ( $\bullet$ ) fiber CAP as a function of drug concentration. Data are shown as mean  $\pm$  S.E.M ( $n \geq 4$ ). Fitted dose-response curves are presented as solid lines.

## 5.4. Second generation iminodihydroquinoline analogues

A second generation library of compounds was designed and synthesized based on the structure of the lead **22** in an attempt to improve potency whilst further exploring the SARs of iminodihydroquinolines. Modifications were focused around the least explored R<sup>1</sup> and R<sup>3</sup> pharmacophore regions (Fig. 60).

### 5.4.1. Effects on C- and A-fiber conduction

All second generation compounds were tested at the high concentration range of 20  $\mu\text{M}$  to 1 mM. This allowed the deduction of complete C-CAP dose-response curves as well as determination of the corresponding A-CAP EC<sub>50</sub>s.

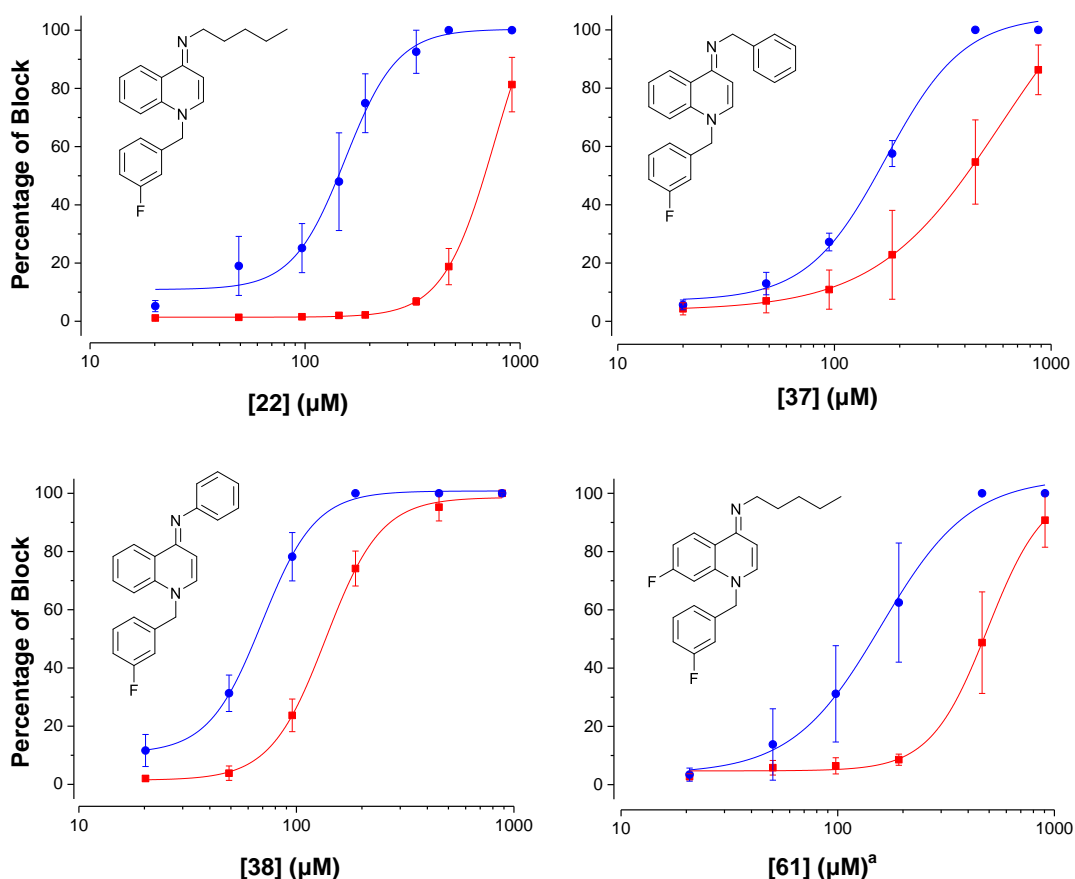


**Figure 60.** Effects of second generation analogues in the skin-nerve preparation. Block of saphenous nerve A $\beta$  (■) and C (●) fiber CAP as a function of drug concentration. Data are shown as mean  $\pm$  S.E.M ( $n \geq 4$ , <sup>a</sup> $n = 3$ ). Fitted dose-response curves are presented as solid lines.

**Table 22.** Summary of half-maximal and maximal effective concentrations ( $EC_{50}$  and  $EC_{90}$ ) for C-fiber blockade in rat saphenous nerve by second generation analogues.

Entry	Cpd	$EC_{50}$ ( $\mu\text{M}$ )	S.E.	$EC_{90}$ ( $\mu\text{M}$ )	S.E.	N
1	<b>22</b>	160.4	9.6	301.4	45.0	4-9
2	<b>37</b>	186.6	18.1	481.4	124.9	4
3	<b>38</b>	71.8	2.0	136.7	6.4	4
4	<b>61</b>	164.5	16.4	481.3	126.5	3

Two compounds, **37** and **38**, bearing benzyl and phenyl  $R^1$ - substituents, respectively, were evaluated at the skin-nerve preparation to examine the requirements of the  $R^1$  pharmacophore region. Substitution of the pentyl chain in **22** with the benzyl group in **37** maintained C-CAP blocking activity with the two compounds exhibiting similar potency values. The introduction of a phenyl ring as the  $R^1$  substituent in **38**, on the other hand, led to a two-fold increase in potency and a C-CAP  $EC_{50}$  of  $71.8 \pm 2.0 \mu\text{M}$ . In terms of C- over A-fiber selectivity, both compounds were significantly less selective than the lead. **38** in particular, was the least selective compound from both libraries blocking more than 65% of A-CAP at C-CAP  $EC_{90}$  (Fig. 61).

Further investigating the effects of modifications at the  $R^3$  pharmacophore region, fluoride, a commonly used hydrogen bioisostere, was introduced as the  $R^3$ -substituent in **61** (Fig. 60). Compound **61** exhibited lower potency ( $EC_{50} = 164.5 \pm 16.4 \mu\text{M}$ ) than the previously explored  $R^3$  halogenated analogues (-Cl and -I) for C-CAP blockade, yet it was equipotent to the hydrogen substituted **22** (Table 22); this suggested spatial requirements are associated with the  $R^3$  pharmacophore region. Regarding C-over A-fiber selectivity, **61** blocked more than 45% of A-CAP at the C-CAP  $EC_{90}$  meaning this is only two-fold selective (Fig. 61).

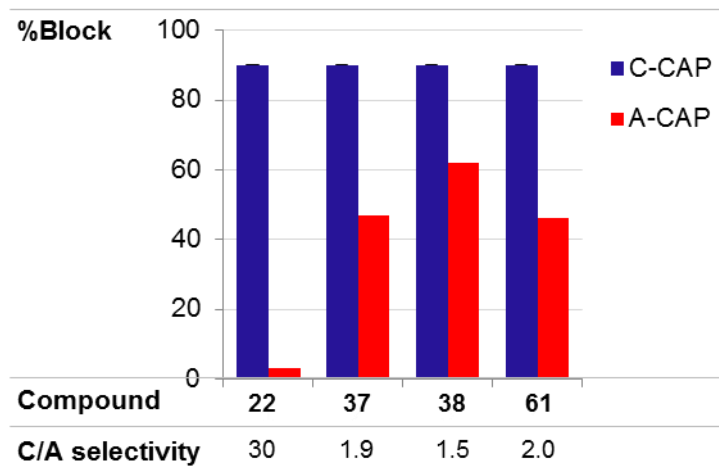


**Figure 61.** Effects of second generation analogues on C- and A-fiber conduction as measured in the skin-nerve preparation. 90% C-CAP block for each compound is plotted alongside the simultaneously recorded value for % A-CAP block at this concentration. C/A-CAP block ratios, at the bottom of the chart, were calculated as a measure of the C/A-fiber selectivity.

Comparing the  $EC_{50}$  values of C-CAP and A-CAP block for the second generation iminodihydroquinolines, confirmed that the selected lead compound from the first library, **22**, was more selective than all the compounds of the second generation library (Fig. 62). At this point, **22** was appointed as the lead preclinical drug candidate for entering pharmacokinetic profiling studies.

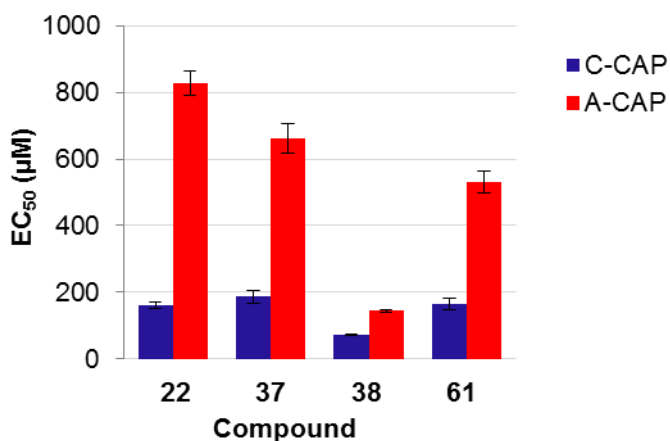


**Figure 62.** Half maximal effective concentrations ( $EC_{50} \pm S.E.$ ,  $n \geq 3$ ) of second generation analogues for C- and A-CAP blockade as measured in the skin-nerve preparation.

### 5.4.2. Na<sub>v</sub> screening

The *in vitro* effects of the second library of iminodihydroquinolines at Na<sub>v</sub>s were evaluated using the IonWorks Barracuda platform (Table 23). Gratifyingly, **22**, as well as analogue **38**, exhibited state- and use-dependency, displaying two-fold lower IC<sub>50</sub> values for channels in those states over resting Na<sub>v</sub>s (tonic block). On the contrary, compound **37** inhibited Na<sub>v</sub>s at all three voltage states with similar levels of potency. The effects of the lead were evaluated at Na<sub>v</sub>1.7, the molecular target of interest, but also at the Na<sub>v</sub>1.4, Na<sub>v</sub>1.5 and Na<sub>v</sub>1.6 isoforms aiming to assay potential off-target toxicity. Unfortunately, **22** was found to block non-selectively all of the Na<sub>v</sub> isoforms investigated. Interestingly, the most and least selective compounds for C- over A-fiber blockade, **22** and **38** respectively, displayed similar IC<sub>50</sub> values for the Na<sub>v</sub>1.6 and Na<sub>v</sub>1.7 isoforms. The significance of this for unraveling the molecular mechanism of action of iminodihydroquinolines at peripheral nerves is discussed in section 5.7.

**Table 23:** IC<sub>50</sub> values of second generation iminodihydroquinolines for hNa<sub>v</sub> inhibition.

Cpd	Na <sub>v</sub> Isoform	IC <sub>50</sub> ± SE (μM)		
		Tonic block	Use-dependent block	State-dependent block
<b>22</b>	Na <sub>v</sub> 1.4	2.98 ± 0.41	1.57 ± 0.20	1.32 ± 0.35
	Na <sub>v</sub> 1.5	9.90 ± 0.67	2.20 ± 0.08	4.03 ± 0.28
	Na <sub>v</sub> 1.6	4.70 ± 0.79	1.59 ± 0.10	1.30 ± 0.06
	Na <sub>v</sub> 1.7	5.42 ± 0.80	1.77 ± 0.11	2.15 ± 0.24
<b>37</b>	Na <sub>v</sub> 1.7	1.65 ± 0.18	1.01 ± 0.08	1.15 ± 0.08
<b>38</b>	Na <sub>v</sub> 1.6	6.59 ± 0.63	2.24 ± 0.12	1.34 ± 0.09
	Na <sub>v</sub> 1.7	6.45 ± 0.60	1.89 ± 0.07	1.78 ± 0.13

## 5.5. Nerve absorption and metabolism pharmacokinetics

The rapid metabolism and tissue clearance exhibited by [ $^{125}$ I]labelled iminodihydroquinoline **2** after iv administration in mice (see page 28), suggested that the plausible routes of administration for this compound class are limited to those avoiding drug passage through the systemic circulation, i.e. local administration. Such routes are the local infiltration, epidural, spinal and topical/surface administration and peripheral nerve block, all widely used in clinical practice for the delivery of LA drugs.<sup>218</sup> Local administration leads to drug deposition at the nerve surface, which upon a series of steps will reach the individual neuronal fibers to exert its effects.

Before assessing the rate of **22** nerve absorption and the impact of this on the onset and maintenance of nerve block, a description of the anatomical features of the rat saphenous nerve is given below to provide a brief overview over the anticipated drug movement pathway. The saphenous nerve consists of afferent A $\beta$ , A $\delta$  and C-fibers, tightly packed together in bundles known as *fasciculi* (Fig. 63). Each fiber is cased by a thin membrane, the endoneurium, and each bundle of fibers is surrounded by two to four layers of flattened connective tissue known as the perineurium. Saphenous nerves are in their majority monofasciculated, yet nerves consisting of two or more fascicles are also known to exist. The outermost layer of connective tissue is the epineurium and encloses the nerve fascicles and the blood vessels supplying the nerve.

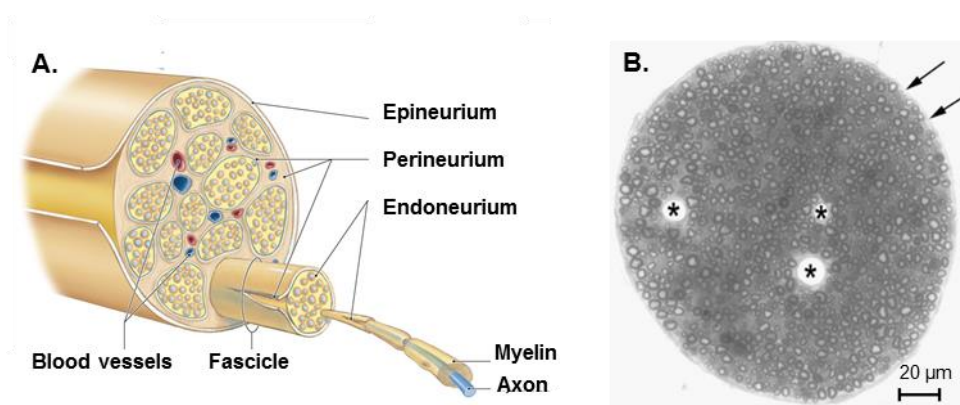


**Figure 63.** Cross sectional aspects of the rat saphenous nerve. A. Schematic representation of the nerve illustrating fascicles and individual nerve fibers. Components in an orderly fashion from the outermost layer to the inner most include the epineurium, perineurium, endoneurium and Swann cells surrounding the axon. B. Light micrograph of a monofasciculated nerve, enveloped by a well-defined perineurium (arrows), showing myelinated fibers and capillary blood vessels (\*) in the endoneurial space.<sup>214</sup>



The average number of myelinated A-fibers in the saphenous nerve is 700 and the ratio of unmyelinated C-fibers to A-fibers has been measured to 3.42:1.<sup>213</sup> A recent study investigating the anatomy of young female rat saphenous nerves has demonstrated that these are longitudinally and laterally symmetrical with no morphological differences between proximal and distal segments, as well as between right and left sides. Myelinated and unmyelinated fibers are found intermingled in the endoneural space.<sup>214</sup>

Following drug administration into the soft tissues near the nerve, drug molecules will move from the extraneural site towards the inner layers of the nerve *via* diffusion according to the concentration gradient. They will first cross the epineurium to reach the perineurium, which is the greatest diffusional barrier, and from there move into the endoneurium to reach their site of action, the individual nerve fibers.

The first step towards assessing the local pharmacokinetics of **22** involved a quick stability study to identify to which degree the compound remained intact after administration. The solutions of **22** applied to the nerve, were analyzed by high performance liquid chromatography (HPLC) at the end of a dose-response experiment; the chromatograms revealed no additional species apart from the parent **22** in the solutions examined. This suggested **22** is stable under the experimental conditions and is most likely the active species for the pronounced effects at the saphenous nerve.

Two experiments were carried out to examine the effects of biological barriers on absorption, onset of nerve conduction blockade, and potency of **22**. The first experiment involved nerve desheathing a procedure by which the outer epineurium and perineurium connective tissues are carefully detached from the nerve, uncovering the free neuronal fibers. The dose-response relationship of **22** at the desheathed nerve was determined by applying a series of ascending drug concentrations for 15 minute periods each, as previously described for the assay using intact nerves (Fig. 64). As expected, **22** was much more potent in blocking C-CAPs in desheathed rather than intact nerves; a 20-fold increase in potency was observed and complete C-fiber blockade was achieved at 50  $\mu$ M. This suggested slow diffusion of **22** through the various layers of connective tissue. Gratifyingly, A-fiber conduction in the desheathed nerve preparation remained unaffected at the concentration point where full C-CAP blockade was achieved, suggesting that the source of differential C- over- A-fiber block is not related to the time course of drug diffusion into the nerve or the nerve's anatomical features.

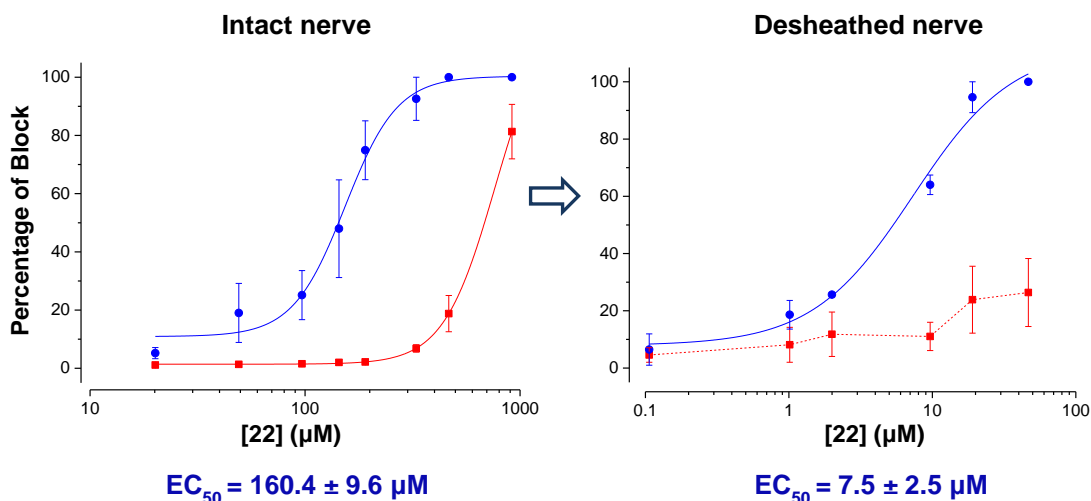


**Figure 64.** Effects of the lead compound **22** in intact (left) and desheathed (right) saphenous nerves. Block of A $\beta$  (■) and C (●) fiber CAP as a function of drug concentration. Data are shown as mean  $\pm$  S.E.M ( $n = 9$  intact,  $n = 2$  desheathed). Fitted dose-response curves are presented as solid lines.

The results of the experiment imply that a temporal component is associated with all dose-response data reported so far, and is a result of diffusion barriers. The rate of diffusion is governed by the concentration gradient, and the speed of onset of drug action is essentially proportional to the log of drug concentration. As a consequence, doubling the concentration of the drug will only marginally speed up the onset of block, although it is likely to block fibers more effectively and prolong the duration of block. Lipophilicity is one of the key molecular properties influencing the rate of diffusion and hence the speed of effect onset. The iminodihydroquinolines tested are likely to exhibit a range of diffusion rates according to their distinct logP values.

To explore the time course of diffusion of **22** into the nerve, a single concentration, just below the  $EC_{50}$ , 130  $\mu\text{M}$ , was applied to the intact saphenous nerve for a time period of 90 minutes (Fig. 65). At 15 minutes, 40% C-CAP blockade was observed, consistent with the previously obtained data for the dose-response relationship of **22**. There was a linear increase in the %C-CAP block with time, from 0 to 45 minutes, at which point complete block was reached. A-fiber conduction remained practically unaffected during the course of the experiment. This confirmed that the differential block observed for the two fiber classes is not a temporal phenomenon but rather a result of the axons being *per se* differentially sensitive to the block.

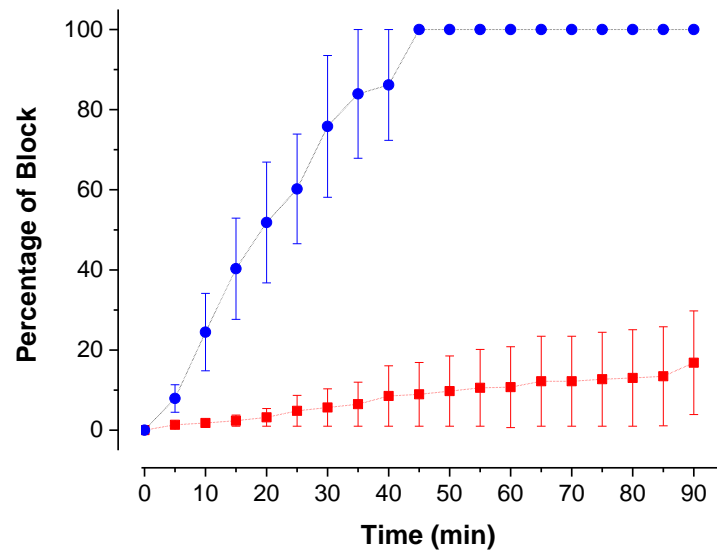


**Figure 65.** Effects of lead compound **22**, applied at a single concentration, 130  $\mu\text{M}$ , at the intact saphenous nerve for 1.5 h. Block of A $\beta$  (■) and C (●) fiber CAP as a function of time. Data are shown as mean  $\pm$  S.E.M ( $n = 4$ ).

The above experiments signify the clinical potential of iminodihydroquinolines as local analgesic drugs. Primarily, complete impulse inhibition and functional impairment of C-fibers has been achieved whilst maintaining conduction of myelinated A $\beta$  afferents over an extended period of time. This may translate to effective pain relief *in vivo* without loss of the discriminative touch sensation. We anticipate that preferential block of C-fibers will also be exerted over the larger A $\alpha$  myelinated fibers, responsible for motor control, hence also avoiding the paralysis side effects exerted by the currently used LAs. In terms of potency, the above experiments demonstrate that complete C-CAP blockade can be achieved at concentrations significantly lower than those initially estimated from the dose-response relationships. A balance is required for dosing, between a concentration high enough to produce effective C-CAP blockade within a reasonable period of time yet without compromising safety.

## 5.6. Comparative assessment towards local anesthetics

Peripheral nerve block induced by LA drugs, as observed clinically, can sometimes lead to differential functional blockade; pain is often alleviated whilst motor function and touch sensation are less affected. This is presumed to be the result of a complex behavior *in vivo*, with numerous investigational studies on the subject yielding contradicting data. Despite widespread belief that the effective concentration of local anesthetics simply increases as a function of larger fiber diameter, the so called “size-principle”, the relationship appears to be much more complex than initially appreciated.<sup>219</sup> Other factors such as the type of fiber, the degree of myelination, the fiber length and the frequency dependence are also important.

With respect to the effects of lidocaine at single fiber APs, a consistent order of fiber block has been reported by many investigators, both *in vitro* and *in vivo*.<sup>220, 221, 222, 223</sup> The A $\delta$ -fibers were found to be the most susceptible of all categories, followed by the larger A $\beta$ -fibers, and the C-fibers being the least susceptible of all (Fig. 66). This could explain the clinical observation that pain sensation is numbed before motor function is affected, as the fast-pain transmitting A $\delta$ -fibers are blocked first. The preferential block of A $\delta$ -fibers however, over the prolonged-pain transmitting C-fibers, is not always beneficial in a clinical setting. It can often mislead an anesthesiologist about the extent of total block; if a region is falsely assigned as “anesthetized” while some C-fibers are still conducting, the residual afferent input might still be able to sensitize the CNS and thereby mediate post-operative pain.

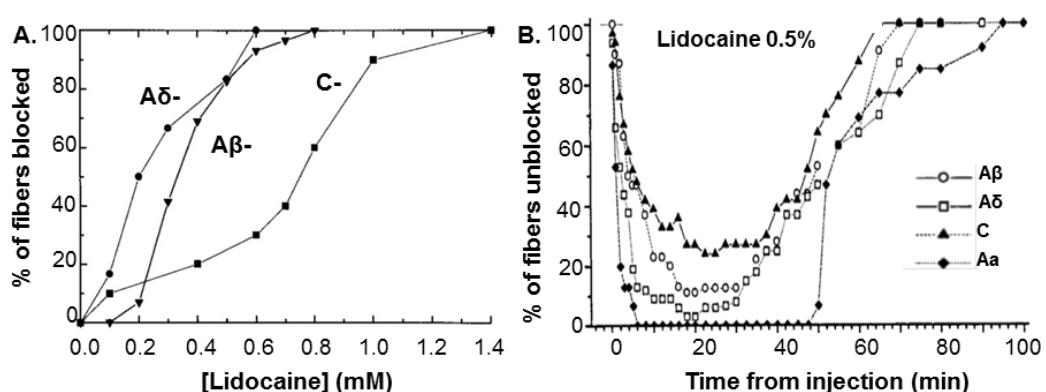


**Figure 66.** Effects of lidocaine in the rat sciatic nerve. (A) Tonic block of individual nerve fiber axons *in vivo*. All categories (A $\beta$ , A $\delta$ , C) are blocked over a range of concentrations from 0.2 to 0.8 mM yet nociceptive C-fibers are evidently significantly less susceptible.<sup>220</sup> (B) Time course of impulse blockade as a response to a non-equilibrium percutaneous bolus injection of 0.5% lidocaine around the nerve.<sup>223</sup> The differential rate and maximum degree of block exhibited by nerve fibers are consistent amongst the two studies. Adapted from references 220 and 223.

The effects of three clinically used LAs, lidocaine, butamben, and dibucaine in C- and A-fiber CAPs were assessed in the skin-nerve preparation for purpose of comparison with the lead compound **22**. Lidocaine is the gold standard for local analgesia and hence was examined first. C-fibers ( $EC_{50}$  value of  $415.9 \pm 90 \mu\text{M}$ ) were found to be slightly more susceptible to lidocaine than A-fibers,  $EC_{50} = 715.8 \pm 102.9 \mu\text{M}$  (Fig. 67, 68). At the concentration point causing 90% of C-CAP block, A-CAP block reached approximately 70% (Fig. 69). An analogous study reported in literature, investigating the effects of lidocaine on the desheathed rat saphenous nerve, also reports a lower C-CAP  $EC_{50}$  ( $= 63 \pm 6 \mu\text{M}$ ) than A-CAP  $EC_{50}$  ( $= 119 \pm 46 \mu\text{M}$ ). However, the difference was not statistically significant and lidocaine was classified as non-selective blocker of all CAP components.<sup>217</sup>

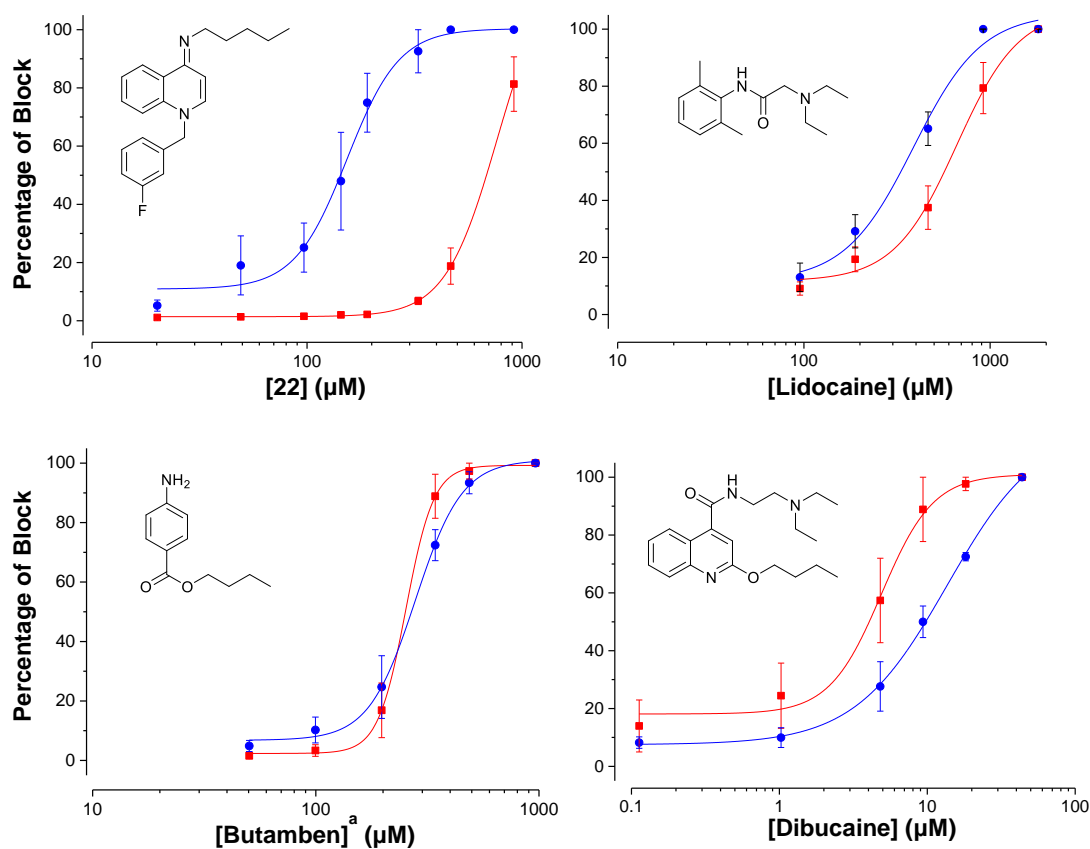


**Figure 67.** Effects of lead **22** and local anesthetics lidocaine, butamben and dibucaine, in the skin-nerve preparation. Block of saphenous nerve A $\beta$  (■) and C (●) fiber CAP as a function of drug concentration. Data are shown as mean  $\pm$  S.E.M ( $n \geq 4$ , <sup>a</sup> $n = 3$ ). Fitted dose-response curves are presented as solid lines.

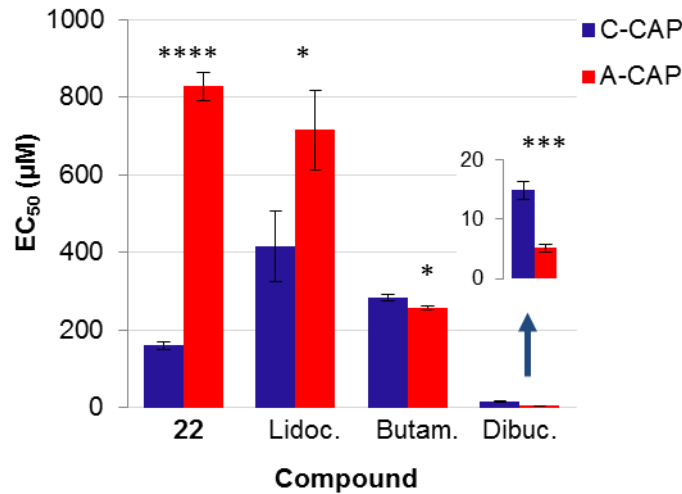


**Figure 68.** Half-maximal effective concentrations of lead **22** and local anesthetics lidocaine butamben and dibucaine ( $EC_{50} \pm S.E.$ ,  $n \geq 3$ ) for C- and A-CAP blockade in the skin-nerve preparation. Asterisks (\*) indicate the significance level of A and C-CAP  $EC_{50}$  difference, as calculated by the unpaired Students  $t$ -test (\*  $P \leq 0.05$ , \*\*\*  $P \leq 0.001$ , \*\*\*\*  $P \leq 0.0001$ ).

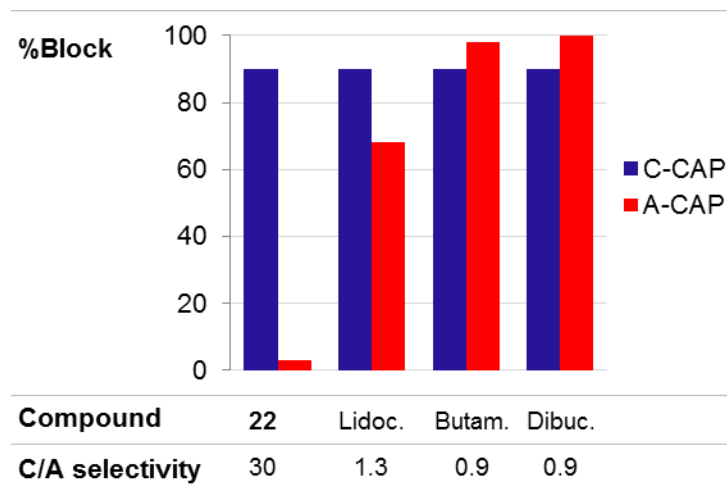


**Figure 69.** Effects of 'lead' **22** and local anesthetics on C- and A-fiber conduction in the skin-nerve preparation. 90% C-CAP block for each compound is plotted alongside the simultaneously recorded value for % A-CAP. C/A ratios, at the bottom of the chart, were calculated as a measure of the C/A-fiber selectivity for each compound.

The second LA examined at the skin-nerve preparation was butyl aminobenzoate (butamben). Butamben was first patented in 1923 for topical use, Butesin Picrate. It was later on formulated as a 5% aqueous suspension by Abbot Laboratories suitable for epidural administration. Butamben was of particular interest in the context of this study. Its epidural administration has been reported to produce long-lasting sensory blockade to cancer patients, with a marked reduction or even

absence of pain obtained, whilst preserving motor, bowel and bladder function.<sup>224</sup> Perplexingly, epidural administration of aqueous butamben solutions in rats did not produce similar selectivity, with the authors of the study attributing this to differences in the physicochemical properties of the suspension, rather than the butamben molecule *per se*.<sup>225</sup> A more recent study by Thériault *et al.* suggests that the observed selectivity could be partially due to enhanced and selective responsiveness of Na<sub>v</sub> channels in nociceptive neurons to butamben.<sup>226</sup> In the skin-nerve preparation butamben caused a dose-dependent inhibition of all phases of the CAP in a concentration range of 0.05 to 1 mM (Fig. 67). A slight preference was observed for A- over C-fiber blockade in terms of EC<sub>50</sub>s (Fig. 68), yet the compound was found to be non-selective at higher concentration dose-response points (C-CAP EC<sub>90</sub>) (Fig. 69).

The last LA evaluated in the skin-nerve assay was cinchocaine also known under the name dibucaine. Cinchocaine was the first LA of the quinoline group to be synthesized and was introduced into medical practice in 1932. Its high CNS and CVS toxicity limited its clinical use yet it remains the subject of several recent medical studies.<sup>227, 228, 229</sup> It has been the starting point for the exploration of other quinoline based derivatives as LAs.<sup>230</sup> Appreciating the common structural origin of iminodihydroquinolines and cinchocaine, its effects on CAP conduction were explored (Fig. 67). Interestingly cinchocaine, exhibited a reversed selectivity relative to iminodihydroquinolines, with A-fibers (EC<sub>50</sub>= 5.1 ± 0.6 μM) being more susceptible to block than C-fibers (EC<sub>50</sub>= 14.8 ± 1.5 μM) (Fig. 68). Like butamben, cinchocaine was non-selective at higher concentration dose-response points (Fig. 69).

Overall, the above findings suggest that the lead compound of this study, **22**, is far superior to all LAs examined, both in terms of C- over A-fiber block selectivity but also, with the exception of dibucaine, in terms of potency for blocking C-fibers.

## 5.7. Unraveling the molecular mechanism of iminodihydroquinoline action at nociceptors

### 5.7.1. Relationship between $\text{Na}_v1.7$ inhibition and C-fiber conduction block

One of the key objectives of the study was to elucidate the molecular mechanism of action of iminodihydroquinolines at nociceptors. As previously described in chapter 1.7,  $\text{Na}_v$  channels play a crucial role in the electrophysiology of nerve conduction, as they are responsible for the depolarization phase of the action potential. The  $\text{Na}_v1.7$  is one of the  $\text{Na}_v$  isoforms predominantly expressed in nociceptors. Having established that iminodihydroquinolines are potent  $\text{Na}_v1.7$  blockers, a positive correlation was anticipated between the levels of  $\text{Na}_v1.7$  inhibition and C-fiber blockade by members of the compound library. To investigate this hypothesis, the iminodihydroquinolines examined in the skin-nerve preparation were selected to represent a range of  $\text{Na}_v1.7$  potencies. The  $\text{IC}_{50}$  values of the 14 compounds tested, spanned the range of  $< 1 \mu\text{M}$  (7 compounds),  $1\text{-}10 \mu\text{M}$  (6 compounds), and  $> 10 \mu\text{M}$  (1 compound). The logarithmic relationship between the  $\text{IC}_{50}$ s for  $\text{Na}_v1.7$  and the  $\text{EC}_{50}$ s for C-CAP blockade of iminodihydroquinolines is plotted in Figure 70. The compound with  $\text{Na}_v1.7$   $\text{IC}_{50}$  higher than  $10 \mu\text{M}$  ( $\text{IC}_{50} = 94.4 \mu\text{M}$ ) was found inactive in the skin-nerve preparation at the concentration range tested, hence it is not included in the plot.

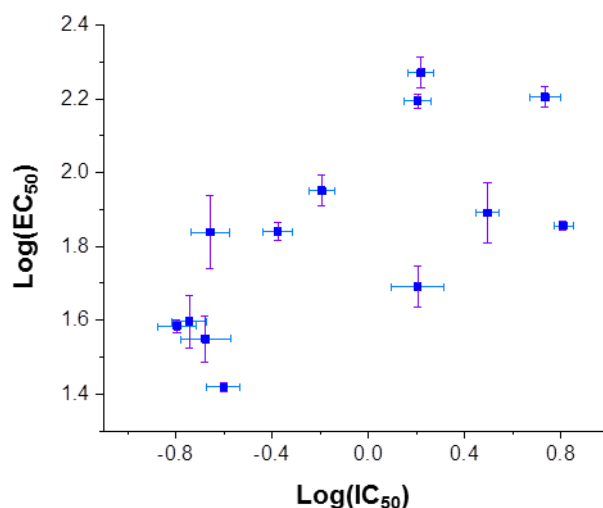


**Figure 70.** Logarithmic relationship between  $\text{IC}_{50}$  of  $h\text{Na}_v1.7$  at resting state, and  $\text{EC}_{50}$  of C-fiber blockade as determined by the automated patch clamp and the skin-nerve assays respectively. Standard deviations and standard errors are plotted as relative log error bars.<sup>231</sup>



As can be seen from the graph above, the potency for C-CAP blockade appears to increase with increasing  $\text{Na}_v1.7$  potency. In an attempt to quantify this relationship, a linear regression model was applied to the data set (Fig. 71.A). The line of 'best fit' had a calculated adjusted  $R^2$  value of 0.40 meaning only 40% of the variability could be accounted for by this relationship. Visually there was a trend with data points appearing to be divided into two groups of different gradients as illustrated in Figure 71.B. Indeed, when applying linear regression models to the newly assigned data sets, the  $R^2$  values of the two were improved compared to the previously applied model A, meaning these relationships were better fitted for describing the data.

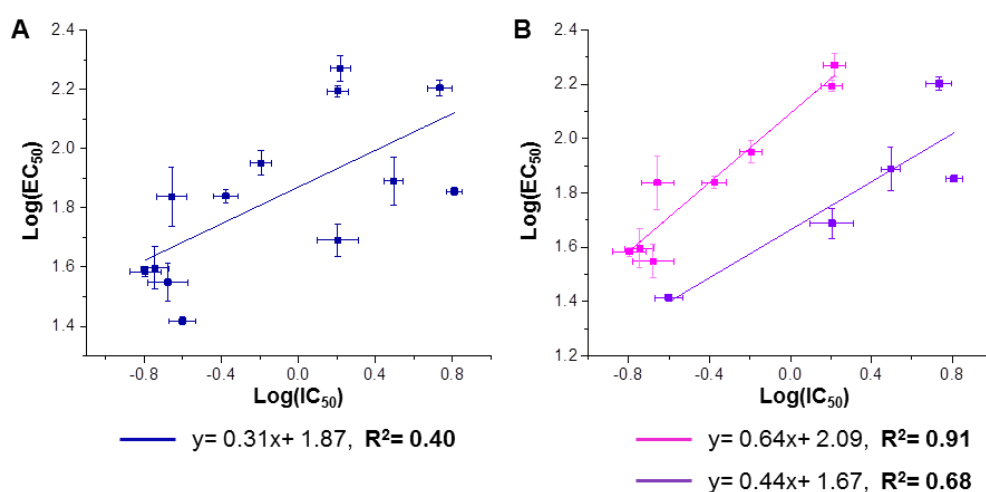


**Figure 71.** Linear regression models for describing the activity of iminodihydroquinolines at  $\text{Na}_v1.7$  and at sensory C-fibers. (A) The linear model characterizing the relationship between all data points, adj.  $R^2 = 0.40$  (B) Two linear models, applied at two group subsets, display increased  $R^2$  values (0.91, 0.68) and are therefore more appropriate predictors of the  $\log(\text{IC}_{50})/\log(\text{EC}_{50})$  relationship. Models and adjusted  $R^2$  values were calculated using the OriginPro software at linear fitting mode with no weighting.

It was hypothesized that the distinct correlations observed for the two groups of Fig. 71.B, could be attributed to differences in the diffusion rates of the compounds. Comparing several physical properties known to affect the diffusion rate of a compound, in particular the  $\log D$ , the molecular weight, the  $\text{pK}_a$  and the polar surface area, no apparent differences were found to exist between the two groups with respect to these parameters.

In summary, the above data provide evidence that  $\text{Na}_v1.7$  inhibition is the underlying mechanism of iminodihydroquinolines' sensory C-fiber blockade, yet the possibility of other targets also being engaged in the process cannot be ruled out.

### 5.7.2. $\text{Na}_v$ isoform selectivity and C- over A-fiber selectivity

We hypothesized that the selective C-fiber conduction blockade exhibited by iminohydroquinolines could potentially be mediated *via* selective inhibition of the  $\text{Na}_v$  isoforms predominantly expressed in this category of somatosensory neurons. More precisely, the C- over A-fiber selectivity was considered to originate from selective inhibition of the  $\text{Na}_v1.7$  over the  $\text{Na}_v1.6$  isoform.

The selectivity of compounds for blocking  $\text{Na}_v1.7$  over  $\text{Na}_v1.6$  isoforms was measured as the ratio between their  $\text{IC}_{50}$  values, as previously described in page 90. Compounds exhibiting a range of  $\text{Na}_v1.7$  over  $\text{Na}_v1.6$  selectivity were tested in the skin-nerve preparation, with some being equipotent for the two, to others showing up to 10-fold selectivity. The C- over A-fiber selectivity for each compound is plotted alongside its  $\text{Na}_v1.7$  over  $\text{Na}_v1.6$  selectivity in Figure 72. Unexpectedly, no correlation was found to exist between the two variables. Lead compound **22**, with the highest selectivity for C-over A-CAP blockade, blocked both  $\text{Na}_v1.7$  and  $\text{Na}_v1.6$  channels with similar levels of potency ( $h\text{Na}_v1.6/h\text{Na}_v1.7 \text{ IC}_{50} \sim 1$ ). In addition, the most and least C-fiber selective compounds of the library, **22** and **38** respectively, showed essentially the same  $\text{Na}_v$  isoform inhibition profile. The results suggest that the selective action of iminodihydroquinolines on nerve conduction is not likely to originate from selective inhibition of  $\text{Na}_v$  channels predominantly expressed in nociceptors, but is rather due to another, currently unknown mechanism.

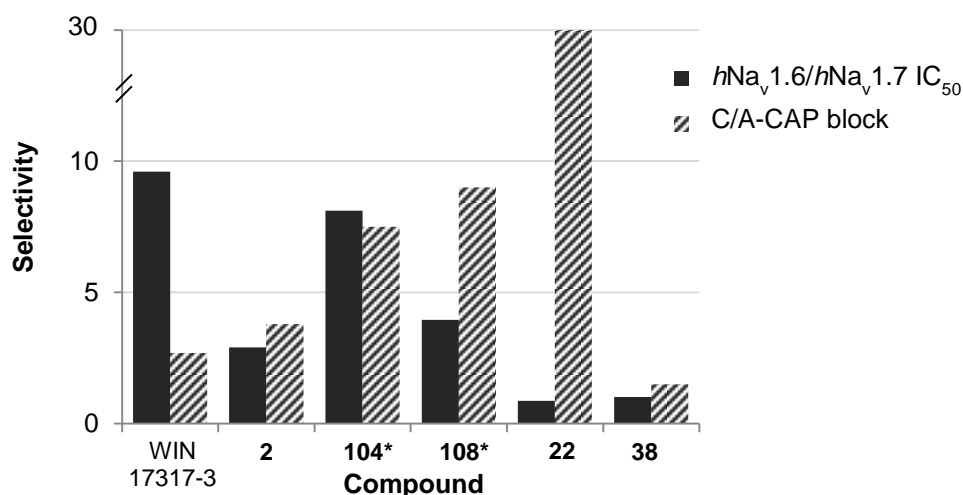


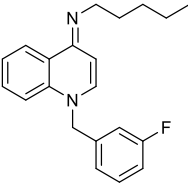
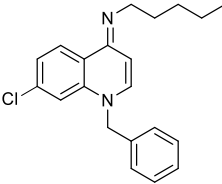
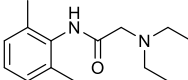
**Figure 72.** Selectivity for  $\text{Na}_v1.7$  over  $\text{Na}_v1.6$  isoform blockade, as calculated from the relative potencies at tonic state in automated patch clamp assays, plotted alongside the selectivity for C- over A-fiber blockade for each compound, calculated as the ratio of 90% C-CAP blockade over the corresponding A-CAP block in the skin nerve preparation.

## 5.8. Summary

In conclusion, iminonidihydroquinolines are potent, selective blockers of C-CAPs in peripheral sensory neurons. Their evoked responses in the skin-nerve preparation and their levels of  $\text{Na}_v$  inhibition as determined with automated patch clamp assays, suggest that the C-CAP blockade is largely mediated *via*  $\text{Na}_v1.7$  inhibition, although other molecular mechanisms or targets may also contribute. The underlying mechanism of the selective C- over A-CAP conduction blockade was found to be unrelated to increased responsiveness of  $\text{Na}_v$  isoforms selectively expressed in nociceptors, but rather to be due to another, currently unknown mechanism.

Compound **22** exhibited the highest C- over A-fiber selectivity of the compound series and was therefore selected as the lead preclinical drug candidate for further characterization *in vivo*. The physicochemical properties of the lead **22** as well as its functional characterization at  $\text{Na}_v1.7$  and the sensory neuronal fibers are summarized in Table 24, alongside those of the ‘hit’ compound WIN17317-3 and the local anesthetic lidocaine.

**Table 24.** Physicochemical properties and functional characterization of **22**, WIN17317-3 and the marketed drug lidocaine.

Compound	<b>22</b>	WIN17317-3	Lidocaine
Chemical structure			
Name	[1-(3-Fluoro-benzyl)-1H-quinolin-4-ylidene]-pentyl-amine	(1-Benzyl-7-chloro-1H-quinolin-4-ylidene)-pentyl-amine	2-Diethylamino-N-(2,6-dimethyl-phenyl)-acetamide
Chemical formula	$\text{C}_{21}\text{H}_{23}\text{FN}_2$	$\text{C}_{21}\text{H}_{23}\text{ClN}_2$	$\text{C}_{14}\text{H}_{22}\text{N}_2\text{O}$
Molecular weight	322.42	338.87	234.34
Melting point	64-65 °C	102-103 °C	68°C
$\text{Na}_v1.7$ $\text{IC}_{50}$ ( $\mu\text{M}$ )	5.42 ± 0.80 (tonic) 1.77 ± 0.11 (10 Hz) 2.15 ± 0.24 (inact.)	0.21 ± 0.05 (tonic) 0.22 ± 0.03 (10 Hz) 0.23 ± 0.04 (inact.)	548 (tonic) 49 (10 Hz) 8 (inact.)
C-CAP $\text{EC}_{50}$ ( $\mu\text{M}$ )	160.4 ± 9.7	34.6 ± 5.1	415.9 ± 90.4
C- over A-CAP selectivity <sup>a</sup>	30	2.7	1.3

**Table 24:** Continued.

Compound		22	WIN 17317-3	Lidocaine
Solubility (mg/mL) <sup>b</sup>	H <sub>2</sub> O	1.4 ± 0.4	0.8 ± 0.2	3.42 ± 0.02 <sup>232</sup>
	PB	2.6 ± 0.3	1.7 ± 0.1	NA
	25%PG:PB	4.0 ± 0.4	1.8 ± 0.3	NA

<sup>a</sup> C/A-CAP selectivity = 90/(%A-CAP at [C-CAP EC<sub>90</sub>]); <sup>b</sup> Compounds tested in the free base form, PB = phosphate buffer (pH= 7.4), PG= propylene glycol, 32°C.

## 6. *In vivo* characterization of a lead preclinical drug candidate in rodents

The two main reasons drug candidates fail during clinical development are that (a) they are not efficacious or (b) they do not exhibit the required safety profile. Experts in the field emphasise the importance of implementing a proactive testing paradigm, conducting the relevant predictive *in vitro* and *in vivo* studies early in the drug discovery process to avoid spending resources on molecules with soon-to-be discovered limiting liabilities.<sup>233, 234</sup> While *in silico* and *in vitro* models are continually being developed and refined, *in vivo* preclinical safety models remain the gold standard for assessing human risk.

The toxicity of any drug is strongly dependent on its absorption, distribution, metabolism and excretion (ADME) profile which in turn is influenced by the selected route of administration. Given the quick metabolism and clearance of [<sup>125</sup>I]2 from the blood, iminodihydroquinolines were developed as candidate analgesic drugs suitable for local administration. As such, they are intended to produce their effects at or near their site of deposition, without requiring transit through the blood to a blood-perfused site. Subsequent to administration, the efficacy as well as the potential toxicity of a given iminodihydroquinoline will depend on its concurrent distribution and dissipation from the site of administration. The potential sources of toxicity can be broadly divided into local and systemic (Fig. 73). Localised toxicity could potentially arise from drug action at neuronal tissues, apart from the intended nociceptors, leading to sensory and motor deficits. Such effects are, however, unlikely to occur in the case of iminodihydroquinolines given the class's high selectivity for C- over A-neuronal fibres. Other local side effects could involve drug action on skeletal muscles; given that iminodihydroquinolines also act as potent Na<sub>v</sub>1.4 inhibitors this parameter must be assessed.

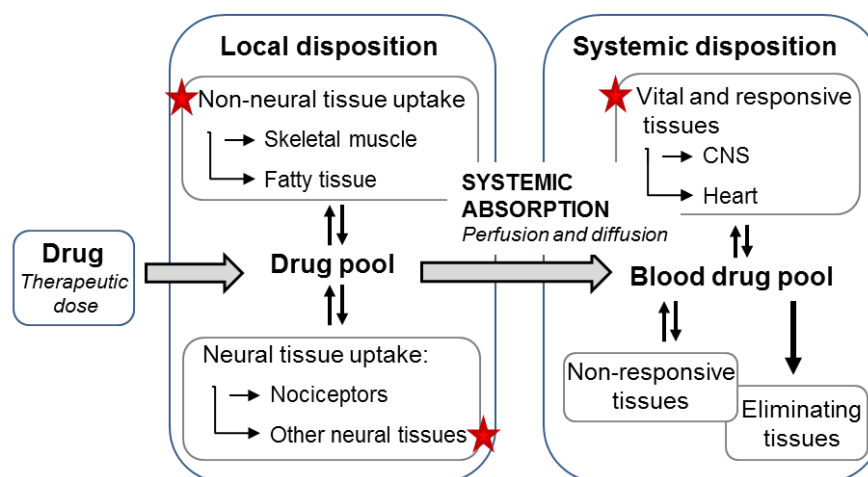


**Figure 73.** A conceptual model depicting the fate of local drugs injected perineurally indicating potential sites for toxicity effects (\*).

Locally administered drugs are cleared from their site of action mainly *via* systemic absorption. In fact, the main adverse effects of clinically used LAs are associated with high plasma concentrations leading to CNS and cardiovascular complications (Fig. 74). Given the high  $Na_v1.2$  (brain) and  $Na_v1.5$  (heart) inhibition exhibited by iminodihydroquinolines *in vitro*, systemic side effects were the main concern for their potential development as local analgesics.

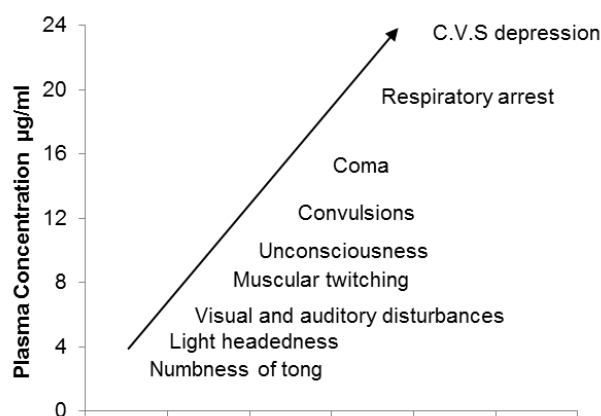


**Figure 74.** Relationship of plasma concentration and signs and symptoms of toxicity for lidocaine. Adapted from reference 219.<sup>219</sup>

The pharmacokinetic profile of [<sup>125</sup>I]**2** showed no significant retention of radioactivity in the mouse brain and heart after iv administration suggesting that the concentration of iminodihydroquinolines will be relatively low in these vital organs even in the case they enter systemic circulation. Given that the lead compound **22** is structurally different to **2**, these parameters had to be reassessed.

To provide preliminary data, two experiments were designed for evaluating the safety profile of **22**. The first involved pharmacokinetic profiling of  $^{18}\text{F}$ -labelled **22** using PET/CT aiming to assess the excretion pathway and the retention of **22**, if any, in vital and potentially responsive tissues (heart, brain). The second experiment involved assessment of the acute toxicity of the compound *in vivo*. A five stage dose escalation study was designed aiming to determine the maximum tolerated dose for **22** and obtain an indication of the safety dose margin.

## **6.1. Assays**

### **6.1.1. Positron emission tomography (PET) for pharmacokinetic profiling**

PET is a non-invasive imaging technique increasingly applied in the field of drug discovery for evaluating the PK/PD of new drug candidates both at preclinical and clinical development stages.<sup>235</sup> The introduction of new radiochemical techniques along with advances in PET technology have been the key contributing factors in the increasing prevalence of PET.<sup>175</sup>

PET relies on unstable radioisotopes undergoing positron decay *via* the release of a positron and a neutrino from the nucleus. The released positron travels a short distance (typically 1 mm - 2 cm depending on its kinetic energy) before annihilating with an electron; their rest masses are converted into two 511 keV photons which are released simultaneously and in opposite directions (Fig. 75). Coincident detection of these photons by a pair of radiation detectors in a PET scanner determines the so called line of response which provides information about the spatial location of the radionuclide. Upon counting millions of annihilation events, a final source map can be reconstructed in the form of a 3D-image.<sup>236</sup>

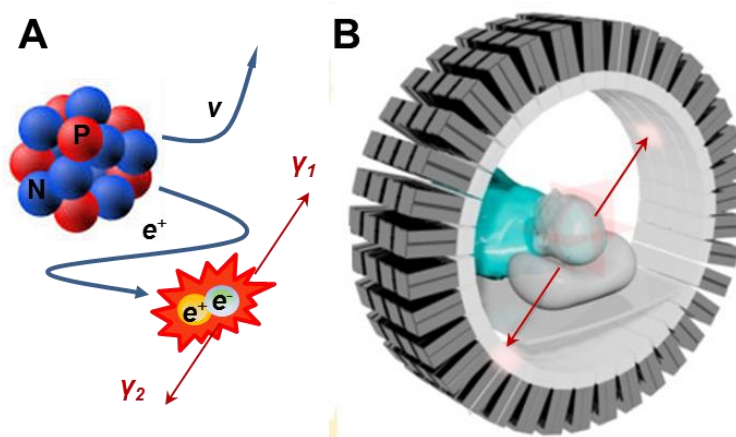


**Figure 75.** Principles of PET. A. A positron ( $e^+$ ) and a neutrino ( $\nu$ ) are ejected from an atom that undergoes positron decay. Two 511 keV photons are produced when the positron annihilates with an electron ( $e^-$ ). B. If both photons are detected within a set timing window, as determined by the PET scanner coincidence timing processor, then a line of response is registered.

The main advantage of PET relative to other molecular imaging modalities (SPECT, MRI) is that it is fully quantitative. It has high sensitivity and it allows emission scans to be acquired as dynamic series and be presented in the form of a motion picture. The series of static recordings are separated in time frames, each depicting a map of the radioactivity concentration in the subject for a certain time interval after tracer injection. This means tracer distribution can be monitored quantitatively at each of the tissues of interest as a function of time. The time frames can be specifically defined according to the needs of each study; in studies requiring pharmacokinetic profiling for example, time frames are selected according to the anticipated tissue kinetics of the ligand under investigation.

For the purpose of this study, [ $^{18}\text{F}$ ]**22** was synthesised as previously described in section 3.2.3. [ $^{18}\text{F}$ ]**22** (specific activity: 2.9 GBq/ $\mu\text{mol}$ ) was administered intravenously to a mouse *via* the tail-vein and dynamic PET imaging was performed for 2 hours using a nanoScan<sup>®</sup> PET-CT system at the UCL Centre of Advanced Biomedical Imaging. The PET study was performed by PDRAs Dr. Kerstin Sander and Dr. Thibault Gendron.



### 6.1.2. The “up-and-down” method for determining acute lethal toxicity

The median lethal dose, LD<sub>50</sub>, a concept first introduced by Trevan in 1927,<sup>237</sup> has been used for many decades as the standardized approach for determining the acute lethal toxicity of new chemical entities. Limitations of LD<sub>50</sub> testing procedures, coupled with increased concern over the use of animals in testing, led to the recent development of alternative approaches using fewer animals and with more humane endpoints.<sup>238, 239</sup>

The “up-and-down method” (Dixon, 1948),<sup>240</sup> also known as the “staircase bioassay”, was employed for the toxicity study of the lead compound **22**. The method has been extensively used in a variety of experimental settings and has been shown to be equally effective as the conventional LD<sub>50</sub> method, while significantly reducing the number of animals used.<sup>241, 240, 242</sup> In brief, the study design involves the selection of an initial dose for administration from the concentration range where this is speculated to produce an effect. Experimental endpoints (positive results) are clearly defined prior to the beginning of the study and a specified time-period, usually seven days, is allowed for these to occur. If no effect is observed during this period, the dose is increased by a defined (log) increment and a new subject is dosed. Alternatively, if a positive result is obtained with the initial dose, the next dosing is decreased accordingly. This procedure is repeated until sufficient data is obtained to answer the imposed question.

According to regulatory requirements, preclinical acute toxicity should ordinarily be examined using two routes of drug administration: (a) the route intended for human administration, and (b) intravenously. Studies should be conducted in at least two mammalian species, including a non-rodent species when reasonable. In this study the effects of iv administration were investigated first. Knowledge regarding the compounds “toxic” blood concentration, and information about systemic absorption and clearance, would help to determine the therapeutic window, and the likelihood of a systemic toxic reaction following a high drug concentration locally, or prolonged drug exposure. Most incidents currently associated with the use of LAs arise from accidental intravascular administration rather than overdose. As it was recently stated “it is not a question of ‘if’ an intravascular injection occurs is a question of when”.<sup>243, 244</sup>

Lethality was the defined endpoint for this study, whilst CNS and cardiac toxicity were set as secondary endpoints. The study was outsourced to Charles River laboratories, Wilmington USA, as our group does not hold a valid project

license for performing such procedures. Male Wistar Han rats were injected with **22** dosed as discussed above *via* the tail vein.

## 6.2. Pharmacokinetic profile of [ $^{18}\text{F}$ ]**22**

The biodistribution of [ $^{18}\text{F}$ ]**22** after iv administration is depicted by the series of PET/CT images in Figure 76. Immediately after injection the  $^{18}\text{F}$ -labelled lead compound **22** can be traced moving up the tail vein and reaching the compartments of the heart. From there, it enters the general circulation reaching the lungs and the brain *via* the pulmonary and carotid arteries and the rest of the body tissues *via* the aorta. Rapid clearance can be seen even at the early time points, with no apparent retention in critical organs, i.e. the brain, heart and lungs. From 2-5 minutes there is gradual accumulation in the liver and kidneys, followed by excretion to the GI tract and bladder. At 30 minutes post injection onwards, the radioactivity is largely limited to the GI tract, bladder and gall bladder. The results confirm clearance via renal and hepatobiliary excretion.

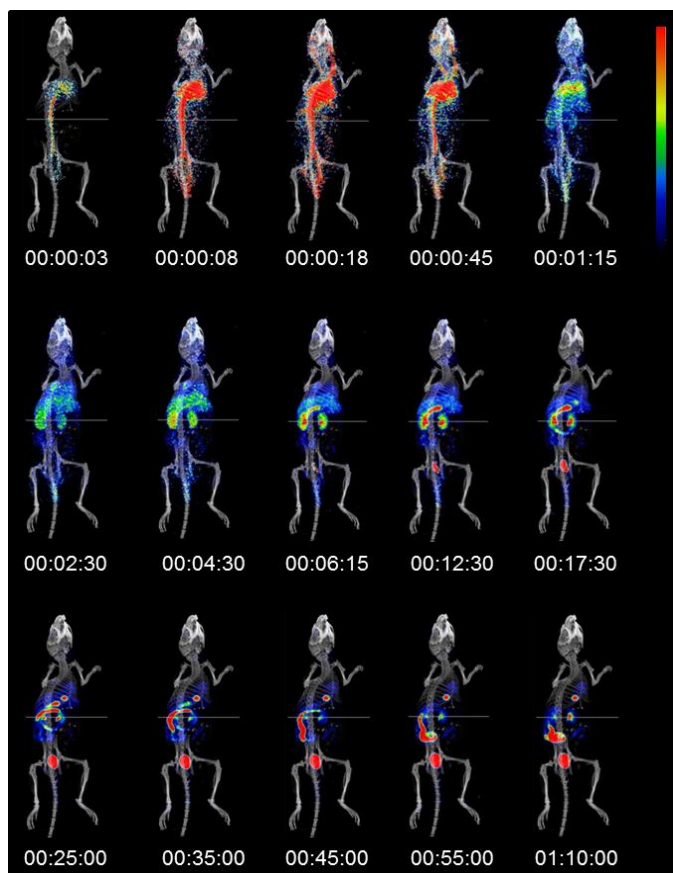


**Figure 76.** Representative PET/CT images illustrating the biodistribution of [ $^{18}\text{F}$ ]**22** in wild-type albino (Balb/C) mouse after iv administration. The radiotracer retention is presented as a percentage of the injected dose per unit tissue volume (%ID/ml).

Overall, [ $^{18}\text{F}$ ]**22** showed no significant brain or heart retention as evident by the two hour summed PET/CT image (Fig. 77). The data are in accordance with the previously described pharmacokinetic profile of [ $^{125}\text{I}$ ]**2**.<sup>3</sup> This confirmed the requirement for a local route of administration and at the same time provided confidence regarding the compounds' therapeutic index, as systemic toxicity is likely to be limited by the rapid clearance from circulation.

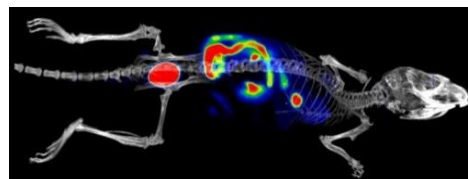


**Figure 77.** Biodistribution of [ $^{18}\text{F}$ ]**22**. Summed PET/CT image, 2 hours.

### 6.3. Maximum tolerated dose of the lead **22** after iv administration in rats

Administration of an initial dose of  $3 \text{ mg}\cdot\text{kg}^{-1}$  of **22** in rats, led to no apparent signs of toxicity, neither did the increased dose of  $7.5 \text{ mg}\cdot\text{kg}^{-1}$ . Escalating to  $30 \text{ mg}\cdot\text{kg}^{-1}$ , immediately post injection, the animal exhibited laboured and irregular breathing and arrhythmic heartbeat. It became non-responsive, ataxic, had some muscle spasms (seizure-like activity) and died soon after dosing. Decreasing the dose by half, to  $15 \text{ mg}\cdot\text{kg}^{-1}$ , led to similar signs of toxicity and the animal also died soon after dosing. Reducing the dose further, to  $10 \text{ mg}\cdot\text{kg}^{-1}$ , caused the animal immediately post dose to exhibit increased heart rate and increased effort for respiration; the animal was hypoactive yet responsive to stimulation. Within an hour of dosing the animal recovered, returning to normal breathing rhythms and became much more responsive. Based on the results of this initial sighting study, the maximum tolerated dose of **22** was estimated in the range of  $7.5 - 10 \text{ mg}\cdot\text{kg}^{-1}$ , with the first signs of CNS and cardiovascular toxicity appearing at  $10 \text{ mg}\cdot\text{kg}^{-1}$ . Table 25 provides a summary on the “up-and-down” test series results.

**Table 25.** “Up-and-down” test series to determine the CNS, cardiovascular toxicity and lethality in rats after iv administration of **22**.

Dose ( $\text{mg}\cdot\text{kg}^{-1}$ )	Test results <sup>a</sup>		
	CNS tox.	CVS tox	Lethality
3	O	O	O
7.5	O	O	O
10	X	X	O
15	X	X	X
30	X	X	X

<sup>a</sup>X= positive result; O= negative result.

The LA lidocaine, produces systemic CNS and cardiac toxicity in mice with an ED<sub>50</sub> of 19.5 and 21.2 mg·kg<sup>-1</sup> respectively;<sup>131</sup> these values are in accordance with those obtained for other species (dog, monkey).<sup>245, 246</sup> **22** with a C-CAP EC<sub>50</sub> = 160.4 ± 9.7 µM is 3-fold more potent in blocking C-fibers relative to lidocaine, C-CAP EC<sub>50</sub> = 415.9 ± 90.4 µM. Taking into account the relative potencies and the maximum tolerated doses for the two compounds, collectively the results suggest that **22** has similar, or superior, safety profile to lidocaine when administered systematically. Nonetheless, the administration of LAs that have higher systemic toxicity than lidocaine but have other therapeutic benefits, for example are longer acting, is commonplace in clinics as exemplified by bupivacaine.

It is worth noting that oral administration of a 100 mg·kg<sup>-1</sup> dose of the parent compound, WIN17317-3, twice daily in mice and hamsters, as part of a study investigating the antiparasitic activity of iminodihydroquinolines, proceeded with no lethality for the five day period of the study.<sup>247</sup> However, administration of 200 mg·kg<sup>-1</sup> twice daily in mice was not tolerated (2/2 animal died).

## 6.4. Summary

To conclude, in this last part of the study, the safety profile of **22** was investigated in preliminary assays. Safety evaluation is a critical step in the preclinical drug discovery process and of particular importance to regulatory authorities for granting permission for the use of more advanced animal models or human tissues. Using an isotopically <sup>18</sup>F-labelled analogue, the pharmacokinetic profile of the lead compound **22** was assessed after iv administration in mice. The results of the study, in combination with those previously obtained for [<sup>125</sup>I]**2**, suggest that iminodihydroquinolines are rapidly metabolised and largely cleared from the blood within ten minutes post injection, showing no significant retention in any of the vital organs (brain, heart), with renal and hepatobiliary being their main routes of excretion. The maximum tolerated dose of **22** after iv administration in rats has been estimated at 7.5 – 10 mg·kg<sup>-1</sup>, allowing a considerable safety margin, given the anticipated slow rate of systemic absorption from a peripheral tissue administration site.

## 7. Conclusions

Of all neurological diseases, pain is one of the most challenging with respect to understanding the relationships between symptoms and mechanisms and rationalizing approaches towards treatment. There is currently a great unmet clinical need for novel, more efficacious and safer pain therapies.<sup>248</sup> The most powerful known method of blocking pain while retaining consciousness is to inject LAs, Na<sub>v</sub> blockers, regionally into areas of the body generating pain. LAs like lidocaine, provide effective pain relief by blocking conduction of pain-signalling neurons; however, adverse effects including action on the CNS (e.g. seizures), on heart's excitable tissue (arrhythmias, conduction defects) and on non-nociceptive fibres of the PNS (anaesthesia, motor- or vaso-paralysis) limit their clinical utility. The work in this thesis describes the development of small molecule iminodihydroquinolines as new generation local analgesic drugs with selective action on pain-signalling neurons.

Previous work by our group has demonstrated that the high affinity, state-dependent Na<sub>v</sub> blocker, WIN17317-3, can potently block nociceptive C-fibers whilst leaving non-nociceptive A-fibers largely unaffected. In the present work, a library of structural analogues of WIN17317-3 was designed, synthesized and evaluated for their effects at human Na<sub>v</sub>s and rodent peripheral sensory neurons *in vitro*. The results revealed selective nociceptor blockade to be a functional property characterizing the iminodihydroquinoline class of compounds. Nociceptor blockade was demonstrated to be mediated, at least partially, through inhibition of the Na<sub>v</sub>1.7 isoform. Intriguingly, the profound C- over A-fiber selectivity could not be explained by selective inhibition of ion channels known to be predominantly expressed at nociceptors (TRPA1, TRPV1, Na<sub>v</sub>1.7, Na<sub>v</sub>1.8,) as it was initially hypothesised.

The selective nociceptor blockade exhibited by iminodihydroquinolines could in a clinical setting translate to effective analgesia without the complete sensory and motor block currently produced by LA drugs. This would be beneficial in a number of clinical situations. For example, analgesia without loss of proprioception or motor function would allow patients undergoing neurosurgery to provide instant feedback on sensation and the ability to control movement thus limiting possible nerve damage. Also, it would enable early mobilization in patients receiving peripheral nerve block or plexus block in cases such as following knee or hip joint replacement.<sup>129</sup> Furthermore, epidural administration for pain relief during labour

would allow the mother to actively participate in the delivery of the child. In a different scenario, the unpleasant loss of sensation and prolonged numbness following dentistry and cosmetic procedures could be avoided.

Appreciating the clinical potential associated with the use of iminodihydroquinolines as local analgesic drugs, a lead compound from the library, **22**, exhibiting excellent C-over A-fiber selectivity and “drug-like” physicochemical properties, was selected for further characterization *in vivo*. **22** was submitted to preliminary safety studies in rodents; the pharmacokinetic profile of <sup>18</sup>F-labelled **22** showed rapid clearance and excretion after iv administration and the maximum tolerated systemic dose of **22** was estimated to be in the range of 7.5-10 mgkg<sup>-1</sup>. Both studies provided confidence regarding the potential safety margin of **22**. **22** was denoted as the lead preclinical drug candidate for entering human nerve conduction studies *ex vivo*, analogous to the rodent skin-nerve preparation studies. The human nerve conduction studies will objectively and quantifiably evaluate whether the remarkable peripheral nerve effects observed in rodents are also exerted in human tissues. If successful, we envision **22**, upon further toxicological studies, progressing to first-in-man microdosing studies for future clinical development as a local analgesic drug.

The discovery of iminodihydroquinolines as selective nociceptor blockers opens new exciting opportunities for the field of pain medicine. Presently, there is a feeling that success in the development of new pain therapeutics is quite limited, lacking real breakthrough analgesic drugs despite improvements in our understanding of pain mechanisms.<sup>63</sup> Whilst many efforts and resources have been concentrated on the selective targeting of peripheral Na<sub>v</sub>s, the clinical usefulness of such agents after a decade of extensive research is still to be demonstrated. Having excluded all known mechanisms to confer C-over A-fiber selectivity (selective Na<sub>v</sub> or TRP isoform inhibition), the elucidation of the molecular mechanism of action of iminodihydroquinolines could provide a completely novel target for analgesia revolutionizing the field of analgesic drug discovery.

## 8. Experimental

### 8.1. Experimental for Chapter 3

All chemistry and radiochemistry experiments were performed at the UCL Department of Chemistry.

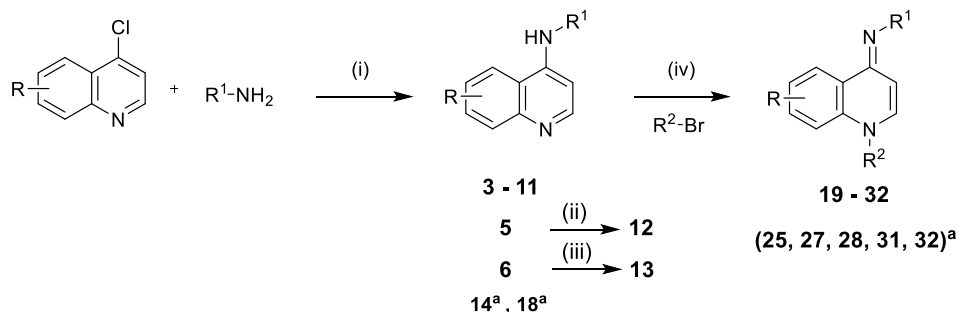
#### General experimental

Reagents were purchased from Sigma-Aldrich, Acros Organics or Fluorochem and were used without further purification. Purification of compounds by column chromatography was performed on BDH silica gel (40-60  $\mu\text{M}$ ) unless otherwise specified. Analytical thin layer chromatography was carried out using Merck Keisegel aluminium-backed plates coated with silica gel. Components were visualized using combinations of ultra-violet lights, ninhydrin, phosphomolybdic acid and potassium permanganate. For compound characterization,  $^1\text{H}$  and  $^{13}\text{C}$  NMR spectra were recorded at room temperature unless otherwise specified. The respective instruments, Bruker Avance 400, 500 or 600 were operated at a frequency of 400, 500 or 600 MHz for  $^1\text{H}$  and 100, 125 or 150 MHz for  $^{13}\text{C}$ , respectively. Proton decoupled  $^{19}\text{F}$  NMR spectra were recorded on a Bruker Avance 300 instrument at a frequency of 282 MHz. All spectra were internally referenced to the respective deuterated solvents. Chemical shifts are reported in ppm using the following abbreviations: s, singlet; d, doublet; t, triplet; q, quintet; m, multiplet; br, broad or a combination of these. Coupling constants (J) are given in Hertz (Hz). Full NMR assignment was performed with the aid of multidimensional and long range experiments. Infrared (IR) spectra were recorded on a Perkin-Elmer 1605 Fourier transform spectrometer or a Perkin-Elmer spectrum 100 FT-IR spectrometer as thin films. High resolution mass spectra were recorded on either a Thermo Finnigan MAT900xp (CI, EI) or a MALDI microMX (TOF) mass spectrometer. Melting points were determined using a Gallenkamp heating block and are uncorrected.

All labelling reactions were performed manually using [ $^{18}\text{F}$ ]fluoride in [ $^{18}\text{O}$ ]H<sub>2</sub>O. Radio-HPLC was performed with an Agilent 1200 HPLC system equipped with a 1200 Series Diode Array Detector and a GABI Star NaI (TI) scintillation detector. The system was used for purification as well as characterization of the radiotracer. The decay-corrected isolated RCY was calculated by relating the amount of isolated radioactive product to the initial amount of [ $^{18}\text{F}$ ]fluoride in [ $^{18}\text{O}$ ]H<sub>2</sub>O. The analytical RCY was determined by integrating the area under the curve in the preparative radio-HPLC chromatogram. No corrections were made to account for losses during the preparative procedure.

### 8.1.1. Synthesis of *N*-substitued-4-imino-1,4-dihydroquinolines.

#### Route A:

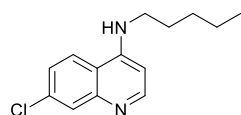


**Scheme 30.** Synthesis of *N*-substitued-4-imino-1,4-dihydroquinolines from 4-chloroquinolines.

Reagents and Conditions: (i) 90-120 °C, 2-48 h; (ii) Acetic anhydride, DCM, 0 °C → rt, 3 h; (iii) DAST, DCM, 0 °C → rt, 48 h; (a) modified reaction conditions; (iv) NaI, acetone, reflux, 3-18 h.

#### (4-alkylamino)quinoline intermediates 3 - 18:

##### (7-Chloro-quinolin-4-yl)-pentyl-amine (3)



White feathery solid

Chemical formula: C<sub>14</sub>H<sub>17</sub>ClN<sub>2</sub>

Molecular weight: 248.75 g.mol<sup>-1</sup>

Yield: 96%

A solution of 4,7-dichloroquinoline (1.00 g, 0.05 mol) in amylamine (2.70 ml, 0.15 mol) was heated at 120 °C to reflux for 18 h under Ar atmosphere. The resulting solution was allowed to cool at R.T. and was then transferred to ice/water (~40 cm<sup>3</sup>) while stirring vigorously. The precipitate formed was filtered, washed with water (2 x 15 ml) and pentane (2 x 15 ml) and dried *in vacuo* to afford pure **3** as a white feathery solid (1.19 g, 96%).

<sup>1</sup>H NMR (600 MHz, CDCl<sub>3</sub>) δ ppm: 8.53 (1H, d, *J* = 5.3, CH-2), 7.96 (1H, d, *J* = 2.2, CH-8), 7.66 (1H, d, *J* = 9.0, CH-5), 7.36 (1H, dd, *J* = 9.0, 2.2, CH-6), 6.39 (1H, d, *J* = 5.3, CH-3), 7.98 (1H, t, *J* = 5.1, NH), 3.30 (2H, td, *J* = 7.3, 5.1, NHCH<sub>2</sub>), 1.77 (2H, qn, *J* = 7.3, NHCH<sub>2</sub>CH<sub>2</sub>), 1.47-1.35 (4H, m, CH<sub>2</sub>CH<sub>2</sub>CH<sub>3</sub>), 0.95 (3H, t, *J* = 7.2, CH<sub>3</sub>)

<sup>13</sup>C NMR (150 MHz, CDCl<sub>3</sub>) δ ppm: 152.0 (CH-2), 149.9 (C<sub>Q</sub>-4), 149.1 (C<sub>Q</sub>-8'), 134.9 (C<sub>Q</sub>-7), 128.8 (CH-8), 125.3 (CH-6), 120.9 (CH-5), 117.6 (C<sub>Q</sub>-4'), 99.1 (CH-3), 43.3 (NHCH<sub>2</sub>), 29.3 (CH<sub>2</sub>CH<sub>2</sub>CH<sub>3</sub>), 28.7 (NHCH<sub>2</sub>CH<sub>2</sub>), 22.6 (CH<sub>2</sub>CH<sub>3</sub>), 14.1 (CH<sub>3</sub>)

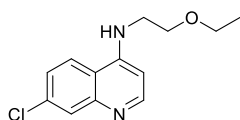
HRMS (CI) *m/z*: Calcd. [M-H]<sup>+</sup> 249.1159  
Measured 249.1160

LRMS (CI) *m/z*: 251 (32), 249 (100, [M-H]<sup>+</sup>)

IR ν<sub>max</sub> (neat/cm<sup>-1</sup>): 3205 (N-H), 3058 (Ar C-H), 2920 (Alkyl C-H), 2854, 1573 (Ar C=C)

*m.p.*: 117 - 118 °C



**(7-Chloro-quinolin-4-yl)-(2-ethoxy-ethyl)-amine (4)**

Off white powder

Chemical formula: C<sub>13</sub>H<sub>15</sub>ClN<sub>2</sub>OMolecular weight: 250.72 g.mol<sup>-1</sup>

Yield: quantitative

A solution of 4,7-dichloroquinoline (0.40 g, 2.02 mmol) in 2-ethoxyethylamine (1 ml, 9.54 mmol) was heated at 120 °C to reflux for 5 h under Ar atmosphere. The resulting solution was allowed to cool at R.T. and was then transferred into an ice/water mixture (~20 cm<sup>3</sup>) whilst stirring vigorously. The resulting off-white precipitate was filtered, washed with water (2 x 15 ml) and pentane (2 x 15 ml) and dried *in vacuo* to afford pure **4** as an off white powder (0.52 g, quantitative yield).

**<sup>1</sup>H NMR (600 MHz, CDCl<sub>3</sub>)** δ ppm: 8.53 (1H, d, *J* = 5.3, CH-2), 7.96 (1H, d, *J* = 2.3, CH-8), 7.69 (1H, d, *J* = 8.9 CH-5), 7.37 (1H, dd, *J* = 8.9, 2.3, CH-6), 6.41 (1H, d, *J* = 5.3, CH-3), 5.47 (1H, b, s, NH), 3.76 (2H, t, *J* = 5.4, NHCH<sub>2</sub>CH<sub>2</sub>), 3.59 (2H, q, *J* = 7.0, OCH<sub>2</sub>CH<sub>3</sub>), 3.47 (2H, q, *J* = 5.4, NHCH<sub>2</sub>), 1.26 (3H, t, *J* = 7.0, CH<sub>3</sub>)

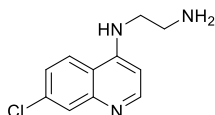
**<sup>13</sup>C NMR (150 MHz, CDCl<sub>3</sub>)** δ ppm: 152.1 (CH-2), 149.9 (C<sub>q</sub>-4), 149.1 (C<sub>q</sub>-8'), 135.0 (C<sub>q</sub>-7), 128.8 (CH-8), 125.5 (CH-6), 121.2 (CH-5), 117.4 (C<sub>q</sub>-4'), 99.4 (CH-3), 68.0 (NHCH<sub>2</sub>CH<sub>2</sub>), 66.8 (OCH<sub>2</sub>CH<sub>3</sub>), 42.9 (NHCH<sub>2</sub>), 15.3 (CH<sub>3</sub>)

**HRMS (CI) m/z:** Calcd. [M-H]<sup>+</sup> 251.0951  
Measured 251.0954

**LRMS (CI) m/z:** 253 (33), 251 (100, [M-H]<sup>+</sup>)

**IR ν<sub>max</sub> (neat/cm<sup>-1</sup>):** 3234 (NH), 2965 (Alkyl C-H), 2855, 2799, 1607, 1578 (Ar C=C), 1546

**m.p.:** 114 –115 °C

**N<sup>1</sup>-(7-chloroquinolin-4-yl)ethane-1,2-diamine (5)**

White powder

Chemical formula: C<sub>11</sub>H<sub>12</sub>ClN<sub>3</sub>Molecular Weight: 221.69 g.mol<sup>-1</sup>

Yield: 90%

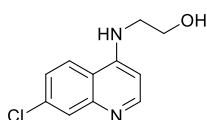
A mixture of 4,7-dichloroquinoline (1.50 g, 7.57 mmol) and ethylenediamine (2.81 ml, 42.05 mmol) was heated to reflux at 110 °C for 5 h. After cooling at R.T., the mixture was poured onto an ice (~50 cm<sup>3</sup>) and NaOH (2M, 50 ml) mixture while stirring vigorously. The precipitate formed was filtered, was washed with water (2 x 100 ml) and pentane (2 x 100 ml) and was dried *in vacuo* to afford **5** as white solid (1.52 g, 90%).

**<sup>1</sup>H NMR (600 MHz, DMSO-d<sub>6</sub>)** δ ppm: 8.37 (1H, d, *J* = 5.3, CH-2), 8.27 (1H, d, *J* = 9.0, CH-5), 7.77 (1H, d, *J* = 2.6, CH-8), 7.43 (1H, dd, *J* = 9.0, 2.6, CH-6), 7.32 (1H, s, br, NH), 6.50 (1H, d, *J* = 5.3, CH-3), 3.31-3.23 (2H, m, NHCH<sub>2</sub>), 2.84 (2H, t, *J* = 6.5, CH<sub>2</sub>NH<sub>2</sub>), (NH<sub>2</sub> hidden below H<sub>2</sub>O peak)

**<sup>13</sup>C NMR (150 MHz, DMSO-d<sub>6</sub>)** δ ppm: 151.9 (CH-2), 150.3 (C<sub>q</sub>-4), 149.0 (C<sub>q</sub>-8'), 133.5 (C<sub>q</sub>-7), 127.4 (CH-8), 124.2 (CH-5), 124.1 (CH-6), 117.4 (C<sub>q</sub>-4'), 98.7 (CH-3), 45.4 (NHCH<sub>2</sub>), 39.7 (CH<sub>2</sub>NH<sub>2</sub>)

**HRMS (EI) m/z:** Calcd. [M]<sup>+</sup> 221.0714  
Measured 221.0716

**LRMS (EI) m/z:** 223 (7), 221 (21, [M]<sup>+</sup>), 193 (37), 192 (53), 191 (100, [M-CH<sub>2</sub>NH<sub>2</sub>]<sup>+</sup>), 163 (51), 156 (74, [M-CH<sub>2</sub>NH<sub>2</sub>-Cl]<sup>+</sup>), 155 (71), 135 (38) 128 (21)

**2-(7-Chloro-quinolin-4-ylamino)-ethanol (6)**

White feathery solid

Chemical formula: C<sub>11</sub>H<sub>11</sub>ClN<sub>2</sub>OMolecular Weight: 222.67 g.mol<sup>-1</sup>

Yield: 91%

A solution of 4,7-dichloroquinoline (1.50 g, 7.57 mmol) in ethanolamine (15 ml, 0.25 mol) was heated at 120 °C under argon atmosphere for 3 h. After cooling at R.T., the solution was transferred to an ice/water mixture (~40 cm<sup>3</sup>) while stirring vigorously. The precipitate formed was filtered, washed with water (3 x 10 ml) and pentane (3 x 10 ml), and dried *in vacuo* to afford pure **6** as a white feathery solid (1.53 g, 91%).

**<sup>1</sup>H NMR (600 MHz, DMSO-d<sub>6</sub>)** δ ppm: 8.38 (1H, d, *J* = 5.4, CH-2), 8.26 (1H, d, *J* = 9.0, CH-5), 7.78 (1H, d, *J* = 2.0, CH-8), 7.44 (1H, dd, *J* = 9.0, 2.0, CH-6), 7.30 (1H, t, *J* = 5.7, NH), 6.49 (1H, d, *J* = 5.4, CH-3), 4.89 (1H, br, s, OH), 3.65 (2H, t, *J* = 5.7, CH<sub>2</sub>OH), 3.35 (2H, q, *J* = 5.7, NHCH<sub>2</sub>)

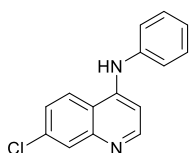
**<sup>13</sup>C NMR (150 MHz, DMSO-d<sub>6</sub>)** δ ppm: 151.9 (CH-2), 150.3 (C<sub>Q</sub>-4), 149.1 (C<sub>Q</sub>-8'), 133.40 (C<sub>Q</sub>-7), 127.5 (CH-8), 124.1 (CH-5), 124.0 (CH-6), 117.5 (C<sub>Q</sub>-4'), 98.7 (CH-3), 58.7 (CH<sub>2</sub>OH), 45.2 (NHCH<sub>2</sub>)

**HRMS (EI) m/z:** Calcd. [M]<sup>+</sup> 222.0560  
Measured 222.0565

**LRMS (EI) m/z:** 224 (16), 222 (55, [M]<sup>+</sup>), 193 (30), 191 (91, [M-CH<sub>2</sub>OH]<sup>+</sup>), 156 (100, [M-CH<sub>2</sub>OH-Cl]<sup>+</sup>), 155 (76), 135 (21), 99 (21)

**IR ν<sub>max</sub> (neat/cm<sup>-1</sup>):** 3300 (OH), 3062 (Ar C-H), 2960 (Alkyl C-H), 2811, 1575 (Ar C=C), 1535 (Ar C=C)

**m.p.:** 218 - 219 °C

**(7-Chloro-quinolin-4-yl)-phenyl-amine (7)**

Pale pink powder

Chemical formula: C<sub>15</sub>H<sub>11</sub>ClN<sub>2</sub>Molecular Weight: 254.71 g.mol<sup>-1</sup>

Yield: 60%

A solution of 4,7-dichloroquinoline (0.40 g, 2.00 mmol) in aniline (0.82 ml, 9.00 mmol), was heated at 110 °C for 1.5 h. The resulting mixture was cooled at R.T. and was then poured onto ice/water (~20 cm<sup>3</sup>) while stirring vigorously. The resulting precipitate was filtered, washed with water and pentane and dried *in vacuo* to afford pure **7** (0.31 g, 60%) as pale pink powder.

**<sup>1</sup>H NMR (600 MHz, DMSO-d<sub>6</sub>)** δ ppm: 9.63 (1H, s, br, NH), 8.52 (1H, d, *J* = 9.0, CH-5), 8.48 (1H, d, *J* = 5.8, CH-2), 7.94 (1H, d, *J* = 2.2, CH-8), 7.66 (1H, dd, *J* = 9.0, 2.2, CH-6), 7.48 (2H, t, *J* = 7.8, meta Ph-CH), 7.40 (2H, d, *J* = 7.8, ortho Ph-CH), 7.25 (1H, t, *J* = 7.8, para Ph-CH), 6.89 (1H, d, *J* = 5.8, CH-3)

**<sup>13</sup>C NMR (150 MHz, DMSO-d<sub>6</sub>)** δ ppm: 149.8 (CH-2), 146.8 (C<sub>Q</sub>-4), 139.3 (Ph-C<sub>Q</sub>), 135.1 (C<sub>Q</sub>-7), 129.7 (meta Ph-CH), 125.6 (CH-6 or CH-8), 125.5 (CH-6 or CH-8), 125.1 (para Ph-CH), 124.9 (CH-5), 123.4 (ortho Ph-CH), 117.7 (C<sub>Q</sub>-4'), 101.4 (CH-3), [C<sub>Q</sub>-8' hidden]

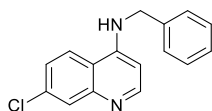
**HRMS (CI) m/z:** Calcd. [M-H]<sup>+</sup> 255.0689  
Measured 255.0686

**LRMS (CI) m/z:** 257 (34), 255 (98, [M-H]<sup>+</sup>), 219 (30, [M-Cl]<sup>+</sup>)

**IR  $\nu_{\max}$  (neat/cm<sup>-1</sup>):** 3165 (NH), 3096 (Ar C-H), 3048, 2995, 2939, 1607 (C=N-), 1591, 1562 (Ar C=C)

**m.p.:** 190 – 191 °C

### Benzyl-(7-chloro-quinolin-4-yl)-amine (8)



Pale yellow solid

Chemical formula: C<sub>16</sub>H<sub>13</sub>ClN<sub>2</sub>

Molecular Weight: 268.74 g.mol<sup>-1</sup>

Yield: 35%

To 4,7-dichloroquinoline (0.40 g, 1.61 mmol), benzylamine (0.90 ml, 8.25 mmol) was added and the resulting solution was stirred at 90 °C for 24 h. After cooling at R.T, the solution was transferred in ice/water (~40 cm<sup>3</sup>) and the mixture was stirred for 15 min. The pale brown precipitate was filtered and was washed with water (2 x 25 ml) and pentane (2 x 25 ml). Purification *via* flash column chromatography (1:1 EtOAc:petroleum ether) afforded pure **8** as a pale yellow solid (0.15 g, 35 %).

**<sup>1</sup>H NMR (CDCl<sub>3</sub>, 500 MHz)**  $\delta$  ppm: 8.45 (1H, d, *J* = 5.5, CH-2) 7.99 (1H, d, *J* = 2.0, CH-8) 7.84 (1H, d, *J* = 8.9, CH-5) 7.30-7.42 (6H, m, CH-6, Ph-CH), 6.43 (1H, d, *J* = 5.5, CH-3), 5.98 (1H, s, br, NH), 4.56 (2H, d, *J* = 4.9, NHCH<sub>2</sub>)

**<sup>13</sup>C NMR (CDCl<sub>3</sub>, 125 MHz)**  $\delta$  ppm: 150.8, 150.4, 147.8, 137.0, 135.6, 129.1, 128.1, 127.8, 127.6, 125.9, 121.6, 117.0, 99.6, 47.6

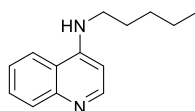
**HRMS (ES+) m/z:** Calcd. [M-H]<sup>+</sup> 269.0846

Measured 269.0839

**LRMS (ES+) m/z:** 271 (35), 269 (100, [M-H]<sup>+</sup>)

**m.p.:** 166 - 167 °C

### Pentyl-quinolin-4-yl-amine (9)



White powder

Chemical formula: C<sub>14</sub>H<sub>18</sub>N<sub>2</sub>

Molecular Weight: 214.31 g.mol<sup>-1</sup>

Yield: 88%

A solution of 4-chloroquinoline (1.00 g, 6.11 mmol) in amylamine (3.90 ml, 33.62 mmol) was heated at 110 °C for 24 h under Ar atmosphere. The solution was allowed to cool at R.T. and was then transferred to an ice/water mixture (~40 cm<sup>3</sup>) while stirring vigorously. The precipitate formed was filtered, was washed with water (2 x 20 ml) and pentane (2 x 20 ml), and was dried *in vacuo* to afford pure **9** as a white powder (1.15 g, 88%).

**<sup>1</sup>H NMR (CDCl<sub>3</sub>, 600 MHz)**  $\delta$  ppm: 8.56 (1H, d, *J* = 5.3, CH-2), 7.98 (1H, d, *J* = 8.4, CH-5), 7.73 (1H, d, *J* = 8.4, CH-8), 7.63 (1H, ddd, *J* = 8.4, 6.8, 1.5, CH-6), 7.43 (1H, ddd, *J* = 8.4, 6.8, 1.5, CH-7), 6.43 (1H, d, *J* = 5.3, CH-3), 5.04 (1H, t, *J* = 5.2, NH), 3.32 (2H, td, *J* = 7.2, 5.2, NHCH<sub>2</sub>), 1.78 (2H, qn, *J* = 7.2, NHCH<sub>2</sub>CH<sub>2</sub>), 1.49-1.36 (4H, m, CH<sub>2</sub>CH<sub>2</sub>CH<sub>3</sub>), 0.95 (3H, t, *J* = 7.2, CH<sub>3</sub>)

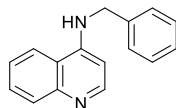
**<sup>13</sup>C NMR (150 MHz, CDCl<sub>3</sub>)**  $\delta$  ppm: 151.2 (CH-2), 149.8 (C<sub>Q</sub>-4), 148.5 (C<sub>Q</sub>-8'), 130.1 (CH-5), 129.1 (CH-6), 124.7 (CH-7), 119.3 (CH-8), 118.8 (C<sub>Q</sub>-4'), 98.9 (CH-3), 43.4 (NCH<sub>2</sub>), 29.4 (CH<sub>2</sub>CH<sub>2</sub>CH<sub>3</sub>), 28.8 (NCH<sub>2</sub>CH<sub>2</sub>), 22.6 (CH<sub>2</sub>CH<sub>3</sub>), 14.2 (CH<sub>3</sub>)

**HRMS (EI) m/z:** Calcd. [M]<sup>+</sup> 214.1464

Measured 214.1471

**LRMS (EI) m/z:** 214 (27, [M]<sup>+</sup>), 157 (100, [M-CH<sub>2</sub>(CH<sub>2</sub>)<sub>2</sub>CH<sub>3</sub>]<sup>+</sup>), 156 (22)  
**m.p.:** 102 – 103 °C

### **N-benzylquinolin-4-amine (10)**



Pale yellow solid  
 Chemical Formula: C<sub>16</sub>H<sub>14</sub>N<sub>2</sub>  
 Molecular Weight: 234.30  
 Yield: 90%

A solution of 4-chloroquinoline (0.46 g, 2.84 mmol) in benzylamine (1.70 ml, 16.49 mmol) was heated at 110 °C for 24 h. After cooling to room temperature, the solution was poured into ice (~100 cm<sup>3</sup>) while stirring vigorously. The organic products were extracted with DCM (2 x 100 ml), the organic extracts were dried over anh. MgSO<sub>4</sub> and were evaporated *in vacuo*. Purification *via* column chromatography (1:19 MeOH:EtOAc) afforded **10** (0.60 g, 90%) as pale yellow solid.

**<sup>1</sup>H NMR (600 MHz, CDCl<sub>3</sub>)** δ ppm: 8.55 (1H, d, *J* = 5.3, CH-2), 8.01 (1H, dd, *J* = 8.5, 1.4, CH-8), 7.77 (1H, dd, *J* = 8.5, 1.4, CH-5), 7.65 (1H, td, *J* = 8.5, 1.4, CH-7), 7.46-7.42 (1H, m, CH-6), 7.42-7.37 (4H, m, ortho Ph-CH, meta Ph-CH), 7.36-7.32 (1H, m, para Ph-CH), 6.46 (1H, d, *J* = 5.3, CH-3), 5.39 (1H, s, br, NH), 4.54 (2H, d, *J* = 5.3, CH<sub>2</sub>)

**<sup>13</sup>C NMR (150 MHz, CDCl<sub>3</sub>)** δ ppm: 151.2 (CH-2), 149.5 (C<sub>Q</sub>-4), 148.5 (C<sub>Q</sub>-8'), 137.6 (Ph-C<sub>Q</sub>), 130.2 (CH-8), 129.2 (CH-7), 129.1 (meta Ph-CH), 128.0 (para Ph-CH), 127.7 (ortho Ph-CH), 124.9 (CH-6), 119.4 (CH-5), 118.8 (C<sub>Q</sub>-4'), 99.5 (CH-3), 47.69 (CH<sub>2</sub>)

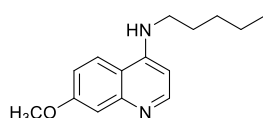
**HRMS (CI) m/z:** Calcd. [M+H]<sup>+</sup> 235.1230  
 Measured 235.1231

**LRMS (CI) m/z:** 235 (100, [M+H]<sup>+</sup>)

**IR ν<sub>max</sub> (neat/cm<sup>-1</sup>):** 3190 (N-H), 3057 (Ar C-H), 3019, 2971, 2911, 1567 (Ar C=C), 1536

**m.p.:** 130 – 131 °C

### **(7-Methoxy-quinolin-4-yl)-pentyl-amine (11)**



Beige solid  
 Chemical formula: C<sub>15</sub>H<sub>20</sub>N<sub>2</sub>O  
 Molecular weight: 244.34 g.mol<sup>-1</sup>  
 Yield: 81%

A solution of 4-chloro-7-methoxyquinoline (0.50 g, 2.58 mmol) in amylamine (2.45 ml, 21.08 mmol) was heated to reflux at 110 °C for 48 h. After cooling at ambient temperature, the mixture was poured onto an ice (~ 100 cm<sup>3</sup>) and NaOH (100 ml, 2M) mixture while stirring vigorously. The precipitate formed was filtered, was washed with water (2 x 100 ml) and petrol (2 x 100 ml) and was dried *in vacuo* to afford **11** as beige solid (0.51 g, 81%).

**<sup>1</sup>H NMR (CDCl<sub>3</sub>, 400 MHz)** δ ppm: 8.49 (1H, d, *J* = 5.4, CH-2), 7.63 (1H, d, *J* = 9.2, CH-5), 7.35 (1H, d, *J* = 2.6, CH-8), 7.08 (1H, dd, *J* = 9.2, 2.6, CH-6), 6.36 (1H, d, *J* = 5.4, CH-3), 4.91 (1H, s, br, NH), 3.94 (3H, s, OCH<sub>3</sub>), 3.55-3.28 (2H, m, NCH<sub>2</sub>), 1.77 (2H, q, *J* = 7.3, NCH<sub>2</sub>CH<sub>2</sub>), 1.52-1.37 (4H, m, CH<sub>2</sub>CH<sub>2</sub>CH<sub>3</sub>), 0.96 (3H, t, *J* = 7.1, CH<sub>3</sub>)

**<sup>13</sup>C NMR (CDCl<sub>3</sub>, 150 MHz)** δ ppm: 160.3 (C<sub>Q</sub>-7), 151.5 (CH-2), 150.4 (C<sub>Q</sub>-4 or C<sub>Q</sub>-8'), 149.9 (C<sub>Q</sub>-4 or C<sub>Q</sub>-8'), 120.6 (CH-5), 117.1 (CH-6), 113.3 (C<sub>Q</sub>-4'), 108.3 (CH-8), 98.0 (CH-3), 55.5 (OCH<sub>3</sub>), 43.3 (NHCH<sub>2</sub>), 29.4 (CH<sub>2</sub>CH<sub>2</sub>CH<sub>3</sub>), 28.9 (NHCH<sub>2</sub>CH<sub>2</sub>), 22.6 (CH<sub>2</sub>CH<sub>3</sub>), 14.2 (CH<sub>2</sub>CH<sub>3</sub>)

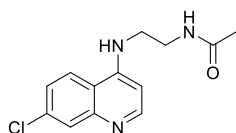
**HRMS (EI) m/z:** Calcd.  $[M+H]^+$  244.1570  
Measured 244.1567

**LRMS (EI) m/z:** 244 (13,  $[M]^+$ ), 187 (13,  $[M-CH_2(CH_2)_2CH_3]^+$ ), 88 (11), 86 (65,  $[NHCH_2(CH_2)_3CH_3]^+$ ), 84 (100)

**IR  $\nu_{max}$  (neat/cm<sup>-1</sup>):** 3357 (N-H), 3078, (Ar C-H), 2999, 2958, 2931, 2858 (aliphatic C-H), 1618 (C=N), 1583, 1535

**m.p.:** 118-119 °C

### ***N*-[2-(7-Chloro-quinolin-4-ylamino)-ethyl]-acetamide (12)**



White powder  
Chemical formula: C<sub>13</sub>H<sub>14</sub>ClN<sub>3</sub>O  
Molecular Weight: 263.72 g.mol<sup>-1</sup>  
Yield: 85%

To **5** (1.52 g, 6.85 mmol) and NEt<sub>3</sub> (2.60 ml, 18.50 mmol) in DCM (3 ml) at 0 °C, acetic anhydride (0.84 ml, 8.87 mmol) was added under argon atmosphere. The mixture was stirred at 0 °C for 1 h and then at ambient temperature for 2 h further. NaHCO<sub>3</sub> (1 M, 15 ml) was added to the reaction mixture. The organic products were extracted with EtOAc (3 x 15 ml) and the organic extracts were dried over anh. MgSO<sub>4</sub> and evaporated *in vacuo* to afford **12** as white crystalline solid (1.55 g, 85%).

**<sup>1</sup>H NMR (600 MHz, DMSO-d<sub>6</sub>)**  $\delta$  ppm: 8.40 (1H, d, *J* = 5.4, CH-2), 8.18 (1H, d, *J* = 9.0, CH-5), 8.13 (1H, s, br, NHCOCH<sub>3</sub>), 7.79 (1H, d, *J* = 2.4, CH-8), 7.46 (1H, dd, *J* = 9.0, 2.4, CH-6), 7.43 (1H, s, br, NHCH<sub>2</sub>CH<sub>2</sub>NHCO), 6.53 (1H, d, *J* = 5.4, CH-3), 3.35-3.29 (4H, m, NHCH<sub>2</sub>CH<sub>2</sub>), 1.83 (3H, s, CH<sub>3</sub>)

**<sup>13</sup>C NMR (150 MHz, DMSO-d<sub>6</sub>)**  $\delta$  ppm: 170.0 (C=O), 152.0 (CH-2), 150.0 (C<sub>Q</sub>-4), 149.1 (C<sub>Q</sub>-8'), 133.4 (C<sub>Q</sub>-7), 127.6 (CH-8), 124.2 (CH-5 or CH-6), 123.9 (CH-5 or CH-6), 117.4 (C<sub>Q</sub>-4'), 98.6 (CH-3), 42.3 (NHCH<sub>2</sub> or NHCH<sub>2</sub>CH<sub>2</sub>), 37.3 (NHCH<sub>2</sub> or NHCH<sub>2</sub>CH<sub>2</sub>), 22.7 (CH<sub>3</sub>)

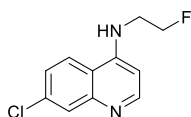
**HRMS (EI) m/z:** Calcd.  $[M]^+$  263.0820  
Measured 263.0807

**LRMS (EI) m/z:** 265 (17), 263 (50,  $[M]^+$ ), 205 (19), 205 (20), 204 (56), 193 (33), 191 (100,  $[M-CH_2NHCOCH_2]^+$ ), 156 (41,  $[M-CH_2NHCOCH_2-Cl]^+$ ), 155 (22), 135 (11)

**IR  $\nu_{max}$  (neat/cm<sup>-1</sup>):** 3323 (N-H), 3181 (N-H), 2951 (Ar C-H), 2929, 2845 (Alkyl C-H), 1645 (C=N), 1607, 1577 (Ar C=C), 1543

**m.p.:** 215 – 216 °C

### **(7-Chloro-quinolin-4-yl)-(2-fluoro-ethyl)-amine (13)**



Off white powder  
Chemical formula: C<sub>11</sub>H<sub>10</sub>ClFN<sub>2</sub>  
Molecular weight: 224.66 g.mol<sup>-1</sup>  
Yield: 63%

To a suspension of **6** (0.30 g, 1.35 mmol) in anhydrous DCM (5 ml) cooled at 0 °C, DAST (0.60 ml, 4.71 mmol) was added under Ar atmosphere. The resulting mixture was stirred at R.T. for 2 days. The reaction was quenched at 0 °C by the slow addition of cold NaOH (1M, 15 ml). The organic products were extracted with DCM (3 x 20 ml). The organic extracts were dried over anh. Na<sub>2</sub>SO<sub>4</sub> and concentrated *in*

*vacuo*. The resulting precipitate was purified by flash column chromatography (EtOAc) to afford pure **13** (0.19 g, 63%) as an off white powder.

**<sup>1</sup>H NMR (600 MHz, CDCl<sub>3</sub>)** δ ppm: 8.58 (1H, d, *J* = 5.3, *CH*-2), 7.99 (1H, d, *J* = 2.2, *CH*-8), 7.71 (1H, d, *J* = 9.0, *CH*-5), 7.39 (1H, dd, *J* = 9.0, 2.2, *CH*-6), 6.45 (1H, d, *J* = 5.3, *CH*-3), 5.37 (1H, br, s, *NH*), 4.77 (2H, dt, <sup>2</sup>*J*<sub>HF</sub> = 46.9 <sup>3</sup>*J*<sub>HH</sub> = 5.0, *CH*<sub>2</sub>F), 3.66 (2H, dq, <sup>3</sup>*J*<sub>HF</sub> = 26.8 <sup>3</sup>*J*<sub>HH</sub> = 5.0, *NHCH*<sub>2</sub>)

**<sup>13</sup>C NMR (150 MHz, CDCl<sub>3</sub>)** δ ppm: 152.0 (*CH*-2), 149.4 (*C*<sub>Q</sub>-4 or *C*<sub>Q</sub>-8'), 149.2 (*C*<sub>Q</sub>-4 or *C*<sub>Q</sub>-8'), 135.2 (*C*<sub>Q</sub>-7), 128.9 (*CH*-8), 125.8 (*CH*-6), 121.0 (*CH*-5), 117.3 (*C*<sub>Q</sub>-4'), 99.3 (*CH*-3), 81.7 (d, <sup>1</sup>*J*<sub>CF</sub> = 168.1, *CH*<sub>2</sub>F), 43.5 (d, <sup>2</sup>*J*<sub>CF</sub> = 20.3, *CH*<sub>2</sub>*CH*<sub>2</sub>F)

**<sup>19</sup>F NMR (282 MHz, CDCl<sub>3</sub>)** δ ppm: -224.24

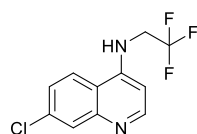
**HRMS (EI) m/z:** Calcd. [M]<sup>+</sup> 224.0511  
Measured 224.0509

**LRMS (EI) m/z:** 226 (26), 224 (100, [M]<sup>+</sup>), 193 (28), 191 (81, [M-CH<sub>2</sub>F]<sup>+</sup>), 156 (75, [M-CH<sub>2</sub>F-Cl]<sup>+</sup>), 155 (49), 88 (66)

**IR ν<sub>max</sub> (neat/cm<sup>-1</sup>):** 3213 (*NH*), 3053(*C=CH*), 3001, 2964 (*Alkyl C-H*), 1608, 1578 (*Ar C=C*), 1542

**m.p.:** 165-166 °C

#### 7-chloro-*N*-(2,2,2-trifluoroethyl)quinolin-4-amine (**14**)



White crystalline solid

Chemical formula: C<sub>11</sub>H<sub>8</sub>ClF<sub>3</sub>N<sub>2</sub>

Molecular Weight: 260.64 g.mol<sup>-1</sup>

Yield: 92%

A mixture of 4,7-dihydroquinoline (0.40 g, 2.01 mmol), 2,2,2-trifluoroethylamine hydrochloride (1.37 g, 10.1 mmol) and triethylamine (1.27 ml, 10.1 mmol) in DMF (1.5 ml) was heated at 100 °C for 4 h. The resulting solution was allowed to cool at R.T. and was then transferred to an ice/water (~30 cm<sup>3</sup>) and NaOH mixture (2M, 5 ml) while stirring vigorously. The precipitate formed was filtered, was washed with water (2 x 10 ml) and pentane (2 x 10 ml) and was dried *in vacuo* to afford a white solid. Re-crystallization (CHCl<sub>3</sub>, MeOH) afforded pure **14** as a white crystalline solid (0.47 g, 92%).

**<sup>1</sup>H NMR (600 MHz, DMSO-*d*<sub>6</sub>)** δ ppm: 8.49 (1H, d, *J* = 5.4, *CH*-2), 8.31 (1H, d, *J* = 9.1, *CH*-5), 7.86 (1H, d, *J* = 2.3, *CH*-8), 7.80 (1H, t, *J* = 6.7, *NH*), 7.53 (1H, dd, *J* = 9.1, 2.3, *CH*-6), 6.83 (1H, d, *J* = 5.4, *CH*-3), 4.24 (2H, qd, <sup>3</sup>*J*<sub>CF</sub> = 9.9, <sup>3</sup>*J*<sub>HH</sub> = 6.7, *NHCH*<sub>2</sub>)

**<sup>13</sup>C NMR (150 MHz, DMSO-*d*<sub>6</sub>)** δ ppm: 151.9 (*CH*-2), 149.7 (*C*<sub>Q</sub>-4), 149.0 (*C*<sub>Q</sub>-8'), 133.8 (*C*<sub>Q</sub>-7), 127.7 (*CH*-8), 125.5 (q, <sup>1</sup>*J*<sub>CF</sub> = 279.9, CF<sub>3</sub>), 124.9 (*CH*-6), 123.9 (*CH*-5), 117.3 (*C*<sub>Q</sub>-4'), 99.9 (*CH*-3), 43.2 (q, <sup>2</sup>*J*<sub>CF</sub> = 32.8, *NCH*<sub>2</sub>)

**<sup>19</sup>F NMR (282 MHz, DMSO-*d*<sub>6</sub>)** δ ppm: -69.8

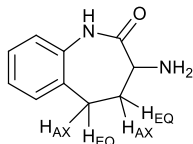
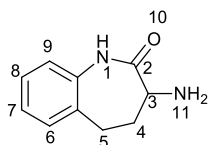
**HRMS (ES+) m/z:** Calcd. [M-H]<sup>+</sup> 261.0406  
Measured 261.0414

**LRMS (ES+) m/z:** 263 (28), 261 (98, [M-H]<sup>+</sup>)

**m.p.:** 201 - 202 °C

**3-azido-1,3,4,5-tetrahydro-2H-benzo[b]azepin-2-one (16)** was synthesized by PDRA Dr. Carlos Perez Medina according to a previously described procedure.<sup>154</sup>

**3-amino-4,5-dihydro-1H-benzo[b]azepin-2(3H)-one (17)**



White powder

Chemical formula: C<sub>10</sub>H<sub>10</sub>N<sub>2</sub>O

Molecular Weight: 176.21 g.mol<sup>-1</sup>

Yield: 61%

To a solution of **16** (0.60 g, 2.97 mol) and NH<sub>4</sub>Cl (0.37 g, 7.00 mmol), in EtOH (8 ml) and H<sub>2</sub>O (2.7 ml), zinc powder (0.26 g, 4.00 mmol) was added and the resulting mixture was heated to reflux at 80 °C for 20 min with vigorous stirring. After cooling at R.T., EtOAc (15 ml) was added followed by NH<sub>3</sub> (aq., 32%, 1 ml). The mixture was filtered, and the filtrate was washed with brine and dried over anh. Na<sub>2</sub>SO<sub>4</sub>. The solvents were evaporated *in vacuo* to afford pure **17** as a white powder (0.32 g, 61%).

**<sup>1</sup>H NMR (600 MHz, CDCl<sub>3</sub>)** δ ppm: 7.83 (1H, s, br, NH-1), 7.22-7.23 (2H, m, CH-6, CH-8), 7.14 (1H, td, *J* = 7.5, 1.4, CH-7), 6.99 (1H, dd, *J* = 8.3, 1.1, CH-9), 3.43 (1H, dd, <sup>3</sup>*J*<sub>H-3, H-4 AXIAL</sub> = 11.4, <sup>3</sup>*J*<sub>H-3, H-4 EQUATORIAL</sub> = 8.1, CH-3), 2.92 (1H, td, <sup>2</sup>*J*<sub>H5-AX, H5-EQ</sub> = 13.6, <sup>3</sup>*J*<sub>H5-AX, H4-AX</sub> = 13.6, <sup>3</sup>*J*<sub>H5-AX, H4-EQ</sub> = 7.8, CH-5<sub>AX</sub>), 2.65 (1H, dd, <sup>2</sup>*J*<sub>H5-AX, H5-EQ</sub> = 13.9, <sup>3</sup>*J*<sub>H5-EQ, H4-AX</sub> = 7.8, CH-5<sub>EQ</sub>), 2.52 (1H, tt, <sup>2</sup>*J*<sub>H4-AX, H4-EQ</sub> = 13.1, <sup>3</sup>*J*<sub>H4-AX, H5-AX</sub> = 13.6, <sup>3</sup>*J*<sub>H4-AX, H5-EQ</sub> = 7.6, <sup>3</sup>*J*<sub>H4-AX, H3</sub> = 7.6, CH-4<sub>AX</sub>), 1.93 (1H, ddd, <sup>2</sup>*J*<sub>H4-AX, H4-EQ</sub> = 13.0, <sup>3</sup>*J*<sub>H4-EQ, H3</sub> = 11.5, <sup>3</sup>*J*<sub>H4-EQ, H5-AX</sub> = 7.9), 1.64 (2H, s, br, NH<sub>2</sub>)

**<sup>13</sup>C NMR (150 MHz, CDCl<sub>3</sub>)** δ ppm: 177.1 (C<sub>Q</sub>-2), 136.7 (C<sub>Q</sub>-9'), 134.7 (C<sub>Q</sub>-5'), 129.8 (CH-6), 127.7 (CH-8), 126.2 (CH-7), 122.1 (CH-9), 51.6 (CH-3), 39.2 (CH<sub>2</sub>-4), 29.16 (CH<sub>2</sub>-5)

**HRMS (EI) m/z:** Calcd. [M]<sup>+</sup> 176.0944

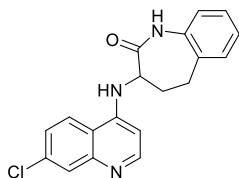
Measured 176.0947

**LRMS (EI) m/z:** 176 (36, [M]<sup>+</sup>), 159 (45), 147 (17, [M-CH<sub>2</sub>NH<sub>2</sub>]<sup>+</sup>), 130 (100), 118 (21), 106 (52)

**IR ν<sub>max</sub> (neat/cm<sup>-1</sup>):** 3356 (NH<sub>2</sub>), 3296, 3025 (Ar C-H), 2945, 2849 (Alkyl C-H), 1662, 1582

**m.p.:** 160-162 °C

**3-((7-chloroquinolin-4-yl)amino)-4,5-dihydro-1H-benzo[b]azepin-2(3H)-one (18)**



Beige powder

Chemical formula: C<sub>19</sub>H<sub>16</sub>ClN<sub>3</sub>O

Molecular Weight: 337.80 g.mol<sup>-1</sup>

Yield: 26%

To a mixture of **17** (0.19 g, 1.11 mmol) and 4,7-dichloroquinoline (0.22 g, 1.11 mmol) in DMF (1.5 ml), NEt<sub>3</sub> (0.30 ml, 2.16 mmol) was added and the resulting mixture was heated at 150 °C for 18 h. After cooling at R.T. the mixture was poured onto an ice (~30 cm<sup>3</sup>) and NaOH (2M, 20 ml) mixture and was stirred for 15 min. The precipitate formed was filtered and was washed with water (2 x 50 ml) and pentane (2 x 50 ml). Purification *via* flash column chromatography (EtOAc → 1:20 MeOH:EtOAc) afforded **18** as a beige solid (97 mg, 26%).

**<sup>1</sup>H NMR (600 MHz, DMSO-d<sub>6</sub>)** δ ppm: 10.03 (1H, s, NHCO), 8.42 (1H, d, *J* = 9.0, quin CH-5), 8.34 (1H, d, *J* = 5.4, quin CH-2), 7.80 (1H, d, *J* = 2.3, quin CH-8), 7.50 (1H, dd, *J* = 9.0, 2.3, quin CH-6), 7.34 (1H, dd, *J* = 7.6, 1.6, bnza CH-6), 7.33-7.29 (2H, m, CHNH, bnza CH-8), 7.17 (1H, td, *J* = 7.6, 1.6, bnza CH-7), 7.13 (1H, dd, *J* = 7.6, 1.6, bnza CH-9), 5.93 (1H, d, *J* = 5.4, quin CH-3), 4.06 (1H, dt, *J* = 11.3, 7.7, bnza CH-3), 2.85-2.78 (2H, m, bnza CH<sub>2</sub>-5), 2.61-2.51 (2H, m, bnza CH<sub>2</sub>-4)

**<sup>13</sup>C NMR (150 MHz, DMSO-d<sub>6</sub>)** δ ppm: 171.2 (C<sub>Q</sub>=O), 151.9 (quin CH-2), 149.6 (quin C<sub>Q</sub>-4), 149.0 (quin C<sub>Q</sub>-8'), 137.6 (bnza C<sub>Q</sub>-9'), 133.6 (bnza C<sub>Q</sub>-5' and quin C<sub>Q</sub>-7), 129.7 (bnza CH-6), 127.6 (bnza CH-8), 127.5 (quin CH-8), 125.3 (bnza CH-7), 124.6 (quin CH-5), 124.4 (quin CH-6), 122.1 (bnza CH-9), 117.5 (quin C<sub>Q</sub>-4'), 99.6 (quin CH-3), 52.8 (bnza CH-3), 34.6 (bnza CH<sub>2</sub>-4), 28.2 (bnza CH<sub>2</sub>-5)

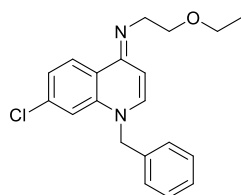
**HRMS (EI) m/z:** Calcd. [M]<sup>+</sup> 337.0976  
Measured 337.0973

**LRMS (EI) m/z:** 339 (17), 337 (44, [M]<sup>+</sup>), 132 (100)

**IR ν<sub>max</sub> (neat/cm<sup>-1</sup>):** 3361 (N-H), 3039 (Ar C-H), 2955, 2850 (Alkyl C-H), 1664 (C=N-), 1609, 1579 (Ar C=C), 1535

#### 4-Imino-1,4-dihydroquinolines **19** - **32**:

##### (*E*)-*N*-(1-benzyl-7-chloroquinolin-4(1*H*)-ylidene)-2-ethoxyethanamine (**19**)



Dark yellow/orange crystals  
Chemical formula: C<sub>20</sub>H<sub>21</sub>ClN<sub>2</sub>O  
Molecular weight: 340.85 g.mol<sup>-1</sup>  
Yield: 17%

To a solution of **4** (0.60 g, 2.40 mmol) and NaI (0.43 g, 2.86 mmol) in acetone (5 ml), benzyl bromide (0.30 ml, 2.64 mmol) was added and the resulting mixture was heated to reflux at 80 °C for 12 h under Ar atmosphere. The solution was allowed to cool at R.T and was then transferred to an ice/water (~30 cm<sup>3</sup>) and NaOH (2 M, 20 ml) mixture whilst stirring vigorously. The precipitate formed was filtered, washed with water (2 x 20 ml) and pentane (2 x 20 ml), and dried *in vacuo*. Recrystallization (CH<sub>3</sub>CN: petroleum ether) afforded pure **19** as dark yellow/orange crystals (0.14 g, 17%).

**<sup>1</sup>H NMR (600 MHz, CDCl<sub>3</sub>)** δ ppm: 8.44 (1H, d, *J* = 8.6, CH-5), 7.35 (2H, t, *J* = 7.4, meta Ph-CH), 7.30 (1H, t, *J* = 7.4, para Ph-CH), 7.17 (2H, d, *J* = 7.4, ortho Ph-CH), 7.12 (1H, d, *J* = 8.6, CH-6), 7.02 (1H, d, *J* = 7.9, CH-2), 7.00 (1H, s, CH-8), 6.07 (1H, d, *J* = 7.9, CH-3), 5.04 (2H, s, CH<sub>2</sub>Ph), 3.82 (2H, t, *J* = 6.8, NCH<sub>2</sub>CH<sub>2</sub>), 3.62 (2H, q, *J* = 7.0, CH<sub>2</sub>CH<sub>3</sub>), 3.53 (2H, t, *J* = 6.8, NCH<sub>2</sub>CH<sub>2</sub>), 1.24 (3H, t, *J* = 7.0, CH<sub>3</sub>)

**<sup>13</sup>C NMR (150 MHz, CDCl<sub>3</sub>)** δ ppm: 154.9 (C<sub>Q</sub>-4), 139.6 (C<sub>Q</sub>-7), 139.5 (CH-2), 136.5 (C<sub>Q</sub>-8'), 135.5 (Ph-C<sub>Q</sub>), 129.3 (meta Ph-CH), 128.3 (para Ph-CH), 127.4 (CH-5), 126.2 (ortho Ph-CH), 123.8 (CH-6), 114.9 (CH-8), 99.9 (CH-3), 71.6 (NCH<sub>2</sub>CH<sub>2</sub>), 66.7 (CH<sub>2</sub>CH<sub>3</sub>), 55.6 (CH<sub>2</sub>Ph), 50.0 (NCH<sub>2</sub>CH<sub>2</sub>), 15.4 (CH<sub>3</sub>), (C<sub>Q</sub>-4' hidden)

**HRMS (ES+) m/z:** Calcd. [M-H]<sup>+</sup> 341.1404  
Measured 341.1421

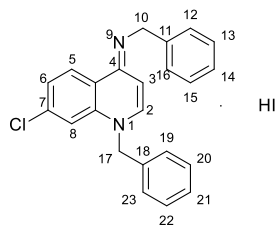
**LRMS (ES+) m/z:** 343 (35), 341 (100, [M-H]<sup>+</sup>)

**IR ν<sub>max</sub> (neat/cm<sup>-1</sup>):** 3031 (Ar C-H), 2967 (Alkyl C-H), 2901, 2824, 1635 (C=N-), 1596 (Ar C=C), 1569



m.p.: 111-112 °C

**(E)-N,1-dibenzyl-7-chloroquinolin-4(1H)-imine hydroiodide (20)**



Dark yellow crystals

Chemical formula:  $C_{23}H_{19}Cl_2 \cdot HI$

Molecular Weight:  $486.78 \text{ g}\cdot\text{mol}^{-1}$

Yield: 98%

To a solution of **8** (0.90 g, 3.35 mmol) and NaI (0.60g, 4.02 mmol) in acetone (15 ml), benzyl bromide (0.44 ml, 3.70 mmol) was added and the mixture was heated at 60 °C for 18 h. The mixture was allowed to cool to ambient temperature and was then poured into an ice (~ 100 cm<sup>3</sup>) and NaOH (2M, 100 ml), mixture while stirring vigorously. The precipitate formed was filtered, was washed with water (2 x 100 ml) and petrol (2 x 100 ml) and was dried *in vacuo*. Recrystallization (MeOH) afforded the hydroiodide salt **20**, as yellow crystalline solid (1.60 g, 98%).

**<sup>1</sup>H NMR (CDCl<sub>3</sub>, 600 MHz)** δ ppm: 11.04-10.89 (1H, m, =NH<sup>+</sup>), 9.45 (1H, d, *J* = 8.9, CH-5), 8.10-8.04 (1H, m, CH-2), 7.61 (1H, d, *J* = 1.9, CH-8), 7.56 (1H, dd, *J* = 8.9, 1.9, CH-6), 7.46 (2H, d, *J* = 7.5, CH-12, CH-16), 7.41-7.35 (3H, m, CH-20, CH-22, CH-24), 7.30 (2H, t, *J* = 7.5, CH-13, CH-15), 7.26-7.22 (1H, m, CH-14), 7.16-7.13 (2H, m, CH-19, CH-23), 6.51 (1H, d, *J* = 7.6, CH-3), 5.56 (2H, s, CH<sub>2</sub>-17), 4.84 (2H, d, *J* = 6.1, CH<sub>2</sub>-10)

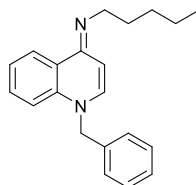
**<sup>13</sup>C NMR (CDCl<sub>3</sub>, 150 MHz)** δ ppm: 156.0 (C<sub>Q</sub>-4), 145.8 (CH-2), 141.3 (C<sub>Q</sub>-7), 138.8 (C<sub>Q</sub>-8<sup>+</sup>), 135.6 (C<sub>Q</sub>-11), 132.5 (C<sub>Q</sub>-18), 129.9 (CH-20, CH-23), 129.5 (CH-24), 129.1 (CH-13, CH-15), 128.9 (CH-5), 128.3 (CH-6 or CH-14), 128.1 (CH-6 or CH-14), 127.7 (CH-12, CH-16), 127.0 (CH-19, CH-23), 117.4 (C<sub>Q</sub>-4<sup>+</sup>), 117.1 (CH-8), 99.8 (CH-3), 58.4 (CH<sub>2</sub>-17), 47.0 (CH<sub>2</sub>-10)

**HRMS (ES<sup>+</sup>) m/z:** Calcd. [M+H]<sup>+</sup> 359.1315  
Measured 359.1312

**LRMS (ES<sup>+</sup>) m/z:** 361 (32), 360 (26), 359 (100, [M+H]<sup>+</sup>), 224 (14), 220 (20), 208 (20), 196 (13), 180 (25), 179 (38)

**IR ν<sub>max</sub> (neat/cm<sup>-1</sup>):** 3178 (N-H), 3087 (Ar C-H), 3057, 3026, 2999, 2939, 2875 (Alkyl C-H), 1606 (C=N), 1571 (Ar C=C), 1527

**(E)-N-(1-benzylquinolin-4(1H)-ylidene)pentan-1-amine (21)**



White solid

Chemical formula:  $C_{21}H_{24}N_2$

Molecular Weight:  $304.43 \text{ g}\cdot\text{mol}^{-1}$

Yield: 86%

To a solution of **9** (0.17 g, 0.80 mmol) and NaI (0.15 g, 1.00 mmol) in acetone (5 ml), benzyl bromide (0.1 ml, 0.88 mmol) was added and the mixture was heated to reflux at 70 °C for 18 hr under Ar atmosphere. The resulting solution was allowed to cool at R.T. and was then transferred to a mixture of ice/water (~20 cm<sup>3</sup>) and NaOH (2M, 10 ml) while stirring vigorously. The precipitate formed was filtered, washed with water (3 x 15 ml) and pentane (2 x 10 ml) and was dried *in vacuo* to afford pure **21** (0.21 g, 86%) as white solid.

**<sup>1</sup>H NMR (600 MHz, CDCl<sub>3</sub>)** δ ppm: 8.65 (1H, d, *J* = 8.2, CH-5), 7.39-7.20 (6H, m, meta Ph-CH, para Ph-CH, CH-2, CH-6, CH-7), 7.16 (2H, d, *J* = 7.6, ortho Ph-CH), 7.12 (1H, d, *J* = 8.5, CH-8), 6.14 (1H, d, *J* = 7.9, CH-3), 5.21 (2H, s, CH<sub>2</sub>Ph), 3.39 (2H, t, *J* = 7.5, NCH<sub>2</sub>), 1.76 (2H, qn, *J* = 7.5, NCH<sub>2</sub>CH<sub>2</sub>), 1.47-1.35 (4H, m, CH<sub>2</sub>CH<sub>2</sub>CH<sub>3</sub>), 0.92 (3H, t, *J* = 7.1, CH<sub>3</sub>)

**<sup>13</sup>C NMR (150 MHz, CDCl<sub>3</sub>)** δ ppm: 154.9 (C<sub>Q</sub>-4), 140.8 (CH-2), 138.5 (C<sub>Q</sub>-8'), 135.7 (Ph-C<sub>Q</sub>), 131.0 (CH-7), 129.2 (meta Ph-CH), 128.2 (para Ph-CH), 126.3 (ortho Ph-CH), 125.8 (CH-5), 124.3 (C<sub>Q</sub>-4'), 124.1 (CH-6), 115.7 (CH-8), 98.9 (CH-3), 56.2 (CH<sub>2</sub>Ph), 48.8 (C=NCH<sub>2</sub>), 30.3 (NCH<sub>2</sub>CH<sub>2</sub>), 30.0 (CH<sub>2</sub>CH<sub>2</sub>CH<sub>3</sub>), 22.8 (CH<sub>2</sub>CH<sub>3</sub>), 14.3 (CH<sub>3</sub>)

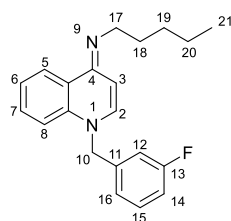
**HRMS (EI) m/z:** Calcd. [M]<sup>+</sup> 304.1934  
Measured 304.1947

**LRMS (EI) m/z:** 304 (27, [M]<sup>+</sup>), 261 (80, [M-CH<sub>2</sub>CH<sub>2</sub>CH<sub>3</sub>]<sup>+</sup>), 247 (100, [M-CH<sub>2</sub>(CH<sub>2</sub>)<sub>2</sub>CH<sub>3</sub>]<sup>+</sup>), 91 (27, [PhCH<sub>2</sub>]<sup>+</sup>)

**IR ν<sub>max</sub> (neat/cm<sup>-1</sup>):** 3055 (Ar C-H), 3027, 2950 (Alkyl C-H), 2922, 2851, 1615 (C=N-C), 1571 (Ar C=C)

**m.p.:** 76.5 – 77.5 °C

### [1- (3-Fluoro-benzyl)-1*H*-quinolin-4-ylidene]-pentyl-amine (**22**)



Pale yellow crystals

Chemical Formula: C<sub>21</sub>H<sub>23</sub>FN<sub>2</sub>

Molecular weight: 322.43

Yield: 71%

To a solution of **9** (0.86 g, 4.01 mmol) in acetone (15 ml), 3-fluorobenzyl bromide (0.54 ml, 4.40 mmol) and NaI (0.78 g, 4.79 mmol) were added and the mixture was heated at 65 °C for 18 h. After cooling to room temperature, DCM (100 ml) was added and the resulting mixture was washed with water (2 x 100 ml). The organic solution was dried over anh. MgSO<sub>4</sub> and evaporated *in vacuo*. Trituration of the remaining residue with petrol, afforded an off-white precipitate. The precipitate was dissolved in EtOH (20 ml), KOBu<sup>t</sup> (0.49 g, 4.37 mmol) was added and the resulting solution was stirred at room temperature for 15 min. The organic product was extracted with DCM (2 x 25 ml), the organic extracts were dried over anh. MgSO<sub>4</sub>, and evaporated to dryness. Recrystallization (pentane, Et<sub>2</sub>O) afforded **22** as pale yellow crystals (0.92 g, 71%).

**<sup>1</sup>H NMR (600 MHz, CDCl<sub>3</sub>)** δ ppm: 8.49 (1H, d, *J* = 8.0, CH-5), 7.33-7.27 (2H, m, CH-7, CH-15), 7.17 (1H, dd, *J* = 8.0, 7.2, CH-6), 7.00 (1H, d, *J* = 8.1, CH-2), 6.99-6.90 (3H, m, CH-8, CH-14, CH-16), 6.87 (1H, dt, <sup>3</sup>*J*<sub>HF</sub> = 9.6, <sup>4</sup>*J*<sub>HH</sub> = 2.1, CH-12), 6.05 (1H, d, *J* = 8.1, CH-3), 5.05 (2H, s, CH<sub>2</sub>-10), 3.36 (2H, t, *J* = 7.5, CH<sub>2</sub>-17), 1.76 (2H, q, *J* = 7.5, CH<sub>2</sub>-18), 1.49-1.36 (4H, m, CH<sub>2</sub>-19, CH<sub>2</sub>-20), 0.94 (2H, t, *J* = 7.2, CH<sub>3</sub>-21)

**<sup>13</sup>C NMR (150 MHz, CDCl<sub>3</sub>)** δ ppm: 163.3 (d, <sup>1</sup>*J*<sub>CF</sub> = 247.6, C<sub>Q</sub>-13), 154.4 (C<sub>Q</sub>-4), 139.1 (d, <sup>3</sup>*J*<sub>CF</sub> = 6.8, C<sub>Q</sub>-11), 139.0 (CH-2), 138.5 (C<sub>Q</sub>-8'), 130.8 (d, <sup>3</sup>*J*<sub>CF</sub> = 8.4, CH-15), 130.2 (CH-7), 126.0 (C<sub>Q</sub>-4'), 125.7 (CH-5), 123.4 (CH-6), 121.67 (d, <sup>4</sup>*J*<sub>CF</sub> = 2.9, CH-16), 115.0 (d, <sup>2</sup>*J*<sub>CF</sub> = 21.2, CH-14), 114.9 (CH-8), 113.2 (d, <sup>2</sup>*J*<sub>CF</sub> = 22.3, CH-12), 99.2 (CH-3), 55.1 (CH<sub>2</sub>-10), 50.3 (CH<sub>2</sub>-17), 31.0 (CH<sub>2</sub>-18), 30.3 (CH<sub>2</sub>-19), 22.9 (CH<sub>2</sub>-20), 14.3 (CH<sub>3</sub>-21)

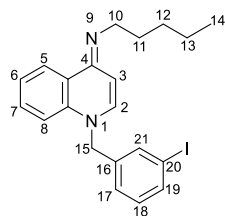
**<sup>19</sup>F NMR (282 MHz, CDCl<sub>3</sub>)** δ ppm: -112.13

**HRMS (ES-) m/z:** Calcd. [M]<sup>+</sup> 322.1845  
Measured 322.1821

**LRMS (ES-) m/z:** 322 (39, [M]<sup>+</sup>), 321(100), 313 (14)

IR  $\nu_{\max}$  (neat/cm<sup>-1</sup>): 2951 (Ar C-H), 2926, 2855 (Aliphatic C-H), 1612 (C=N), 1575, 1542  
 m.p.: 64-65 °C

### *N*-(1-(3-iodobenzyl)quinolin-4(1*H*)-ylidene)pentan-1-amine (23)



Pale yellow solid

Chemical formula: C<sub>21</sub>H<sub>23</sub>IN<sub>2</sub>

Molecular Weight: 430.33 g.mol<sup>-1</sup>

Yield: 79%

To a solution of **9** (0.50 g, 2.33 mmol) in acetone (10 ml), 3-iodobenzylbromide (0.76 g, 2.56 mmol) and NaI (0.39 g, 2.60 mmol) were added, and the mixture was heated at 65 °C for 18 h. After cooling to room temperature, the mixture was poured in ice (~100 cm<sup>3</sup>) and stirred vigorously for 15 min. The precipitate formed was filtered, and was washed with water and petrol. The precipitate was dissolved in EtOH (5 ml), KOBu<sup>t</sup> (0.36 g, 3.21 mmol) was added and the mixture was stirred at room temperature for 15 min. The organic products were extracted with DCM (2 x 25 ml). The organic extracts were dried over anh. MgSO<sub>4</sub> and evaporated to afford **23** as pale yellow solid (0.79 g, 79%).

<sup>1</sup>H NMR (600 MHz, CDCl<sub>3</sub>)  $\delta$  ppm: 8.55 (1H, dd, *J* = 8.1, 1.7, CH-5), 7.61 (1H, d, *J* = 7.7, 1.7, CH-19), 7.54 (1H, t, *J* = 1.7, CH-21) 7.34 (1H, ddd, *J* = 8.5, 7.1, 1.7, CH-7), 7.20 (1H, dd, *J* = 8.1, 7.1, CH-6), 7.12-7.07 (2H, m, CH-2, CH-17), 7.04 (1H, t, *J* = 7.7, CH-18), 6.96 (1H, d, *J* = 8.5, CH-8), 6.07 (1H, d, *J* = 8.1, CH-3), 5.05 (2H, s, CH<sub>2</sub>-15), 3.37 (2H, t, *J* = 7.5, CH<sub>2</sub>-10), 1.76 (2H, qn, *J* = 7.5, CH<sub>2</sub>-11), 1.48-1.36 (4H, m, CH<sub>2</sub>-12, CH<sub>2</sub>-13), 0.93 (3H, t, *J* = 7.1, CH<sub>3</sub>-14)

<sup>13</sup>C NMR (150 MHz, CDCl<sub>3</sub>)  $\delta$  ppm: 154.6 (C<sub>Q</sub>-4), 139.5 (CH-2), 138.6 (Ph-C<sub>Q</sub>), 138.4 (C<sub>Q</sub>-8'), 137.2 (CH-19), 135.1 (CH-21), 130.9 (CH-18), 130.6 (CH-7), 125.8 (CH-5), 125.4 (C<sub>Q</sub>-4'), 125.3 (CH-17), 123.8 (CH-6), 115.1 (CH-8), 99.2 (CH-3), 95.1 (C<sub>Q</sub>-20), 55.0 (CH<sub>2</sub>-15), 49.8 (CH<sub>2</sub>-10), 30.8 (CH<sub>2</sub>-11), 30.2 (CH<sub>2</sub>-12), 22.9 (CH<sub>2</sub>-13), 14.4 (CH<sub>3</sub>-14)

HRMS (EI) *m/z*: Calcd. [M]<sup>+</sup> 430.0906

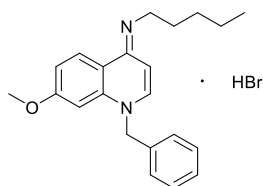
Measured 430.0900

LRMS (EI) *m/z*: 430 (38, [M]<sup>+</sup>), 387 (90, [M-CH<sub>2</sub>CH<sub>2</sub>CH<sub>3</sub>]<sup>+</sup>), 373 (100, [M-HCH<sub>2</sub>(CH<sub>2</sub>)<sub>2</sub>CH<sub>3</sub>]<sup>+</sup>), 360 (13, [M+H-CH<sub>2</sub>(CH<sub>2</sub>)<sub>3</sub>CH<sub>3</sub>]<sup>+</sup>), 217 (21, [CH<sub>2</sub>Ph]<sup>+</sup>), 90 (7)

IR  $\nu_{\max}$  (neat/cm<sup>-1</sup>): 3053 (Ar C-H), 2950, 2913, 2845 (Aliphatic C-H), 2811, 1631 (C=N), 1606, 1586 (Ar C=C), 1569, 1557

m.p.: 118 – 119 °C

### 1-benzyl-7-methoxy-4-(pentylamino)quinolin-1-ium bromide (24)



White powder

Chemical formula: C<sub>22</sub>H<sub>26</sub>N<sub>2</sub>O · HBr

Molecular weight: 415.38 g.mol<sup>-1</sup>

Yield: 42%

To a solution of **11** (0.43 g, 1.77 mmol) in acetone (15 ml), benzyl bromide (210  $\mu$ l, 1.77 mmol) was added and the mixture was heated at 60 °C for 3 h. After cooling to

ambient temperature, the mixture was poured into an ice (~ 100 cm<sup>3</sup>) and NaOH (100 ml, 2M) mixture while stirring vigorously. The organic products were extracted with DCM (2 x 100 ml), dried over anh. MgSO<sub>4</sub> and evaporated *in vacuo*. To the remaining residue, EtOAc (50 ml) was added and the mixture was stirred for 10 min. The precipitate formed was filtered, was washed with EtOAc (2 x 50 ml) and petrol (2 x 50 ml) and was dried *in vacuo* to afford **24** as white powder (0.31 g, 42%).

**<sup>1</sup>H NMR (CDCl<sub>3</sub>, 600 MHz)** δ ppm: 10.01 (1H, t, *J* = 5.9, NH<sup>+</sup>), 9.14 (1H, d, *J* = 9.3, CH-5), 8.24 (1H, d, *J* = 7.5, CH-2), 7.36-7.28 (3H, m, meta Ph-CH, para Ph-CH), 7.20 (2H, d, *J* = 7.9, ortho Ph-CH), 7.03 (1H, dd, *J* = 9.3, 2.5, CH-6), 6.87 (1H, d, *J* = 2.5, CH-8), 6.36 (1H, d, *J* = 7.5, CH-3), 5.71 (2H, s, CH<sub>2</sub>Ph), 3.78 (3H, s, OCH<sub>3</sub>), 3.52 (2H, td, *J* = 7.0, 5.9, NCH<sub>2</sub>), 1.79 (2H, q, *J* = 7.0, NCH<sub>2</sub>CH<sub>2</sub>), 1.42-1.31 (4H, m, CH<sub>2</sub>CH<sub>2</sub>CH<sub>3</sub>), 0.89 (3H, t, *J* = 7.0, CH<sub>2</sub>CH<sub>3</sub>)

**<sup>13</sup>C NMR (CDCl<sub>3</sub>, 150 MHz)** δ ppm: 163.7 (C<sub>Q</sub>-7), 155.1 (C<sub>Q</sub>-4), 145.3 (CH-2), 140.0 (C<sub>Q</sub>-8'), 133.9 (Ph-C<sub>Q</sub>), 129.5 (meta Ph-CH), 128.9 (CH-5 or para Ph-CH), 128.8 (CH-5 or para Ph-CH), 126.7 (ortho Ph-CH), 116.4 (CH-6), 112.6 (C<sub>Q</sub>-4'), 99.7 (CH-8), 97.3 (CH-3), 58.4 (CH<sub>2</sub>Ph), 56.2 (OCH<sub>3</sub>), 43.6 (NCH<sub>2</sub>), 29.2 (CH<sub>2</sub>CH<sub>2</sub>CH<sub>3</sub>), 28.2 (NCH<sub>2</sub>CH<sub>2</sub>), 22.5 (CH<sub>2</sub>CH<sub>3</sub>), 14.2 (CH<sub>3</sub>)

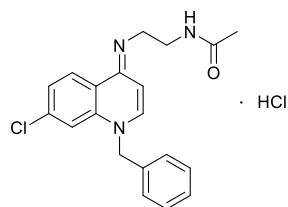
**HRMS (EI) m/z:** Calcd. [M]<sup>+</sup> 334.2040  
Measured 334.5056

**LRMS (EI) m/z:** 335 (8, [M+H]<sup>+</sup>), 334 (32, [M]<sup>+</sup>), 292 (17), 291 (66, [M-CH<sub>2</sub>CH<sub>2</sub>CH<sub>3</sub>]<sup>+</sup>), 278 (25), 277 (100, [M-CH<sub>2</sub>(CH<sub>2</sub>)<sub>2</sub>CH<sub>3</sub>]<sup>+</sup>), 264 (13, [M+H-CH<sub>2</sub>(CH<sub>2</sub>)<sub>3</sub>CH<sub>3</sub>]<sup>+</sup>), 91 (17, [CH<sub>2</sub>Ph]<sup>+</sup>)

**IR ν<sub>max</sub> (neat/cm<sup>-1</sup>):** 3458, 3173 (N-H), 3011 (Ar C-H), 2970, 2946 (aliphatic C-H), 1739, 1614, 1562 (Ar C=C), 1532

**m.p.:** 221 - 222 °C

**(E)-2-acetamido-N-(1-benzyl-7-chloroquinolin-4(1H)-ylidene)ethanaminium chloride (25)**



Off white powder

Chemical formula: C<sub>20</sub>H<sub>20</sub>ClN<sub>3</sub>O · HCl

Molecular Weight: 390.30 g.mol<sup>-1</sup>

Yield: 25%

To a solution of **12** (1.54 g, 5.84 mmol) in DMSO (6 ml), benzyl bromide (0.77 ml, 6.48 mmol) and Et<sub>3</sub>N (0.98 ml, 6.97) were added and the resulting solution was heated at 110 °C for 24 h. After cooling at room temperature, the mixture was poured to an ice (~50 cm<sup>3</sup>) and NaOH (2M, 50 ml) mixture while stirring vigorously. The organic products were extracted with EtOAc (2 x 100 ml) and the organic extracts were dried over anh. MgSO<sub>4</sub> and evaporated *in vacuo*. The resulting residue was purified *via* column chromatography using basic Al<sub>2</sub>O<sub>3</sub> as the solid phase (EtOAc → 1:9 MeOH:EtOAc). The isolated product was dissolved in a mixture of DCM and isopropanol (9:1, 100 ml) and was neutralised to pH 7 with HCl (1 M). The organic layer was isolated, dried over anh MgSO<sub>4</sub> and evaporated *in vacuo* to afford **25** as the hydrochloride salt as off white solid (0.57 g, 25%).

**<sup>1</sup>H NMR (CDCl<sub>3</sub>, 600 MHz)** δ ppm: 10.81 (1H, s, br, NHCH<sub>2</sub>CH<sub>2</sub>NHCO), 9.53 (1H, d, *J* = 9.0, CH-5), 8.62 (1H, s, br, NHCOCH<sub>3</sub>), 8.09 (1H, d, *J* = 7.5, CH-2), 7.66 (1H, dd, *J* = 9.0, 2.0, CH-6), 7.62 (1H, d, *J* = 2.0, CH-8), 7.45-7.39 (3H, m, meta Ph CH, para Ph CH), 7.15 (2H, dd, *J* =

7.6, 1.9, ortho Ph CH), 6.72 (1H, d,  $J = 7.5$ , CH-3), 5.55 (2H, s, CH<sub>2</sub>Ph), 3.76-3.72 (4H, m, NHCH<sub>2</sub>CH<sub>2</sub>), 2.06 (3H, s, CH<sub>3</sub>)

<sup>13</sup>C NMR (CDCl<sub>3</sub>, 150 MHz)  $\delta$  ppm: 172.3 (C=O), 156.6 (C<sub>Q</sub>-4), 145.4 (CH-2), 141.5 (C<sub>Q</sub>-7), 138.7 (C<sub>Q</sub>-8'), 132.4 (C<sub>Q</sub>-Ph), 130.0 (meta Ph CH), 129.7 (para Ph CH or CH-5), 129.3 (para Ph CH or CH-5), 128.5 (CH-6), 126.7 (ortho Ph CH), 117.4 (C<sub>Q</sub>-4'), 116.8 (CH-8), 99.0 (CH-3), 58.3 (CH<sub>2</sub>Ph), 44.4 (NHCH<sub>2</sub> or NHCH<sub>2</sub>CH<sub>2</sub>), 37.8 (NHCH<sub>2</sub> or NHCH<sub>2</sub>CH<sub>2</sub>), 23.2 (CH<sub>3</sub>)

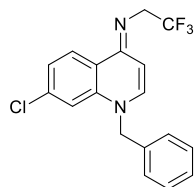
HRMS (ES+) m/z: Calcd. [M+H]<sup>+</sup> 354.1373  
Measured 354.1371

LRMS (ES+) m/z: 356 (29), 354 (100)

IR  $\nu_{\max}$  (neat/cm<sup>-1</sup>): 3219 (N-H), 3089 (Ar C-H), 3001, 2942, 2823 (Alkyl C-H), 1661 (C=N-), 1617, 1579 (Ar C=C), 1545, 1529

m.p.: 233 - 234 °C

### (E)-N-(1-benzyl-7-chloroquinolin-4(1H)-ylidene)-2,2,2-trifluoroethanamine (26)



White powder

Chemical formula: C<sub>18</sub>H<sub>14</sub>ClF<sub>3</sub>N<sub>2</sub>

Molecular Weight: 350.76 g.mol<sup>-1</sup>

Yield: 73%

To a suspension of **14** (0.12 g, 0.46 mmol) and NaI (0.08 g, mmol) in acetone (4 ml), benzyl bromide (0.06 ml, 0.50 mmol) was added and the resulting mixture was heated to reflux at 70 °C for 3 h under Ar atmosphere. The solution was allowed to cool at R.T. and was then transferred on vigorous stirring, to a mixture of ice/water (~20 cm<sup>3</sup>) and NaOH (2 M, 5 ml). The precipitate formed was filtered, was washed with water (3 x 10 ml) and petrol (3 x 10 ml), and dried *in vacuo* to afford pure **26** (0.12 g, 73%) as a white solid.

<sup>1</sup>H NMR (600 MHz, CDCl<sub>3</sub>)  $\delta$  ppm: 8.51 (1H, d,  $J = 8.3$ , CH-5), 7.36 (2H, t,  $J = 7.4$ , meta Ph-CH), 7.32 (1H, t,  $J = 7.4$ , para Ph-CH), 7.18-7.14 (3H, m, CH-6, ortho Ph-CH), 7.11 (1H, d,  $J = 7.9$ , CH-2), 7.05 (1H, d,  $J = 1.3$ , CH-8), 5.88 (1H, d,  $J = 7.9$ , CH-3), 5.08 (2H, s, CH<sub>2</sub>Ph), 3.82 (2H, q,  $^3J_{\text{HF}} = 9.7$ , NCH<sub>2</sub>)

<sup>13</sup>C NMR (150 MHz, CDCl<sub>3</sub>)  $\delta$  ppm: 156.6 (C<sub>Q</sub>-4), 140.2 (CH-2), 139.3 (C<sub>Q</sub>-8'), 136.8 (C<sub>Q</sub>-7), 135.2 (Ph-C<sub>Q</sub>), 129.4 (meta Ph-CH), 128.4 (para Ph-CH), 127.8 (CH-5), 126.3 (q,  $^1J_{\text{CF}} = 275.7$ , CF<sub>3</sub>), 126.2 (ortho Ph-CH), 124.3 (CH-6), 123.9 (C<sub>Q</sub>-4'), 115.0 (CH-8), 99.0 (CH-3), 55.8 (CH<sub>2</sub>Ph), 52.0 (q,  $^2J_{\text{CF}} = 30.5$ , NCH<sub>2</sub>)

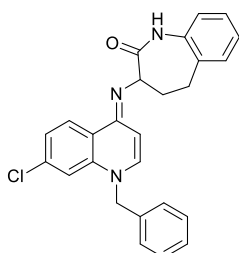
<sup>19</sup>F NMR (282 MHz, CDCl<sub>3</sub>)  $\delta$  ppm: -71.23

HRMS (ES+) m/z: Calcd. [M-H]<sup>+</sup> 351.0876  
Measured 351.0868

LRMS (ES+) m/z: 353 (35), 351 (100, [M-H]<sup>+</sup>)

IR  $\nu_{\max}$  (neat/cm<sup>-1</sup>): 3032 (Ar C-H), 2895 (Alkyl C-H), 2825, 1631 (C=N-), 1600, 1572 (Ar C=C)

m.p.: 163 - 164 °C

**(E)-3-((1-benzyl-7-chloroquinolin-4(1H)-ylidene)amino)-4,5-dihydro-1H-benzo[b]azepin-2(3H)-one (27)**

Yellow powder

Chemical formula: C<sub>26</sub>H<sub>22</sub>ClN<sub>3</sub>OMolecular Weight: 427.92 g.mol<sup>-1</sup>

Yield: 49%

A mixture of **15** (0.10 g, 0.29 mmol) and benzyl bromide (0.05 ml, 0.42 mmol) in DMF (1 ml) was heated at 100 °C for 24 h. After cooling to R.T., the mixture was poured into an ice (~30 cm<sup>3</sup>) and NaOH (2 M, 30 ml) mixture while stirring vigorously. The precipitate formed was filtered, was washed with water (2 x 50 ml) and pentane (2 x 50 ml) and was dried *in vacuo*. Purification *via* column chromatography (EtOAc → 1:2:20 NEt<sub>3</sub>:MeOH:EtOAc) followed by trituration with Et<sub>2</sub>O, afforded pure **27** as a yellow solid (0.06 g, 49%).

**<sup>1</sup>H NMR (600 MHz, DMSO-d<sub>6</sub>)** δ ppm: 9.74 (1H, s, NH), 8.22 (1H, d, *J* = 8.7, quin CH-5), 7.64 (1H, d, *J* = 8.0, quin CH-2), 7.40 (1H, s, quin CH-8), 7.34 (2H, t, *J* = 7.6, meta Ph-CH), 7.29-7.26 (2H, m, bnza CH-6, para Ph-CH), 7.25-7.21 (2H, m, quin CH-6, bnza CH-8), 7.20 (2H, d, *J* = 7.6, ortho Ph-CH), 7.10 (1H, td, *J* = 7.6, 1.5, bnza CH-7), 7.01 (1H, dd, *J* = 7.6, 1.5, bnza CH-9), 5.60 (1H, d, *J* = 8.0, quin CH-3), 5.30 (2H, d, *J* = 4.4, CH<sub>2</sub>Ph), 4.03 (1H, t, *J* = 8.9, bnza COCH-3), 2.86-2.74 (2H, m, bnza CH<sub>2</sub>-5), 2.45-2.40 (2H, m, bnza CH<sub>2</sub>-4)

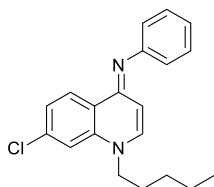
**<sup>13</sup>C NMR (150 MHz, DMSO-d<sub>6</sub>)** δ ppm: 172.7 (C<sub>Q</sub>=O), 153.6 (quin C<sub>Q</sub>-4), 141.8 (quin CH-2), 139.2 (quin C<sub>Q</sub>-8'), 138.2 (bnza C<sub>Q</sub>-9'), 136.5 (Ph-C<sub>Q</sub>), 135.5 (quin C<sub>Q</sub>-7), 134.3 (bnza C<sub>Q</sub>-5'), 129.3 (bnza CH-6), 128.9 (meta Ph-CH), 127.7 (bnza CH-8 and para Ph-CH), 127.2 (quin CH-5), 126.4 (ortho Ph-CH), 124.7 (bnza CH-7), 123.3 (quin CH-6), 123.0 (quin C<sub>Q</sub>-4'), 121.6 (bnza CH-9), 115.6 (quin CH-8), 99.5 (quin CH-3), 58.5 (bnza CH-3), 54.3 (CH<sub>2</sub>Ph), 37.5 (bnza CH<sub>2</sub>-4), 28.8 (bnza CH<sub>2</sub>-5)

**HRMS (EI) m/z:** Calcd. [M]<sup>+</sup> 427.1451  
Measured 427.1458

**LRMS (EI) m/z:** 427 (17, [M<sup>+</sup>]), 268 (22, [M+H-Bnza]<sup>+</sup>), 91 (12), 84 (73), 66 (100)

**IR ν<sub>max</sub> (neat/cm<sup>-1</sup>):** 3049 (Ar C-H), 2922, 1676 (C=N-), 1631, 1614, 1599 (Ar C=C), 1549

**m.p.:** 220 - 221 °C

**(7-Chloro-1-pentyl-1H-quinolin-4-ylidene)-phenyl-amine (28)**

Bright yellow crystals

Chemical formula: C<sub>20</sub>H<sub>21</sub>ClN<sub>2</sub>Molecular Weight: 324.85 g.mol<sup>-1</sup>

Yield: 24%

To a solution of **7** (0.80 g, 3.14 mmol) in THF (20 ml), NaH (60% in mineral oil, 0.19 g, 4.71 mmol) was added slowly and the mixture was stirred at R.T. for 10 min. 1-Bromopentane (0.78 ml, 6.28 mmol) was then added and the resulting mixture was heated at 65 °C for 3 days. After cooling at R.T., water (75 ml) was slowly added to the mixture. The organic products were extracted with EtOAc (3 x 50 ml) and the organic extracts were dried over anh. MgSO<sub>4</sub>. Purification *via* column

chromatography (EtOAc → 1:10 MeOH:EtOAc), followed by recrystallization (Et<sub>2</sub>O) afforded pure **28** as bright yellow crystals (0.25 g, 24%).

**<sup>1</sup>H NMR (600 MHz, CDCl<sub>3</sub>)** δ ppm: 8.53 (1H, d, *J* = 8.7, CH-5), 7.33 (2H, t, *J* = 7.7, meta Ph-CH), 7.22 (1H, dd, *J* = 8.7, 1.9, CH-6), 7.17 (1H, d, *J* = 1.9, CH-8), 7.02 (1H, t, *J* = 7.7, para Ph-CH), 6.92 (2H, d, *J* = 7.7, ortho Ph-CH), 6.83 (1H, d, *J* = 8.0, CH-2), 5.88 (1H, d, *J* = 8.0, CH-3), 3.82 (2H, t, *J* = 7.3, NCH<sub>2</sub>), 1.77 (2H, qn, *J* = 7.3, NCH<sub>2</sub>CH<sub>2</sub>), 1.41-1.31 (4H, m, CH<sub>2</sub>CH<sub>2</sub>CH<sub>3</sub>) 0.92 (3H, t, *J* = 6.9, CH<sub>3</sub>)

**<sup>13</sup>C NMR (150 MHz, CDCl<sub>3</sub>)** δ ppm: 154.4 (C<sub>Q</sub>-4), 152.7 (Ph-C<sub>Q</sub>), 139.9 (C<sub>Q</sub>-8'), 139.6 (CH-2), 137.1 (C<sub>Q</sub>-7), 129.4 (meta Ph-CH), 128.1 (CH-5), 124.0 (C<sub>Q</sub>-4'), 123.7 (CH-6), 122.3 (para Ph-CH), 121.5 (ortho Ph-CH), 114.3 (CH-8), 101.1 (CH-3), 52.5 (NCH<sub>2</sub>), 29.0 (CH<sub>2</sub>CH<sub>2</sub>CH<sub>3</sub>), 28.3 (NCH<sub>2</sub>CH<sub>2</sub>), 22.4 (CH<sub>2</sub>CH<sub>3</sub>), 14.1 (CH<sub>3</sub>)

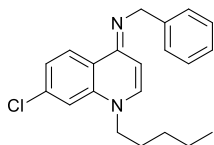
**HRMS (EI) m/z:** Calcd. [M]<sup>+</sup> 324.1388  
Measured 324.1395

**LRMS (EI) m/z:** 326 (30), 325 (35), 324 (100, [M]<sup>+</sup>), 323 (53), 255 (13), 253 (36, [M-CH<sub>2</sub>(CH<sub>2</sub>)<sub>3</sub>CH<sub>3</sub>]<sup>+</sup>), 218 (12 M-CH<sub>2</sub>(CH<sub>2</sub>)<sub>3</sub>CH<sub>3</sub>-Cl]<sup>+</sup>)

**IR ν<sub>max</sub> (neat/cm<sup>-1</sup>):** 3072 (Ar C-H), 3022, 2955, 2870 (Alkyl C-H), 2846, 1624 (C=N-), 1602, 1584 (Ar C=C), 1555

**m.p:** 90 - 91 °C

### (E)-N-(7-chloro-1-pentylquinolin-4(1H)-ylidene)-1-phenylmethanamine (**29**)



Dark yellow/orange solid

Chemical formula: C<sub>21</sub>H<sub>23</sub>ClN<sub>2</sub>

Molecular Weight: 338.87 g.mol<sup>-1</sup>

Yield: 92%

To a solution of **8** (0.14 g, 0.52 mmol), in acetone (2 mL), NaI (0.17 g, 1.13 mmol) and 1-bromopentane (0.13 ml, 1.01 mmol) were added and the resulting mixture was heated to reflux at 65 °C for 32 h. The resulting mixture was allowed to cool at R.T and the organic products were extracted with EtOAc, dried over anh. Na<sub>2</sub>SO<sub>4</sub> and evaporated. Purification *via* column chromatography (EtOAc → 1:20 NEt<sub>3</sub>:EtOAc) afforded pure **29** as a dark yellow/orange solid (0.16 g, 92%).

**<sup>1</sup>H NMR (CDCl<sub>3</sub>, 600 MHz)** δ ppm: 8.60 (1H, d, *J* = 8.7, CH-5), 7.44 (2H, d, *J* = 7.6, ortho Ph-CH), 7.32 (2H, t, *J* = 7.6, meta-Ph-CH), 7.22 (1H, t, *J* = 7.6, para Ph-CH), 7.16 (1H, dd, *J* = 8.7, 1.9, CH-6), 7.13 (1H, d, *J* = 1.9, CH-8), 6.92 (1H, d, *J* = 8.0, CH-2), 5.99 (1H, d, *J* = 8.0, CH-3), 4.59 (2H, s, CH<sub>2</sub>Ph), 3.82 (2H, t, *J* = 7.3, NCH<sub>2</sub>CH<sub>2</sub>), 1.77 (2H, qn, *J* = 7.3, NCH<sub>2</sub>CH<sub>2</sub>), 1.41-1.31 (4H, m, CH<sub>2</sub>CH<sub>2</sub>CH<sub>3</sub>), 0.92 (3H, t, *J* = 7.0, CH<sub>3</sub>)

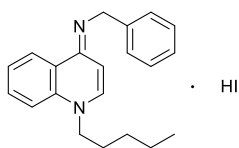
**<sup>13</sup>C NMR (150 MHz, CDCl<sub>3</sub>)** δ ppm: 155.1 (C<sub>Q</sub>-4), 141.8 (Ph-C<sub>Q</sub>), 139.3 (C<sub>Q</sub>-8'), 139.3 (CH-2), 136.5 (C<sub>Q</sub>-7), 128.4 (meta Ph-CH), 127.8 (CH-5), 127.7 (ortho Ph-CH), 126.4 (para Ph-CH), 124.3 (C<sub>Q</sub>-4'), 123.6 (CH-6), 114.2 (CH-8), 99.4 (CH-3), 53.3 (CH<sub>2</sub>Ph), 52.5 (NCH<sub>2</sub>), 29.0 (CH<sub>2</sub>CH<sub>2</sub>CH<sub>3</sub>), 28.3 (NCH<sub>2</sub>CH<sub>2</sub>), 22.5 (CH<sub>2</sub>CH<sub>3</sub>), 14.1 (CH<sub>3</sub>)

**HRMS (ES<sup>+</sup>) m/z:** Calcd. [M-H]<sup>+</sup> 339.1628  
Measured 339.1631

**LRMS (ES<sup>+</sup>) m/z:** 341 (35), 339 (100, [M-H]<sup>+</sup>)

**IR ν<sub>max</sub> (neat/cm<sup>-1</sup>):** 3060 (Ar C-H), 3028, 2947, 2922, 2861 (Alkyl C-H), 1629 (C=N-), 1596, 1561 (Ar C=C)

**m.p:** 93 - 94 °C

**(E)-N-(1-pentylquinolin-4(1H)-ylidene)-1-phenylmethanaminium iodide (30)**

Pale yellow crystals

Chemical formula: C<sub>21</sub>H<sub>24</sub>N<sub>2</sub> · HI

Molecular Weight: 432.34

Yield: 51%

To a solution of **10** (0.57 g, 2.43 mmol) in acetone (5 ml), 1-bromopentane (0.33 ml, 2.66 mmol) and NaI (0.44 g, 2.93 mmol) were added and the mixture was heated at 65 °C for 18 h. After cooling to room temperature, the mixture was poured into an ice (~100 cm<sup>3</sup>) and NaOH (2 M, 100 ml) mixture while stirring vigorously. The precipitate formed was washed with water and ether. Recrystallization (CH<sub>3</sub>CN) afforded **30** (0.53 g, 51%) as pale yellow crystals.

**<sup>1</sup>H NMR (600 MHz, DMSO)** δ ppm: 9.95 (1H, s, br, NH<sup>+</sup>), 8.65 (1H, dd, *J* = 8.5, 1.5, CH-5), 8.58 (1H, d, *J* = 7.5, CH-2), 8.15 (1H, d, *J* = 8.8, CH-8), 8.03 (1H, ddd, *J* = 8.8, 7.0, 1.5, CH-7), 7.79 (1H, dd, *J* = 8.5, 7.0, CH-6), 7.43 (2H, d, *J* = 7.6, ortho Ph-CH), 7.37 (2H, t, *J* = 7.6, meta Ph-CH), 7.29 (1H, t, *J* = 7.6, para Ph-CH), 6.83 (1H, d, *J* = 7.5, CH-3), 4.80 (2H, s, CH<sub>2</sub>Ph), 4.51 (2H, t, *J* = 7.4, NCH<sub>2</sub>CH<sub>2</sub>), 1.78 (2H, q, *J* = 7.4, NCH<sub>2</sub>CH<sub>2</sub>), 1.33-1.22 (4H, m, CH<sub>2</sub>CH<sub>2</sub>CH<sub>3</sub>), 0.84 (3H, t, *J* = 6.7, CH<sub>3</sub>)

**<sup>13</sup>C NMR (150 MHz, DMSO)** δ ppm: 155.3 (C<sub>Q</sub>-4), 146.6 (CH-2), 137.5 (C<sub>Q</sub>-8'), 137.0 (Ph-C<sub>Q</sub>), 133.9 (CH-7), 128.7 (meta Ph-CH), 127.5 (para Ph-CH), 127.3 (ortho Ph-CH), 126.7 (CH-6), 124.0 (CH-5), 118.5 (CH-8), 118.2 (C<sub>Q</sub>-4'), 98.8 (CH-3), 53.8 (NCH<sub>2</sub>CH<sub>2</sub>), 46.4 (CH<sub>2</sub>Ph), 28.5 (NCH<sub>2</sub>CH<sub>2</sub>), 28.0 (CH<sub>2</sub>CH<sub>2</sub>CH<sub>3</sub>), 21.8 (CH<sub>2</sub>CH<sub>3</sub>), 13.9 (CH<sub>3</sub>)

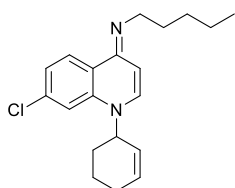
**HRMS (CI) m/z:** Calcd. [M+H<sup>+</sup>] 305.2012

Measured 305.2007

**LRMS (CI) m/z:** 305 (100, [M+H]<sup>+</sup>)

**IR ν<sub>max</sub> (neat/cm<sup>-1</sup>):** 3381, 3234 (N-H), 3085 (Ar C-H), 2953, 2927, 2850 (Aliphatic C-H), 1613 (C=N), 1572 (Ar C=C), 1536

**m.p.:** 163 – 165 °C

**(7-Chloro-1-cyclohex-2-enyl-1H-quinolin-4-ylidene)-pentyl-amine (31)**

Viscous dark yellow/brown oil

Chemical formula: C<sub>20</sub>H<sub>25</sub>ClN<sub>2</sub>Molecular weight: 328.88 g.mol<sup>-1</sup>

Yield: 28%

To a suspension of **3** (0.50 g, 2.01 mmol) and NaI (0.35 g, 2.34 mmol) in anhydrous DMF (5 ml), 4-bromocyclohexene (2.50 ml, 2.01 mmol) was added and the resulting mixture was heated at 80 °C to reflux for 4 days. The resulting brown solution was allowed to cool at R.T. and was then poured into an ice/NaOH (2M) mixture. The organic products were extracted with DCM (3 x 15 ml). The organic extracts were dried over anh. Na<sub>2</sub>SO<sub>4</sub> and the solvents were evaporated *in vacuo*. The resulting viscous brown residue was purified by flash column chromatography (EtOAc → 1:20 NEt<sub>3</sub>: EtOAc) to afford pure **31** as a dark yellow/brown oil (0.18 g, 28%).

**<sup>1</sup>H NMR (600 MHz, CDCl<sub>3</sub>)** δ ppm: 9.35 (1H, d, *J* = 9.0, CH-5), 8.01 (1H, d, *J* = 7.8, CH-2), 7.66 (1H, d, *J* = 1.9, CH-8), 7.55 (1H, dd, *J* = 9.0, 1.9, CH-6), 6.49 (1H, dtd, *J* = 10.0, 3.9, 1.8, CHCH=CH), 6.37 (1H, d, *J* = 7.8, CH-3), 5.74 (1H, dtd, *J* = 10.0, 3.8, 2.2, =CHCH<sub>2</sub>), 5.24 (1H, br, s, NCH), 3.56 (2H, td, *J* = 7.8, 3.6, NCH<sub>2</sub>), 2.28-2.24 (1H, m, =CHCH<sub>2</sub>), 2.23-2.17 (2H, m,



=CHCH<sub>2</sub>, NCHCH<sub>2</sub>), 1.91-1.85 (1H, m, NCHCH<sub>2</sub>), 1.84-1.78 (1H, m, =CHCH<sub>2</sub>CH<sub>2</sub>), 1.75 (2H, qn, *J* = 7.4, NCH<sub>2</sub>CH<sub>2</sub>), 1.64-1.56 (1H, m, =CHCH<sub>2</sub>CH<sub>2</sub>), 1.41-1.31 (4H, m, CH<sub>2</sub>CH<sub>2</sub>CH<sub>3</sub>), 0.88 (3H, t, *J* = 7.1, CH<sub>3</sub>)

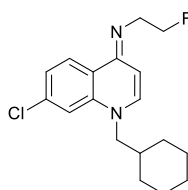
<sup>13</sup>C NMR (150 MHz, CDCl<sub>3</sub>) δ ppm: 155.8 (C<sub>Q</sub>-4), 141.1 (CH-2), 140.3 (C<sub>Q</sub>-8'), 138.5 (C<sub>Q</sub>-7), 137.5 (CHCH=CH), 130.3 (CH-5), 127.3 (CH-6), 123.1 (=CHCH<sub>2</sub>), 118.6 (C<sub>Q</sub>-4'), 115.2 (CH-8), 97.9 (CH-3), 55.8 (NCH), 44.6 (NCH<sub>2</sub>), 29.2 (CH<sub>2</sub>CH<sub>2</sub>CH<sub>3</sub> or CH<sub>2</sub>CH<sub>3</sub>), 29.0 (NCHCH<sub>2</sub>), 27.9 (NCH<sub>2</sub>CH<sub>2</sub>), 24.8 (=CHCH<sub>2</sub>), 22.6 (CH<sub>2</sub>CH<sub>2</sub>CH<sub>3</sub> or CH<sub>2</sub>CH<sub>3</sub>), 18.7 (=CHCH<sub>2</sub>CH<sub>2</sub>), 14.2 (CH<sub>3</sub>)

HRMS (ES+) *m/z*: Calcd. [M-H]<sup>+</sup> 329.1776  
Measured 329.1785

LRMS (ES+) *m/z*: 331 (14), 329 (42, [M-H]<sup>+</sup>), 251 (35), 249 (100)

IR ν<sub>max</sub> (neat/cm<sup>-1</sup>): 3024 (C=C-H), 2925 (Alkyl C-H), 2855, 1721 (C=N-), 1598 (Ar C=C), 1569

**(E)-N-(7-chloro-1-(cyclohexylmethyl)quinolin-4(1H)-ylidene)-2-fluoroethanamine (32)**



Beige solid

Chemical formula: C<sub>18</sub>H<sub>22</sub>ClFN<sub>2</sub>

Molecular Weight: 320.83 g.mol<sup>-1</sup>

Yield: 27%

To a solution of **13** (0.10 g, 0.44 mmol), and NaI (0.22 g, 1.47 mmol) in DMF (2 ml), bromomethylcyclohexane (0.19 ml, 1.32 mmol) was added and the mixture was heated to reflux at 120 °C for 4 days under Ar atmosphere. After cooling at R.T. the solution was transferred to a mixture of ice/water (~20 cm<sup>3</sup>) and NaOH (2M, 5 ml). The organic product was extracted with DCM (3 x 15 ml) and the organic extracts were dried over anh. Na<sub>2</sub>SO<sub>4</sub> and concentrated *in vacuo*. Purification *via* flash column chromatography (EtOAc → 1:20 NEt<sub>3</sub>:EtOAc) afforded pure **32** (0.04 g, 27%) as a beige powder.

<sup>1</sup>H NMR (600 MHz, CDCl<sub>3</sub>) δ ppm: 8.45 (1H, d, *J* = 8.7, CH-5), 7.15 (1H, dd, *J* = 8.7, 1.8, CH-6), 7.08 (1H, d, *J* = 1.8, CH-8), 6.87 (1H, d, *J* = 8.0, CH-2), 5.90 (1H, d, *J* = 8.0, CH-3), 4.78 (2H, dt, <sup>2</sup>J<sub>HF</sub> = 47.6, <sup>3</sup>J<sub>HH</sub> = 5.8, CH<sub>2</sub>F), 3.62 (2H, d, *J* = 7.4 Hz, NCH<sub>2</sub>CH), 3.57 (2H, dt, <sup>3</sup>J<sub>HF</sub> = 25.1, <sup>3</sup>J<sub>HH</sub> = 5.8, CH<sub>2</sub>CH<sub>2</sub>F), 1.81 (1H, ttq, *J* = 11.5, 7.4, 3.7, CH(CH<sub>2</sub>)<sub>2</sub>), 1.77-1.66 (5H, m, cyclohexyl CH<sub>2</sub>), 1.29-1.11 (3H, m, cyclohexyl CH<sub>2</sub>), 1.03-0.93 (2H, m, cyclohexyl CH<sub>2</sub>)

<sup>13</sup>C NMR (150 MHz, CDCl<sub>3</sub>) δ ppm: 155.7 (C<sub>Q</sub>-4), 139.9 (CH-2), 139.5 (C<sub>Q</sub>-8'), 136.4 (C<sub>Q</sub>-7), 127.5 (CH-5), 124.2 (C<sub>Q</sub>-4'), 123.5 (CH-6), 114.4 (CH-8), 98.6 (CH-3), 85.1 (d, <sup>1</sup>J<sub>CF</sub> = 168.1, CH<sub>2</sub>F), 58.8 (NCH<sub>2</sub>CH), 50.1 (d, <sup>2</sup>J<sub>CF</sub> = 22.5, CH<sub>2</sub>CH<sub>2</sub>F), 36.6 (CH(CH<sub>2</sub>)<sub>2</sub>), 30.9 (cyclohexyl CH<sub>2</sub>), 26.3 (cyclohexyl CH<sub>2</sub>), 25.6 (cyclohexyl CH<sub>2</sub>)

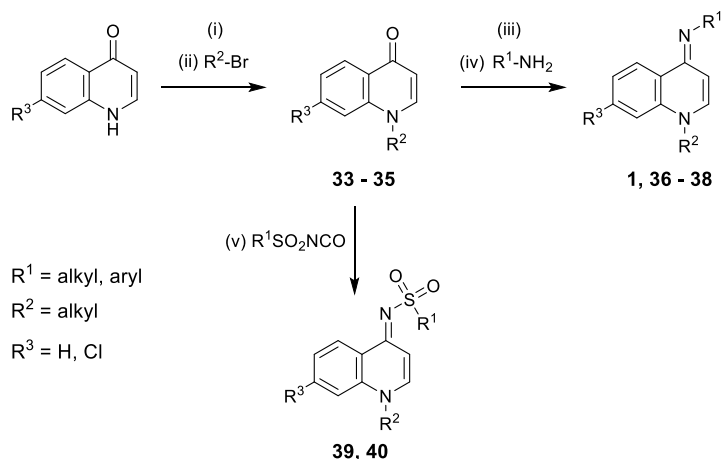
<sup>19</sup>F NMR (282 MHz, CDCl<sub>3</sub>) δ ppm: -220.43

HRMS (ES+) *m/z*: Calcd. [M-H]<sup>+</sup> 321.1534  
Measured 321.1520

LRMS (ES+) *m/z*: 323 (30), 321 (100, [M-H]<sup>+</sup>), 225 (23)

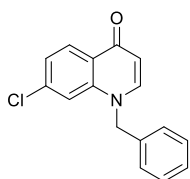
IR ν<sub>max</sub> (neat/cm<sup>-1</sup>): 2945 (Aryl C-H), 2841 (Alkyl C-H), 1634 (C=N-), 1601, 1572 (Ar C=C)

*m.p.*: 147-148 °C

**Route B:**

**Scheme 31.** Synthesis of iminodihydroquinolines starting from 4-quinolones.

Reagents and Conditions: (i) NaH, 0 °C, 15 min (ii) DMF, 80-110 °C, 18-24 h (iii) POCl<sub>3</sub>, 110 °C, 3 h (iv) R<sup>2</sup>-NH<sub>2</sub>, MeOH, rt, 5-18h (v) CH<sub>3</sub>CN, 70 °C, 24 h

**N-substituted 4-quinolines 33 - 35:****1-benzyl-7-chloroquinolin-4(1H)-one (33)**

White crystalline solid

Chemical formula: C<sub>16</sub>H<sub>12</sub>ClNO

Molecular Weight: 269.73 g.mol<sup>-1</sup>

Yield: 57%

To a solution of **EYF119** (0.75 g, 4.18 mmol) and NaH (60% in mineral oil, 0.33 g, 8.35 mmol) in DMF (8 ml), benzyl bromide (1.5 ml, 12.6 mmol) was added under Ar atmosphere and the resulting solution was heated at 90 °C for 18 h. After cooling at R.T, the solvent was evaporated *in vacuo* and water (100 ml) was added to the remaining residue. The organic products were extracted with DCM (3 x 75 ml) and the combined organic extracts were dried over anh. MgSO<sub>4</sub> and concentrated *in vacuo*. Purification by flash column chromatography (EtOAc) afforded pure **33** (0.64 g, 57%) as white crystals.

<sup>1</sup>H NMR (600 MHz, CDCl<sub>3</sub>) δ ppm: 8.39 (1H, d, *J* = 8.5, CH-5), 7.61 (1H, d, *J* = 7.8, CH-2), 7.40-7.32 (3H, m, meta Ph-CH, para Ph-CH), 7.31-7.28 (2H, m, CH-6, CH-8), 7.15 (2H, d, *J* = 7.7, ortho Ph-CH), 6.33 (1H, d, *J* = 7.8, CH-3), 5.26 (2H, s, CH<sub>2</sub>).

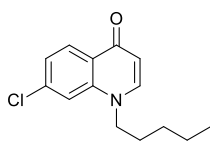
<sup>13</sup>C NMR (150 MHz, CDCl<sub>3</sub>) δ ppm: 177.8 (C<sub>Q</sub>-4), 143.8 (CH-2), 140.9 (C<sub>Q</sub>-8'), 138.8 (CH-7), 134.6 (Ph-C<sub>Q</sub>), 129.5 (meta Ph-CH), 128.9 (para Ph-CH or CH-5), 128.7 (para Ph-CH or CH-5), 126.2 (ortho Ph-CH), 125.8 (C<sub>Q</sub>-4'), 124.6 (CH-6), 115.9 (CH-8), 111.1 (CH-3), 56.6 (CH<sub>2</sub>Ph)

HRMS (EI) *m/z*: Calcd. [M]<sup>+</sup> 269.0607  
Measured 269.0602

LRMS (EI) *m/z*: 271 (12), 269 (35, [M]<sup>+</sup>), 91 (100, PhCH<sub>2</sub><sup>+</sup>)

IR *v*<sub>max</sub> (neat/cm<sup>-1</sup>): 3064 (Ar C-H), 3038, 1616 (C=N-), 1598, 1578 (Ar C=C), 1537

*m.p.*: 197-198 °C

**7-chloro-1-pentylquinolin-4(1H)-one (34)**

White solid

Chemical formula: C<sub>14</sub>H<sub>16</sub>ClNOMolecular weight: 249.74 g.mol<sup>-1</sup>

Yield: 31%

To a suspension of **EYF119** (0.57 g, 4.76 mmol) in DMF (5 ml), NaH (60% in mineral oil, 0.28 g, 7.10 mmol) was added, followed by 1-bromopentane (1.19 ml, 9.60 mmol) and the resulting mixture was heated at 80 °C for 24 h. After cooling at ambient temperature, water (20 ml) was added slowly and the organic products were extracted with DCM (3 x 50 ml). The organic extracts were dried over anh. MgSO<sub>4</sub> and evaporated *in vacuo*. Purification *via* column chromatography (2:3 petroleum ether:EtOAc) afforded **34** as white solid (0.37 g, 31%).

<sup>1</sup>H NMR (CDCl<sub>3</sub>, 600 MHz) δ ppm: 8.39 (1H, d, *J* = 8.7, CH-5), 7.49 (1H, d, *J* = 7.8, CH-2), 7.39 (1H, d, *J* = 1.8, CH-8), 7.31 (1H, dd, *J* = 8.7, 1.8, CH-6), 6.25 (1H, d, *J* = 7.8, CH-3), 4.04 (2H, t, *J* = 7.4, NCH<sub>2</sub>), 1.84 (2H, q, *J* = 7.4, NCH<sub>2</sub>CH<sub>2</sub>), 1.42-1.31 (4H, m, CH<sub>2</sub>CH<sub>2</sub>CH<sub>3</sub>), 0.92 (3H, t, *J* = 6.9, CH<sub>3</sub>)

<sup>13</sup>C NMR (CDCl<sub>3</sub>, 150 MHz) δ ppm: 177.6 (C<sub>Q</sub>-4), 143.5 (CH-2), 140.5 (C<sub>Q</sub>-8'), 138.6 (C<sub>Q</sub>-7), 129.1 (CH-5), 125.9 (C<sub>Q</sub>-4'), 124.3 (CH-6), 115.2 (CH-8), 110.7 (CH-3), 53.5 (NCH<sub>2</sub>), 28.9 (NCH<sub>2</sub>CH<sub>2</sub> or CH<sub>2</sub>CH<sub>2</sub>CH<sub>3</sub>), 28.6 (NCH<sub>2</sub>CH<sub>2</sub> or CH<sub>2</sub>CH<sub>2</sub>CH<sub>3</sub>), 22.4 (CH<sub>2</sub>CH<sub>3</sub>), 14.1 (CH<sub>3</sub>)

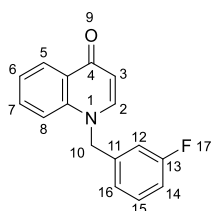
HRMS (ES<sup>+</sup>) *m/z*: Calcd. [M+H]<sup>+</sup> 250.0999

Measured 250.0990

LRMS (ES<sup>+</sup>) *m/z*: 252 (20), 250 (83, [M+H]<sup>+</sup>), 182 (20), 180 (100)

IR ν<sub>max</sub> (neat/cm<sup>-1</sup>): 3459 (weak, O-H), 3029 (Ar C-H), 2997, 2969, 2958, 2930, 2866 (aliphatic C-H), 1740 (C=O), 1622 (C=C), 1583, 1542

*m.p.*: 82 - 83 °C

**1-(3-fluorobenzyl)quinolin-4(1H)-one (35)**

White powder

Chemical Formula: C<sub>16</sub>H<sub>12</sub>FNO

Molecular Weight: 253.28

Yield: 68%

To a solution of 4-quinolinone (1.00 g, 6.89 mmol) and NaH (60% in mineral oil, 0.33 g, 8.25 mmol) in DMF (8 ml), 3-fluorobenzyl bromide (0.85 ml, 6.93 mmol) was added under an atmosphere of argon and the resulting solution was heated at 110 °C for 18 h. After cooling to ambient temperature, the mixture was concentrated *in vacuo* and water (100 ml) was added to the remaining residue. The organic products were extracted with DCM (3 x 100 ml) and the combined organic extracts were washed with sat. LiCl (50 ml) and water (2 x 100 ml), were dried over anh. MgSO<sub>4</sub> and were concentrated *in vacuo*. Trituration of the remaining precipitate with ether, afforded **35** (0.12 g, 68%) as white powder.

<sup>1</sup>H NMR (600 MHz, CDCl<sub>3</sub>) δ ppm: 8.46 (1H, dd, *J* = 8.2, 1.3, CH-5), 7.62 (1H, d, *J* = 7.7, CH-2), 7.54 (1H, ddd, *J* = 8.4, 7.0, 1.3, CH-7), 7.35 (1H, ddd, *J* = 7.0, 8.2, 1.3, CH-6), 7.31 (1H, td, <sup>3</sup>*J*<sub>HH</sub> = 8.2, <sup>4</sup>*J*<sub>HF</sub> = 5.9, CH-15), 7.24 (1H, dd, *J* = 8.4, 1.3, CH-8), 7.00 (1H, td, <sup>3</sup>*J*<sub>HH</sub> = 8.2, <sup>3</sup>*J*<sub>HF</sub> = 8.2, <sup>4</sup>*J*<sub>HH</sub> = 2.6, CH-14), 6.91 (1H, dd, *J* = 8.2, 1.7, CH-16), 6.84 (1H, ddd, <sup>3</sup>*J*<sub>HF</sub> = 9.4, <sup>4</sup>*J*<sub>HH</sub> = 2.6, 1.7, CH-12), 6.34 (1H, d, *J* = 7.7, CH-3), 5.30 (2H, s, CH<sub>2</sub>)

**<sup>13</sup>C NMR (150 MHz, CDCl<sub>3</sub>)** δ ppm: 178.4 (C<sub>Q</sub>-4), 163.4 (d, <sup>1</sup>J<sub>CF</sub>= 248.9, C<sub>Q</sub>-13), 143.7 (CH-2), 140.1 (C<sub>Q</sub>-8'), 137.9 (d, <sup>3</sup>J<sub>CF</sub>= 6.9, C<sub>Q</sub>-11), 132.5 (CH-7), 131.1 (d, <sup>3</sup>J<sub>CF</sub>= 8.3, CH-15), 127.5 (C<sub>Q</sub>-4'), 127.3 (CH-5), 124.0 (CH-6), 121.7 (d, <sup>4</sup>J<sub>CF</sub>= 3.0, CH-16), 116.0 (CH-8), 115.5 (d, <sup>2</sup>J<sub>CF</sub>= 21.2, CH-14), 113.3 (d, <sup>2</sup>J<sub>CF</sub>= 22.2, CH-12), 110.8 (CH-3), 56.1 (d, <sup>4</sup>J<sub>CF</sub>= 2.1, CH<sub>2</sub>)

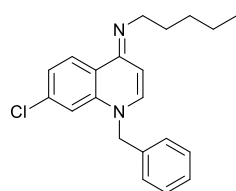
**HRMS (EI) m/z:** Calcd. [M]<sup>+</sup> 253.0903  
Measured 253.0904

**LRMS (EI) m/z:** 254 (8), 253 (43, [M<sup>+</sup>]), 110 (7), 109 (100, [M-CH<sub>2</sub>Ph-F]<sup>+</sup>), 86 (17), 84 (30), 83 (9)

**IR ν<sub>max</sub> (neat/cm<sup>-1</sup>):** 3079 (Ar C-H), 2960, 1622 (C=O), 1614, 1587 (Ar C=C), 1551

#### 4-iminodidhydroquinolines **1**, **36** - **40**:

##### (E)-N-(1-benzyl-7-chloroquinolin-4(1H)-ylidene)pentan-1-amine (**1**)



Pale yellow crystalline solid  
Chemical formula: C<sub>21</sub>H<sub>23</sub>ClN<sub>2</sub>  
Molecular Weight: 338.87 g.mol<sup>-1</sup>  
Yield: 51%

A solution of **33** (0.25 g, 0.93 mmol) in POCl<sub>3</sub> (4 ml), was heated to reflux for 1.5 h. After cooling at R.T., the mixture was evaporated *in vacuo*, and the resulting residue was triturated with ether. The resulting precipitate was dissolved in MeOH (2 ml), amylamine (0.57 ml, 4.90 mmol) was added dropwise and the solution was stirred R.T. for 3 h. The solution was poured into an ice (~30 cm<sup>3</sup>) and NaOH (2 M, 20 ml) mixture while stirring vigorously. The precipitate formed was filtered, was washed with water (2 x 20 ml) and pentane (2 x 20 ml) and dried *in vacuo*. Recrystallisation (CHCl<sub>3</sub>) afforded pure **1** (0.16 g, 51%) as pale yellow crystals.

**<sup>1</sup>H NMR (600 MHz, CDCl<sub>3</sub>)** δ ppm: 8.41 (1H, d, *J*= 8.5, CH-5), 7.35 (2H, t, *J*= 7.5, meta Ph-CH), 7.27-7.30 (1H, t, *J*= 7.5, para Ph-CH), 7.18 (2H, d, *J*= 7.5, ortho Ph-CH), 7.09 (1H, dd, *J*= 8.5, 2.1, CH-6), 6.99-6.94 (2H, m, CH-2, CH-8), 6.02 (1H, d, *J*= 8.2, CH-3), 5.02 (2H, s, CH<sub>2</sub>Ph), 3.32 (2H, t, *J*= 7.4, NCH<sub>2</sub>CH<sub>2</sub>), 1.74 (2H, qn, *J*= 7.4, NCH<sub>2</sub>CH<sub>2</sub>), 1.47-1.36 (4H, m, CH<sub>2</sub>CH<sub>2</sub>CH<sub>3</sub>), 0.93 (3H, t, *J*= 7.0, CH<sub>3</sub>)

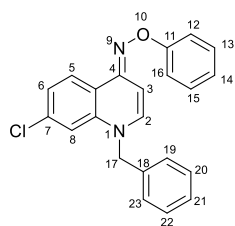
**<sup>13</sup>C NMR (150 MHz, CDCl<sub>3</sub>)** δ ppm: 153.7 (C<sub>Q</sub>-4), 139.7 (CH-2), 139.1 (C<sub>Q</sub>-8'), 136.2 (CH-7), 135.7 (Ph-C<sub>Q</sub>), 129.3 (meta Ph-CH), 128.2 (para Ph-CH) 127.2 (CH-5), 126.2 (ortho Ph-CH), 124.5 (C<sub>Q</sub>-4'), 123.6 (CH-6), 114.8 (CH-8), 99.7 (CH-3), 55.5 (CH<sub>2</sub>Ph), 50.3 (NCH<sub>2</sub>CH<sub>2</sub>), 31.0 (NCH<sub>2</sub>CH<sub>2</sub>), 30.2 (CH<sub>2</sub>CH<sub>2</sub>CH<sub>3</sub>), 22.9 (CH<sub>2</sub>CH<sub>3</sub>), 14.3 (CH<sub>3</sub>)

**HRMS (ES+) m/z:** Calcd. [M+H]<sup>+</sup> 339.1628  
Measured 339.1633

**LRMS (ES+) m/z:** 341 (50), 340 (33), 339 (100, [MH]<sup>+</sup>)

**IR ν<sub>max</sub> (neat/cm<sup>-1</sup>):** 3032 (Ar C-H), 2951, 2917 (Alkyl C-H), 2840, 1632 (C=N-), 1595, 1566 (Ar C=C)

**m.p.:** 93 – 94 °C

**(E)-1-benzyl-7-chloroquinolin-4(1H)-one O-phenyl oxime (36)**

Pale brown crystals

Chemical formula: C<sub>22</sub>H<sub>17</sub>ClN<sub>2</sub>OMolecular weight: 360.84 g.mol<sup>-1</sup>

Yield: 74%

A solution of **33** (0.48 g, 1.78 mmol) in POCl<sub>3</sub> (5 ml), was heated at 100 °C for 2 h. The solution was cooled to ambient temperature, DCM (5 ml) was added and the mixture was evaporated *in vacuo*. DCM (5 ml) was added and the mixture was evaporated again. The remaining residue was dissolved in MeOH (2 ml), and a freshly prepared solution *o*-phenylhydroxylamine in DCM (\*), was added dropwise. The mixture was heated at 60 °C for 2 h and at ambient temperature for 18 h, and was then poured onto an ice (~ 100 cm<sup>3</sup>) and NaOH (100 ml, 2 M) mixture while stirring vigorously. The organic products were extracted with EtOAc (2 x 100 ml), and the organic extracts were dried over anh. MgSO<sub>4</sub> and evaporated *in vacuo*. Purification *via* flash column chromatography (EtOAc), followed by recrystallization (Et<sub>2</sub>O) afforded **36** as pale brown crystals (0.48 g, 74%).

<sup>1</sup>H NMR (CDCl<sub>3</sub>, 600 MHz) δ ppm: 8.30 (1H, d, *J* = 8.7, CH-5), 7.37 (2H, t, *J* = 7.5, CH-20, CH-22), 7.34-7.30 (5H, m, CH-12, CH-13, CH-15, CH-16, CH-21), 7.19 (2H, d, *J* = 7.5, CH-19, CH-23), 7.12 (1H, dd, *J* = 8.7, 2.0, CH-6), 7.00 (1H, d, *J* = 2.0, H-8), 6.99-6.97 (1H, m, CH-14), 6.93 (1H, d, *J* = 8.0, CH-2), 6.57 (1H, d, *J* = 8.0, CH-3), 5.02 (2H, s, CH<sub>2</sub>-17)

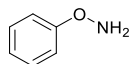
<sup>13</sup>C NMR (CDCl<sub>3</sub>, 150 MHz) δ ppm: 160.3 (C<sub>Q</sub>-11), 149.4 (C<sub>Q</sub>-4), 139.1 (C<sub>Q</sub>-8'), 139.0 (CH-2), 136.4 (C<sub>Q</sub>-7), 135.4 (C<sub>Q</sub>-18), 129.4 (CH-13, CH-15 or CH-20, CH-22), 129.3 (CH-13, CH-15 or CH-20, CH-22), 128.3 (CH-21), 126.2 (CH-19, CH-23), 126.0 (CH-5), 123.8 (CH-6), 121.2 (CH-14), 118.7 (C<sub>Q</sub>-4'), 115.0 (CH-8), 114.5 (CH-12, CH-16), 96.8 (CH-3), 55.6 (CH<sub>2</sub>-17)

HRMS (EI) *m/z*:      Calcd. [M]<sup>+</sup>            360.1024  
                                  Measured                360.1026

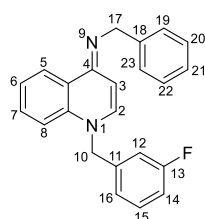
LRMS (EI) *m/z*: 362 (32), 360 (100, [M]<sup>+</sup>), 270 (14), 269 (49, [M-CH<sub>2</sub>Ph]<sup>+</sup>), 267 (64, [M-OPh]<sup>+</sup>), 241 (11), 141 (28), 86 (45), 84 (71)

IR ν<sub>max</sub> (neat/cm<sup>-1</sup>): 3067 (Ar C-H), 3030, 1634 (C=N), 1593 (aromatic C=C), 1584, 1557, 1542

*m.p.*: 93 - 94 °C

***o*-phenylhydroxylamine (\*)**

To a solution of *o*-phenylhydroxylamine hydrochloride (0.52 g, 3.57 mmol) in DCM (2 ml) and H<sub>2</sub>O (1 ml), Na<sub>2</sub>CO<sub>3</sub> (1.96 ml, 2 M) was added and the mixture was stirred at ambient temperature for 30 min. DCM (10 ml) was added and the organic layer was separated, dried over anh. MgSO<sub>4</sub> and concentrated to a volume of 3-4 ml.

**Benzyl-[1-(3-fluoro-benzyl)-1H-quinolin-4-ylidene]-amine (37)**

Off white crystalline solid

Chemical formula: C<sub>23</sub>H<sub>19</sub>FN<sub>2</sub>Molecular weight: 342.42 g.mol<sup>-1</sup>

Yield: 57%

A solution of **35** (0.25 g, 1.00 mmol) in POCl<sub>3</sub> (3 ml), was heated to reflux for 2 h. After cooling to ambient temperature, DCM (2 x 20 ml) was added the mixture was evaporated *in vacuo*. The remaining residue was triturated with ether. The resulting precipitate was dissolved in MeOH (1 ml), benzylamine (1.00 ml, 9.21 mmol) was added dropwise and the solution was stirred at room temperature for 18 h. The solution was poured into an ice (~50 cm<sup>3</sup>) and NaOH (2 M, 50 ml) mixture while stirring vigorously. The precipitate formed was filtered, was washed with water and petrol and was dried *in vacuo*. Recrystallisation (Et<sub>2</sub>O) afforded **37** (0.20 g, 57%) as off white crystals.

<sup>1</sup>H NMR (600 MHz, CDCl<sub>3</sub>) δ ppm: 8.64 (1H, dd, *J* = 8.1, 1.7, CH-5), 7.50 (2H, d, *J* = 7.9, CH-19, CH-23), 7.37-7.32 (3H, m, CH-7, CH-20, CH-22), 7.30 (1H, td, <sup>3</sup>*J*<sub>HH</sub> = 8.0, <sup>4</sup>*J*<sub>HF</sub> = 5.8, CH-15), 7.25-7.18 (2H, m, CH-6, CH-21), 7.03 (1H, d, *J* = 8.1, CH-2), 7.00-6.94 (3H, m, CH-8, CH-14, CH-16), 6.88 (1H, ddd, <sup>3</sup>*J*<sub>HF</sub> = 9.5, <sup>4</sup>*J*<sub>HH</sub> = 2.5, 1.7, CH-12), 6.10 (1H, d, *J* = 8.1, CH-3), 5.07 (2H, s, CH<sub>2</sub>-10), 4.65 (2H, s, CH<sub>2</sub>-17)

<sup>13</sup>C NMR (150 MHz, CDCl<sub>3</sub>) δ ppm: 163.3 (d, <sup>1</sup>*J*<sub>CF</sub> = 247.6, C<sub>Q</sub>-13), 155.5 (C<sub>Q</sub>-4), 142.1 (CH-2), 139.3 (C<sub>Q</sub>-8'), 139.0 (d, <sup>3</sup>*J*<sub>CF</sub> = 6.8, C<sub>Q</sub>-11), 138.5 (CH-21), 130.8 (d, <sup>3</sup>*J*<sub>CF</sub> = 8.3, CH-15), 130.3 (C<sub>Q</sub>-18), 128.3 (CH-20, CH-22), 127.8 (CH-19, CH-23), 126.3 (CH-7), 126.1 (C<sub>Q</sub>-4'), 125.9 (CH-5), 123.5 (CH-6), 121.7 (d, <sup>4</sup>*J*<sub>CF</sub> = 2.9, CH-16), 115.1 (d, <sup>2</sup>*J*<sub>CF</sub> = 21.1, CH-14), 115.0 (CH-8), 113.2 (d, <sup>2</sup>*J*<sub>CF</sub> = 22.3, CH-12), 99.5 (CH-3), 55.2 (CH<sub>2</sub>-10), 53.6 (CH<sub>2</sub>-17)

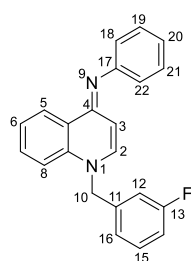
<sup>19</sup>F NMR (282 MHz, CDCl<sub>3</sub>) δ ppm: -111.67

HRMS (ES+) *m/z*: Calcd. [M+H]<sup>+</sup> 343.1611  
Measured 343.1838

LRMS (ES+) *m/z*: 344 (33), 343 (100, [M+H]<sup>+</sup>), 304 (12), 302 (12), 210 (7), 196 (5)

IR ν<sub>max</sub> (neat/cm<sup>-1</sup>): 3056 (Ar C-H), 3022, 2848 (Aliphatic C-H), 1629 (C=N), 1589 (Ar C=C), 1571

*m.p.*: 118 - 119 °C

**[1-(3-Fluoro-benzyl)-1H-quinolin-4-ylidene]-phenyl-amine (38)**

Bright yellow crystalline solid

Chemical formula: C<sub>22</sub>H<sub>17</sub>FN<sub>2</sub>Molecular weight: 328.39 g.mol<sup>-1</sup>

Yield: 88%

A solution of **35** (0.70 g, 2.76 mmol) in POCl<sub>3</sub> (10 ml), was heated to reflux for 2 h. After cooling to ambient temperature, DCM (2 x 20 ml) was added the mixture was evaporated *in vacuo*. The remaining residue was triturated with ether. The resulting precipitate was dissolved in MeOH (2 ml), aniline (1.39 ml, 15.22 mmol) was added dropwise and the solution was stirred at room temperature for 4 h. The solution was

poured into an ice (~50 cm<sup>3</sup>) and NaOH (2 M, 50 ml) mixture while stirring vigorously. The organic products were extracted with EtOAc (2 x 100 ml), were dried over anhydrous MgSO<sub>4</sub> and evaporated *in vacuo*. Purification via column chromatography (EtOAc) followed by recrystallisation (CHCl<sub>3</sub>) afforded **38** (0.80 g, 88%) as bright yellow crystals.

**<sup>1</sup>H NMR (600 MHz, CDCl<sub>3</sub>)** δ ppm: 8.61 (1H, dd, *J* = 8.1, 1.7, CH-5), 7.41 (1H, ddd, *J* = 8.6, 7.2, 1.7, CH-7), 7.35 (2H, t, *J* = 7.8, CH-19, CH-21), 7.31 (1H, td, <sup>3</sup>*J*<sub>HH</sub> = 8.0, <sup>4</sup>*J*<sub>HF</sub> = 5.8, CH-15), 7.28-7.24 (1H, m, CH-6), 7.06-7.01 (2H, m, CH-14, CH-20), 7.00-6.95 (5H, m, CH-2, CH-8, CH-16, CH-18, CH-22), 6.88 (1H, ddd, <sup>3</sup>*J*<sub>HF</sub> = 9.5, <sup>4</sup>*J*<sub>HH</sub> = 2.5, 1.7, CH-12), 5.99 (1H, d, *J* = 8.0, CH-3), 5.09 (2H, s, CH<sub>2</sub>-10)

**<sup>13</sup>C NMR (150 MHz, CDCl<sub>3</sub>)** δ ppm: 163.3 (d, <sup>1</sup>*J*<sub>CF</sub> = 247.7, C<sub>Q</sub>-13), 154.8 (C<sub>Q</sub>-4), 152.9 (C<sub>Q</sub>-17), 139.8 (C<sub>Q</sub>-8'), 139.1 (CH-2), 138.8 (d, <sup>3</sup>*J*<sub>CF</sub> = 6.8, C<sub>Q</sub>-11), 131.1 (CH-7), 130.9 (d, <sup>3</sup>*J*<sub>CF</sub> = 8.3, CH-15), 129.3 (CH-19, CH-21), 126.4 (CH-5), 125.5 (C<sub>Q</sub>-4'), 123.8 (CH-6), 122.3 (CH-20), 121.7 (d, <sup>4</sup>*J*<sub>CF</sub> = 2.8, CH-16), 121.5 (CH-18, CH-22), 115.2 (CH-8), 115.1 (d, <sup>2</sup>*J*<sub>CF</sub> = 21.2, CH-14), 113.2 (d, <sup>2</sup>*J*<sub>CF</sub> = 22.4, CH-12), 101.3 (CH-3), 55.3 (CH<sub>2</sub>-10)

**<sup>19</sup>F NMR (282 MHz, CDCl<sub>3</sub>)** δ ppm: -111.26

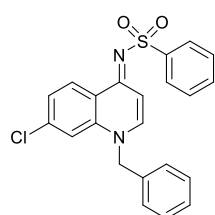
**HRMS (ES-) m/z:** Calcd. [M]<sup>+</sup> 327.1298  
Measured 327.1297

**LRMS (ES-) m/z:** 328 (48, [M<sup>+</sup>]), 327 (100), 319 (14), 261 (27)

**IR ν<sub>max</sub> (neat/cm<sup>-1</sup>):** 3064 (Ar C-H), 3012, 1629 (C=N), 1609, 1585 (Ar C=C), 1553

**m.p.:** 138 - 141 °C

### ***N*-(1-Benzyl-7-chloro-1*H*-quinolin-4-ylidene)-benzenesulfonamide (39)**



White crystals

Chemical formula: C<sub>22</sub>H<sub>17</sub>ClN<sub>2</sub>O<sub>2</sub>S

Molecular weight: 408.90 g.mol<sup>-1</sup>

Yield: 70%

To a suspension of **33** (0.50 g, 1.85 mmol) in CH<sub>3</sub>CN (10 ml), benzenesulfonyl isocyanate (0.49 ml, 3.66 mmol) was added and the resulting mixture was heated at 70 °C for 24 h. After cooling at ambient temperature, MeOH (5 ml) was added and the mixture was stirred for five min. The precipitate formed was filtered, was dried *in vacuo* and recrystallized (CHCl<sub>3</sub>, DCM) to afford **39** (0.53 g, 70%) as white crystalline solid.

**<sup>1</sup>H NMR (CDCl<sub>3</sub>, 600 MHz)** δ ppm: 8.60 (1H, d, *J* = 8.9, CH-5), 8.08 (2H, dd, *J* = 8.1, 1.6, ortho Ph-CH), 7.70 (1H, d, *J* = 7.7, CH-2), 7.55-7.44 (4H, m, meta Ph-CH, para Ph-CH, CH-3), 7.40-7.35 (4H, m, meta Bz-CH, para Bz-CH, CH-8), 7.33 (1H, dd, *J* = 8.9, 1.9, CH-6), 7.12 (2H, dd, *J* = 7.7, 1.7, ortho Bz-CH), 5.38 (2H, s, CH<sub>2</sub>)

**<sup>13</sup>C NMR (150 MHz, CDCl<sub>3</sub>)** δ ppm: 161.0 (C<sub>Q</sub>-4), 143.5 (Ph-C<sub>Q</sub>), 143.4 (CH-2), 139.6 (C<sub>Q</sub>-7 or C<sub>Q</sub>-8'), 139.5 (C<sub>Q</sub>-7 or C<sub>Q</sub>-8'), 133.6 (Bz-C<sub>Q</sub>), 131.7 (para Ph-CH), 129.7 (meta Bz-CH), 129.3 (CH-5), 129.1 (para Bz-CH), 128.7 (meta Ph-CH), 126.7 (ortho Ph-CH), 126.4 (ortho Bz-CH), 126.2 (CH-6), 123.6 (C<sub>Q</sub>-4'), 115.8 (CH-8), 106.3 (CH-3), 57.4 (CH<sub>2</sub>)

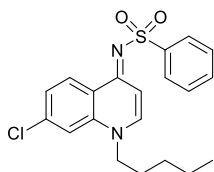
**HRMS (EI) m/z:** Calcd. [M]<sup>+</sup> 408.0694  
Measured 408.0699

**LRMS (EI) m/z:** 410 (23), 408 (57, [M<sup>+</sup>]), 346 (18), 344 (53), 343 (15), 91 (100, [CH<sub>2</sub>Ph]<sup>+</sup>)

**IR ν<sub>max</sub> (neat/cm<sup>-1</sup>):** 3076 (Ar C-H), 3026, 2970, 1741 (S=O), 1603 (C=C), 1537, 1528

m.p.: 231 - 232 °C

**(E)-N-(7-chloro-1-pentylquinolin-4(1H)-ylidene)benzenesulfonamide (40)**



White feathery solid

Chemical formula: C<sub>20</sub>H<sub>21</sub>ClN<sub>2</sub>O<sub>2</sub>S

Molecular weight: 388.91 g.mol<sup>-1</sup>

Yield: 85%

To a suspension of **34** (0.07 g, 0.28 mmol) in CH<sub>3</sub>CN (2 ml) benzenesulfonyl isocyanate (75.0 μl, 0.56 mmol) was added and the resulting mixture was heated at 70 °C for 24 h. After cooling to ambient temperature, MeOH (2 ml) was added and the mixture was evaporated *in vacuo*. The remaining residue was purified *via* column chromatography (2:3 petroleum ether:EtOAc) followed by recrystallization (CHCl<sub>3</sub>) to afford **40** (93 mg, 85%) as white feathery solid.

<sup>1</sup>H NMR (CDCl<sub>3</sub>, 600 MHz) δ ppm: 8.61 (1H, d, *J* = 8.9, CH-5), 8.07-8.04 (2H, m, ortho Ph-CH), 7.59 (1H, d, *J* = 7.6, CH-2), 7.51-7.45 (3H, m, meta Ph-CH, para Ph-CH), 7.44 (1H, d, *J* = 1.6, CH-8), 7.38 (1H, d, *J* = 7.6, CH-3), 7.37 (1H, dd, *J* = 8.9, 1.6, CH-6), 4.16 (2H, t, *J* = 7.6, NCH<sub>2</sub>), 1.84 (2H, q, *J* = 7.6, NCH<sub>2</sub>CH<sub>2</sub>), 1.41-1.30 (4H, m, CH<sub>2</sub>CH<sub>2</sub>CH<sub>3</sub>), 0.91 (3H, t, *J* = 7.0, CH<sub>3</sub>)

<sup>13</sup>C NMR (CDCl<sub>3</sub>, 150 MHz) δ ppm: 160.9 (C<sub>Q</sub>-4), 143.5 (Ph-C<sub>Q</sub>), 143.0 (CH-2), 139.6 (C<sub>Q</sub>-7 or C<sub>Q</sub>-8'), 139.0 (C<sub>Q</sub>-7 or C<sub>Q</sub>-8'), 131.6 (para Ph-CH), 129.5 (CH-5), 128.7 (meta Ph-CH), 126.7 (ortho Ph-CH), 126.0 (CH-6), 123.7 (C<sub>Q</sub>-4'), 115.1 (CH-8), 106.2 (CH-3), 54.3 (NCH<sub>2</sub>), 28.8 (NCH<sub>2</sub>CH<sub>2</sub>, CH<sub>2</sub>CH<sub>2</sub>CH<sub>3</sub>), 22.3 (CH<sub>2</sub>CH<sub>3</sub>), 14.0 (CH<sub>3</sub>)

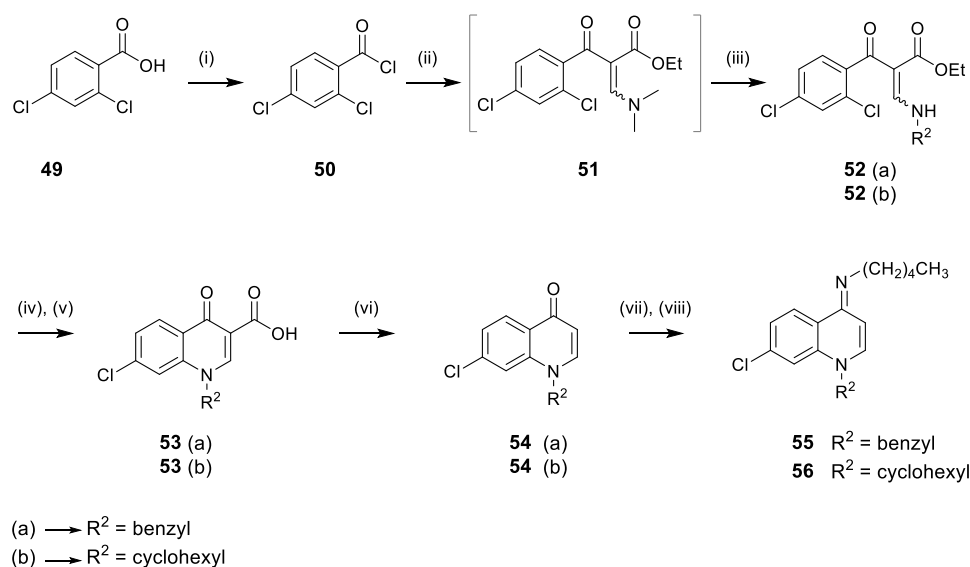
HRMS (EI) *m/z*:      Calcd. [M]<sup>+</sup>            388.1007  
                                  Measured                388.1001

LRMS (EI) *m/z*: 390 (27), 388 (73, [M]<sup>+</sup>), 326 (31), 325 (38), 324 (100), 323 (62), 253 (15), 84 (17), 77 (16)

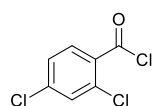
IR *v*<sub>max</sub> (neat/cm<sup>-1</sup>): 2970 (Ar C-H), 2950, 2928, 2869 (aliphatic C-H), 1741 (S=O), 1617 (C=N), 1601 (C=C), 1539, 1531

m.p.: 143 – 144 °C



**Route C:****Scheme 32.** Synthesis of iminodihydroquinolines **55** and **56** from 2,4-dichlorobenzoic acid.

Reagents and conditions: (i) (COCl)<sub>2</sub>, DMF (cat.), DCM, rt, 2h, quant. (ii) ethyl 3-(*N,N*-dimethylamino)acrylate, NEt<sub>3</sub>, CH<sub>3</sub>CN, 70 °C, 3-5 h (iii) NH<sub>2</sub>-R<sup>2</sup>, 70 °C, 18 h (iv) NaH, THF, reflux, 4-6.5 h (v) NaOH, THF/EtOH (6:1), 50-60 °C, 6 h (vi) HCl (aq.), biphenyl ether, 260 °C, 7 h (vii) POCl<sub>3</sub>, 100 °C, 2 h (viii) *n*-pentylamine, rt, 2-3 h.

**2,4-Dichloro-benzoyl chloride (50)**

Yellow oil

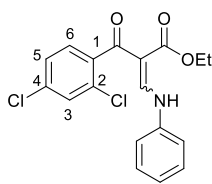
Chemical formula: C<sub>7</sub>H<sub>3</sub>Cl<sub>3</sub>OMolecular Weight: 209.46 g.mol<sup>-1</sup>

Yield: quantitative

To a solution of 2,4-dichlorobenzoic acid (5.05 g, 26.28 mmol) in DCM (300 ml) under an atmosphere of argon, oxalyl chloride (2.75 ml, 31.52 mmol) was added followed by DMF (4 drops) and the solution was stirred at ambient temperature for 2 h. The solvents were evaporated *in vacuo*, and to the remaining residue toluene was added (150 ml) and the mixture was evaporated again to afford **50** as yellow oil (5.45 g, quantitative).

<sup>1</sup>H NMR (CDCl<sub>3</sub>, 600 MHz) δ ppm: 8.07 (1H, d, *J* = 8.6, CH-6), 7.51 (1H, d, *J* = 2.1, CH-3), 7.40 (1H, dd, *J* = 8.6, 2.1, CH-5)

<sup>13</sup>C NMR (CDCl<sub>3</sub>, 150 MHz) δ ppm: 164.2, 140.9, 135.2, 134.8, 131.6, 131.0, 127.6

**Ethyl 2-(2,4-dichlorobenzoyl)-3-(phenylamino)acrylate (52a)**

Beige solid

Chemical formula:  $C_{18}H_{15}Cl_2NO_3$ Molecular weight:  $364.22 \text{ g}\cdot\text{mol}^{-1}$ 

Yield: 31%

Mixture of stereoisomers: 77:33 (**52a**:**52a''**)

To a solution of  $CH_3CN$  (40 ml) and  $NEt_3$  (14.94 ml, 0.11 mmol), ethyl 3-(*N,N*-dimethylamino)acrylate (5.75 ml, 40.17 mmol) and **50** (5.61 g, 26.78 mmol) were added, and the resulting mixture was heated at 70 °C for 3 h under argon atmosphere. After cooling at ambient temperature, aniline (2.44 ml, 26.78 mmol) was added and the mixture was heated at 70 °C for 18 h further. After cooling at ambient temperature,  $H_2O$  (40 ml) and  $CH_3CN$  (40 ml) were added and the resulting mixture was stirred for 15 min. The organic products were extracted with EtOAc (3 x 100 ml), and the organic products were dried over anhydrous  $MgSO_4$  and evaporated *in vacuo*. Purification *via* column chromatography (1:5 petroleum ether:EtOAc) afforded **52a** as beige solid (3.03 g, 31%).

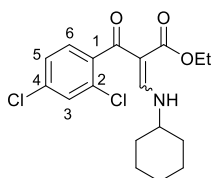
$^1H$  NMR ( $CDCl_3$ , 600 MHz)  $\delta$  ppm: 12.71 (1H, d,  $J=13.2$ , NH), 11.26 (1H, d,  $J=13.8$ , NH''), 8.67 (1H, d,  $J=14.1$ , C=CH'), 8.65 (1H, d,  $J=13.6$ , C=CH), 7.46-7.39 (2H, m, meta Ph-H, meta Ph-H''), 7.38 (1H, d,  $J=2.0$ , CH-3), 7.37 (1H, d,  $J=2.0$ , CH-3''), 7.31-7.18 (5H, m, CH-5, CH-5'', CH-6, CH-6'', ortho Ph-H, ortho Ph-H'', para Ph-H, para Ph-H''), 4.04 (2H, q,  $J=7.0$ ,  $CH_2$ ), 4.01 (2H, q,  $J=7.3$ ,  $CH_2$ ''), 1.02 (3H, t,  $J=7.2$ ,  $CH_3$ ), 0.88 (3H, t,  $J=7.2$ ,  $CH_3$ '')

$^{13}C$  NMR ( $CDCl_3$ , 150 MHz)  $\delta$  ppm: 193.5 ( $C_{QO}$ ), 190.5 ( $C_{QO}$ ), 168.5 ( $C_{QO}$ ), 166.5 ( $C_{QO}$ ), 153.3 (CH), 152.7 (CH), 141.2 ( $C_Q$ ), 140.9 ( $C_Q$ ), 138.7 ( $C_Q$ ), 138.6 ( $C_Q$ ), 135.0 ( $C_Q$ ), 134.9 ( $C_Q$ ), 130.9 ( $C_Q$ ), 130.1 (CH), 130.0 (CH), 129.2 (CH), 129.0 (CH), 128.9 (CH), 128.3 (CH), 127.0 (CH), 126.9 (CH), 126.4 (CH), 126.0 (CH), 118.2 (CH), 117.8 (CH), 103.4 ( $C_Q$ ), 103.3 ( $C_Q$ ), 60.4 ( $CH_2$ ), 60.2 ( $CH_2$ ''), 13.9 ( $CH_3$ ), 13.5 ( $CH_3$ '')

HRMS (EI)  $m/z$ : Calcd.  $[M]^+$  363.0423  
Measured 363.0427

LRMS (EI)  $m/z$ : 365 (7), 363 (10,  $[M]^+$ ), 330 (26), 328 (83,  $[C_{18}H_{15}ClNO_3]^+$ ), 300 (25), 284 (27), 282 (86), 175 (62), 173 (100,  $[C_7H_3Cl_2NO]^+$ ), 145 (34,  $[C_6H_3Cl_2]^+$ )

m.p.: 74 - 75 °C

**3-Cyclohexylamino-2-(2,4-dichloro-benzoyl)-acrylic acid ethyl ester (52b)**

White solid

Chemical formula:  $C_{18}H_{21}Cl_2NO_3$ Molecular weight:  $370.27 \text{ g}\cdot\text{mol}^{-1}$ 

Yield: 61%

Mixture of stereoisomers: 83:17 (**52b**:**52b''**)

To  $CH_3CN$  (5 ml),  $Et_3N$  (1.33 ml, 9.54 mmol), ethyl 3-(*N,N*-dimethylamino)acrylate (0.51 ml, 3.58 mmol), and **50** (0.50 g, 2.39 mmol) were added and the resulting mixture was heated at 70 °C for 5 h under argon atmosphere. After cooling at ambient temperature, cyclohexylamine (0.28 ml, 2.39 mmol) was added and the mixture was heated at 70 °C for 18 h further. After cooling at ambient temperature,  $H_2O$  (10 ml) was added and the resulting mixture was stirred for 15 min. The resulting precipitate

was filtered, was washed with a solution of H<sub>2</sub>O and CH<sub>3</sub>CN (1:1, 100 ml) and dried *in vacuo* to afford **52b** as white solid (0.54 g, 61%).

**<sup>1</sup>H NMR (CDCl<sub>3</sub>, 600 MHz)** δ ppm: 11.11 (1H, s, br, NH), 9.60 (1H, s, br, NH'), 8.27 (1H, d, *J*=14.8, C=CH'), 8.18 (1H, d, *J*=14.2, C=CH), 7.34 (1H, d, *J*=1.9, CH-3), 7.33 (1H, d, *J*=1.9, CH-3'), 7.21-7.25 (1H, m, CH-5, CH-5'), 7.16 (1H, d, *J*=8.2, CH-6'), 7.13 (1H, d, *J*=8.2, CH-6), 3.96 (2H, q, *J*=7.1, CH<sub>2</sub>CH<sub>3</sub>), 3.91 (2H, q, *J*=7.1, CH<sub>2</sub>'CH<sub>3</sub>), 3.29-3.40 (1H, m, NHCH(CH<sub>2</sub>)<sub>2</sub>), 1.96-2.06 (2H, m, CH<sub>2</sub>), 1.77-1.87 (2H, m, CH<sub>2</sub>), 1.62-1.69 (1H, m, CH<sub>2</sub>), 1.33-1.53 (4H, m, CH<sub>2</sub>), 1.19-1.30 (1H, m, CH<sub>2</sub>), 0.96 (3H, t, *J*=7.1, CH<sub>3</sub>), 0.82 (3H, t, *J*=7.1, CH<sub>3</sub>')

**<sup>13</sup>C NMR (CDCl<sub>3</sub>, 150 MHz)** δ ppm: 192.3 (C<sub>Q</sub>O), 190.2 (C<sub>Q</sub>O), 168.8 (C<sub>Q</sub>O), 166.9 (C<sub>Q</sub>O), 159.0 (CH), 158.8 (CH), 142.0 (C<sub>Q</sub>), 141.5 (C<sub>Q</sub>), 134.3 (C<sub>Q</sub>), 134.2 (C<sub>Q</sub>), 131.1 (C<sub>Q</sub>), 130.8 (C<sub>Q</sub>), 128.9 (CH), 128.8 (CH), 128.6 (CH), 128.1 (CH), 126.8 (CH), 126.7 (CH), 100.4 (C<sub>Q</sub>), 100.0 (C<sub>Q</sub>), 59.9 (CH<sub>2</sub>), 59.6 (CH<sub>2</sub>), 59.1 (CH), 58.9 (CH), 33.8 (CH<sub>2</sub>), 33.7 (CH<sub>2</sub>), 25.1 (CH<sub>2</sub>), 24.5 (CH<sub>2</sub>), 14.0 (CH<sub>3</sub>), 13.5 (CH<sub>3</sub>)

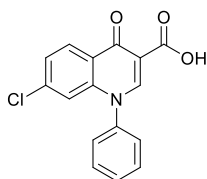
**HRMS (CI) m/z:** Calcd. [M]<sup>+</sup> 370.0977  
Measured 370.0971

**LRMS (CI) m/z:** 372 (66), 370 (100, [M]<sup>+</sup>), 334 (51), 324 (40, C<sub>16</sub>H<sub>16</sub>Cl<sub>2</sub>NO<sub>2</sub><sup>+</sup>)

**IR ν<sub>max</sub> (neat/cm<sup>-1</sup>):** 3211 (NH), 3078 (C=C-H), 2981 (Ar-H), 2935 (CH<sub>2</sub>, CH<sub>3</sub>), 2857 (-CH), 1670 (C=O), 1612 (C=C)

**m.p.:** 124 - 125 °C

### 7-Chloro-4-oxo-1-phenyl-1,4-dihydro-quinoline-3-carboxylic acid (**53a**)



White crystalline solid

Chemical formula: C<sub>16</sub>H<sub>10</sub>ClNO<sub>3</sub>

Molecular weight: 299.71 g.mol<sup>-1</sup>

Yield: 58%

To a solution of NaH (60% in mineral oil, 0.50 g, 12.48 mmol) in THF (70 ml), **52a** (3.03 g, 8.32 mmol) was added slowly and the mixture was heated at 65 °C for 4 h under an atmosphere of argon. The resulting mixture was cooled to ambient temperature, and was neutralised to pH 7 by addition of acetic acid (glacial). The solution was evaporated *in vacuo*, and to the remaining residue water (200 ml) was added. The precipitate formed was filtered and was re-dissolved in a mixture of THF (60 ml) and EtOH (10 ml). NaOH (6.24 ml, 2M) was added, and the resulting solution was heated at 60 °C for 5 h. The solvents were evaporated *in vacuo* and water (200 ml) was added to the remaining residue. The aqueous layer was acidified to pH 3 by HCl (1M) addition. The organic products were extracted with DCM (3 x 100 ml), and the organic extracts were dried over anh. MgSO<sub>4</sub> and evaporated *in vacuo* to afford **53a** as white solid (2.70 g, 58%).

**<sup>1</sup>H NMR (DMSO-d<sub>6</sub>, 600 MHz)** δ ppm: 14.76 (1H, s, br, COOH), 8.73 (1H, s, CH-2), 8.44 (1H, d, *J*=8.7, CH-5), 7.77-7.68 (6H, m, Ph-CH, CH-6), 7.04 (1H, d, *J*=1.9, CH-8)

**<sup>13</sup>C NMR (DMSO-d<sub>6</sub>, 150 MHz)** δ ppm: 177.6 (C<sub>Q</sub>-4), 165.4 (COOH), 149.9 (CH-2) 141.9 (C<sub>Q</sub>-8'), 139.6 (C<sub>Q</sub>-Ph), 139.0 (C<sub>Q</sub>-7), 130.7 (CH-6 or para Ph-CH), 130.5 (meta Ph-CH), 128.1 (CH-5), 127.5 (ortho Ph-CH), 126.9 (CH-6 or para Ph-CH), 123.9 (C<sub>Q</sub>-4'), 118.1 (CH-8), 108.6 (CH-3)

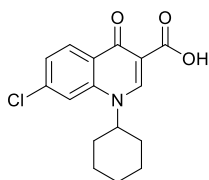
**HRMS (ES+) m/z:** Calcd. [M+H]<sup>+</sup> 300.0427  
Measured 300.0433

**LRMS (ES+) m/z:** 302 (33), 300 (100, [M+H]<sup>+</sup>), 256 (12), 254 (25, [M-COOH]<sup>+</sup>), 191 (10)

**IR  $\nu_{\max}$  (neat/cm<sup>-1</sup>):** 3072 (Ar C-H), 2623 (broad, O-H), 1726 (C=O), 1602 (C=N), 1585 (Ar C=C), 1551, 1536, 1501

**m.p.:** > 250 °C

### 7-Chloro-1-cyclohexyl-4-oxo-1,4-dihydro-quinoline-3-carboxylic acid (**53b**)



White powder

Chemical formula: C<sub>16</sub>H<sub>16</sub>ClNO<sub>3</sub>

Molecular Weight: 305.76 g.mol<sup>-1</sup>

Yield: quantitative

To a solution of **52b** (0.06 g, 0.18 mmol) in THF (6 ml) and EtOH (1 ml), NaOH (0.14 ml, 2 M) was added, and the mixture was heated at 60 °C for 6 h. The solvents were evaporated *in vacuo* and to the remaining residue water (150 ml) was added. The aqueous layer was acidified to pH 3 with HCl (1 M) and the organic products were extracted with DCM (3 x 100 ml). The organic extracts were dried over anh. MgSO<sub>4</sub> and evaporated to afford **53b** as white solid (0.05 g, quantitative).

**<sup>1</sup>H NMR (CDCl<sub>3</sub>, 600 MHz)**  $\delta$  ppm: 14.79 (1H, s, COOH), 8.89 (1H, s, CH-2), 8.51 (1H, d, *J* = 8.6, CH-5), 7.69 (1H, d, *J* = 1.7, CH-8), 7.54 (1H, dd, *J* = 8.6, 1.7, CH-6), 4.45 (1H, tt, *J* = 11.9, 3.2, NCH(CH<sub>2</sub>)<sub>2</sub>), 2.19 (2H, d, *J* = 11.9, cyclohexyl CH<sub>2</sub>-2, cyclohexyl CH<sub>2</sub>-6), 2.12-2.05 (2H, m, cyclohexyl CH<sub>2</sub>-3, cyclohexyl CH<sub>2</sub>-5), 1.92-1.79 (3H, m, cyclohexyl CH<sub>2</sub>-2, cyclohexyl CH<sub>2</sub>-4, cyclohexyl CH<sub>2</sub>-6), 1.60 (2H, qt, *J* = 13.5, 3.5, cyclohexyl CH<sub>2</sub>-3, cyclohexyl CH<sub>2</sub>-5), 1.34 (1H, qt, *J* = 13.3, 3.9, cyclohexyl CH<sub>2</sub>-4)

**<sup>13</sup>C NMR (CDCl<sub>3</sub>, 150 MHz)**  $\delta$  ppm: 176.6 (C<sub>Q</sub>-4), 167.0 (C<sub>Q</sub>OOH), 144.8 (CH-2), 140.9 (C<sub>Q</sub>-7 or C<sub>Q</sub>-8'), 140.5 (C<sub>Q</sub>-7 or C<sub>Q</sub>-8'), 129.3 (CH-5), 126.9 (CH-6), 125.3 (C<sub>Q</sub>-4'), 115.8 (CH-8), 109.4 (C<sub>Q</sub>-3), 60.8 (NCH(CH<sub>2</sub>)<sub>2</sub>), 33.0 (cyclohexyl CH<sub>2</sub>-2, cyclohexyl CH<sub>2</sub>-6), 25.9 (cyclohexyl CH<sub>2</sub>-3, cyclohexyl CH<sub>2</sub>-5), 25.2 (cyclohexyl CH<sub>2</sub>-4)

**HRMS (CI) m/z:** Calcd. [M+H]<sup>+</sup> 306.0897

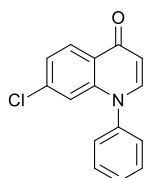
Measured 306.0904

**LRMS (CI) m/z:** 308 (31), 306 (100, [M+H]<sup>+</sup>)

**IR  $\nu_{\max}$  (neat/cm<sup>-1</sup>):** 3084 (Ar C-H), 2936, 2863 (alkyl C-H), 2658 (broad O-H), 1714 (C=O), 1604, 1555 (Ar C=C), 1534, 1501

**m.p.:** > 250 °C

### 7-Chloro-1-phenyl-1H-quinolin-4-one (**54a**)



Pale pink solid

Chemical formula: C<sub>15</sub>H<sub>10</sub>ClNO

Molecular weight: 255.70 g.mol<sup>-1</sup>

Yield: 18%

A mixture of **53a** (1.48 g, 4.68 mmol) and HCl (0.47 ml, 10 M) was heated in biphenyl ether (16 g) at 260 °C for 7 h. The solution was allowed to cool to ~ 40 °C, and petroleum ether (200 ml) was added while stirring vigorously. The precipitate formed was filtered, was washed with petroleum ether (2 x 100 ml) and was dried *in vacuo*. Purification *via* flash column chromatography (EtOAc → 1:19 MeOH:EtOAc) afforded **54a** (0.21 g, 18%) as pale pink solid.

**<sup>1</sup>H NMR (CDCl<sub>3</sub>, 600 MHz)** δ ppm: 8.41 (1H, d, *J* = 8.7, *CH*-5), 7.69-7.59 (4H, m, *CH*-2, meta Ph-*CH*, para Ph-*CH*), 7.42-7.38 (2H, m, ortho Ph-*CH*), 7.36 (1H, dd, *J* = 8.7, 1.9, *CH*-6), 7.01 (1H, d, *J* = 1.9, *CH*-8), 6.59 (1H, d, *J* = 8.0, *CH*-3)

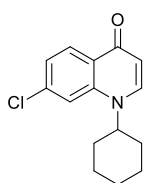
**<sup>13</sup>C NMR (CDCl<sub>3</sub>, 150 MHz)** δ ppm: 177.2 (*C*<sub>Q</sub>-4), 143.7 (*CH*-2), 142.1 (*C*<sub>Q</sub>-8'), 140.7 (Ph-*C*<sub>Q</sub>), 139.0 (*C*<sub>Q</sub>-7), 130.8 (para Ph-*CH*), 130.2 (meta Ph-*CH*), 128.4 (*CH*-5), 127.5 (ortho Ph-*CH*), 125.3 (*CH*-6), 124.5 (*C*<sub>Q</sub>-4'), 117.1 (*CH*-8), 110.5 (*CH*-3)

**HRMS (EI) *m/z*:** Calcd. [*M*]<sup>+</sup> 255.0445  
Measured 255.0440

**LRMS (EI) *m/z*:** 257 (30), 255 (100, [*M*]<sup>+</sup>), 229 (11), 227 (37), 191 (12), 165 (13), 110 (11), 96 (14), 78 (14, [*M*+H-Ph]<sup>+</sup>)

**m.p.:** 192-193 °C

### 7-Chloro-1-cyclohexyl-1*H*-quinolin-4-one (54b)



Beige powder

Chemical formula: C<sub>15</sub>H<sub>16</sub>ClNO

Molecular Weight: 261.75 g.mol<sup>-1</sup>

Yield: 24%

A mixture of **53b** (2.61 g, 8.53 mmol) and HCl (0.86 ml, 10 M) in biphenyl ether (25 g) was heated at 260 °C for 7 h. The solution was allowed to cool to ~40 °C, and petrol was added (200 ml), while stirring vigorously. The precipitate formed was filtered, was washed with petrol and was dried *in vacuo*. Purification *via* flash column chromatography (EtOAc → 1:1:18 NEt<sub>3</sub>:MeOH:EtOAc) afforded **54b** (0.54 g, 24%) as beige solid.

**<sup>1</sup>H NMR (CDCl<sub>3</sub>, 600 MHz)** δ ppm: 8.42 (1H, d, *J* = 8.7, *CH*-5), 7.71 (1H, d, *J* = 8.0, *CH*-2), 7.51 (1H, d, *J* = 1.8, *CH*-8), 7.32 (1H, dd, *J* = 8.7, 1.8, *CH*-6), 6.30 (1H, d, *J* = 8.0, *CH*-3), 4.27 (1H, tt, *J* = 11.8, 3.5, NCH(CH<sub>2</sub>)<sub>2</sub>), 2.12 (2H, d, *J* = 11.8, cyclohexyl *CH*<sub>2</sub>-2, cyclohexyl *CH*<sub>2</sub>-6), 2.05-1.98 (2H, m, cyclohexyl *CH*<sub>2</sub>-3, cyclohexyl *CH*<sub>2</sub>-5), 1.89-1.82 (1H, m, cyclohexyl *CH*<sub>2</sub>-4), 1.69 (2H, qd, *J* = 12.5, 3.5, cyclohexyl *CH*<sub>2</sub>-2, cyclohexyl *CH*<sub>2</sub>-6), 1.57 (2H, qt, *J* = 13.2, 3.5, cyclohexyl *CH*<sub>2</sub>-3, cyclohexyl *CH*<sub>2</sub>-5), 1.30 (1H, qt, *J* = 13.2, 4.0, cyclohexyl *CH*<sub>2</sub>-4)

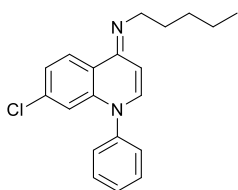
**<sup>13</sup>C NMR (CDCl<sub>3</sub>, 150 MHz)** δ ppm: 177.2 (*C*<sub>Q</sub>-4), 140.9 (*C*<sub>Q</sub>-8'), 138.7 (*C*<sub>Q</sub>-7), 138.4 (*CH*-2), 129.2 (*CH*-5), 126.0 (*C*<sub>Q</sub>-4'), 124.1 (*CH*-6), 114.5 (*CH*-8), 110.8 (*CH*-3), 58.8 (NCH(CH<sub>2</sub>)<sub>2</sub>), 32.8 (cyclohexyl *CH*<sub>2</sub>-2, cyclohexyl *CH*<sub>2</sub>-6), 26.0 (cyclohexyl *CH*<sub>2</sub>-3, cyclohexyl *CH*<sub>2</sub>-5), 25.5 (cyclohexyl *CH*<sub>2</sub>-4)

**HRMS (EI) *m/z*:** Calcd. [*M*]<sup>+</sup> 261.0915  
Measured 261.0922

**LRMS (EI) *m/z*:** 263 (6), 261 (25, [*M*]<sup>+</sup>), 182 (19), 181 (38), 180 (51), 179 (100, [*M*+H-cyclohexyl]<sup>+</sup>), 152 (12), 151 (19), 150 (25)

**IR *v*<sub>max</sub> (neat/cm<sup>-1</sup>):** 3471, 3074 (Ar C-H), 2933, 2858 (alkyl C-H), 1628 (C=O), 1589 (Ar C=C), 1538

**m.p.:** 130-131 °C

**(E)-7-chloro-N-pentyl-1-phenylquinolin-4(1H)-imine (55)**

Pale brown crystalline solid (needles)

Chemical formula:  $C_{20}H_{21}ClN_2$

Molecular weight:  $324.85 \text{ g}\cdot\text{mol}^{-1}$

Yield: 96%

A solution of **54a** (0.22 g, 0.84 mmol) in  $\text{POCl}_3$  (4 ml), was heated at  $100^\circ\text{C}$  for 2 h. The resulting solution was cooled to ambient temperature, DCM (4 ml) was added and the resulting mixture was evaporated *in vacuo*. DCM (4 ml) was added and the mixture was evaporated again. To the remaining residue, *n*-pentylamine (0.54 ml, 4.66 mmol) was added dropwise and the mixture was stirred at ambient temperature for 2 h. The resulting solution was poured into an ice ( $\sim 50 \text{ cm}^3$ ) and NaOH (50 ml, 2 M) mixture while stirring vigorously. The organic products were extracted with EtOAc (2 x 100 ml) and the organic extracts were dried over anhydrous  $\text{MgSO}_4$  and evaporated *in vacuo*. Purification *via* flash column chromatography using basic  $\text{Al}_2\text{O}_3$  as the solid phase (EtOAc  $\rightarrow$  1:9 MeOH:EtOAc), followed by recrystallization (MeOH) afforded **55** as pale brown crystalline solid (0.26 g, 96%).

$^1\text{H NMR}$  ( $\text{CDCl}_3$ , 600 MHz)  $\delta$  ppm: 8.41 (1H, d,  $J = 8.8$ , CH-5), 7.56 (2H, t,  $J = 7.6$ , meta Ph-CH), 7.50 (1H, t,  $J = 7.6$ , para Ph-CH), 7.34 (2H, d,  $J = 7.6$ , ortho Ph-CH), 7.12 (1H, dd,  $J = 8.8, 1.8$ , CH-6), 6.96 (1H, d,  $J = 8.1$ , CH-2), 6.72 (1H, d,  $J = 1.8$ , CH-8), 6.06 (1H, d,  $J = 8.1$ , CH-3), 3.36 (2H, t,  $J = 7.5$ ,  $\text{NCH}_2$ ), 1.75 (2H, q,  $J = 7.5$ ,  $\text{NCH}_2\text{CH}_2$ ), 1.47-1.35 (4H, m,  $\text{CH}_2\text{CH}_2\text{CH}_3$ ), 0.93 (3H, t,  $J = 7.1$ ,  $\text{CH}_3$ )

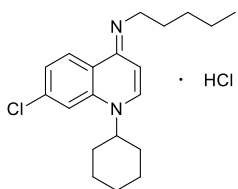
$^{13}\text{C NMR}$  ( $\text{CDCl}_3$ , 150 MHz)  $\delta$  ppm: 153.5 ( $\text{C}_Q$ -4), 141.7 (Ph- $\text{C}_Q$ ), 140.7 ( $\text{C}_Q$ -8'), 138.0 (CH-2), 135.8 ( $\text{C}_Q$ -7), 130.5 (meta Ph-CH), 129.0 (para Ph-CH), 127.9 (ortho Ph-CH), 127.0 (CH-5), 123.8 (CH-6), 115.8 (CH-8), 99.5 (CH-3), 50.4 ( $\text{NCH}_2$ ), 31.0 ( $\text{NCH}_2\text{CH}_2$ ), 30.2 ( $\text{CH}_2\text{CH}_2\text{CH}_3$ ), 22.9 ( $\text{CH}_2\text{CH}_3$ ), 14.4 ( $\text{CH}_3$ ), [ $\text{C}_Q$ -4', hidden]

HRMS (EI)  $m/z$ : Calcd.  $[\text{M}]^+$  324.1388  
Measured 324.1392

LRMS (EI)  $m/z$ : 324 (13,  $[\text{M}]^+$ ), 283 (13), 281 (41,  $[\text{M}-\text{CH}_2\text{CH}_2\text{CH}_3]^+$ ), 269 (29), 267 (100,  $[\text{M}-\text{CH}_2(\text{CH}_2)_2\text{CH}_3]^+$ ), 254 (14,  $[\text{M}-\text{CH}_2(\text{CH}_2)_3\text{CH}_3+\text{H}]^+$ ), 86 (17), 84 (29)

IR  $\nu_{\text{max}}$  (neat/ $\text{cm}^{-1}$ ): 3038 (Ar C-H), 2959, 2930, 2841, 2812 (aliphatic C-H), 1634 (C=N), 1595 (Ar C=C), 1572, 1549

m.p.:  $78\text{-}79^\circ\text{C}$

**(E)-7-chloro-1-cyclohexyl-N-pentylquinolin-4(1H)-imine hydrochloride (56)**

White solid

Chemical formula:  $C_{20}H_{27}ClN_2 \cdot \text{HCl}$

Molecular weight:  $367.36 \text{ g}\cdot\text{mol}^{-1}$

Yield: 68%

A solution of **54b** (0.29 g, 1.11 mmol) in  $\text{POCl}_3$  (4 ml), was heated at  $100^\circ\text{C}$  for 2 h. The resulting solution was cooled to ambient temperature, DCM (4 ml) was added and the mixture was evaporated *in vacuo*. DCM (4 ml) was added and the mixture was evaporated again. To the remaining residue, *n*-pentylamine (0.71 ml, 6.11 mmol) was added dropwise and the mixture was stirred at ambient temperature for 3

h. The resulting solution was poured into an ice (~ 50 cm<sup>3</sup>) and NaOH (2M, 50 ml) mixture while stirring vigorously. The organic products were extracted with EtOAc (2 x 100 ml) and the organic extracts were dried over anh. MgSO<sub>4</sub> and evaporated *in vacuo*. Purification *via* flash column chromatography using basic Al<sub>2</sub>O<sub>3</sub> as the solid phase (EtOAc → 1:9 EtOAc:MeOH), followed by recrystallization (CHCl<sub>3</sub>) afforded **56** as white solid (0.27 g, 68%).

**<sup>1</sup>H NMR (CDCl<sub>3</sub>, 600 MHz)** δ ppm: 11.36 (1H, t, *J* = 7.0, =NH<sup>t</sup>), 9.61 (1H, d, *J* = 9.0, CH-5), 8.13 (1H, d, *J* = 7.8, CH-2), 7.67 (1H, d, *J* = 1.9, CH-8), 7.61 (1H, dd, *J* = 9.0, 1.9, CH-6), 6.52 (1H, d, *J* = 7.8, CH-3), 4.49 (1H, tt, *J* = 11.9, 3.7, NH(CH<sub>2</sub>)<sub>2</sub>), 3.59 (2H, q, *J* = 7.0, =NCH<sub>2</sub>), 2.18 (2H, d, *J* = 11.7 cyclohexyl CH<sub>2</sub>-2, cyclohexyl CH<sub>2</sub>-6), 2.10-2.03 (2H, m, cyclohexyl CH<sub>2</sub>-3, cyclohexyl CH<sub>2</sub>-5), 1.92-1.85 (cyclohexyl CH<sub>2</sub>-4), 1.84-1.73 (4H, m, =NCH<sub>2</sub>CH<sub>2</sub>, cyclohexyl CH<sub>2</sub>-2, cyclohexyl CH<sub>2</sub>-6), 1.62 (2H, qt, *J* = 13.1, 3.7, cyclohexyl CH<sub>2</sub>-3, cyclohexyl CH<sub>2</sub>-5), 1.42-1.29 (5H, m, CH<sub>2</sub>CH<sub>2</sub>CH<sub>3</sub>, cyclohexyl CH<sub>2</sub>-4), 0.87 (3H, *J* = 7.1, CH<sub>3</sub>)

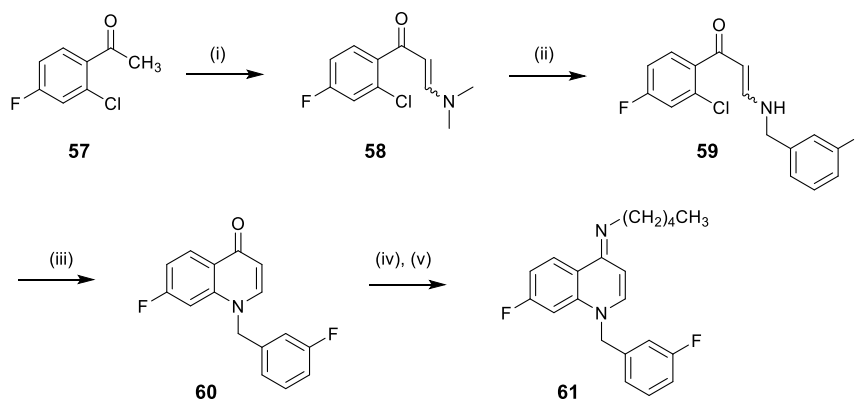
**<sup>13</sup>C NMR (CDCl<sub>3</sub>, 150 MHz)** δ ppm: 155.2 (C<sub>Q</sub>-4), 140.9 (C<sub>Q</sub>-7), 140.3 (CH-2), 138.6 (C<sub>Q</sub>-8'), 130.1 (CH-5), 127.7 (CH-6), 117.6 (C<sub>Q</sub>-4'), 115.3 (CH-8), 98.5 (CH-3), 60.7 (NCH(CH<sub>2</sub>)<sub>2</sub>), 44.0 (=NCH<sub>2</sub>), 33.1 (cyclohexyl CH<sub>2</sub>-2, cyclohexyl CH<sub>2</sub>-6), 29.3 (CH<sub>2</sub>CH<sub>2</sub>CH<sub>3</sub>), 27.9 (=NCH<sub>2</sub>CH<sub>2</sub>), 25.9 (cyclohexyl CH<sub>2</sub>-3, cyclohexyl CH<sub>2</sub>-5), 25.2 (cyclohexyl CH<sub>2</sub>-4), 22.5 (CH<sub>2</sub>CH<sub>3</sub>), 14.2 (CH<sub>3</sub>)

**HRMS (CI) m/z:** Calcd. [M+H]<sup>+</sup> 331.1940  
Measured 331.1949

**LRMS (EI) m/z:** 333 (33), 331 (100, [M+H]<sup>+</sup>), 289 (6), 287 (17, [M-CH<sub>2</sub>CH<sub>2</sub>CH<sub>3</sub>]<sup>+</sup>), 275 (7), 273 (23, [M-CH<sub>2</sub>(CH<sub>2</sub>)<sub>2</sub>CH<sub>3</sub>]<sup>+</sup>), 191 (8)

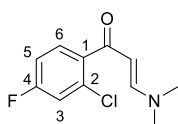
**IR ν<sub>max</sub> (neat/cm<sup>-1</sup>):** 3371 (N-H), 2992 (Ar C-H), 2926, 2853 (Alkyl C-H), 1606 (C=N), 1581 (Ar C=C), 1525

**m.p:** 231 - 232 °C



**Scheme 33.** Synthesis of iminodihydroquinoline **61** from 4-fluoro-2-chloroacetophenone.

Reagents and conditions: (i) *N,N*-dimethylformamide dimethyl acetal, toluene, reflux, 24 h (ii) 3-fluorobenzyl amine, acetic acid, 60 °C, 8 h (iii) NaH, DMF, 80 °C, 3 h (iv) POCl<sub>3</sub>, 100 °C, 2.5 h (v) *n*-pentylamine, MeOH, rt, 5 h.

**(E)-1-(2-chloro-4-fluorophenyl)-3-(dimethylamino)prop-2-en-1-one (58)**

Yellow/brown viscous oil  
 Chemical Formula: C<sub>11</sub>H<sub>11</sub>ClFNO  
 Molecular weight: 227.66  
 Yield: 61%

To a solution of 4-fluoro-2-chloroacetophenone (1.79 g, 10.40 mmol) in toluene (15 ml), *N,N*-dimethylformamide dimethyl acetal (1.65 ml, 12.42 mmol) was added and the resulting solution was heated to reflux at 110 °C for 24 h under an atmosphere of argon. After cooling to room temperature the solution was evaporated *in vacuo* and the remaining residue was purified by column chromatography (1:1 petroleum ether:EtOAc → EtOAc) to afford **58** as yellow/brown viscous oil (1.45 g, 61%).

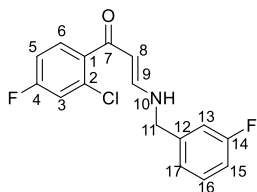
<sup>1</sup>H NMR (600 MHz, CDCl<sub>3</sub>) δ ppm: 7.40 (1H, br, CH-6), 7.12 (1H, dd, *J* = 8.7, 2.7, CH-3), 6.98 (1H, td, *J* = 8.3, 2.5, CH-5), 5.35 (1H, d, *J* = 12.5, CHN(CH<sub>3</sub>)<sub>2</sub>), 3.10 (3H, s, br, CH<sub>3</sub>), 2.88 (3H, s, br, CH<sub>3</sub>)

<sup>13</sup>C NMR (150 MHz, CDCl<sub>3</sub>) δ ppm: 162.5 (d, <sup>1</sup>*J*<sub>CF</sub> = 256.4, C<sub>Q</sub>-4), 132.1 (d, <sup>3</sup>*J*<sub>CF</sub> = 10.6, C<sub>Q</sub>-2), 130.5 (d, <sup>3</sup>*J*<sub>CF</sub> = 9.0, CH-6), 117.4 (d, <sup>2</sup>*J*<sub>CF</sub> = 23.1, CH-3), 114.0 (d, <sup>2</sup>*J*<sub>CF</sub> = 21.2, CH-5), 45.3 (CH<sub>3</sub>), 37.3 (CH<sub>3</sub>)

HRMS (CI) *m/z*: Calcd. [M+H]<sup>+</sup> 228.0586  
 Measured 228.0586

LRMS (CI) *m/z*: 230 (33), 231 (21), 228 (100, [M+H]<sup>+</sup>), 227 (22), 212 (9), 210 (26), 193 (33, [M-Cl]<sup>+</sup>), 157 (10, [M- C=CN(CH<sub>3</sub>)<sub>2</sub>]<sup>+</sup>), 98 (14, [COC=CN(CH<sub>3</sub>)<sub>2</sub>]<sup>+</sup>)

IR *v*<sub>max</sub> (neat/cm<sup>-1</sup>): 3042 (Ar C-H), 3019, 2920, 2805 (aliphatic C-H), 1640 (C=O), 1578 (Ar C=C), 1538

**(E)-1-(2-chloro-4-fluorophenyl)-3-((3-fluorobenzyl)amino)prop-2-en-1-one (59)**

Viscous orange oil  
 Chemical Formula: C<sub>16</sub>H<sub>12</sub>ClF<sub>2</sub>NO  
 Molecular weight: 307.72  
 Yield: 48%

To a mixture of **58** (1.28 g, 5.62 mmol) in acetic acid (20 ml), 3-fluorobenzyl amine (0.47 ml, 5.69 mmol) was added and the mixture was heated at 60 °C for 8 h. After cooling to room temperature, the solution was evaporated *in vacuo* and the remaining residue was purified by column chromatography (2:3 petroleum ether:EtOAc) to afford **59** as viscous orange oil (0.84 g, 48%).

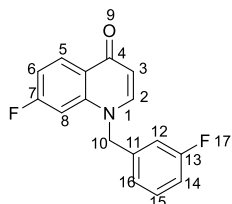
<sup>1</sup>H NMR (600 MHz, CDCl<sub>3</sub>) δ ppm: 10.43 (1H, s, br, NH-10), 7.51 (1H, dd, <sup>3</sup>*J*<sub>HH</sub> = 8.6, <sup>4</sup>*J*<sub>HF</sub> = 6.2, CH-6), 7.34 (1H, ddd, <sup>3</sup>*J*<sub>HH</sub> = 9.2, 7.8, <sup>4</sup>*J*<sub>HF</sub> = 5.5, CH-16), 7.12 (1H, dd, <sup>3</sup>*J*<sub>HF</sub> = 8.6, <sup>4</sup>*J*<sub>HH</sub> = 2.5, CH-3), 7.08 (1H, dd, <sup>3</sup>*J*<sub>HH</sub> = 7.3, <sup>4</sup>*J*<sub>HH</sub> = 1.8, CH-17), 7.03-6.98 (3H, m, CH-5, CH-13, CH-15), 6.97-6.94 (1H, m, CH-9), 5.47 (1H, d, *J* = 7.4, CH-8), 4.46 (2H, d, *J* = 6.0, CH<sub>2</sub>-11)

<sup>13</sup>C NMR (150 MHz, CDCl<sub>3</sub>) δ ppm: 190.3 (C<sub>Q</sub>-7), 163.2 (d, <sup>1</sup>*J*<sub>CF</sub> = 247.7, C<sub>Q</sub>-4 or C<sub>Q</sub>-14), 162.8 (d, <sup>1</sup>*J*<sub>CF</sub> = 252.8, C<sub>Q</sub>-4 or C<sub>Q</sub>-14), 154.1 (CH-9), 140.1 (d, <sup>3</sup>*J*<sub>CF</sub> = 6.9, C<sub>Q</sub>-12), 137.0 (d, <sup>4</sup>*J*<sub>CF</sub> = 3.5, C<sub>Q</sub>-1), 132.3 (d, <sup>3</sup>*J*<sub>CF</sub> = 10.5, C<sub>Q</sub>-2), 131.0 (d, <sup>3</sup>*J*<sub>CF</sub> = 9.1, CH-6), 130.6 (d, <sup>3</sup>*J*<sub>CF</sub> = 8.3, CH-16), 122.9 (d, <sup>4</sup>*J*<sub>CF</sub> = 3.0, CH-16), 117.7 (d, <sup>2</sup>*J*<sub>CF</sub> = 24.8, CH-3), 115.0 (d, <sup>2</sup>*J*<sub>CF</sub> = 20.9, CH-13 or CH-15), 114.4 (d, <sup>2</sup>*J*<sub>CF</sub> = 21.8, CH-13 or CH-15), 114.1 (d, <sup>2</sup>*J*<sub>CF</sub> = 21.0, CH-5), 93.3 (CH-8), 52.4 (d, <sup>4</sup>*J*<sub>CF</sub> = 2.0, CH<sub>2</sub>-11)



**HRMS (ES-) m/z:** Calcd. [M-H]<sup>-</sup> 306.0497  
 Measured 306.0497  
**LRMS (ES-) m/z:** 308 (33), 306 (100, [M-H]<sup>-</sup>)  
**IR v<sub>max</sub> (neat/cm<sup>-1</sup>):** 3269 (N-H), 3063 (Ar C-H), 2919, 2851 (aliphatic C-H), 1630 (C=O), 1589 (Ar C=C)

### 7-Fluoro-1-(3-fluoro-benzyl)-1H-quinolin-4-one (60)



Yellow solid

Chemical formula: C<sub>16</sub>H<sub>11</sub>F<sub>2</sub>NO

Molecular weight: 271.27 g.mol<sup>-1</sup>

Yield: 14%

To a solution of **59** (0.84 g, 2.72 mmol) in DMF (15 ml) cooled to 0 °C, NaH (60% in mineral oil, 0.11 g, 2.75 mmol) was added portion wise. The mixture was then heated at 80 °C for 3 h. After cooling to room temperature, water was added (150 ml). The organic products were extracted with EtOAc (2 x 100 ml), and the organic extracts were dried over anh. MgSO<sub>4</sub> and evaporated *in vacuo*. The remaining residue was purified by column chromatography (EtOAc -> 1:9 MeOH:EtOAc) to afford **60** as yellow solid (0.10 g, 14%).

**<sup>1</sup>H NMR (600 MHz, CDCl<sub>3</sub>)** δ ppm: 8.47 (1H, dd, <sup>3</sup>J<sub>HH</sub>= 8.8, <sup>4</sup>J<sub>HF</sub>= 6.5, CH-5), 7.60 (1H, d, J= 7.8, CH-2), 7.35 (1H, ddd, <sup>3</sup>J<sub>HH</sub>= 8.3, 7.8, <sup>4</sup>J<sub>HF</sub>= 5.9, CH-15), 7.08 (1H, td, <sup>3</sup>J<sub>HF</sub>= 8.8, <sup>3</sup>J<sub>HH</sub>= 8.8, <sup>4</sup>J<sub>HH</sub>= 2.3, CH-6), 7.03 (1H, td, <sup>3</sup>J<sub>HF</sub>= 8.3, <sup>3</sup>J<sub>HH</sub>= 8.3, <sup>4</sup>J<sub>HH</sub>= 1.8, CH-14), 6.92 (1H, dd, J= 7.8, 1.8, CH-16), 6.89 (1H, dd, <sup>3</sup>J<sub>HF</sub>= 10.6, <sup>4</sup>J<sub>HH</sub>= 2.3, CH-8), 6.84 (1H, dt, <sup>3</sup>J<sub>HF</sub>= 9.4, <sup>4</sup>J<sub>HH</sub>= 1.8, CH-12), 6.34 (1H, d, J= 7.8, CH-3), 5.24 (2H, s, CH<sub>2</sub>-10)

**<sup>13</sup>C NMR (150 MHz, CDCl<sub>3</sub>)** δ ppm: 177.6 (C<sub>Q</sub>-4), 165.1 (d, <sup>1</sup>J<sub>CF</sub>= 252.1, C<sub>Q</sub>-7), 163.4 (d, <sup>1</sup>J<sub>CF</sub>= 248.7, C<sub>Q</sub>-13), 143.9 (CH-2), 141.6 (d, <sup>2</sup>J<sub>CF</sub>= 11.6, C<sub>Q</sub>-8'), 137.2 (d, <sup>3</sup>J<sub>CF</sub>= 6.9, C<sub>Q</sub>-11), 131.3 (d, <sup>3</sup>J<sub>CF</sub>= 8.4, CH-15), 130.3 (d, <sup>3</sup>J<sub>CF</sub>= 10.7, CH-5), 124.1 (C<sub>Q</sub>-4'), 121.6 (d, <sup>4</sup>J<sub>CF</sub>= 3.1, CH-16), 115.8 (d, <sup>2</sup>J<sub>CF</sub>= 21.0, CH-14), 113.2 (d, <sup>2</sup>J<sub>CF</sub>= 22.4, CH-12), 112.8 (d, <sup>2</sup>J<sub>CF</sub>= 22.8, CH-6), 111.2 (CH-3), 102.2 (d, <sup>2</sup>J<sub>CF</sub>= 26.6, CH-8), 56.2 (CH<sub>2</sub>-10)

**<sup>19</sup>F NMR (282 MHz, CDCl<sub>3</sub>)** δ ppm: -104.93, -111.23

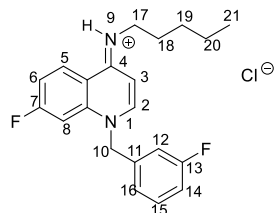
**HRMS (EI) m/z:** Calcd. [M]<sup>+</sup> 271.0803  
 Measured 271.0793

**LRMS (EI) m/z:** 272 (10), 271 (58, [M]<sup>+</sup>), 109 (100, [CH<sub>2</sub>PhF]<sup>+</sup>), 107 (10)

**IR v<sub>max</sub> (neat/cm<sup>-1</sup>):** 3079 (Ar C-H), 3055, 2920, 2850 (aliphatic C-H), 1629, 1605, 1576

**m.p.:** 129-131 °C

### [7-Fluoro-1-(3-fluoro-benzyl)-1H-quinolin-4-ylidene]-pentyl-amine hydrochloride (61)



White powder

Chemical formula: C<sub>21</sub>H<sub>22</sub>F<sub>2</sub>N<sub>2</sub> · HCl

Molecular Weight: 376.88 g.mol<sup>-1</sup>

Yield: 50%

A solution of **60** (0.10 g, 0.37 mmol) in POCl<sub>3</sub> (3 ml), was heated to reflux for 2.5 h. After cooling to room temperature, the mixture was evaporated *in vacuo*, DCM (2 x

20 ml) was added and the mixture was evaporated again. The remaining residue was triturated with ether. The resulting precipitate was dissolved in MeOH (2 ml), amylamine (0.23 ml, 1.98 mmol) was added dropwise and the solution was stirred at room temperature for 5 h. The solution was poured into an ice (~30 cm<sup>3</sup>) and NaOH (2 M, 30 ml) mixture while stirring vigorously. The organic products were extracted with DCM (2 x 100 ml), the organic extracts were dried over anh. MgSO<sub>4</sub> and were evaporated *in vacuo*. Trituration with Et<sub>2</sub>O afforded the hydrochloride salt **61** (70 mg, 50%) as white powder.

**<sup>1</sup>H NMR (600 MHz, CDCl<sub>3</sub>)** δ ppm: 11.36 (1H, br, s, NH<sup>+</sup>), 9.59 (1H, dd, <sup>3</sup>J<sub>HH</sub>= 9.4, <sup>4</sup>J<sub>HF</sub>= 5.6, CH-5), 8.32 (1H, d, J= 7.5, CH-2), 7.35 (1H, td, <sup>3</sup>J<sub>HH</sub>= 8.2, <sup>4</sup>J<sub>HF</sub>= 5.7, CH-15), 7.29-7.25 (1H, m, CH-6), 7.16 (1H, dd, <sup>3</sup>J<sub>HF</sub>= 9.9, <sup>4</sup>J<sub>HH</sub>= 2.5, CH-8), 7.04 (1H, td, <sup>3</sup>J<sub>HF</sub>= 8.2, <sup>3</sup>J<sub>HF</sub>= 8.2, <sup>4</sup>J<sub>HH</sub>= 2.2, CH-14), 6.96 (1H, dt, J= 8.2, 2.2, CH-16), 6.85 (1H, dt, <sup>3</sup>J<sub>HF</sub>= 8.9, <sup>4</sup>J<sub>HH</sub>= 2.2, CH-12), 6.50 (1H, d, J= 7.5, CH-3), 5.67 (2H, s, CH<sub>2</sub>-10), 3.61-3.55 (2H, m, CH<sub>2</sub>-17), 1.82 (2H, q, J= 7.4, CH<sub>2</sub>-18), 1.45-1.31 (4H, m, CH<sub>2</sub>-19, CH<sub>2</sub>-20), 0.89 (3H, t, J= 7.1, CH<sub>3</sub>-21)

**<sup>13</sup>C NMR (150 MHz, CDCl<sub>3</sub>)** δ ppm: 165.5 (d, <sup>1</sup>J<sub>CF</sub>= 257.6, C<sub>Q</sub>-7), 163.4 (d, <sup>1</sup>J<sub>CF</sub>= 249.5, C<sub>Q</sub>-13), 155.7 (C<sub>Q</sub>-4), 145.8 (CH-2), 139.8 (d, <sup>3</sup>J<sub>CF</sub>= 11.8, C<sub>Q</sub>-8'), 135.8 (d, <sup>3</sup>J<sub>CF</sub>= 7.6, C<sub>Q</sub>-11), 131.5 (d, <sup>3</sup>J<sub>CF</sub>= 8.3, CH-15), 131.3 (d, <sup>3</sup>J<sub>CF</sub>= 9.8, CH-5), 122.1 (d, <sup>4</sup>J<sub>CF</sub>= 2.9, CH-16), 116.4 (d, <sup>2</sup>J<sub>CF</sub>= 20.9, CH-14), 116.2 (d, <sup>2</sup>J<sub>CF</sub>= 23.9, CH-6), 115.6 (C<sub>Q</sub>-4'), 113.6 (d, <sup>2</sup>J<sub>CF</sub>= 22.7, CH-12), 103.3 (d, <sup>2</sup>J<sub>CF</sub>= 26.4, CH-8), 98.2 (CH-3), 57.6 (CH<sub>2</sub>-10), 44.2 (CH<sub>2</sub>-17), 29.3 (CH<sub>2</sub>-19), 28.0 (CH<sub>2</sub>-18), 22.5 (CH<sub>2</sub>-20), 14.1 (CH<sub>3</sub>-21)

**<sup>19</sup>F NMR (282 MHz, CDCl<sub>3</sub>)** δ ppm: -110.64, -99.87

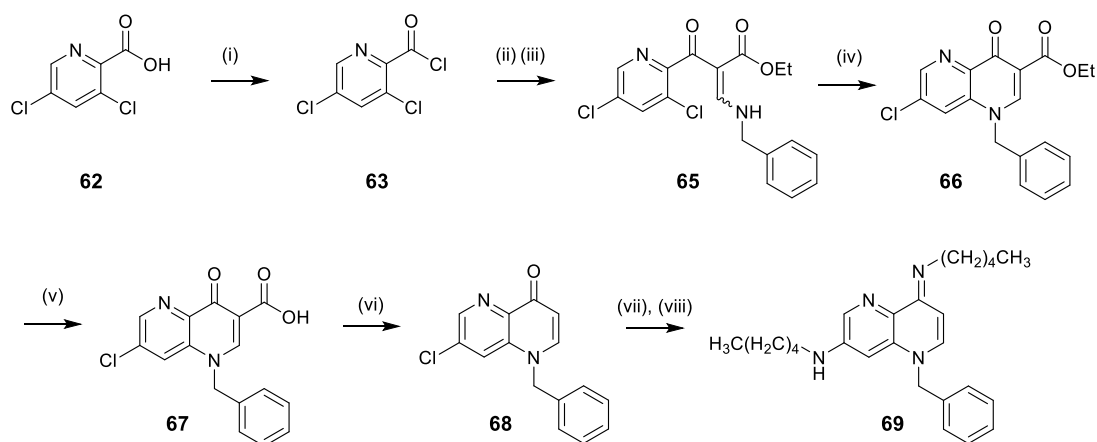
**HRMS (CI) m/z:** Calcd. [M<sup>+</sup>] 340.1746  
Measured 340.1745

**LRMS (CI) m/z:** 342 (95), 341 (77), 340 (100, [M]<sup>+</sup>), 297 (23, [M-CH<sub>2</sub>CH<sub>2</sub>CH<sub>3</sub>]<sup>+</sup>), 283 (27, [M-CH<sub>2</sub>(CH<sub>2</sub>)<sub>2</sub>CH<sub>3</sub>]<sup>+</sup>), 233 (19), 109 (11), 85 (17, [CH<sub>2</sub>(CH<sub>2</sub>)<sub>3</sub>CH<sub>3</sub>]<sup>+</sup>)

**IR ν<sub>max</sub> (neat/cm<sup>-1</sup>):** 3167 (N-H), 3020 (Ar C-H), 2929, 2871 (aliphatic C-H), 1613 (C=N), 1584 (Ar C=C), 1561, 1546

**m.p.:** 239 - 240 °C

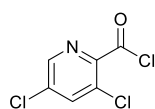
### 8.1.2. Synthesis of *N*-substituted-4-imino-1,4-dihydro-naphthyridines



**Scheme 34.** Synthesis of the naphthyridine **69**.

Reagents and conditions: (i)  $(\text{COCl})_2$ , DMF (cat.), DCM, rt, 2 h (ii) Ethyl 3-(*N,N*-dimethylamino)acrylate,  $\text{NEt}_3$ ,  $\text{CH}_3\text{CN}$ , 65 °C, 3.5 h (iii) Benzylamine, 70 °C, 18 h (d) NaH, THF, 50 °C, 4 h (iv) NaOH, THF, 60 °C, 3 h (v) HCl (aq.), biphenyl ether, 280 °C, 7 h (vi)  $\text{POCl}_3$ , 110 °C, 2 h (vii) *n*-pentylamine, rt → 18 h, 80 °C → 6 h.

#### 3,5-Dichloro-pyridine-2-carbonyl chloride (**63**)



Pale brown needles

Chemical formula:  $\text{C}_6\text{H}_2\text{Cl}_3\text{NO}$

Molecular Weight: 210.44  $\text{g}\cdot\text{mol}^{-1}$

Yield: quantitative

To a solution of 3,5-dichloro-2-pyridine carboxylic acid (3.34 g, 17.42 mmol) in DCM (300 ml), oxalyl chloride (1.83 ml, 20.98 mmol) was added followed by DMF (3 drops), and the mixture was stirred at R.T. for 2 h. The solvents were evaporated *in vacuo*, toluene (100 ml) was added and the mixture was evaporated again to afford **63** as pale brown solid (3.65 g, quantitative yield).

$^1\text{H NMR}$  ( $\text{CDCl}_3$ , 500 MHz)  $\delta$  ppm: 8.60 (1H, d,  $J=2.0$ , CH-6), 7.90 (1H, d,  $J=2.0$ , CH-4)

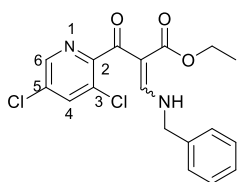
$^{13}\text{C NMR}$  ( $\text{CDCl}_3$ , 125 MHz)  $\delta$  ppm: 165.9 ( $\text{C}_\text{Q}=\text{O}$ ), 146.9 (CH-6), 144.6 ( $\text{C}_\text{Q}$ -2), 138.8 (CH-4), 136.5 ( $\text{C}_\text{Q}$ -3 or  $\text{C}_\text{Q}$ -5), 132.4 ( $\text{C}_\text{Q}$ -3 or  $\text{C}_\text{Q}$ -5)

HRMS (EI)  $m/z$ : Calcd.  $[\text{M}-\text{Cl}]^+$  173.9513  
Measured 173.9518

LRMS (EI)  $m/z$ : 176 (68), 174 (100,  $[\text{M}-\text{Cl}]^+$ ), 148 (45), 146 (70,  $[\text{M}-\text{COCl}]^+$ ), 112 (26), 110 (39)

IR  $\nu_{\text{max}}$  (neat/ $\text{cm}^{-1}$ ): 3068 (Ar C-H), 1760 (C=O), 1710, (C=N-), 1556 (Ar C=C), 1527

m.p.: 58 - 59 °C

**3-Benzylamino-2-(2,4-dichloro-benzoyl)-acrylic acid ethyl ester (65)**

White crystalline solid

Chemical formula: C<sub>18</sub>H<sub>16</sub>Cl<sub>2</sub>N<sub>2</sub>O<sub>3</sub>Molecular Weight: 379.24 g.mol<sup>-1</sup>

Yield: 45%

Mixture of stereoisomers: 83:17 (**65:65''**)

To a solution of NEt<sub>3</sub> (6.63 ml, 45.38 mmol) in CH<sub>3</sub>CN (20 ml), ethyl-3,3-dimethylaminoacrylate (2.55 ml, 17.81 mmol) and **63** (2.50 g, 11.88 mmol) were added and the mixture was heated at 65 °C for 3.5 h. After cooling to R.T., benzylamine (1.30 ml, 11.88 mmol) was added and the mixture was heated again at 65 °C for 18 h. After cooling at R.T., H<sub>2</sub>O (30 ml) was added, and after 15 min of stirring the mixture was allowed to stand for 45 min. The precipitate formed was filtered, was washed with a mixture of CH<sub>3</sub>CN and H<sub>2</sub>O (1:1) (3 x 100 ml), and was dried *in vacuo* to afford **65** as a white solid (2.03 g, 45%).

<sup>1</sup>H NMR (CDCl<sub>3</sub>, 600 MHz) δ ppm: 11.28 (1H, s, br, NH), 9.84 (1H, s, br, NH'), 8.42 (1H, d, *J* = 13.0, CHNH"), 8.41 (1H, d, *J* = 2.0, CH-6), 8.40 (1H, d, *J* = 2.3, CH-6"), 8.26 (1H, d, *J* = 14.1, CHNH), 7.44-7.33 (3H, m, meta Ph-*H*, meta Ph-*H'*, para Ph-*H*, para Ph-*H'*), 7.31-7.27 (2H, m, ortho Ph-*H*, ortho Ph-*H'*), 4.64 (2H, d, *J* = 6.6, CH<sub>2</sub>Ph), 4.63 (2H, d, *J* = 6.3, CH<sub>2</sub>Ph"), 3.98 (2H, q, *J* = 7.1, CH<sub>2</sub>CH<sub>3</sub>), 3.88 (2H, q, *J* = 7.2, CH<sub>2</sub>CH<sub>3</sub>"), 0.99 (3H, t, *J* = 7.2, CH<sub>3</sub>), 0.77 (3H, t, *J* = 7.1, CH<sub>3</sub>")

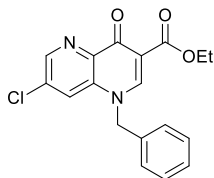
<sup>13</sup>C NMR (CDCl<sub>3</sub>, 150 MHz) δ ppm: 191.0 (C<sub>Q</sub>), 188.6 (C<sub>Q</sub>), 168.2 (C<sub>Q</sub>), 166.2 (C<sub>Q</sub>), 161.5 (CH), 160.8 (CH), 156.8 (C<sub>Q</sub>), 156.0 (C<sub>Q</sub>), 145.6 (CH), 145.4 (CH), 136.5 (CH), 136.4 (CH), 135.5 (C<sub>Q</sub>), 135.3 (C<sub>Q</sub>), 131.2 (C<sub>Q</sub>), 131.1 (C<sub>Q</sub>), 129.3 (C<sub>Q</sub>), 128.7 (CH), 127.8 (CH), 127.7 (CH), 127.6 (C<sub>Q</sub>), 100.1 (C<sub>Q</sub>), 99.5 (C<sub>Q</sub>), 60.0 (CH<sub>2</sub>), 59.7 (CH<sub>2</sub>), 54.4 (CH<sub>2</sub>), 54.3 (CH<sub>2</sub>), 14.1 (CH<sub>3</sub>), 13.6 (CH<sub>3</sub>)

HRMS (ES+) *m/z*: Calcd. [M+Na]<sup>+</sup> 401.0436  
Measured 401.0434

LRMS (ES+) *m/z*: 401 (11, [M+Na]<sup>+</sup>), 335 (72), 333 (100, [M-OCH<sub>2</sub>CH<sub>3</sub>]<sup>+</sup>)

IR ν<sub>max</sub> (neat/cm<sup>-1</sup>): 3197 (N-H), 3029, (Ar C-H), 2978, 2931, 1686 (C=O), 1620, (C=N-), 1571 (Ar C=C)

*m.p.*: 130 - 131 °C

**1-Benzyl-7-chloro-4-oxo-1,4-dihydro-[1,5]naphthyridine-3-carboxylic acid ethyl ester (66)**

Yellow powder

Chemical formula: C<sub>18</sub>H<sub>15</sub>ClN<sub>2</sub>O<sub>3</sub>Molecular Weight: 342.78 g.mol<sup>-1</sup>

Yield: 94%

To a solution of **65** (2.00 g, 5.27 mmol) in THF (50 ml) cooled at 0 °C, NaH (60% in mineral oil, 0.30 g, 7.38 mmol) was added slowly and the mixture was heated at 50 °C for 4 h. The mixture was quenched at ambient temperature by the dropwise addition of acetic acid (glacial, 1 ml). The solvent was evaporated *in vacuo*, and the remaining residue was taken up in water (200 ml). The precipitate formed was filtered, was washed with water (2 x 100 ml) and was dried *in vacuo* to afford **66** as yellow powder (1.69 g, 94%).

**<sup>1</sup>H NMR (CDCl<sub>3</sub>, 600 MHz)** δ ppm: 8.70 (1H, d, *J* = 2.0, CH-6), 8.55 (1H, s, CH-2), 7.68 (1H, d, *J* = 2.0, CH-8), 7.46-7.33 (3H, m, meta Ph-CH, para Ph-CH), 7.17 (2H, d, *J* = 7.9, ortho Ph-CH), 5.37 (2H, s, CH<sub>2</sub>Ph), 4.40 (2H, q, *J* = 7.2, CH<sub>2</sub>CH<sub>3</sub>), 1.40 (3H, t, *J* = 7.2, CH<sub>3</sub>)

**<sup>13</sup>C NMR (CDCl<sub>3</sub>, 150 MHz)** δ ppm: 172.8 (C<sub>Q</sub>-4), 164.8 (C<sub>Q</sub>OOCH<sub>2</sub>), 149.5 (CH-2), 146.9 (CH-6), 141.9 (C<sub>Q</sub>-4' or C<sub>Q</sub>-7), 136.8 (C<sub>Q</sub>-8'), 134.9 (C<sub>Q</sub>-4' or C<sub>Q</sub>-7), 133.1 (Ph-C<sub>Q</sub>), 129.9 (meta Ph-CH), 129.3 (para Ph-CH), 126.2 (ortho Ph-CH), 124.5 (CH-8), 114.7 (C<sub>Q</sub>-3), 61.5 (CH<sub>2</sub>CH<sub>3</sub>), 57.3 (CH<sub>2</sub>Ph), 14.3 (CH<sub>3</sub>)

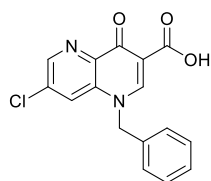
**HRMS (ES+) m/z:** Calcd. [M+Na]<sup>+</sup> 365.0699  
Measured 365.0687

**LRMS (ES+) m/z:** 367 (34), 365 (100, [M+Na]<sup>+</sup>), 345 (34), 343 (97, [M+H]<sup>+</sup>), 315 (22), 132 (18)

**IR v<sub>max</sub> (neat/cm<sup>-1</sup>):** 3075, 3052 (Ar C-H), 2925, 2853 (Alkyl C-H), 1721 (C=O), 1631 (C=N-), 1608, 1576 (Ar C=C), 1528

**m.p.:** 200 - 204 °C (dec.)

### 1-Benzyl-7-chloro-4-oxo-1,4-dihydro-[1,5]naphthyridine-3-carboxylic acid (**67**)



Beige powder

Chemical formula: C<sub>16</sub>H<sub>11</sub>ClN<sub>2</sub>O<sub>3</sub>

Molecular Weight: 314.72 g.mol<sup>-1</sup>

Yield: 90%

A mixture of **66** (1.66 g, 4.84 mmol) and NaOH (1 M, 5.33 ml) in THF (50 ml), was heated to 60 °C for 3 h. After cooling to ambient temperature the solvent was evaporated *in vacuo* and the remaining residue was dissolved in water (50 ml). The aqueous solution was washed with DCM (2 x 50 ml) and was acidified to pH 5 by addition of HCl (aq. 37 %). The precipitate formed was filtered, was washed with water (2 x 100 ml) and was dried *in vacuo* to afford **67** as a beige solid (1.37 g, 90%).

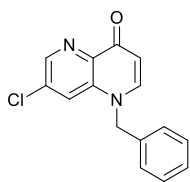
**<sup>1</sup>H NMR (600 MHz, DMSO-d<sub>6</sub>)** δ ppm: 14.95 (1H, s, COOH), 9.28 (1H, s, CH-2), 8.93 (1H, d, *J* = 2.0, CH-6), 8.55 (1H, d, *J* = 2.0, CH-8), 7.37 (2H, t, *J* = 7.3, meta Ph-CH), 7.34-7.24 (3H, m, ortho Ph-CH, para Ph-CH), 5.89 (2H, s, CH<sub>2</sub>)

**<sup>13</sup>C NMR (150 MHz, DMSO-d<sub>6</sub>)** δ ppm: 177.1 (C<sub>Q</sub>-4), 165.6 (C<sub>Q</sub>OOH), 150.6 (CH-2), 147.6 (CH-6), 139.2 (C<sub>Q</sub>-4'), 137.7 (C<sub>Q</sub>-8'), 134.8 (Ph-C<sub>Q</sub> or C<sub>Q</sub>-7), 134.7 (Ph-C<sub>Q</sub> or C<sub>Q</sub>-7), 129.1 (meta Ph-CH), 128.3 (para Ph-CH), 126.9 (ortho Ph-CH), 126.4 (CH-8), 111.3 (C<sub>Q</sub>-3), 55.9 (CH<sub>2</sub>Ph)

**HRMS (ES+) m/z:** Calcd. [M+H]<sup>+</sup> 315.0536  
Measured 315.0539

**LRMS (ES+) m/z:** 339 (18), 337 (73, [M+Na]<sup>+</sup>), 334 (48), 317 (31), 315 (100, [M+H]<sup>+</sup>), 132 (60)

**IR v<sub>max</sub> (neat/cm<sup>-1</sup>):** 3016 (Ar C-H), 2920, 2849 (Alkyl C-H), 1729 (C=O), 1612 (C=N-), 1578 (Ar C=C), 1551, 1524, 1507

**1-benzyl-7-chloro-1,5-naphthyridin-4(1H)-one (68)**

Orange/brown powder

Chemical formula: C<sub>15</sub>H<sub>11</sub>ClN<sub>2</sub>OMolecular Weight: 270.71 g.mol<sup>-1</sup>

Yield: 74%

To a mixture of **67** (0.50g, 1.59 mmol) in biphenyl ether (15 g), HCl (36%, 0.32 ml) was added and the mixture was stirred at ambient temperature for 10 min. The mixture was then heated at 280 °C for 7 h. The resulting solution was cooled at 40 °C and petroleum ether (150 ml) was added while stirring vigorously. The precipitate formed was filtered and was washed with petrol (2 x 100 ml). Purification *via* column chromatography (EtOAc → 1:2:17 NEt<sub>3</sub>:MeOH:EtOAc) to afford **68** as a brown powder (0.32g, 74%).

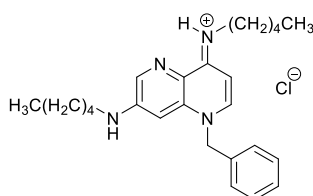
<sup>1</sup>H NMR (600 MHz, DMSO-d<sub>6</sub>) δ ppm: 8.64 (1H, d, *J* = 2.0, CH-6), 8.25 (1H, d, *J* = 2.0, CH-8), 8.23 (1H, d, *J* = 7.8, CH-2), 7.35 (2H, t, *J* = 7.7, meta Ph-CH), 7.29 (1H, t, *J* = 7.7, para Ph-CH), 7.21 (2H, t, *J* = 7.7, ortho Ph-CH), 6.37 (1H, d, *J* = 7.8, CH-3), 5.55 (2H, s, CH<sub>2</sub>)

<sup>13</sup>C NMR (150 MHz, DMSO-d<sub>6</sub>) δ ppm: 175.4 (C<sub>Q</sub>-4), 145.4 (CH-2), 144.7 (CH-6), 139.6 (C<sub>Q</sub>-4'), 137.5 (C<sub>Q</sub>-8'), 135.7 (Ph-C<sub>Q</sub>), 133.1 (C<sub>Q</sub>-7), 129.0 (meta Ph-CH), 128.0 (para Ph-CH), 126.4 (ortho Ph-CH), 125.1 (CH-8), 112.6 (CH-3), 54.5 (CH<sub>2</sub>Ph)

HRMS (CI) m/z: Calcd. [M+H]<sup>+</sup> 271.0638  
Measured 271.0632

LRMS (CI) m/z: 273 (15), 271 (37, [M+H]<sup>+</sup>), 245 (23), 218 (75), 91 (100)

IR ν<sub>max</sub> (neat/cm<sup>-1</sup>): 3025 (Ar C-H), 2975, 2942, 2879 (Alkyl C-H), 2735, 2600, 2528, 2494, 1622, 1575 (Ar C=C), 1524

**(E)-N-(1-benzyl-7-(pentylamino)-1,5-naphthyridin-4(1H)-ylidene)pentan-1-aminium chloride (69)**

Brown solid

Chemical formula: C<sub>25</sub>H<sub>34</sub>N<sub>4</sub> · HClMolecular Weight: 427.02 g.mol<sup>-1</sup>

Yield: 59%

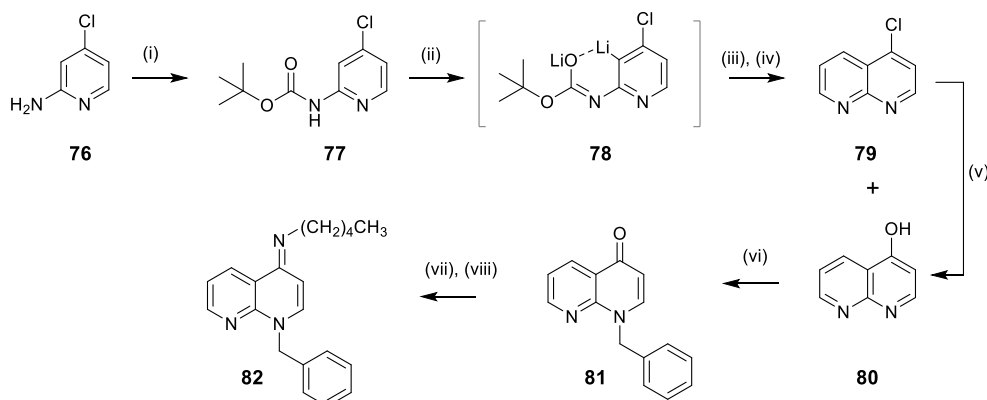
A solution of **68** (0.28 g, 1.02 mmol) in POCl<sub>3</sub> (5 ml), was heated to reflux at 110 °C for 2 h. After cooling at ambient temperature, the mixture was evaporated *in vacuo*, DCM (50 ml) was added and the mixture was evaporated again. The remaining residue was triturated with ether. To the resulting precipitate amylamine (6.00 ml, 0.05 mol) was added dropwise, and the solution was stirred R.T. for 18 h and at 80 °C for 6 h further. The solution was poured into an ice (~30 cm<sup>3</sup>) and NaOH (2 M, 20 ml) mixture while stirring vigorously. The organic products were extracted with DCM (2 x 50 ml), the organic extracts were dried over anh. MgSO<sub>4</sub> and were evaporated *in vacuo*. Purification *via* flash column chromatography (EtOAc → 1:2:7 NEt<sub>3</sub>:MeOH:EtOAc) afforded **69** as a brown solid (0.26 g, 59%).

HRMS (ES+) m/z: Calcd. [M+H]<sup>+</sup> 391.2862  
Measured 391.2856

LRMS (EI) m/z: 392 (32), 391 (100, [M+H]<sup>+</sup>)

IR  $\nu_{\max}$  (neat/cm<sup>-1</sup>): 3211 (N-H), 3047, 2956 (Ar C-H), 2927, 2857 (Alkyl C-H), 1622 (C=N-), 1601, 1578 (Ar C=C), 1546, 1523

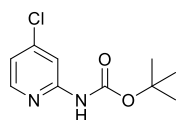
m.p.: 160 - 161 °C



**Scheme 35.** Synthesis of naphthyridine 82.

Reagents and conditions: (i) Di-*tert*-butyl dicarbonate, LiHMDS, THF, -5–0 °C, 2 h (ii) *n*-BuLi, HMPA, THF, -78 °C, 1 h (iii) -78 °C, 1.5 h (iv) HCl (aq.), 100 °C, 3 h (v) CH<sub>3</sub>COOH, 125 °C, 1.5 h (vi) Benzyl bromide, K<sub>2</sub>CO<sub>3</sub>, DMF, 80 °C, 3 h (vii) POCl<sub>3</sub>, 110 °C, 1.5 h (viii) *n*-pentylamine, MeOH, rt, 18 h.

***tert*-butyl (4-chloropyridin-2-yl)carbamate (77)**



White powder

Chemical formula: C<sub>10</sub>H<sub>13</sub>ClN<sub>2</sub>O<sub>2</sub>

Molecular Weight: 228.67 g.mol<sup>-1</sup>

Yield: 77%

To a solution of LiHMDS (48.0 mmol, 1M in THF) cooled at -5 °C under Ar atmosphere, a solution of 4-chloro-pyridine-2-amine (3.70 g, 28.9 mmol) in THF (50 ml) was added and the mixture was stirred at -5 °C for 5 min. A solution of di-*tert*-butyl-dicarbonate (4.40 g, 20.0 mol) in THF (40 ml) was then added, and the resulting mixture was stirred at 0 °C for 2 h. The resulting solution was allowed to warm to R.T and the solvents were evaporated *in vacuo*. To the resulting residue, water was added (100 ml) and the pH of the solution was adjusted to 6 by the slow addition of HCl (1M). The organic products were extracted with EtOAc (3 x 75 ml), the combined organic extracts were washed with NaHCO<sub>3</sub> (1M) (2 x 100 ml), water (2 x 100 ml) and brine (100 ml), were dried over anh. MgSO<sub>4</sub> and were evaporated *in vacuo*. The resulting precipitate was triturated with MeOH (2 x 20 ml) and dried *in vacuo* to afford pure **77** as white powder (3.52 g, 77%).

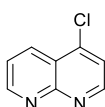
<sup>1</sup>H NMR (600 MHz, CDCl<sub>3</sub>) δ ppm: 8.54 (1H, s, br, NH), 8.18 (1H, d, *J* = 5.5, CH-6), 8.07 (1H, d, *J* = 1.8, CH-3), 6.96 (1H, dd, *J* = 5.5, 1.8, CH-5), 1.54 (9H, s, (CH<sub>3</sub>)<sub>3</sub>)

<sup>13</sup>C NMR (150 MHz, CDCl<sub>3</sub>) δ ppm: 153.4 (C<sub>Q</sub>=O or C<sub>Q</sub>-2), 152.4 (C<sub>Q</sub>=O or C<sub>Q</sub>-2), 148.5 (CH-6), 146.0 (C<sub>Q</sub>-4), 118.9 (CH-5), 112.6 (CH-3), 81.6 (C<sub>Q</sub>(CH<sub>3</sub>)<sub>3</sub>) 28.4 ((CH<sub>3</sub>)<sub>3</sub>)

HRMS (EI) *m/z*: Calcd. [M]<sup>+</sup> 228.0660  
Measured 228.0663

**LRMS (EI) m/z:** 230 (10), 228 (25, [M]<sup>+</sup>), 174 (14), 172 (39, [M+H-C(CH<sub>3</sub>)]<sup>+</sup>), 157 (18), 155 (55, [M-OC(CH<sub>3</sub>)]<sup>+</sup>), 130 (32), 128 (100, [M+H-COOC(CH<sub>3</sub>)]<sup>+</sup>), 114 (8), 112 (27, [M-NHCOOC(CH<sub>3</sub>)]<sup>+</sup>), 27)  
**IR v<sub>max</sub> (neat/cm<sup>-1</sup>):** 3057 (Ar C-H), 3021, 2973 (alkyl C-H), 2921, 2847, 1719 (C=O), 1574 (C=N-), 1512 (Ar C=C)  
**m.p.:** 145 - 146 °C

#### 4-chloro-1,8-naphthyridine (79)



Brown amorphous solid  
 Chemical formula: C<sub>8</sub>H<sub>5</sub>ClN<sub>2</sub>  
 Molecular Weight: 164.59 g.mol<sup>-1</sup>  
 Yield: 39%

To a solution of **77** (3.78 g, 16.5 mmol) in THF (50 ml) cooled at -78 °C under Ar atmosphere, HMPA (5.30 ml, 38.4 mmol) was added, followed by *n*-Buli (15 ml, 2.5M in hexane) and the resulting solution was stirred at -78 °C for 1 h. 3-Dimethylaminoacrolein (1.66 ml, 16.5 mmol) was then added dropwise and the resulting mixture was stirred at -78 °C for 1.5 h. The reaction was quenched by the dropwise addition of HCl (2M, aq.) to pH 8. The organic layer was separated and then extracted with HCl (2 M, aq) (2 x 40 ml). The acidic extracts were heated to reflux for 3 h. After cooling at R.T, K<sub>2</sub>CO<sub>3</sub> (anh., 40 g) was added, and the resulting mixture was extracted with EtOAc (3 x 10 ml), decanting the organic extracts. The organic extracts were dried over anh. MgSO<sub>4</sub>, and evaporated. Purification by column chromatography (EtOAc → 1:20 MeOH:EtOAc) afforded pure **79** as brown solid (1.05 g, 39%).

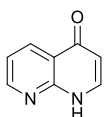
**<sup>1</sup>H NMR (600 MHz, CDCl<sub>3</sub>)** δ ppm: 9.17 (1H, dd, *J*= 4.2, 2.0, CH-7), 9.04 (1H, d, *J*= 4.7, CH-2) 8.64 (1H, dd, *J*= 8.4, 2.0, CH-5), 7.63 (1H, dd, *J*= 8.4, 4.2, CH-6), 7.61 (1H, d, *J*= 4.7, CH-3)

**<sup>13</sup>C NMR (150 MHz, CDCl<sub>3</sub>)** δ ppm: 156.4 (C<sub>Q</sub>-8'), 154.5 (CH-7), 153.2 (CH-2), 143.4 (C<sub>Q</sub>-4), 134.1 (CH-5), 123.2 (CH-6), 122.4 (CH-3), 121.9 (C<sub>Q</sub>-4')

**HRMS (EI) m/z:** Calcd. [M]<sup>+</sup> 164.0136  
 Measured 164.0137

**LRMS (EI) m/z:** 166 (32), 164 (100, [M]<sup>+</sup>), 129 (38, [M-Cl]<sup>+</sup>), 102 (43), 75 (16)  
**IR v<sub>max</sub> (neat/cm<sup>-1</sup>):** 3362, 3029 (Ar C-H), 1623, (C=N-), 1585 (Ar C=C), 1546, 1516  
**m.p.:** 52 - 53 °C

#### 1,8-naphthyridin-4(1H)-one (80)



Brown amorphous solid  
 Chemical formula: C<sub>8</sub>H<sub>6</sub>N<sub>2</sub>O  
 Molecular Weight: 146.15 g.mol<sup>-1</sup>  
 Yield: 92%

A solution of **79** (0.74 g, 4.48 mmol) in glacial acetic acid (1.85 ml) was heated to reflux at 125 °C for 1.5 h. After cooling at R.T, Et<sub>2</sub>O (100 ml) was added and the precipitate formed was filtered, was washed with Et<sub>2</sub>O (2 x 50 ml) and pentane (2 x 50 ml), and was dried *in vacuo*. Recrystallization (CHCl<sub>3</sub>, MeOH) afforded pure **80** (0.60 g, 92%) as brown solid.



**<sup>1</sup>H NMR (600 MHz, DMSO-*d*<sub>6</sub>)** δ ppm: 13.52 (1H, s, br, NH), 8.92 (1H, dd, *J* = 4.4, 2.0, CH-7), 8.59 (1H, dd, *J* = 8.1, 2.0, CH-5), 8.35 (1H, d, *J* = 7.2, CH-2), 7.59 (1H, dd, *J* = 8.1, 4.4, CH-6), 6.65 (1H, d, *J* = 7.2, CH-3)

**<sup>13</sup>C NMR (150 MHz, DMSO-*d*<sub>6</sub>)** δ ppm: 175.1 (C<sub>Q</sub>-4), 154.6 (CH-7), 149.8 (C<sub>Q</sub>-8'), 143.2 (CH-2), 134.4 (CH-5), 121.4 (CH-6), 118.53 (C<sub>Q</sub>-4'), 108.4 (CH-3)

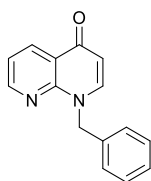
**HRMS (EI) m/z:** Calcd. [M]<sup>+</sup> 146.0475  
Measured 146.0478

**LRMS (EI) m/z:** 146 (100, [M]<sup>+</sup>), 118 (48, [M-CO]<sup>+</sup>), 91 (18), 78 (19)

**IR v<sub>max</sub> (neat/cm<sup>-1</sup>):** 3225, 3029 (Ar C-H), 2844, 2780, 1593 (Ar C=C), 1510

**m.p.:** 207 - 211 °C (dec.)

### 1-benzyl-1,8-naphthyridin-4(1*H*)-one (**81**)



Light brown powder

Chemical formula: C<sub>15</sub>H<sub>12</sub>N<sub>2</sub>O

Molecular Weight: 236.27 g.mol<sup>-1</sup>

Yield: 80%

To a solution of **80** (0.51 g, 3.42 mmol) in DMF (5 ml), K<sub>2</sub>CO<sub>3</sub> (0.57 g, 4.12 mmol) was added and the mixture was stirred at rt for 10 min. Benzyl bromide (0.42 ml, 3.54 mmol) was then added and the resulting mixture was stirred at 80 °C for 3 h. After cooling at R.T., the mixture was poured onto an ice (~50 cm<sup>3</sup>) and NaOH (2M, 30 ml) mixture and was stirred for 10 min. The organic products were extracted with DCM (2 x 100 ml), the organic extracts were dried over MgSO<sub>4</sub> and were evaporated *in vacuo*. The crude residue was purified by column chromatography (EtOAc → 1:10 MeOH:EtOAc) to afford pure **81** as a tan solid (0.66 g, 80%).

**<sup>1</sup>H NMR (600 MHz, CDCl<sub>3</sub>)** δ ppm: 8.75-8.70 (2H, m, CH-5, CH-7), 7.75 (1H, d, *J* = 7.8, CH-2), 7.36 (1H, dd, *J* = 7.9, 4.6, H-6), 7.35-7.28 (3H, m, meta Ph-CH, para Ph-CH), 7.24 -7.28 (2H, m, ortho Ph-CH), 6.38 (1H, d, *J* = 7.8, CH-3), 5.62 (2H, s, CH<sub>2</sub>)

**<sup>13</sup>C NMR (150 MHz, CDCl<sub>3</sub>)** δ ppm: 178.8 (C<sub>Q</sub>-4), 152.6 (CH-5 or CH-7), 150.1 (C<sub>Q</sub>-8'), 143.2 (CH-2), 136.4 (Ph-C<sub>Q</sub>), 136.2 (CH-5 or CH-7), 129.2 (meta Ph-CH), 128.3 (para Ph-CH), 127.6 (ortho Ph-CH), 121.9 (C<sub>Q</sub>-4'), 120.1 (CH-6), 111.5 (CH-3), 53.0 (CH<sub>2</sub>Ph)

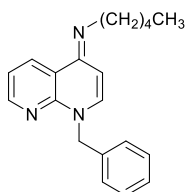
**HRMS (EI) m/z:** Calcd. [M]<sup>+</sup> 236.0944  
Measured 236.0948

**LRMS (EI) m/z:** 236 (59, [M]<sup>+</sup>), 91 (100, [PhCH<sub>2</sub>]<sup>+</sup>)

**IR v<sub>max</sub> (neat/cm<sup>-1</sup>):** 3057 (Ar C-H), 2988, 1641, 1616, 1578 (Ar C=C), 1549

**m.p.:** 124 - 126 °C

### (1-Benzyl-1*H*-[1,8]naphthyridin-4-ylidene)-pentyl-amine (**82**)



Dark orange needles/crystals

Chemical formula: C<sub>20</sub>H<sub>23</sub>N<sub>3</sub>

Molecular Weight: 305.42 g.mol<sup>-1</sup>

Yield: 90%

A solution of **81** (0.53 g, 2.23 mmol) in POCl<sub>3</sub> (8 ml) was heated to reflux at 110 °C for 1.5 h. After cooling at R.T., DCM (10 ml) was added, and the solvents were evaporated *in vacuo*. The resulting residue was dissolved in MeOH (8 ml),

amylamine (0.52 ml, 4.47 mmol) was added dropwise and the mixture was stirred at R.T. for 18 h. The mixture was poured into an ice (~50 cm<sup>3</sup>) and NaOH (2M, 30 ml) mixture and was stirred for 10 min. The organic products were extracted with DCM (3 x 100 ml), the organic extracts were dried over anh. MgSO<sub>4</sub> and were evaporated *in vacuo*. Purification *via* flash column chromatography (EtOAc → 1:20 NEt<sub>3</sub>:EtOAc), followed by recrystallisation (petroleum ether) afforded pure **82** as an orange solid (0.61 g, 90%).

**<sup>1</sup>H NMR (600 MHz, CDCl<sub>3</sub>, heated at 60 °C)** δ ppm: 8.74 (1H, m, *CH*-7), 8.45 (1H, dd, *J*= 5.5, 1.9, *CH*-5), 7.35-7.25 (5H, m, Ph-*CH*), 7.11 (1H, dd, *J*= 7.9, 4.6, *CH*-6), 7.03 (1H, d, *J*= 8.2, *CH*-2), 6.02 (1H, d, *J*= 8.2, *CH*-3), 5.37 (2H, s, CH<sub>2</sub>Ph), 3.36 (2H, t, *J*=7.2, NCH<sub>2</sub>), 1.76 (2H, qn, *J*= 7.2, NCH<sub>2</sub>CH<sub>2</sub>), 1.50-1.38 (4H, m, CH<sub>2</sub>CH<sub>2</sub>CH<sub>3</sub>), 0.96 (3H, t, *J*= 7.2, CH<sub>3</sub>)

**<sup>13</sup>C NMR (150 MHz, CDCl<sub>3</sub>, RT)** δ ppm: 154.8 (C<sub>Q</sub>), 149.8 (CH), 149.7 (C<sub>Q</sub>), 138.0 (CH), 137.6 (C<sub>Q</sub>), 134.1 (CH), 128.8 (CH), 127.7 (CH), 127.4 (CH), 121.1 (C<sub>Q</sub>), 119.2 (CH), 100.1 (CH), 51.7 (CH<sub>2</sub>), 50.5 (CH<sub>2</sub>), 30.9 (CH<sub>2</sub>), 30.2 (CH<sub>2</sub>), 22.9 (CH<sub>2</sub>), 14.3 (CH<sub>3</sub>)

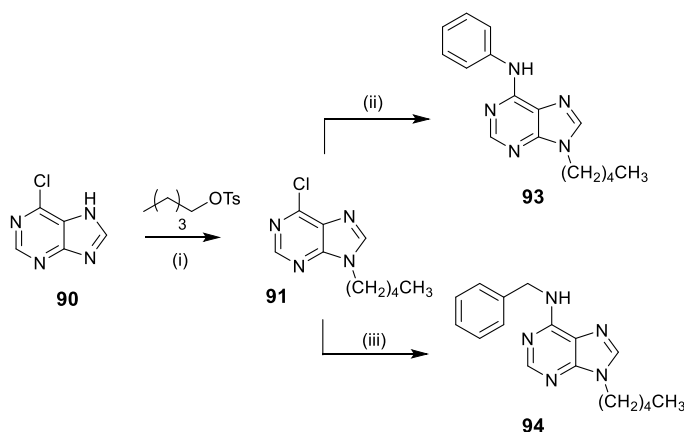
**HRMS (EI) m/z:** Calcd. [M]<sup>+</sup> 305.1886  
Measured 305.1893

**LRMS (EI) m/z:** 305 (6, [M]<sup>+</sup>), 262 (13, [M-CH<sub>2</sub>CH<sub>2</sub>CH<sub>3</sub>]<sup>+</sup>), 248 (22, [M-CH<sub>2</sub>(CH<sub>2</sub>)<sub>2</sub>CH<sub>3</sub>]<sup>+</sup>), 158 (10), 130 (9), 91 (100, [PhCH<sub>2</sub><sup>+</sup>])

**IR ν<sub>max</sub> (neat/cm<sup>-1</sup>):** 3063 (Ar C-H), 3026, 2950, 2923, 2856, 2838 (Alkyl C-H), 2809, 1630, 1588 (Ar C=C), 1570

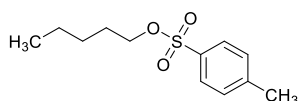
**m.p.:** 52 - 53 °C

### 8.1.3. Synthesis of *N*9-substitued-6-aminoaryl-purines and *N*-substituted-4-imino-1,4-dihydro-pyridines



**Scheme 36.** Synthesis of purines **93** and **94**.

Reagents and conditions: (i) NaH, DMF, rt, 24 h (ii) Aniline, NEt<sub>3</sub>, *n*-pentanol, 110 °C, 24 h (iii) Benzylamine, EtOH, reflux, 3 h

**Pentyl 4-methylbenzenesulfonate**

Colourless oil

Chemical formula: C<sub>12</sub>H<sub>18</sub>O<sub>3</sub>SMolecular weight: 242.33 g.mol<sup>-1</sup>

Yield: 57%

To a solution of tosyl chloride (4.75 g, 24.91 mmol) in DCM (15 ml) cooled at 0 °C, pentan-1-ol (1.22 ml, 11.27 mmol) and pyridine (5 ml, 61.82 mmol) were added and the mixture was stirred at ambient temperature for 48 h. DCM was added until the cloudy solution turned clear. The solution was then washed with KHSO<sub>4</sub> (2 M, aq) (2 x 150 ml), with NaHCO<sub>3</sub> (1 M, aq), (2 x 150 ml) and brine (2 x 150 ml). The combined organic layers were dried over anh. MgSO<sub>4</sub> and evaporated *in vacuo*. Purification *via* flash column chromatography (petroleum ether → 1:19 Et<sub>2</sub>O:petroleum ether) afforded **pentyl 4-methylbenzenesulfonate** as colourless oil (1.56 g, 57%).

<sup>1</sup>H NMR (CDCl<sub>3</sub>, 600 MHz) δ ppm: 7.78 (2H, d, *J* = 8.3, ortho Ph-CH), 7.34 (2H, d, *J* = 8.3, meta Ph-CH), 4.01 (2H, t, *J* = 6.7, OCH<sub>2</sub>), 2.44 (3H, s, Ph-CH<sub>3</sub>), 1.63 (2H, q, *J* = 6.7, OCH<sub>2</sub>CH<sub>2</sub>), 1.32-1.17 (4H, m, CH<sub>2</sub>CH<sub>2</sub>CH<sub>3</sub>), 0.84 (3H, t, *J* = 7.0, CH<sub>2</sub>CH<sub>3</sub>)

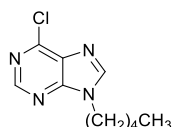
<sup>13</sup>C NMR (CDCl<sub>3</sub>, 150 MHz) δ ppm: 144.8 (C<sub>Q</sub>-SO<sub>2</sub>), 133.3 (Ph-C<sub>Q</sub>-CH<sub>3</sub>), 129.9 (meta Ph-CH), 128.0 (ortho Ph-CH), 70.9 (OCH<sub>2</sub>), 28.6 (OCH<sub>2</sub>CH<sub>2</sub>), 27.6 (CH<sub>2</sub>CH<sub>2</sub>CH<sub>3</sub>), 22.2 (CH<sub>2</sub>CH<sub>3</sub>), 21.8 (Ph-CH<sub>3</sub>), 14.1 (CH<sub>2</sub>CH<sub>3</sub>)

HRMS (CI) *m/z*: Calcd. [M+H]<sup>+</sup> 243.1055

Measured 243.1057

LRMS (CI) *m/z*: 485 (100), 397 (30), 243 (24)

IR *v*<sub>max</sub> (neat/cm<sup>-1</sup>): 2958 (Ar C-H), 2932, 2871 (aliphatic C-H), 1598 (Ar C=C)

**6-Chloro-9-pentyl-9H-purine (91)**

Light yellow oil

Chemical formula: C<sub>10</sub>H<sub>13</sub>ClN<sub>4</sub>Molecular weight: 224.69 g.mol<sup>-1</sup>

Yield: 48%

To a solution of 6-chloropurine (0.56 g, 3.62 mmol) in DMF (15 ml), NaH (60% in mineral oil, 0.16 g, 4.17 mmol) was added followed by **EYF162** (1.00 g, 4.13 mmol). The mixture was stirred at ambient temperature for 24 h. DCM (50 ml) was added and the resulting solution was washed with water (3 x 30 ml) and sat. LiCl (2 x 20 ml). The organic solution was dried over anh. MgSO<sub>4</sub> and evaporated *in vacuo*. Purification *via* column chromatography (EtOAc) afforded **91** as yellow oil (0.39 g, 48%).

<sup>1</sup>H NMR (CDCl<sub>3</sub>, 600 MHz) δ ppm: 8.74 (1H, s, CH-2), 8.11 (1H, s, CH-8), 4.28 (2H, t, *J* = 7.3, NCH<sub>2</sub>), 1.92 (2H, q, *J* = 7.3, NCH<sub>2</sub>CH<sub>2</sub>), 1.40-1.28 (4H, m, CH<sub>2</sub>CH<sub>2</sub>CH<sub>3</sub>), 0.88 (3H, t, *J* = 7.1, CH<sub>3</sub>)

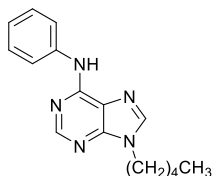
<sup>13</sup>C NMR (CDCl<sub>3</sub>, 150 MHz) δ ppm: 152.0 (CH-2), 151.9 (C<sub>Q</sub>-4), 151.1 (C<sub>Q</sub>-6), 145.2 (CH-8), 131.7 (C<sub>Q</sub>-5), 44.7 (NCH<sub>2</sub>), 29.7 (NCH<sub>2</sub>CH<sub>2</sub>), 28.8 (CH<sub>2</sub>CH<sub>2</sub>CH<sub>3</sub>), 22.2 (CH<sub>2</sub>CH<sub>3</sub>), 14.0 (CH<sub>3</sub>)

HRMS (EI) *m/z*: Calcd. [M]<sup>+</sup> 224.0823

Measured 224.0821

**LRMS (EI) m/z:** 226 (21), 224 (66, [M]<sup>+</sup>), 209 (15, [M-CH<sub>3</sub>]<sup>+</sup>), 195 (41, [M-CH<sub>2</sub>CH<sub>3</sub>]<sup>+</sup>), 182 (16, [M-CH<sub>2</sub>CH<sub>2</sub>CH<sub>3</sub>]<sup>+</sup>), 169 (30), 168 (100), 167 (73, [M-CH<sub>2</sub>(CH<sub>2</sub>)<sub>2</sub>CH<sub>3</sub>]<sup>+</sup>), 154 (73, [M+H-pentyl]<sup>+</sup>)  
**IR v<sub>max</sub> (neat/cm<sup>-1</sup>):** 3073 (Ar C-H), 2957, 2931, 2864 (aliphatic C-H), 1591 (Ar C=C), 1556

### 9-pentyl-N-phenyl-9H-purin-6-amine (93)



White crystalline solid  
 Chemical formula: C<sub>16</sub>H<sub>19</sub>N<sub>5</sub>  
 Molecular weight: 281.36 g.mol<sup>-1</sup>  
 Yield: 75%

To a solution of **91** (0.35 g, 1.58 mmol) in *n*-pentanol (5 ml), aniline (0.29 ml, 3.18 mmol), and NEt<sub>3</sub> (0.88 ml, 6.31 mmol) were added and the resulting mixture was heated at 110 °C for 24 h, under argon atmosphere. The resulting mixture was concentrated *in vacuo* and was purified *via* column chromatography (1:4 petroleum ether:EtOAc) followed by recrystallization (CHCl<sub>3</sub>, Et<sub>2</sub>O) to afford **93** as white crystalline solid (0.33 g, 75%).

**<sup>1</sup>H NMR (CDCl<sub>3</sub>, 600 MHz)** δ ppm: 8.55 (1H, s, CH-2), 7.82 (CH-8), 7.80 (2H, d, *J* = 7.7, ortho Ph-CH), 7.75 (1H, s, br, NH), 7.39 (2H, t, *J* = 7.7, meta Ph-CH), 7.11 (1H, t, *J* = 7.4, para Ph-CH), 4.22 (2H, t, *J* = 7.3, NCH<sub>2</sub>), 1.92 (2H, q, *J* = 7.3, NCH<sub>2</sub>CH<sub>2</sub>), 1.40-1.29 (4H, m, CH<sub>2</sub>CH<sub>2</sub>CH<sub>3</sub>), 0.90 (3H, t, *J* = 7.1, CH<sub>3</sub>)

**<sup>13</sup>C NMR (CDCl<sub>3</sub>, 150 MHz)** δ ppm: 152.9 (CH-2), 152.4 (C<sub>Q</sub>-6), 149.8 (C<sub>Q</sub>-4), 140.7 (CH-8), 138.8 (Ph-C<sub>Q</sub>), 129.2 (meta Ph-CH), 123.7 (para Ph-CH), 120.5 (C<sub>Q</sub>-5), 120.4 (ortho Ph-CH), 44.2 (NCH<sub>2</sub>), 30.0 (NCH<sub>2</sub>CH<sub>2</sub>), 28.9 (CH<sub>2</sub>CH<sub>2</sub>CH<sub>3</sub>), 22.3 (CH<sub>2</sub>CH<sub>3</sub>), 14.0 (CH<sub>3</sub>)

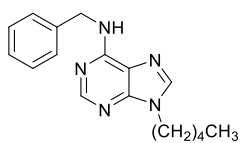
**HRMS (ES+) m/z:** Calcd. [M+H]<sup>+</sup> 282.1719  
 Measured 282.1719

**LRMS (ES+) m/z:** 283 (20), 282 (100, [M+H]<sup>+</sup>), 213 (10), 212 (68), 180 (13), 164 (9)

**IR v<sub>max</sub> (neat/cm<sup>-1</sup>):** 3281 (N-H), 3199, 3050 (Ar C-H), 2952, 2930, 2868 (aliphatic C-H), 1736, 1624 (Ar C=C), 1574

**m.p.:** 113-114 °C

### N-benzyl-9-pentyl-9H-purin-6-amine (94)



White powder  
 Chemical formula: C<sub>17</sub>H<sub>21</sub>N<sub>5</sub>  
 Molecular weight: 295.39 g.mol<sup>-1</sup>  
 Yield: 90%

To a solution of **91** (0.45 g, 2.00 mmol) in ethanol (15 ml), benzylamine (1.08 ml, 10.00 mmol), was added and the resulting mixture was heated at 70 °C, under argon atmosphere for 3 h. The resulting mixture was concentrated *in vacuo* and was purified by column chromatography (1:5 petroleum ether:EtOAc) followed by recrystallization (CHCl<sub>3</sub>) to afford **94** as white solid (0.53 g, 90%).

**<sup>1</sup>H NMR (CDCl<sub>3</sub>, 600 MHz)** δ ppm: 8.43 (1H, s, br, CH-2), 7.66 (1H, s, br, CH-8), 7.39 (2H, d, *J* = 7.6, ortho Ph-CH), 7.33 (2H, t, *J* = 7.6, meta Ph-CH), 7.28 (1H, t, *J* = 7.6, para Ph-CH), 6.21 (1H, s, br, NH), 4.87 (2H, s, br, CH<sub>2</sub>Ph), 4.17 (2H, t, *J* = 7.3, NCH<sub>2</sub>), 1.88 (2H, q, *J* = 7.3, NCH<sub>2</sub>CH<sub>2</sub>), 1.40-1.27 (4H, m, CH<sub>2</sub>CH<sub>2</sub>CH<sub>3</sub>), 0.89 (3H, t, *J* = 7.2, CH<sub>3</sub>)

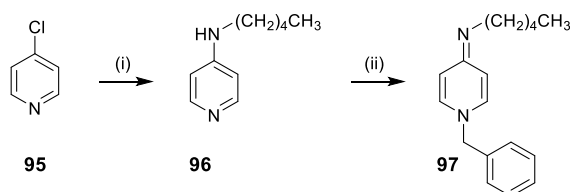
**$^{13}\text{C}$  NMR (CDCl<sub>3</sub>, 150 MHz)**  $\delta$  ppm: 154.8 (C<sub>Q</sub>-6), 153.2 (CH-2), 149.4 (C<sub>Q</sub>-4), 139.9 (CH-8), 138.6 (Ph-C<sub>Q</sub>), 128.8 (meta Ph-CH), 127.9 (ortho Ph-CH), 127.6 (para Ph-CH), 119.9 (C<sub>Q</sub>-5), 44.7 (CH<sub>2</sub>Ph), 44.0 (NCH<sub>2</sub>), 30.0 (NCH<sub>2</sub>CH<sub>2</sub>), 28.9 (CH<sub>2</sub>CH<sub>2</sub>CH<sub>3</sub>), 22.3 (CH<sub>2</sub>CH<sub>3</sub>), 14.0 (CH<sub>3</sub>)

**HRMS (EI) m/z:** Calcd. [M]<sup>+</sup> 295.1792  
Measured 295.1791

**LRMS (EI) m/z:** 296 (18), 295 (100, [M]<sup>+</sup>), 294 (21), 280 (8, [M-CH<sub>3</sub>]<sup>+</sup>), 252 (5, [M-CH<sub>2</sub>CH<sub>2</sub>CH<sub>3</sub>]<sup>+</sup>), 239 (11), 238 (16, [M-CH<sub>2</sub>(CH<sub>2</sub>)<sub>2</sub>CH<sub>3</sub>]<sup>+</sup>), 224 (10, [M-CH<sub>2</sub>(CH<sub>2</sub>)<sub>3</sub>CH<sub>3</sub>]<sup>+</sup>), 106 (7, [NH<sub>2</sub>CH<sub>2</sub>Ph]<sup>+</sup>)

**IR  $\nu_{\text{max}}$  (neat/cm<sup>-1</sup>):** 3268 (N-H), 3222, 3195, 3147, 3062, 3034 (Ar C-H), 2949, 2929, 2870 (aliphatic C-H), 1620 (Ar C=C), 1581, 1538

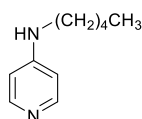
**m.p.:** 78 - 79 °C



### Scheme 37. Synthesis of pyridine **97**.

Reagents and conditions: (i) *n*-Pentylamine, 110 °C, 48 h (ii) Benzyl bromide, NaI, acetone, reflux, 8 h.

### *N*-pentylpyridin-4-amine (**96**)



Beige crystals

Chemical formula: C<sub>10</sub>H<sub>16</sub>N<sub>2</sub>

Molecular Weight: 164.25 g.mol<sup>-1</sup>

Yield: 51%

A solution of 4-chloropyridine hydrochloride (2.50 g, 16.65 mmol) in amylamine (10.64 ml, 0.09 mol) was heated to reflux at 110 °C for 48 h. After cooling to R.T, the solution was poured on ice (~50 cm<sup>3</sup>) while stirring vigorously. The organic products were extracted with DCM (2 x 100 ml) and the organic extracts were dried over anh. MgSO<sub>4</sub>, and were evaporated *in vacuo*. Purification *via* column chromatography (EtOAc → 1:5:20 NEt<sub>3</sub>:MeOH:EtOAc) afforded pure **96** as beige crystals (1.40 g, 51%).

**$^1\text{H}$  NMR (CDCl<sub>3</sub>, 500 MHz)**  $\delta$  ppm: 8.16 (2H, dd, *J* = 5.0, 1.6, CH-2, CH-6), 6.41 (2H, dd, *J* = 5.0, 1.6, CH-3, CH-5), 4.24 (1H, s, br, NH), 3.12 (1H, td, *J* = 7.2, 5.5, NHCH<sub>2</sub>), 1.61 (2H, qn, *J* = 7.2, NHCH<sub>2</sub>CH<sub>2</sub>), 1.40-1.33 (4H, m, CH<sub>2</sub>CH<sub>2</sub>CH<sub>3</sub>), 0.91 (3H, t, *J* = 6.8, CH<sub>3</sub>)

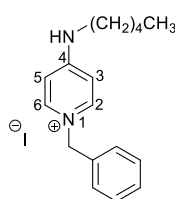
**$^{13}\text{C}$  NMR (CDCl<sub>3</sub>, 125 MHz)**  $\delta$  ppm: 153.6 (C<sub>Q</sub>-4), 149.9 (CH-2, CH-6), 107.5 (CH-3, CH-5), 42.7 (NHCH<sub>2</sub>), 29.2 (NHCH<sub>2</sub>CH<sub>2</sub> or CH<sub>2</sub>CH<sub>2</sub>CH<sub>3</sub>), 28.9 (NHCH<sub>2</sub>CH<sub>2</sub> or CH<sub>2</sub>CH<sub>2</sub>CH<sub>3</sub>), 17.6 (CH<sub>2</sub>CH<sub>3</sub>), 14.1 (CH<sub>3</sub>)

**HRMS (EI) m/z:** Calcd. [M]<sup>+</sup> 164.1308  
Measured 164.1310

**LRMS (EI) m/z:** 164 (22, [M]<sup>+</sup>), 107 (100, [M-CH<sub>2</sub>(CH<sub>2</sub>)<sub>2</sub>CH<sub>3</sub>]<sup>+</sup>)

**IR  $\nu_{\text{max}}$  (neat/cm<sup>-1</sup>):** 3230 (N-H), 3138, 3026 (Ar C-H), 2995, 2927, 2862 (Alkyl C-H), 1603 (C=N-), 1531 (Ar C=C)

**m.p.:** 63 - 64 °C

***N*-(1-benzylpyridin-4(1*H*)-ylidene)pentan-1-amine hydroiodide (97)**

White crystals

Chemical formula: C<sub>17</sub>H<sub>22</sub>N<sub>2</sub> · HIMolecular Weight: 382.28 g.mol<sup>-1</sup>

Yield: 62%

A mixture of **96** (1.00 g, 6.09 mmol), benzyl bromide (0.79 ml, 6.69 mmol) and NaI (1.09 g, 7.30 mmol) in acetone (5 ml), was heated to reflux at 65 °C for 8 h. After cooling to R.T, the mixture was poured in an ice (~50 cm<sup>3</sup>) and NaOH (2M, 50 ml) mixture while stirring vigorously. The organic products were extracted with DCM (2 x 100 ml). The organic extracts were dried over anh. MgSO<sub>4</sub>, and evaporated *in vacuo*. Purification *via* flash column chromatography (EtOAc → 1:5:20 NEt<sub>3</sub>:MeOH:EtOAc) followed by recrystallization (propan-2-ol) afforded **97** as the hydroiodide salt as white crystals (1.44 g, 62%).

<sup>1</sup>H NMR (CDCl<sub>3</sub>, 600 MHz) δ ppm: 8.68 (1H, t, *J* = 6.7, NH), 8.16 (1H, dd, *J* = 7.4, 2.0, CH-2), 8.06 (1H, dd, *J* = 7.4, 2.0, CH-6), 7.60 (1H, dd, *J* = 7.4, 2.9, CH-5), 7.39-7.29 (5H, m, Ph-CH), 6.55 (1H, dd, *J* = 7.4, 2.9, CH-3), 5.43 (2H, s, CH<sub>2</sub>Ph), 3.23 (2H, q, *J* = 6.7, NCH<sub>2</sub>CH<sub>2</sub>), 1.73 (2H, qn, *J* = 6.7, NCH<sub>2</sub>CH<sub>2</sub>), 1.43-1.20 (4H, m, CH<sub>2</sub>CH<sub>2</sub>CH<sub>3</sub>), 0.85 (3H, t, *J* = 7.1, CH<sub>3</sub>)

<sup>13</sup>C NMR (CDCl<sub>3</sub>, 150 MHz) δ ppm: 157.1 (C<sub>Q</sub>-4), 143.0 (CH-2), 140.6 (CH-6), 133.9 (Ph-C<sub>Q</sub>), 129.6 (ortho Ph-CH or meta Ph-CH), 129.5 (para Ph-CH), 128.6 (ortho Ph-CH or meta Ph-CH), 111.5 (CH-5), 105.5 (CH-3), 61.0 (CH<sub>2</sub>Ph), 43.4 (NHCH<sub>2</sub>), 29.2 (CH<sub>2</sub>CH<sub>2</sub>CH<sub>3</sub>), 27.9 (NHCH<sub>2</sub>CH<sub>2</sub>), 22.4 (CH<sub>2</sub>CH<sub>3</sub>), 14.1 (CH<sub>3</sub>)

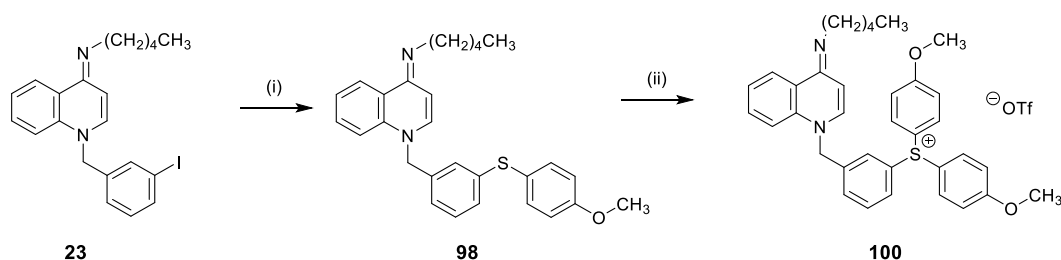
HRMS (CI) *m/z*: Calcd. [M+H]<sup>+</sup> 255.1861

Measured 255.1859

LRMS (CI) *m/z*: 255 (100, [M+H]<sup>+</sup>)

IR ν<sub>max</sub> (neat/cm<sup>-1</sup>): 3210 (N-H), 3125, 3043 (Ar C-H), 3016, 2948, 2924, 2862 (alkyl C-H), 1641 (C=N-), 1575 (Ar C=C), 1551, 1517

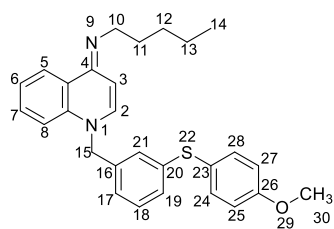
m.p.: 108 - 109 °C

**8.1.4. Synthesis of sulfonium salt 100****Scheme 38.** Synthesis of the sulfonium salt **100**.

Reagents and conditions: (i) 4-methoxythiophenol, Pd<sub>2</sub>(dba)<sub>3</sub>, DPEPhos, <sup>t</sup>BuOK, toluene, 100 °C, 3 h (ii) 99, Cu(II) benzoate, TFSA, chlorobenzene, 125 °C, 2.5 h.

***N*-(1-(3-iodobenzyl)quinolin-4(1*H*)-ylidene)pentan-1-amine (23)**

Synthesis described in page 148.

**(1-[3-(4-Methoxy-phenylsulfanyl)-benzyl]-1*H*-quinolin-4-ylidene)-pentyl-amine, (98)**

Yellow oil

Chemical formula: C<sub>28</sub>H<sub>30</sub>N<sub>2</sub>OSMolecular Weight: 442.62 g.mol<sup>-1</sup>

Yield: 63%

In a flame dried, three-necked round bottom flask, Pd<sub>2</sub>dba<sub>3</sub> (19 mg, 0.02 mmol), DPEPhos (23 mg, 0.04 mmol) and toluene (35 ml) were added and the resulting solution was stirred under an atmosphere of argon for 10 min. **23** (0.89 g, 2.07 mmol), 4-methoxythiophenol (254 μl, 2.07 mmol) and K<sup>t</sup>OBu (0.28 g, 2.49 mmol) were added and the mixture was heated at 100 °C for 3 h. The mixture was cooled to room temperature, was passed over a pad of celite and was evaporated *in vacuo*. The resulting residue was purified by column chromatography using basic Al<sub>2</sub>O<sub>3</sub> as the solid phase (EtOAc → 3:17 MeOH:EtOAc) to afford **98** as viscous yellow oil (0.57 g, 63%).

*Note: 98 and 100 have very similar R<sub>f</sub> values therefore their separation using standard chromatographic means is not feasible; the reaction needs to proceed to completion for isolation of pure product.*

<sup>1</sup>H NMR (600 MHz, CDCl<sub>3</sub>) δ ppm: 9.22 (1H, dd, *J* = 8.2, 1.4, CH-5), 7.99 (1H, d, *J* = 7.6, CH-2), 7.64–7.53 (2H, m, CH-6, CH-7), 7.34–7.30 (3H, m, CH-8, CH-24, CH-28), 7.18 (1H, t, *J* = 7.8, CH-18), 7.02 (1H, dt, *J* = 7.8, 1.8, CH-19), 6.84 (2H, d, *J* = 8.9, CH-25, CH-27), 6.83–6.80 (1H, m, CH-17), 6.77 (1H, t, *J* = 1.8, CH-21), 6.32 (1H, d, *J* = 7.6, CH-3), 5.40 (2H, s, CH<sub>2</sub>-15), 3.83 (3H, s, CH<sub>3</sub>-30), 3.52 (2H, t, *J* = 7.5, CH<sub>2</sub>-10), 1.78 (2H, qn, *J* = 7.5, CH<sub>2</sub>-11), 1.43–1.33 (4H, m, CH<sub>2</sub>-12, CH<sub>2</sub>-13), 0.91 (3H, t, *J* = 7.0, CH<sub>3</sub>-14)

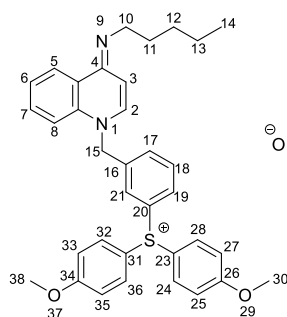
<sup>13</sup>C NMR (150 MHz, CDCl<sub>3</sub>) δ ppm: 160.5 (C<sub>Q</sub>-26), 156.2 (C<sub>Q</sub>-4), 144.5 (CH-2), 141.5 (C<sub>Q</sub>-16), 137.7 (C<sub>Q</sub>-8'), 136.3 (CH-24, CH-28), 134.9 (C<sub>Q</sub>-20), 133.6 (CH-7), 130.0 (CH-18), 127.8 (CH-5), 127.3 (CH-19), 126.8 (CH-6), 124.5 (CH-21), 123.1 (CH-17), 122.2 (C<sub>Q</sub>-23), 119.5 (C<sub>Q</sub>-4'), 116.5 (CH-8), 115.3 (CH-25, CH-27), 97.8 (CH-3), 57.2 (CH<sub>2</sub>-15), 55.6 (CH<sub>3</sub>-30), 44.5 (CH<sub>2</sub>-10), 29.4 (CH<sub>2</sub>-12), 27.9 (CH<sub>2</sub>-11), 22.6 (CH<sub>2</sub>-13), 14.2 (CH<sub>3</sub>-14)

HRMS (EI) *m/z*: Calcd. [M]<sup>+</sup> 442.2079  
Measured 442.2081

LRMS (EI) *m/z*: 442 (69, [M]<sup>+</sup>), 399 (100, [M-CH<sub>2</sub>CH<sub>2</sub>CH<sub>3</sub>]<sup>+</sup>), 385 (70, [M-HCH<sub>2</sub>(CH<sub>2</sub>)<sub>2</sub>CH<sub>3</sub>]<sup>+</sup>), 371 (16, [M-CH<sub>2</sub>(CH<sub>2</sub>)<sub>2</sub>CH<sub>3</sub>]<sup>+</sup>), 229 (20), 213 (9)

IR ν<sub>max</sub> (neat/cm<sup>-1</sup>): 3207, 3052 (Ar C-H), 2950, 2921, 2847 (Aliphatic C-H), 1619 (C=N), 1588 (Ar C=C), 1569

**(E)-bis(4-methoxyphenyl)(3-((4-(pentylimino)quinolin-1(4H)-yl)methyl)phenyl)sulfonium trifluoromethanesulfonate (100)**



Yellow oil

Chemical formula:  $C_{36}H_{37}F_3N_2O_5S_2$

Molecular weight:  $698.82 \text{ g}\cdot\text{mol}^{-1}$

Yield: 32%

To a solution of **98** (0.22 g, 0.49 mmol) in chlorobenzene (2.5 ml), trifluoromethanesulfonic acid (41  $\mu\text{l}$ , 0.47 mmol) was added and the solution was stirred at room temperature for 10 min. Bis(4-methoxyphenyl)iodonium triflate (0.20 g, 0.40 mmol) and copper (II) benzoate dihydrate (13 mg, 0.04 mmol) were then added and the mixture was heated at 125 °C for 2.5 h under an atmosphere of argon. After cooling to room temperature,  $\text{Et}_2\text{O}$  (10 ml) was added and the top layer was decanted. The resulting dark brown residue was purified by column chromatography ( $\text{CHCl}_3 \rightarrow 1:9 \text{ MeOH}:\text{CHCl}_3$ ). The oil obtained was diluted in DCM (20 ml) and was washed twice with NaOH (2M, 20 ml). The organic layer was dried over anhydrous  $\text{MgSO}_4$  and evaporated *in vacuo* to afford **100** as viscous pale yellow oil (0.90 g, 32%).

$^1\text{H NMR}$  (600 MHz,  $\text{CDCl}_3$ )  $\delta$  ppm: 8.47 (1H, dd,  $J = 8.1, 1.5$ , CH-5), 7.57 (1H, t,  $J = 7.8$ , CH-18), 7.53 (4H, d,  $J = 9.1$ , CH-24, CH-28, CH-32, CH-36), 7.52-7.49 (1H, m, CH-17), 7.45 (1H, dq,  $J = 8.0, 1.2$ , CH-19), 7.33-7.28 (2H, m, CH-2, CH-7), 7.27-7.25 (1H, m, CH-21), 7.17 (1H, ddd,  $J = 8.1, 7.1, 1.1$ , CH-6), 7.09 (4H, d,  $J = 9.1$ , CH-25, CH-27, CH-33, CH-35), 6.91 (1H, dd,  $J = 8.4, 1.1$ , CH-8), 6.02 (1H, d,  $J = 8.1$ , CH-3), 5.29 (2H, s,  $\text{CH}_2$ -15), 3.88 (6H, s,  $\text{CH}_3$ -30,  $\text{CH}_3$ -38), 3.33 (2H, t,  $J = 7.4$ ,  $\text{CH}_2$ -10), 1.74 (2H, qn,  $J = 7.4$ ,  $\text{CH}_2$ -11), 1.47-1.35 (4H, m,  $\text{CH}_2$ -12,  $\text{CH}_2$ -13), 0.93 (3H, t,  $J = 7.1$ ,  $\text{CH}_3$ -14)

$^{13}\text{C NMR}$  (150 MHz,  $\text{CDCl}_3$ )  $\delta$  ppm: 164.7 ( $\text{C}_\text{Q}$ -26,  $\text{C}_\text{Q}$ -34), 154.3 ( $\text{C}_\text{Q}$ -4), 141.1 ( $\text{C}_\text{Q}$ -16), 140.2 (CH-2), 138.0 ( $\text{C}_\text{Q}$ -8'), 133.2 (CH-24, CH-28, CH-32, CH-36), 131.9 (CH-17 or CH-18), 131.8 (CH-17 or CH-18), 130.6 (CH-7), 129.0 (CH-19), 127.8 (CH-21), 127.1 ( $\text{C}_\text{Q}$ -20), 125.7 (CH-5), 125.1 ( $\text{C}_\text{Q}$ -4'), 123.7 (CH-6), 121.0 ( $\text{C}_\text{Q}$ , q,  $^1J_{\text{CF}} = 319.9$ ,  $\text{CF}_3$ ), 117.4 (CH-25, CH-27, CH-33, CH-35), 115.2 (CH-8), 113.6 ( $\text{C}_\text{Q}$ -23,  $\text{C}_\text{Q}$ -31), 99.3 (CH-3), 56.2 ( $\text{CH}_3$ -30,  $\text{CH}_3$ -38), 54.5 ( $\text{CH}_2$ -15), 49.6 ( $\text{CH}_2$ -10), 30.7 ( $\text{CH}_2$ -11), 30.2 ( $\text{CH}_2$ -12), 22.9 ( $\text{CH}_2$ -13), 14.3 ( $\text{CH}_3$ -14)

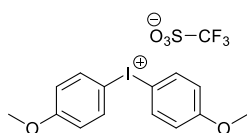
$^{19}\text{F NMR}$  (282 MHz,  $\text{CDCl}_3$ )  $\delta$  ppm: -78.23

HRMS (EI)  $m/z$ : Calcd.  $[\text{M}]^+$  549.2576  
Measured 549.2571

LRMS (EI)  $m/z$ : 549 (5,  $[\text{M}]^+$ ), 491 (12), 442 (55,  $[\text{M}-\text{PhOCH}_3]^+$ ), 399 (90,  $[\text{M}-\text{PhOCH}_3-\text{CH}_2\text{CH}_2\text{CH}_3]^+$ ), 385 (69,  $[\text{M}+\text{H}-\text{PhOCH}_3-\text{CH}_2(\text{CH}_2)_2\text{CH}_3]^+$ ), 371 (17,  $[\text{M}-\text{PhOCH}_3-\text{CH}_2(\text{CH}_2)_3\text{CH}_3]^+$ ), 246 (100,  $[\text{S}(\text{PhOCH}_3)_2]^+$ ), 231 (34), 214 (23), 84 (23)

IR  $\nu_{\text{max}}$  (neat/ $\text{cm}^{-1}$ ): 3060 (Ar C-H), 2925, 2848 (Aliphatic C-H), 1631 (C=N), 1586 (Ar C=C), 1572



**Bis(4-methoxyphenyl)iodonium trifluoromethanesulfonate (99)**

Light brown oil

Chemical formula: C<sub>15</sub>H<sub>14</sub>F<sub>3</sub>IO<sub>5</sub>SMolecular weight: 490.23 g.mol<sup>-1</sup>

Yield: 80%

To a solution of iodine (0.52 g, 2.0 mmol) and 3-chloroperbenzoic acid (0.8 g, 4.6 mmol) in DCM (15 ml) were added anisole (0.68 g, 6.2 mmol) and para-toluenesulfonic acid monohydrate (1.2 g, 6.3 mmol), and the mixture was stirred for 15 min at 40 °C. The red solution was cooled to 0 °C (ice bath) and trifluoromethanesulfonic acid (0.35 ml, 4 mmol) was added. The red slurry was stirred for 1 h at room temperature, diluted with DCM and purified by column chromatography (DCM: diethyl ether = 2: 1, DCM, DCM: methanol = 96: 4). The product was obtained as a light brown oil (1.2 g, 80%).

**<sup>1</sup>H NMR (600 MHz, DMSO-d<sub>6</sub>)** δ ppm: 8.12 (4H, d, *J* = 9.0, ortho Ph-*H*), 7.06 (4H, d, *J* = 9.0, meta Ph-*H*), 3.79 (6H, s, OCH<sub>3</sub>)

**<sup>13</sup>C NMR (150 MHz, DMSO-d<sub>6</sub>)** δ ppm: 161.8 (C<sub>Q</sub> para Ph), 136.9 (CH ortho Ph), 120.7 (C<sub>Q</sub>, q, <sup>1</sup>*J*<sub>CF</sub> = 321.3, CF<sub>3</sub>), 117.4 (CH meta Ph), 106.2 (C<sub>Q</sub> Ph), 55.7 (OCH<sub>3</sub>)

**<sup>19</sup>F NMR (282 MHz, DMSO-d<sub>6</sub>)** δ ppm: -78.2

<b>HRMS (EI) m/z:</b>	Calcd. [M] <sup>+</sup>	341.0039
	Measured	341.0031

### 8.1.5. Radiochemistry

#### [<sup>18</sup>F]N-(1-(3-Fluorobenzyl)quinolin-4(1*H*)-ylidene)pentan-1-amine ([<sup>18</sup>F]22)

[<sup>18</sup>F]Fluoride (650 MBq) in water was trapped on a Sep-Pak<sup>®</sup> QMA cartridge, released with a solution (0.5 ml) of Kryptofix 222 (30 mM) and potassium bicarbonate (30 mM) in acetonitrile: water (85:15). After removing the solvent by heating at 90 °C under a stream of nitrogen, acetonitrile (0.5 ml) was added, and the distillation was continued at 90 °C. This procedure was repeated and the reaction vial was subsequently capped. Compound **100** (5 mg) dissolved in DMSO (0.5 ml) was subsequently added and the mixture was stirred at 120 °C for 15 minutes. After cooling, the reaction was quenched with water (1.5 ml) and purified by radio-HPLC using an Agilent Zorbax<sup>®</sup> 300SB-C18 column (250 × 9.4 mm) at room temperature and with a flow rate of 3 ml/min. The mobile phase consisted of water and methanol, each containing 0.5% TFA. The radioactive product was isolated using a gradient starting with 10% methanol content kept constant for 5 min and then increased to 50%. The methanol content was subsequently raised from 50 to 60% in 10 min, further to 63% in 5 min, to 70% in 5 min, and finally to 90% in 5 min. Only the most concentrated fraction of the product peak was isolated. The obtained solution was diluted with water to a final volume of 20 ml, trapped on a Sep-Pak<sup>®</sup> SPE C-18 light cartridge, and the labelled product was released with ethanol (0.5 ml). After having reduced the volume to <0.1 ml under a stream of nitrogen, the solution was diluted with saline to give a final ethanol concentration of 5% and sterilized by filtration. Quality control was performed on an analytical Agilent Zorbax<sup>®</sup> 300SB-C18 column (150 × 4.6 mm) at room temperature and with a flow rate of 1 ml/min. The mobile phase consisted of water and methanol, each containing 0.5% TFA. Gradient elution started with 30% methanol content that was kept constant for 5 min, then increased to 50%, raised to 60% in 10 min, then further to 63% in 5 min. The radiochemical purity of [<sup>18</sup>F]22 was >98% and the specific activity of the tracer was 2.9 GBq/μmol. The identity of the radiochemical product was confirmed by coelution with the non-radioactive analogue.

## 8.2. Experimental for Chapter 4

The automated patch clamp electrophysiology study was outsourced to ChanTest Corporation. The experimental details below are reported as provided by the company.

### Chemicals

Chemicals were purchased from Sigma-Aldrich unless otherwise noted and were of ACS reagent grade purity or higher. Test compound and control solutions were prepared fresh daily by diluting stock solutions into a HEPES-buffered physiological saline (HB-PS) solution (composition in mM): NaCl, 137; KCl, 4.0; CaCl<sub>2</sub>, 1.8; MgCl<sub>2</sub>, 1; HEPES, 10; Glucose, 10; pH adjusted to 7.4 with NaOH. Test compound and control solutions contained 0.3% DMSO and 0.05% F-127.

### Cell culture procedures

Chinese hamster ovarian (CHO) cells were stably transfected with specific human Na<sub>v</sub>1.x channel cDNAs. Cells were cultured in Ham's F-12 supplemented with 10% fetal bovine serum, 100 U/mL penicillin G sodium, 100 µg/mL streptomycin sulfate, and the appropriate selection antibiotics. Before testing the cells in culture dishes these were washed twice with Hank's Balanced Salt Solution and treated with accutase for approximately 20 minutes. Immediately before use in the IonWorks Quattro™ system, the cells were washed with HB-PS to remove the accutase and re-suspended in approximately 3 mL of HB-PS. All experiments were performed at ambient temperature.

### Controls

Lidocaine was used as hNa<sub>v</sub>1.x positive control. A solution of HB-PS + 0.3% DMSO + 0.05% F-127 was used as vehicle control; HB-PS provides the appropriate ionic composition for *in vitro* hERG current recording.

### Automated patch clamp electrophysiological procedures

The test compound formulations were loaded in a glass-lined 384-well compound plate, and placed in the plate well of IonWorks Quattro™ or IonWorks™ Barracuda (Molecular Devices Corporation, Union City CA). Each test compound concentration was applied to naïve cells ( $n \geq 4$ , where  $n$  = the number cells/concentration).

In preparation for a recording session, intracellular solution was loaded into the intracellular compartment of the PPC planar electrode. Cell suspension was pipetted into the wells of the PPC planar electrode. After establishment of a whole-cell configuration, membrane currents were recorded using patch clamp amplifier in the IonWorks Quattro™ or the IonWorks™ Barracuda system. Before digitization, the current records were low-pass filtered at one-fifth of the sampling frequency. Block of Na<sub>v</sub> channels was measured using the stimulus voltage pattern described in section 4.2.

### 8.3. Experimental for Chapter 5

The skin-nerve experiments were performed at the UCL Institute of Neurology.

All animal work was performed in compliance with the United Kingdom Home Office's Animals (Scientific Procedures) Act 1986 and with approval of the University College London (UCL) Animal Ethics Committee.

#### Isolated Nerve Preparation

The skin-nerve *in vitro* preparation was used to record electrically evoked A- and C-fiber sensory nerve compound action potentials (CAP). Female Sprague-Dawley rats, weighing 300 to 400 g, were killed by cervical dislocation. The skin of the hind limb and the attached saphenous nerve were removed as previously described by Reeh *et. al.*<sup>210</sup> The preparation was mounted corium-side up in an organ bath and superfused with oxygenated synthetic interstitial fluid (SIF) consisting of 108 mM NaCl, 3.5 mM KCl, 3.5 mM MgSO<sub>4</sub>, 26 mM NaHCO<sub>3</sub>, 1.5 mM CaCl<sub>2</sub>, 9.6 mM sodium gluconate, 5.55 mM glucose, 7.6 mM sucrose, and 10 mM HEPES, at pH 7.4. The temperature of the bath was maintained at 32°C. The proximal end of the nerve was isolated from SIF by liquid paraffin. Recordings were obtained with a pair of gold-wire electrodes, a custom-made low-noise differential amplifier in common rejection mode, a low-pass filter of 1 kHz, and a high-pass filter of 1 Hz. A self-sealing stainless steel ring (inner diameter, 6 mm; outer diameter, 8 mm) was placed on top of a section of the saphenous nerve. In some experiments, the nerve section covered by the stainless steel ring was desheathed before the experiment. The whole nerve was stimulated using Ag/AgCl electrodes with a non-insulated tip diameter of 2 mm (EPO5; World Precision Instruments, Hertfordshire, UK) at a frequency of 1 Hz (A-volley) or 0.25 Hz (C-volley), a stimulus width of 0.2 ms (A-volley) or 2 ms (C-volley), and an intensity of 5 to 20 V. The amplitude of the CAP was measured peak-to-peak and expressed as a percentage of control for different treatments. Drug solutions were diluted into SIF from 100 µM or 100 mM stock solutions in DMSO and warmed to 32°C before the experiment.

## 8.4. Experimental for Chapter 6

### A. Pharmacokinetic profiling of [<sup>18</sup>F]22 using PET/CT

The study was performed at the UCL Centre of Advanced Biomedical Imaging by Dr. Thibault Gendron and Dr. Kerstin Sander.

All animal work was performed in compliance with the United Kingdom Home Office's Animals (Scientific Procedures) Act 1986 and with approval of the University College London (UCL) Animal Ethics Committee.

Wild-type albino mice (FVB or Balb/C, Charles River Laboratories, UK) were allowed to acclimatize for at least one week and were given food and water *ad libitum*. Dynamic PET imaging was performed using a nanoScan® PET-CT system manufactured by Mediso (Medical Imaging Systems, Budapest, Hungary). Mice were anaesthetized with isoflurane (2% in oxygen) and placed on the preheated bed of the scanner (set at 38 °C). The respective radiotracer (5–10 MBq in 100–250 µl saline solution) was injected into the tail vein via intravenous cannulation. After injection, the catheter was carefully removed. Breathing rate and body temperature of the animals were closely monitored during the dynamic PET scans and, if necessary, the isoflurane dose was adjusted. Scans were recorded over two hours, and the animals were subsequently sacrificed by cervical dislocation. Quantification of tissue uptake was carried out using the software package VivoQuant 1.23 (inviCRO, Boston, USA).

### B. Maximum tolerated dose finding study of 22 in rats

The study was outsourced to Charles River Laboratories, Wilmington, MA. The experimental details reported below are as provided by the company.

22 was prepared as solution in vehicle on the day of each experiment. The dosing vehicle was 5% glucose in HPLC grade water (chemicals purchased by Sigma).

A total of 5 male Wistar Han rats were received from Charles River Laboratories, Raleigh, North Carolina. Following an acclimation period, the animals were assigned to the study based on acceptable health as determined by a staff veterinarian. Animals were placed into 5 groups of 1 animal per group. Each animal in Groups 1-5 received the appropriate 22 dose by intravenous administration (tail vein) over an approximate 3 minute dosing period. The volume of each dose delivered (mlkg<sup>-1</sup>) was based on each individual animal's body weight recorded on the morning of dose administration. Dosing was performed in five dose sessions each one week apart.

Body weights were recorded daily for seven days post dosing. Following dosing and at the time of each weight collection, the animals were observed for any clinically relevant abnormalities. Animals observed as normal had similar heart rate and breathing patterns as non-dosed animals.

## 9. References

1. Benzon, H. T.; Raja, S. N., *Essentials of Pain Medicine*. Elsevier/Saunders: 2011.
2. Fishman, S.; Ballantyne, J.; Rathmell, J. P.; Bonica, J. J., *Bonica's Management of Pain*. Lippincott, Williams & Wilkins: 2010.
3. Pérez-Medina, C.; Patel, N.; Robson, M.; Lythgoe, M. F.; Årstad, E., Synthesis and evaluation of a 125I-labeled iminodihydroquinoline-derived tracer for imaging of voltage-gated sodium channels. *Bioorganic & Medicinal Chemistry Letters* **2013**, *23* (18), 5170-5173.
4. Merskey, H., Pain terms: A supplementary note. *PAIN* **1982**, *14* (3), 205-206.
5. Grichnik, K. P.; Ferrante, F. M., The difference between acute and chronic pain. *The Mount Sinai journal of medicine, New York* **1991**, *58* (3), 217-20.
6. Russo, C. M.; Brose, W. G., Chronic pain. *Annual review of medicine* **1998**, *49*, 123-33.
7. Wolfe, M. D.; O'Connor, A. B., Management of Neuropathic Pain in Hospitalized Patients. *Hospital Medicine Clinics* **2013**, *2* (4), e587-e602.
8. Shipton, E., *Pain - Acute and Chronic*, 2Ed. Taylor & Francis: 1999.
9. Portenoy, R. K., Mechanisms of clinical pain. Observations and speculations. *Neurologic clinics* **1989**, *7* (2), 205-30.
10. Woolf, C. J.; Ma, Q., Nociceptors--noxious stimulus detectors. *Neuron* **2007**, *55* (3), 353-64.
11. Costigan, M.; Scholz, J.; Woolf, C. J., Neuropathic pain: a maladaptive response of the nervous system to damage. *Annual review of neuroscience* **2009**, *32*, 1-32.
12. Goldberg, D. S.; McGee, S. J., Pain as a global public health priority. *BMC public health* **2011**, *11*, 770.
13. Breivik, H.; Collett, B.; Ventafridda, V.; Cohen, R.; Gallacher, D., Survey of chronic pain in Europe: prevalence, impact on daily life, and treatment. *European journal of pain (London, England)* **2006**, *10* (4), 287-333.
14. Singh, G., Recent considerations in nonsteroidal anti-inflammatory drug gastropathy. *The American journal of medicine* **1998**, *105* (1b), 31s-38s.
15. Medicine, I. o., *Relieving Pain in America: A Blueprint for Transforming Prevention, Care, Education, and Research*. The National Academies Press: Washington, DC, 2011; p 382.
16. Fein, A., Nociceptors and the perception of pain. *University of Connecticut Health Center* **2012**, *4*, 61-67.
17. Melzack, R.; Wall, P. D., Pain Mechanisms: A New Theory. *Science* **1965**, *150* (3699), 971-979.
18. Grady, K. M.; Severn, A. M.; Eldridge, P. R., *Key Topics in Pain Management, Third Edition*. Taylor & Francis: 2006.
19. Zeilhofer, H. U.; Wildner, H.; Yevenes, G. E., Fast synaptic inhibition in spinal sensory processing and pain control. *Physiological reviews* **2012**, *92* (1), 193-235.
20. Ossipov, M. H., The Perception and Endogenous Modulation of Pain. *Scientifica* **2012**, *2012*, 25.
21. Basbaum, A. I.; Fields, H. L., Endogenous pain control mechanisms: review and hypothesis. *Annals of neurology* **1978**, *4* (5), 451-62.
22. Holdcroft, A.; Jaggar, S., *Core Topics in Pain*. Cambridge University Press: 2005.
23. Koltzenburg, M.; McMahon, S. B.; Tracey, I.; Turk, D. C., *Wall & Melzack's Textbook of Pain, Expert Consult - Online and Print, 6: Wall & Melzack's Textbook of Pain*. Elsevier/Saunders: 2013.
24. Koltzenburg, M., The changing sensitivity in the life of the nociceptor. *Pain* **1999**, *82*, Supplement 1 (0), S93-S102.
25. Djouhri, L.; Bleazard, L.; Lawson, S. N., Association of somatic action potential shape with sensory receptive properties in guinea-pig dorsal root ganglion neurones. *The Journal of physiology* **1998**, *513* (Pt 3), 857-872.
26. Dubin, A. E.; Patapoutian, A., Nociceptors: the sensors of the pain pathway. *The Journal of Clinical Investigation* **2010**, *120* (11), 3760-3772.
27. Raja, S. N.; Meyer, R. A.; Campbell, J. N., Peripheral mechanisms of somatic pain. *Anesthesiology* **1988**, *68* (4), 571-90.
28. Robinson, D. R.; Gebhart, G. F., Inside information – The unique features of visceral sensation. *Molecular interventions* **2008**, *8* (5), 242-253.

29. Gebhart, G. F., Visceral polymodal receptors. *Progress in brain research* **1996**, *113*, 101-12.
30. Woolf, C. J.; Costigan, M., Transcriptional and posttranslational plasticity and the generation of inflammatory pain. *Proceedings of the National Academy of Sciences of the United States of America* **1999**, *96* (14), 7723-7730.
31. Zheng, J., Molecular Mechanism of TRP Channels. *Comprehensive Physiology* **2013**, *3* (1), 221-242.
32. Caterina, M. J.; Schumacher, M. A.; Tominaga, M.; Rosen, T. A.; Levine, J. D.; Julius, D., The capsaicin receptor: a heat-activated ion channel in the pain pathway. *Nature* **1997**, *389* (6653), 816-24.
33. Story, G. M.; Peier, A. M.; Reeve, A. J.; Eid, S. R.; Mosbacher, J.; Hricik, T. R.; Earley, T. J.; Hergarden, A. C.; Andersson, D. A.; Hwang, S. W.; McIntyre, P.; Jegla, T.; Bevan, S.; Patapoutian, A., ANKTM1, a TRP-like channel expressed in nociceptive neurons, is activated by cold temperatures. *Cell* **2003**, *112* (6), 819-29.
34. Paulsen, C. E.; Armache, J.-P.; Gao, Y.; Cheng, Y.; Julius, D., Structure of the TRPA1 ion channel suggests regulatory mechanisms. *Nature* **2015**, *520* (7548), 511-517.
35. Voets, T.; Droogmans, G.; Wissenbach, U.; Janssens, A.; Flockerzi, V.; Nilius, B., The principle of temperature-dependent gating in cold- and heat-sensitive TRP channels. *Nature* **2004**, *430* (7001), 748-54.
36. Wood, J. N.; Eijkelkamp, N., Noxious mechanosensation - molecules and circuits. *Current opinion in pharmacology* **2012**, *12* (1), 4-8.
37. Chalfie, M., Neurosensory mechanotransduction. *Nat Rev Mol Cell Biol* **2009**, *10* (1), 44-52.
38. Chen, C.-C.; Wong, C.-W., Neurosensory mechanotransduction through acid-sensing ion channels. *Journal of Cellular and Molecular Medicine* **2013**, *17* (3), 337-349.
39. Poole, K.; Herget, R.; Lapatsina, L.; Ngo, H.-D.; Lewin, G. R., Tuning Piezo ion channels to detect molecular-scale movements relevant for fine touch. *Nat Commun* **2014**, *5*.
40. Petrus, M.; Peier, A. M.; Bandell, M.; Hwang, S. W.; Huynh, T.; Olney, N.; Jegla, T.; Patapoutian, A., A role of TRPA1 in mechanical hyperalgesia is revealed by pharmacological inhibition. *Mol Pain* **2007**, *3*, 40.
41. Gutman, G. A.; Chandy, K. G.; Adelman, J. P.; Aiyar, J.; Bayliss, D. A.; Clapham, D. E.; Covarrubias, M.; Desir, G. V.; Furuichi, K.; Ganetzky, B.; Garcia, M. L.; Grissmer, S.; Jan, L. Y.; Karschin, A.; Kim, D.; Kuperschmidt, S.; Kurachi, Y.; Lazdunski, M.; Lesage, F.; Lester, H. A.; McKinnon, D.; Nichols, C. G.; O'Kelly, I.; Robbins, J.; Robertson, G. A.; Rudy, B.; Sanguinetti, M.; Seino, S.; Stuehmer, W.; Tamkun, M. M.; Vandenbergh, C. A.; Wei, A.; Wulff, H.; Wymore, R. S., International Union of Pharmacology. XLI. Compendium of Voltage-Gated Ion Channels: Potassium Channels. *Pharmacological Reviews* **2003**, *55* (4), 583-586.
42. Tsantoulas, C.; McMahon, S. B., Opening paths to novel analgesics: the role of potassium channels in chronic pain. *Trends in neurosciences* **2014**, *37* (3), 146-58.
43. Catterall, W. A.; Perez-Reyes, E.; Snutch, T. P.; Striessnig, J., International Union of Pharmacology. XLVIII. Nomenclature and structure-function relationships of voltage-gated calcium channels. *Pharmacol Rev* **2005**, *57* (4), 411-25.
44. Jessell, T. M.; Yoshioka, K.; Jahr, C. E., Amino acid receptor-mediated transmission at primary afferent synapses in rat spinal cord. *The Journal of experimental biology* **1986**, *124*, 239-58.
45. Duggan, A. W.; Hendry, I. A.; Morton, C. R.; Hutchison, W. D.; Zhao, Z. Q., Cutaneous stimuli releasing immunoreactive substance P in the dorsal horn of the cat. *Brain Res* **1988**, *451* (1-2), 261-73.
46. Doan, L., Voltage-gated calcium channels and pain. *Techniques in Regional Anesthesia and Pain Management* **2010**, *14* (2), 42-47.
47. Gold, M. S.; Gebhart, G. F., Nociceptor sensitization in pain pathogenesis. *Nature medicine* **2010**, *16* (11), 1248-57.
48. Treede, R. D.; Meyer, R. A.; Raja, S. N.; Campbell, J. N., Peripheral and central mechanisms of cutaneous hyperalgesia. *Progress in neurobiology* **1992**, *38* (4), 397-421.
49. Koltzenburg, M.; Torebjork, H. E.; Wahren, L. K., Nociceptor modulated central sensitization causes mechanical hyperalgesia in acute chemogenic and chronic neuropathic pain. *Brain : a journal of neurology* **1994**, *117* ( Pt 3), 579-91.

50. Chen, L.; Yang, G.; Grosser, T., Prostanoids and inflammatory pain. *Prostaglandins & other lipid mediators* **2013**, *104-105*, 58-66.
51. Leung, L.; Cahill, C. M., TNF- $\alpha$  and neuropathic pain - a review. *Journal of Neuroinflammation* **2010**, *7*, 27-27.
52. Vargas-Schaffer, G., Is the WHO analgesic ladder still valid?: Twenty-four years of experience. *Canadian Family Physician* **2010**, *56* (6), 514-517.
53. Vane, J. R.; Botting, R. M., Mechanism of action of nonsteroidal anti-inflammatory drugs. *The American journal of medicine* **1998**, *104* (3a), 2S-8S; discussion 21S-22S.
54. Bombardier, C.; Laine, L.; Reicin, A.; Shapiro, D.; Burgos-Vargas, R.; Davis, B.; Day, R.; Ferraz, M. B.; Hawkey, C. J.; Hochberg, M. C.; Kvien, T. K.; Schnitzer, T. J., Comparison of Upper Gastrointestinal Toxicity of Rofecoxib and Naproxen in Patients with Rheumatoid Arthritis. *New England Journal of Medicine* **2000**, *343* (21), 1520-1528.
55. FitzGerald, G. A., Coxibs and Cardiovascular Disease. *New England Journal of Medicine* **2004**, *351* (17), 1709-1711.
56. Pickering, G.; Lorient, M. A.; Libert, F.; Eschaliier, A.; Beaune, P.; Dubray, C., Analgesic effect of acetaminophen in humans: first evidence of a central serotonergic mechanism. *Clinical pharmacology and therapeutics* **2006**, *79* (4), 371-8.
57. Inturrisi, C. E., Clinical pharmacology of opioids for pain. *The Clinical journal of pain* **2002**, *18* (4 Suppl), S3-13.
58. Pradhan, A. A.; Smith, M. L.; Kieffer, B. L.; Evans, C. J., Ligand-directed signalling within the opioid receptor family. *British journal of pharmacology* **2012**, *167* (5), 960-9.
59. Lynch, M. E.; Watson, C. P. N., The pharmacotherapy of chronic pain: A review. *Pain Research & Management : The Journal of the Canadian Pain Society* **2006**, *11* (1), 11-38.
60. Dharmshaktu, P.; Tayal, V.; Kalra, B. S., Efficacy of antidepressants as analgesics: a review. *Journal of clinical pharmacology* **2012**, *52* (1), 6-17.
61. McQuay, H.; Carroll, D.; Jadad, A. R.; Wiffen, P.; Moore, A., *Anticonvulsant drugs for management of pain: a systematic review*. 1995; Vol. 311, p 1047-1052.
62. Todorovic, S. M.; Rastogi, A. J.; Jevtovic-Todorovic, V., Potent analgesic effects of anticonvulsants on peripheral thermal nociception in rats. *British journal of pharmacology* **2003**, *140* (2), 255-260.
63. Kissin, I., The development of new analgesics over the past 50 years: a lack of real breakthrough drugs. *Anesthesia and analgesia* **2010**, *110* (3), 780-9.
64. Woodcock, J.; Witter, J.; Dionne, R. A., Stimulating the development of mechanism-based, individualized pain therapies. *Nat Rev Drug Discov* **2007**, *6* (9), 703-710.
65. Palmer, A. M.; Carter, N., The role of sodium channels in disease. *Drug news & perspectives* **2001**, *14* (9), 568-76.
66. Anger, T.; Madge, D. J.; Mulla, M.; Riddall, D., Medicinal chemistry of neuronal voltage-gated sodium channel blockers. *Journal of medicinal chemistry* **2001**, *44* (2), 115-37.
67. Catterall, W. A., Structural biology: A 3D view of sodium channels. *Nature* **2001**, *409* (6823), 988-991.
68. Marban, E.; Yamagishi, T.; Tomaselli, G. F., Structure and function of voltage-gated sodium channels. *The Journal of physiology* **1998**, *508* ( Pt 3), 647-57.
69. Yu, F. H.; Catterall, W. A., Overview of the voltage-gated sodium channel family. *Genome biology* **2003**, *4* (3), 207.
70. Payandeh, J.; Scheuer, T.; Zheng, N.; Catterall, W. A., The crystal structure of a voltage-gated sodium channel. *Nature* **2011**, *475* (7356), 353-8.
71. Payandeh, J.; Gamal El-Din, T. M.; Scheuer, T.; Zheng, N.; Catterall, W. A., Crystal structure of a voltage-gated sodium channel in two potentially inactivated states. *Nature* **2012**, *486* (7401), 135-139.
72. Zhang, X.; Ren, W.; DeCaen, P.; Yan, C.; Tao, X.; Tang, L.; Wang, J.; Hasegawa, K.; Kumasaka, T.; He, J.; Wang, J.; Clapham, D. E.; Yan, N., Crystal structure of an orthologue of the NaChBac voltage-gated sodium channel. *Nature* **2012**, *486* (7401), 130-134.
73. McCusker, E. C.; Bagn eris, C.; Naylor, C. E.; Cole, A. R.; D'Avanzo, N.; Nichols, C. G.; Wallace, B. A., Structure of a bacterial voltage-gated sodium channel pore reveals mechanisms of opening and closing. *Nat Commun* **2012**, *3*, 1102.



74. Hodgkin, A. L.; Huxley, A. F., A quantitative description of membrane current and its application to conduction and excitation in nerve. *The Journal of physiology* **1952**, *117* (4), 500-544.
75. Ulbricht, W., Sodium channel inactivation: molecular determinants and modulation. *Physiological reviews* **2005**, *85* (4), 1271-301.
76. Cannon, S. C.; Bean, B. P., Sodium channels gone wild: resurgent current from neuronal and muscle channelopathies. *The Journal of Clinical Investigation* **2010**, *120* (1), 80-83.
77. Catterall, W. A.; Goldin, A. L.; Waxman, S. G., International Union of Pharmacology. XLVII. Nomenclature and structure-function relationships of voltage-gated sodium channels. *Pharmacol Rev* **2005**, *57* (4), 397-409.
78. England, S.; de Groot, M. J., Subtype-selective targeting of voltage-gated sodium channels. *British journal of pharmacology* **2009**, *158* (6), 1413-25.
79. Eijkelkamp, N.; Linley, J. E.; Baker, M. D.; Minett, M. S.; Cregg, R.; Werdehausen, R.; Rugiero, F.; Wood, J. N., Neurological perspectives on voltage-gated sodium channels. *Brain : a journal of neurology* **2012**, *135* (Pt 9), 2585-612.
80. Harriott, A. M.; Gold, M. S., Contribution of Primary Afferent Channels to Neuropathic Pain. *Current pain and headache reports* **2009**, *13* (3), 197-207.
81. Waxman, S. G.; Kocsis, J. D.; Black, J. A., *Type III sodium channel mRNA is expressed in embryonic but not adult spinal sensory neurons, and is reexpressed following axotomy*. 1994; Vol. 72, p 466-470.
82. Kiss, T., Persistent Na-channels: origin and function. A review. *Acta biologica Hungarica* **2008**, *59 Suppl*, 1-12.
83. Waxman, S. G.; Zamponi, G. W., Regulating excitability of peripheral afferents: emerging ion channel targets. *Nat Neurosci* **2014**, *17* (2), 153-163.
84. Black, J. A.; Renganathan, M.; Waxman, S. G., Sodium channel Na(v)1.6 is expressed along nonmyelinated axons and it contributes to conduction. *Brain research. Molecular brain research* **2002**, *105* (1-2), 19-28.
85. Black, J. A.; Frézel, N.; Dib-Hajj, S. D.; Waxman, S. G., Expression of Nav1.7 in DRG neurons extends from peripheral terminals in the skin to central preterminal branches and terminals in the dorsal horn. *Molecular Pain* **2012**, *8*, 82-82.
86. Dib-Hajj, S. D.; Yang, Y.; Black, J. A.; Waxman, S. G., The Na(V)1.7 sodium channel: from molecule to man. *Nature reviews. Neuroscience* **2013**, *14* (1), 49-62.
87. Cummins, T. R.; Sheets, P. L.; Waxman, S. G., The roles of sodium channels in nociception: implications for mechanisms of pain. *Pain* **2007**, *131* (3), 243-257.
88. Khasar, S. G.; Gold, M. S.; Levine, J. D., A tetrodotoxin-resistant sodium current mediates inflammatory pain in the rat. *Neuroscience letters* **1998**, *256* (1), 17-20.
89. Fjell, J.; Hjelmstrom, P.; Hormuzdiar, W.; Milenkovic, M.; Aglieco, F.; Tyrrell, L.; Dib-Hajj, S.; Waxman, S. G.; Black, J. A., Localization of the tetrodotoxin-resistant sodium channel NaN in nociceptors. *Neuroreport* **2000**, *11* (1), 199-202.
90. Dib-Hajj, S.; Black, J. A.; Cummins, T. R.; Waxman, S. G., NaN/Nav1.9: a sodium channel with unique properties. *Trends in neurosciences* **2002**, *25* (5), 253-9.
91. Hains, B. C.; Saab, C. Y.; Klein, J. P.; Craner, M. J.; Waxman, S. G., Altered sodium channel expression in second-order spinal sensory neurons contributes to pain after peripheral nerve injury. *The Journal of neuroscience : the official journal of the Society for Neuroscience* **2004**, *24* (20), 4832-9.
92. Lindia, J. A.; Kohler, M. G.; Martin, W. J.; Abbadie, C., Relationship between sodium channel NaV1.3 expression and neuropathic pain behavior in rats. *Pain* **2005**, *117* (1-2), 145-53.
93. Samad, O. A.; Tan, A. M.; Cheng, X.; Foster, E.; Dib-Hajj, S. D.; Waxman, S. G., Virus-mediated shRNA Knockdown of Nav1.3 in Rat Dorsal Root Ganglion Attenuates Nerve Injury-induced Neuropathic Pain. *Mol Ther* **2013**, *21* (1), 49-56.
94. Cummins, T. R.; Aglieco, F.; Renganathan, M.; Herzog, R. I.; Dib-Hajj, S. D.; Waxman, S. G., Nav1.3 sodium channels: rapid repriming and slow closed-state inactivation display quantitative differences after expression in a mammalian cell line and in spinal sensory neurons. *The Journal of neuroscience : the official journal of the Society for Neuroscience* **2001**, *21* (16), 5952-61.
95. Sittl, R.; Lampert, A.; Huth, T.; Schuy, E. T.; Link, A. S.; Fleckenstein, J.; Alzheimer, C.; Grafe, P.; Carr, R. W., Anticancer drug oxaliplatin induces acute cooling-aggravated neuropathy via sodium channel subtype Na(V)1.6-resurgent and persistent

- current. *Proceedings of the National Academy of Sciences of the United States of America* **2012**, *109* (17), 6704-9.
96. Xie, W.; Strong, J. A.; Ye, L.; Mao, J. X.; Zhang, J. M., Knockdown of sodium channel Nav1.6 blocks mechanical pain and abnormal bursting activity of afferent neurons in inflamed sensory ganglia. *Pain* **2013**, *154* (8), 1170-80.
  97. Xie, W.; Strong, J. A.; Zhang, J. M., Local knockdown of the Nav1.6 sodium channel reduces pain behaviors, sensory neuron excitability, and sympathetic sprouting in rat models of neuropathic pain. *Neuroscience* **2015**, *291*, 317-30.
  98. Toledo-Aral, J. J.; Brehm, P.; Haleboua, S.; Mandel, G., A single pulse of nerve growth factor triggers long-term neuronal excitability through sodium channel gene induction. *Neuron* **1995**, *14* (3), 607-11.
  99. Nassar, M. A.; Stirling, L. C.; Forlani, G.; Baker, M. D.; Matthews, E. A.; Dickenson, A. H.; Wood, J. N., Nociceptor-specific gene deletion reveals a major role for Nav1.7 (PN1) in acute and inflammatory pain. *Proceedings of the National Academy of Sciences of the United States of America* **2004**, *101* (34), 12706-11.
  100. Shields, S. D.; Cheng, X.; Üçeyler, N.; Sommer, C.; Dib-Hajj, S. D.; Waxman, S. G., Sodium Channel Nav1.7 Is Essential for Lowering Heat Pain Threshold after Burn Injury. *The Journal of Neuroscience* **2012**, *32* (32), 10819-10832.
  101. Dib-Hajj, S. D.; Cummins, T. R.; Black, J. A.; Waxman, S. G., From genes to pain: Nav1.7 and human pain disorders. *Trends in neurosciences* **2007**, *30* (11), 555-563.
  102. Cummins, T. R.; Dib-Hajj, S. D.; Waxman, S. G., Electrophysiological properties of mutant Nav1.7 sodium channels in a painful inherited neuropathy. *The Journal of neuroscience : the official journal of the Society for Neuroscience* **2004**, *24* (38), 8232-6.
  103. Fertleman, C. R.; Baker, M. D.; Parker, K. A.; Moffatt, S.; Elmslie, F. V.; Abrahamsen, B.; Ostman, J.; Klugbauer, N.; Wood, J. N.; Gardiner, R. M.; Rees, M., SCN9A mutations in paroxysmal extreme pain disorder: allelic variants underlie distinct channel defects and phenotypes. *Neuron* **2006**, *52* (5), 767-74.
  104. Goldberg, Y. P.; MacFarlane, J.; MacDonald, M. L.; Thompson, J.; Dube, M. P.; Mattice, M.; Fraser, R.; Young, C.; Hossain, S.; Pape, T.; Payne, B.; Radomski, C.; Donaldson, G.; Ives, E.; Cox, J.; Youngusband, H. B.; Green, R.; Duff, A.; Boltshauser, E.; Grinspan, G. A.; Dimon, J. H.; Sibley, B. G.; Andria, G.; Toscano, E.; Kerdraon, J.; Bowsher, D.; Pimstone, S. N.; Samuels, M. E.; Sherrington, R.; Hayden, M. R., Loss-of-function mutations in the Nav1.7 gene underlie congenital indifference to pain in multiple human populations. *Clinical genetics* **2007**, *71* (4), 311-9.
  105. Nassar, M. A.; Levato, A.; Stirling, L. C.; Wood, J. N., Neuropathic pain develops normally in mice lacking both Na(v)1.7 and Na(v)1.8. *Mol Pain* **2005**, *1*, 24.
  106. Minett, M. S.; Falk, S.; Santana-Varela, S.; Bogdanov, Y. D.; Nassar, M. A.; Heegaard, A. M.; Wood, J. N., Pain without nociceptors? Nav1.7-independent pain mechanisms. *Cell Rep* **2014**, *6* (2), 301-12.
  107. Coggeshall, R. E.; Tate, S.; Carlton, S. M., Differential expression of tetrodotoxin-resistant sodium channels Nav1.8 and Nav1.9 in normal and inflamed rats. *Neuroscience letters* **2004**, *355* (1-2), 45-8.
  108. Tanaka, M.; Cummins, T. R.; Ishikawa, K.; Dib-Hajj, S. D.; Black, J. A.; Waxman, S. G., SNS Na<sup>+</sup> channel expression increases in dorsal root ganglion neurons in the carrageenan inflammatory pain model. *Neuroreport* **1998**, *9* (6), 967-72.
  109. Akopian, A. N.; Souslova, V.; England, S.; Okuse, K.; Ogata, N.; Ure, J.; Smith, A.; Kerr, B. J.; McMahon, S. B.; Boyce, S.; Hill, R.; Stanfa, L. C.; Dickenson, A. H.; Wood, J. N., The tetrodotoxin-resistant sodium channel SNS has a specialized function in pain pathways. *Nat Neurosci* **1999**, *2* (6), 541-8.
  110. Jarvis, M. F.; Honore, P.; Shieh, C. C.; Chapman, M.; Joshi, S.; Zhang, X. F.; Kort, M.; Carroll, W.; Marron, B.; Atkinson, R.; Thomas, J.; Liu, D.; Krambis, M.; Liu, Y.; McGaraughty, S.; Chu, K.; Roeloffs, R.; Zhong, C.; Mikusa, J. P.; Hernandez, G.; Gauvin, D.; Wade, C.; Zhu, C.; Pai, M.; Scanio, M.; Shi, L.; Drizin, I.; Gregg, R.; Matulenko, M.; Hakeem, A.; Gross, M.; Johnson, M.; Marsh, K.; Wagoner, P. K.; Sullivan, J. P.; Faltynek, C. R.; Krafte, D. S., A-803467, a potent and selective Nav1.8 sodium channel blocker, attenuates neuropathic and inflammatory pain in the rat. *Proceedings of the National Academy of Sciences of the United States of America* **2007**, *104* (20), 8520-5.

111. Joshi, S. K.; Mikusa, J. P.; Hernandez, G.; Baker, S.; Shieh, C. C.; Neelands, T.; Zhang, X. F.; Niforatos, W.; Kage, K.; Han, P.; Krafte, D.; Faltynek, C.; Sullivan, J. P.; Jarvis, M. F.; Honore, P., Involvement of the TTX-resistant sodium channel Nav 1.8 in inflammatory and neuropathic, but not post-operative, pain states. *Pain* **2006**, *123* (1-2), 75-82.
112. Faber, C. G.; Lauria, G.; Merkies, I. S.; Cheng, X.; Han, C.; Ahn, H. S.; Persson, A. K.; Hoeijmakers, J. G.; Gerrits, M. M.; Pierro, T.; Lombardi, R.; Kapetis, D.; Dib-Hajj, S. D.; Waxman, S. G., Gain-of-function Nav1.8 mutations in painful neuropathy. *Proceedings of the National Academy of Sciences of the United States of America* **2012**, *109* (47), 19444-9.
113. Gold, M. S.; Weinreich, D.; Kim, C. S.; Wang, R.; Treanor, J.; Porreca, F.; Lai, J., Redistribution of Na(V)1.8 in uninjured axons enables neuropathic pain. *The Journal of neuroscience : the official journal of the Society for Neuroscience* **2003**, *23* (1), 158-66.
114. Cummins, T. R.; Waxman, S. G., Downregulation of tetrodotoxin-resistant sodium currents and upregulation of a rapidly repriming tetrodotoxin-sensitive sodium current in small spinal sensory neurons after nerve injury. *The Journal of neuroscience : the official journal of the Society for Neuroscience* **1997**, *17* (10), 3503-14.
115. Amaya, F.; Wang, H.; Costigan, M.; Allchorne, A. J.; Hatcher, J. P.; Egerton, J.; Stean, T.; Morisset, V.; Grose, D.; Gunthorpe, M. J.; Chessell, I. P.; Tate, S.; Green, P. J.; Woolf, C. J., The voltage-gated sodium channel Na(v)1.9 is an effector of peripheral inflammatory pain hypersensitivity. *The Journal of neuroscience : the official journal of the Society for Neuroscience* **2006**, *26* (50), 12852-60.
116. Lollignier, S.; Amsalem, M.; Maingret, F.; Padilla, F.; Gabriac, M.; Chapuy, E.; Eschalier, A.; Delmas, P.; Bussierolles, J., Nav1.9 Channel Contributes to Mechanical and Heat Pain Hypersensitivity Induced by Subacute and Chronic Inflammation. *PLoS ONE* **2011**, *6* (8), e23083.
117. Lollignier, S.; Bonnet, C.; Gaudioso, C.; Noël, J.; Ruel, J.; Amsalem, M.; Ferrier, J.; Rodat-Despoix, L.; Bouvier, V.; Aissouni, Y.; Prival, L.; Chapuy, E.; Padilla, F.; Eschalier, A.; Delmas, P.; Bussierolles, J., The Nav1.9 Channel Is a Key Determinant of Cold Pain Sensation and Cold Allodynia. *Cell Reports* **2015**, *11* (7), 1067-1078.
118. Huang, J.; Han, C.; Estacion, M.; Vasylyev, D.; Hoeijmakers, J. G.; Gerrits, M. M.; Tyrrell, L.; Lauria, G.; Faber, C. G.; Dib-Hajj, S. D.; Merkies, I. S.; Waxman, S. G., Gain-of-function mutations in sodium channel Na(v)1.9 in painful neuropathy. *Brain : a journal of neurology* **2014**, *137* (Pt 6), 1627-42.
119. Ruetsch, Y. A.; Boni, T.; Borgeat, A., From cocaine to ropivacaine: the history of local anesthetic drugs. *Current topics in medicinal chemistry* **2001**, *1* (3), 175-82.
120. Scheuer, T., Local anaesthetic block of sodium channels: raising the barrier. *The Journal of physiology* **2007**, *581* (Pt 2), 423-423.
121. Lipkind, G. M.; Fozzard, H. A., Molecular Model of Anticonvulsant Drug Binding to the Voltage-Gated Sodium Channel Inner Pore. *Molecular pharmacology* **2010**, *78* (4), 631-638.
122. Bagal, S. K.; Chapman, M. L.; Marron, B. E.; Prime, R.; Storer, R. I.; Swain, N. A., Recent progress in sodium channel modulators for pain. *Bioorganic & Medicinal Chemistry Letters* **2014**, *24* (16), 3690-3699.
123. Schmalhofer, W. A.; Calhoun, J.; Burrows, R.; Bailey, T.; Kohler, M. G.; Weinglass, A. B.; Kaczorowski, G. J.; Garcia, M. L.; Koltzenburg, M.; Priest, B. T., ProTx-II, a selective inhibitor of NaV1.7 sodium channels, blocks action potential propagation in nociceptors. *Molecular pharmacology* **2008**, *74* (5), 1476-84.
124. Yang, S.; Xiao, Y.; Kang, D.; Liu, J.; Li, Y.; Undheim, E. A.; Klint, J. K.; Rong, M.; Lai, R.; King, G. F., Discovery of a selective NaV1.7 inhibitor from centipede venom with analgesic efficacy exceeding morphine in rodent pain models. *Proceedings of the National Academy of Sciences of the United States of America* **2013**, *110* (43), 17534-9.
125. Clare, J. J., Targeting voltage-gated sodium channels for pain therapy. *Expert opinion on investigational drugs* **2010**, *19* (1), 45-62.
126. McGowan, E.; Hoyt, S. B.; Li, X.; Lyons, K. A.; Abbadie, C., A peripherally acting Na(v)1.7 sodium channel blocker reverses hyperalgesia and allodynia on rat models of inflammatory and neuropathic pain. *Anesthesia and analgesia* **2009**, *109* (3), 951-8.

127. Beggs, S.; Liu, X. J.; Kwan, C.; Salter, M. W., Peripheral nerve injury and TRPV1-expressing primary afferent C-fibers cause opening of the blood-brain barrier. *Mol Pain* **2010**, *6*, 74.
128. Theile, J. W.; Cummins, T. R., Recent Developments Regarding Voltage-Gated Sodium Channel Blockers for the Treatment of Inherited and Acquired Neuropathic Pain Syndromes. *Frontiers in Pharmacology* **2011**, *2*, 54.
129. Roberson, D. P.; Binshtok, A. M.; Blasl, F.; Bean, B. P.; Woolf, C. J., Targeting of sodium channel blockers into nociceptors to produce long-duration analgesia: a systematic study and review. *British journal of pharmacology* **2011**, *164* (1), 48-58.
130. Schwarz, S. K.; Cheung, H. M.; Ries, C. R.; Lee, S. M.; Wang, J. T.; MacLeod, B. A., Lumbar intrathecal administration of the quaternary lidocaine derivative, QX-314, produces irritation and death in mice. *Anesthesiology* **2010**, *113* (2), 438-44.
131. Cheung, H. M.; Lee, S. M.; MacLeod, B. A.; Ries, C. R.; Schwarz, S. K., A comparison of the systemic toxicity of lidocaine versus its quaternary derivative QX-314 in mice. *Canadian journal of anaesthesia = Journal canadien d'anesthesie* **2011**, *58* (5), 443-50.
132. Wanner, S. G.; Glossmann, H.; Knaus, H. G.; Baker, R.; Parsons, W.; Rupprecht, K. M.; Brochu, R.; Cohen, C. J.; Schmalhofer, W.; Smith, M.; Warren, V.; Garcia, M. L.; Kaczorowski, G. J., WIN 17317-3, a new high-affinity probe for voltage-gated sodium channels. *Biochemistry* **1999**, *38* (34), 11137-46.
133. Michne, W. F.; Guiles, J. W.; Treasurywala, A. M.; Castonguay, L. A.; Weigelt, C. A.; Oconnor, B.; Volberg, W. A.; Grant, A. M.; Chadwick, C. C.; Krafte, D. S.; et al., Novel inhibitors of potassium ion channels on human T lymphocytes. *Journal of medicinal chemistry* **1995**, *38* (11), 1877-83.
134. Liang, J.; Brochu, R. M.; Cohen, C. J.; Dick, I. E.; Felix, J. P.; Fisher, M. H.; Garcia, M. L.; Kaczorowski, G. J.; Lyons, K. A.; Meinke, P. T.; Priest, B. T.; Schmalhofer, W. A.; Smith, M. M.; Tarpley, J. W.; Williams, B. S.; Martin, W. J.; Parsons, W. H., Discovery of potent and use-dependent sodium channel blockers for treatment of chronic pain. *Bioorg Med Chem Lett* **2005**, *15* (11), 2943-7.
135. Ok, D.; Li, C.; Abbadie, C.; Felix, J. P.; Fisher, M. H.; Garcia, M. L.; Kaczorowski, G. J.; Lyons, K. A.; Martin, W. J.; Priest, B. T.; Smith, M. M.; Williams, B. S.; Wyratt, M. J.; Parsons, W. H., Synthesis and SAR of 1,2-trans-(1-hydroxy-3-phenylprop-1-yl)cyclopentane carboxamide derivatives, a new class of sodium channel blockers. *Bioorg Med Chem Lett* **2006**, *16* (5), 1358-61.
136. Ono, S.; Kimura, T.; Kubo, T., Characterization of voltage-dependent calcium channel blocking peptides from the venom of the tarantula *Grammostola rosea*. *Toxicon : official journal of the International Society on Toxinology* **2011**, *58* (3), 265-76.
137. Brenneis, C.; Kistner, K.; Puopolo, M.; Segal, D.; Roberson, D.; Sisignano, M.; Labocha, S.; Ferreirós, N.; Strominger, A.; Cobos, E. J.; Ghasemlou, N.; Geisslinger, G.; Reeh, P. W.; Bean, B. P.; Woolf, C. J., Phenotyping the Function of TRPV1-Expressing Sensory Neurons by Targeted Axonal Silencing. *The Journal of Neuroscience* **2013**, *33* (1), 315-326.
138. Lev, S.; Minke, B., CONSTITUTIVE ACTIVITY OF TRP CHANNELS: METHODS FOR MEASURING THE ACTIVITY AND ITS OUTCOME. *Methods in enzymology* **2010**, *484*, 591.
139. Wermuth, C.; Ganellin, C.; Lindberg, P.; Mitscher, L., Glossary of terms used in medicinal chemistry (IUPAC Recommendations 1998). *Pure and Applied Chemistry* **1998**, *70* (5), 1129-1143.
140. Merz, K. M.; Ringe, D.; Reynolds, C. H., *Drug Design: Structure- and Ligand-Based Approaches*. Cambridge University Press: 2010.
141. Lounnas, V.; Ritschel, T.; Kelder, J.; McGuire, R.; Bywater, R. P.; Foloppe, N., CURRENT PROGRESS IN STRUCTURE-BASED RATIONAL DRUG DESIGN MARKS A NEW MINDSET IN DRUG DISCOVERY. *Computational and Structural Biotechnology Journal* **2013**, *5* (6), 1-14.
142. Amzel, L. M., Structure-based drug design. *Current Opinion in Biotechnology* **1998**, *9* (4), 366-369.
143. Güner, O. F., *Pharmacophore Perception, Development, and Use in Drug Design*. International University Line: 2000.
144. Hajduk, P. J.; Greer, J., A decade of fragment-based drug design: strategic advances and lessons learned. *Nat Rev Drug Discov* **2007**, *6* (3), 211-219.

145. Lee, C. H.; Ruben, P. C., Interaction between voltage-gated sodium channels and the neurotoxin, tetrodotoxin. *Channels* **2008**, *2* (6), 407-412.
146. Arnott, J. A.; Planey, S. L., The influence of lipophilicity in drug discovery and design. *Expert opinion on drug discovery* **2012**, *7* (10), 863-75.
147. Manallack, D. T., The pK(a) Distribution of Drugs: Application to Drug Discovery. *Perspectives in Medicinal Chemistry* **2007**, *1*, 25-38.
148. Prasanna, S.; Doerksen, R. J., Topological Polar Surface Area: A Useful Descriptor in 2D-QSAR. *Current medicinal chemistry* **2009**, *16* (1), 21-41.
149. Leeson, P., Drug discovery: Chemical beauty contest. *Nature* **2012**, *481* (7382), 455-456.
150. Filler, R.; Saha, R., Fluorine in medicinal chemistry: a century of progress and a 60-year retrospective of selected highlights. *Future medicinal chemistry* **2009**, *1* (5), 777-91.
151. Shah, P.; Westwell, A. D., The role of fluorine in medicinal chemistry. *Journal of enzyme inhibition and medicinal chemistry* **2007**, *22* (5), 527-40.
152. Purser, S.; Moore, P. R.; Swallow, S.; Gouverneur, V., Fluorine in medicinal chemistry. *Chemical Society reviews* **2008**, *37* (2), 320-30.
153. Singh, R. P.; Shreeve, J. n. M., Recent Advances in Nucleophilic Fluorination Reactions of Organic Compounds Using Deoxofluor and DAST. *Synthesis* **2002**, *2002* (17), 2561-2578.
154. Perez-Medina, C.; Patel, N.; Robson, M.; Badar, A.; Lythgoe, M. F.; Arstad, E., Evaluation of a <sup>125</sup>I-labelled benzazepinone derived voltage-gated sodium channel blocker for imaging with SPECT. *Organic & Biomolecular Chemistry* **2012**, *10* (47), 9474-9480.
155. Lin, W.; Zhang, X.; He, Z.; Jin, Y.; Gong, L.; Mi, A., REDUCTION OF AZIDES TO AMINES OR AMIDES WITH ZINC AND AMMONIUM CHLORIDE AS REDUCING AGENT. *Synthetic Communications* **2002**, *32* (21), 3279-3284.
156. (a) Osornio, Y. M.; Miranda, L. D.; Cruz-Almanza, R.; Muchowski, J. M., Radical cyclizations to quinolone and isoquinolone systems under oxidative and reductive conditions. *Tetrahedron Letters* **2004**, *45* (13), 2855-2858; (b) Alvarez, M.; Salas, M.; Rigat, L.; de Veciana, A.; Joule, J. A., Hetero-ring lithiation of N-methyl-4-quinolone and N-methylquinoline-4-thione. *Journal of the Chemical Society, Perkin Transactions 1* **1992**, (3), 351-356.
157. Morel, A. F.; Larghi, E. L.; Selvero, M. M., Mild, Efficient and Selective Silver Carbonate Mediated O-Alkylation of 4-Hydroxy-2-quinolones: Synthesis of 2,4-Dialkoxyquinolines. *Synlett* **2005**, *2005* (18), 2755-2758.
158. Joule, J. A.; Mills, K., *Heterocyclic Chemistry*. Wiley: 2013.
159. Van Es, T.; Staskun, B. *N*,1-Dialkyl-7-(alkylamino)-4-(alkylimino)-1,4-dihydroquinoline-3-carboxamides and Their 4-Oxo Derivatives: Synthesis and Properties 2001, p. p.102-117. SA ePublications. [http://reference.sabinet.co.za/webx/access/electronic\\_journals/chem/chem\\_v54\\_a6.pdf](http://reference.sabinet.co.za/webx/access/electronic_journals/chem/chem_v54_a6.pdf)
160. Brighente, I. M. C.; Yunes, R. A., The general mechanisms of attack of nitrogen nucleophiles on carbonyl compounds: facts that determine the change of the rate-pH profiles. *Journal of the Brazilian Chemical Society* **1997**, *8*, 549-553.
161. Ku, G.; Harrison, B. L.; Stemerick, D. M., Heterocyclic benzenesulfonylimine derivatives as inhibitors of il-1 action. Google Patents: 1999.
162. Da Silva, A. D.; De Almeida, M. V.; De Souza, M. V.; Couri, M. R., Biological activity and synthetic methodologies for the preparation of fluoroquinolones, a class of potent antibacterial agents. *Current medicinal chemistry* **2003**, *10* (1), 21-39.
163. Ahmed, A.; Daneshtalab, M., Nonclassical biological activities of quinolone derivatives. *Journal of pharmacy & pharmaceutical sciences : a publication of the Canadian Society for Pharmaceutical Sciences, Societe canadienne des sciences pharmaceutiques* **2012**, *15* (1), 52-72.
164. Boteva, A. A.; Krasnykh, O. P., The methods of synthesis, modification, and biological activity of 4-quinolones (review). *Chem Heterocycl Comp* **2009**, *45* (7), 757-785.
165. Grohe, K.; Heitzer, H., Cycloaracylierung von Enaminen, I. Synthese von 4-Chinolon-3-carbonsäuren. *Liebigs Annalen der Chemie* **1987**, *1987* (1), 29-37.

166. Cecchetti, V.; Fravolini, A.; Lorenzini, M. C.; Tabarrini, O.; Terni, P.; Xin, T., Studies on 6-Aminoquinolones: Synthesis and Antibacterial Evaluation of 6-Amino-8-methylquinolones. *Journal of medicinal chemistry* **1996**, *39* (2), 436-445.
167. Kędzia, J.; Modranka, J.; Janecki, T., Efficient syntheses of 3-phosphorylquinolin-4-ones and 3-phosphoryl-1,8-naphthyridin-4-ones. *Tetrahedron Letters* **2011**, *52* (49), 6623-6626.
168. Litvinov, V. P., Chemistry and biological activities of 1,8-naphthyridines. *Russian Chemical Reviews* **2004**, *73* (7), 637.
169. A. S. Anwair, M., *Studies of Physicochemical Properties and Reactivity of Naphthyridine Derivatives: An Overview*. 2013; Vol. 2.
170. Zhichkin, P.; Beer, C. M. C.; Rennells, W. M.; Fairfax, D. J., A One-Pot Method for the Synthesis of Naphthyridines via Modified Friedländer Reaction. *Synlett* **2006**, *2006* (03), 0379-0382.
171. Jia, C.-S.; Zhang, Z.; Tu, S.-J.; Wang, G.-W., Rapid and efficient synthesis of poly-substituted quinolines assisted by p-toluene sulphonic acid under solvent-free conditions: comparative study of microwave irradiation versus conventional heating. *Organic & Biomolecular Chemistry* **2006**, *4* (1), 104-110.
172. Cho, I. S.; Gong, L.; Muchowski, J. M., Synthesis of quinolines via ortho-lithiated N-acylanilines. A modified Friedlaender synthesis. *The Journal of Organic Chemistry* **1991**, *56* (26), 7288-7291.
173. Rosemeyer, H., The Chemodiversity of Purine as a Constituent of Natural Products. *Chemistry & Biodiversity* **2004**, *1* (3), 361-401.
174. Galante, E.; Okamura, T.; Sander, K.; Kikuchi, T.; Okada, M.; Zhang, M.-R.; Robson, M.; Badar, A.; Lythgoe, M.; Koepp, M.; Årstad, E., Development of Purine-Derived 18F-Labeled Pro-drug Tracers for Imaging of MRP1 Activity with PET. *Journal of medicinal chemistry* **2014**, *57* (3), 1023-1032.
175. Fischman, A. J.; Alpert, N. M.; Rubin, R. H., Pharmacokinetic imaging: a noninvasive method for determining drug distribution and action. *Clinical pharmacokinetics* **2002**, *41* (8), 581-602.
176. Tredwell, M.; Gouverneur, V., 18F Labeling of Arenes. *Angewandte Chemie International Edition* **2012**, *51* (46), 11426-11437.
177. Brooks, A. F.; Topczewski, J. J.; Ichiishi, N.; Sanford, M. S.; Scott, P. J. H., Late-stage [18F]fluorination: new solutions to old problems. *Chemical Science* **2014**, *5* (12), 4545-4553.
178. Maeda, M.; Fukumura, T.; Kojima, M., The dimethylsulfonium moiety as a leaving group in aromatic radiofluorination using tetra-n-butylammonium [18F]fluoride. *International Journal of Radiation Applications and Instrumentation. Part A. Applied Radiation and Isotopes* **1987**, *38* (4), 307-310.
179. Mu, L.; Fischer, C. R.; Holland, J. P.; Becaude, J.; Schubiger, P. A.; Schibli, R.; Ametamey, S. M.; Graham, K.; Stellfeld, T.; Dinkelborg, L. M.; Lehmann, L., 18F-Radiolabeling of Aromatic Compounds Using Triarylsulfonium Salts. *European Journal of Organic Chemistry* **2012**, *2012* (5), 889-892.
180. Sander, K.; Gendron, T.; Yiannaki, E.; Cybulska, K.; Kalber, T. L.; Lythgoe, M. F.; Årstad, E., Sulfonium Salts as Leaving Groups for Aromatic Labelling of Drug-like Small Molecules with Fluorine-18. *Sci. Rep.* **2015**, *5*.
181. (a) Deng, W.; Zou, Y.; Wang, Y.-F.; Liu, L.; Guo, Q.-X., CuI-Catalyzed Coupling Reactions of Aryl Iodides and Bromides with Thiols Promoted by Amino Acid Ligands. *Synlett* **2004**, *2004* (07), 1254-1258; (b) Rout, L.; Sen, T. K.; Punniyamurthy, T., Efficient CuO-Nanoparticle-Catalyzed C-S Cross-Coupling of Thiols with Iodobenzene. *Angewandte Chemie* **2007**, *119* (29), 5679-5682.
182. Schopfer, U.; Schlapbach, A., A general palladium-catalysed synthesis of aromatic and heteroaromatic thioethers. *Tetrahedron* **2001**, *57* (15), 3069-3073.
183. Årstad, E.; Sander, K.; Gendron, T., Compounds and their synthesis. Google Patents: 2014.
184. Crivello, J. V.; Lam, J. H. W., A new preparation of triarylsulfonium and -selenonium salts via the copper(II)-catalyzed arylation of sulfides and selenides with diaryliodonium salts. *The Journal of Organic Chemistry* **1978**, *43* (15), 3055-3058.
185. Zhu, M.; Jalalian, N.; Olofsson, B., One-Pot Synthesis of Diaryliodonium Salts Using Toluenesulfonic Acid: A Fast Entry to Electron-Rich Diaryliodonium Tosylates and Triflates. *Synlett* **2008**, *2008* (04), 592-596.

186. Fermini, B.; Priest, B., *Ion Channels*. Springer: 2008.
187. Liem, L. K.; Simard, J. M.; Song, Y.; Tewari, K., The patch clamp technique. *Neurosurgery* **1995**, *36* (2), 382-92.
188. Trivedi, S.; Dekermendjian, K.; Julien, R.; Huang, J.; Lund, P. E.; Krupp, J.; Kronqvist, R.; Larsson, O.; Bostwick, R., Cellular HTS assays for pharmacological characterization of Na(V)1.7 modulators. *Assay and drug development technologies* **2008**, *6* (2), 167-79.
189. Castle, N.; Printzenhoff, D.; Zellmer, S.; Antonio, B.; Wickenden, A.; Silvia, C., Sodium channel inhibitor drug discovery using automated high throughput electrophysiology platforms. *Combinatorial chemistry & high throughput screening* **2009**, *12* (1), 107-22.
190. Dunlop, J.; Bowlby, M.; Peri, R.; Vasilyev, D.; Arias, R., High-throughput electrophysiology: an emerging paradigm for ion-channel screening and physiology. *Nat Rev Drug Discov* **2008**, *7* (4), 358-68.
191. Farre, C.; Fertig, N., HTS techniques for patch clamp-based ion channel screening - advances and economy. *Expert opinion on drug discovery* **2012**, *7* (6), 515-24.
192. Finkel, A.; Wittel, A.; Yang, N.; Handran, S.; Hughes, J.; Costantin, J., Population patch clamp improves data consistency and success rates in the measurement of ionic currents. *Journal of biomolecular screening* **2006**, *11* (5), 488-96.
193. Sorota, S.; Zhang, X. S.; Margulis, M.; Tucker, K.; Priestley, T., Characterization of a hERG screen using the IonWorks HT: comparison to a hERG rubidium efflux screen. *Assay and drug development technologies* **2005**, *3* (1), 47-57.
194. Huang, C.-J.; Harootunian, A.; Maher, M. P.; Quan, C.; Raj, C. D.; McCormack, K.; Numann, R.; Negulescu, P. A.; Gonzalez, J. E., Characterization of voltage-gated sodium-channel blockers by electrical stimulation and fluorescence detection of membrane potential. *Nat Biotech* **2006**, *24* (4), 439-446.
195. Ojima, I., *Fluorine in Medicinal Chemistry and Chemical Biology*. Wiley: 2009.
196. Smart, B. E., Fluorine substituent effects (on bioactivity). *Journal of Fluorine Chemistry* **2001**, *109* (1), 3-11.
197. Dalvit, C.; Invernizzi, C.; Vulpetti, A., Fluorine as a hydrogen-bond acceptor: experimental evidence and computational calculations. *Chemistry (Weinheim an der Bergstrasse, Germany)* **2014**, *20* (35), 11058-68.
198. Brown, A. D.; De, G. M. J.; Marron, B. E.; Rawson, D. J.; Ryckmans, T.; Storer, R. I.; Stuppel, P. A.; Swain, N. A.; West, C. W., Benzenesulfonamides useful as sodium channel inhibitors. Google Patents: 2012.
199. Chakravarty, P. K.; Fisher, M. H.; Gonzalez, E.; Ok, H.; Palucki, B.; Park, M. K.; Parsons, W. H.; Sisco, R.; Zhou, B., Substituted triazoles as sodium channel blockers. Google Patents: 2005.
200. Hoyt, S. B.; London, C.; Abbadie, C.; Felix, J. P.; Garcia, M. L.; Jochnowitz, N.; Karanam, B. V.; Li, X.; Lyons, K. A.; McGowan, E.; Priest, B. T.; Smith, M. M.; Warren, V. A.; Thomas-Fowlkes, B. S.; Kaczorowski, G. J.; Duffy, J. L., A novel benzazepinone sodium channel blocker with oral efficacy in a rat model of neuropathic pain. *Bioorganic & Medicinal Chemistry Letters* **2013**, *23* (12), 3640-3645.
201. Fleming, F. F.; Yao, L.; Ravikumar, P. C.; Funk, L.; Shook, B. C., Nitrile-Containing Pharmaceuticals: Efficacious Roles of the Nitrile Pharmacophore. *Journal of medicinal chemistry* **2010**, *53* (22), 7902-7917.
202. *Kirk-Othmer Encyclopedia of Chemical Technology*. Wiley: 2006.
203. Bissantz, C.; Kuhn, B.; Stahl, M., A medicinal chemist's guide to molecular interactions. *Journal of medicinal chemistry* **2010**, *53* (14), 5061-84.
204. Graves, P. R.; Kwiek, J. J.; Fadden, P.; Ray, R.; Hardeman, K.; Coley, A. M.; Foley, M.; Haystead, T. A., Discovery of novel targets of quinoline drugs in the human purine binding proteome. *Molecular pharmacology* **2002**, *62* (6), 1364-72.
205. Wermuth, C. G., *The Practice of Medicinal Chemistry*. Elsevier Science: 2011.
206. King, A. M.; Yang, X. F.; Wang, Y.; Dustrude, E. T.; Barbosa, C.; Due, M. R.; Piekarz, A. D.; Wilson, S. M.; White, F. A.; Salome, C.; Cummins, T. R.; Khanna, R.; Kohn, H., Identification of the benzyloxyphenyl pharmacophore: a structural unit that promotes sodium channel slow inactivation. *ACS chemical neuroscience* **2012**, *3* (12), 1037-49.
207. Kaczorowski, G. J.; Garcia, M. L.; Bode, J.; Hess, S. D.; Patel, U. A., The Importance of Being Profiled: Improving Drug Candidate Safety and Efficacy Using Ion Channel Profiling. *Frontiers in Pharmacology* **2011**, *2*.

- 
208. Koltzenburg, M.; Stucky, C. L.; Lewin, G. R., Receptive properties of mouse sensory neurons innervating hairy skin. *Journal of neurophysiology* **1997**, *78* (4), 1841-50.
209. Cain, D. M.; Khasabov, S. G.; Simone, D. A., Response properties of mechanoreceptors and nociceptors in mouse glabrous skin: an in vivo study. *Journal of neurophysiology* **2001**, *85* (4), 1561-74.
210. Reeh, P. W., Sensory receptors in mammalian skin in an in vitro preparation. *Neuroscience letters* **1986**, *66* (2), 141-6.
211. Moshourab, R.; Schmidt, Y.; Machelska, H., Skin-nerve preparation to assay the function of opioid receptors in peripheral endings of sensory neurons. *Methods in molecular biology (Clifton, N.J.)* **2015**, *1230*, 215-28.
212. Tsunozaki, M.; Lennertz, R. C.; Vilceanu, D.; Katta, S.; Stucky, C. L.; Bautista, D. M., A 'toothache tree' alkylamide inhibits Adelta mechanonociceptors to alleviate mechanical pain. *The Journal of physiology* **2013**, *591* (Pt 13), 3325-40.
213. Alpsan, D.; Lal, S., Combined light- and electron-microscopic study of the rat saphenous nerve. *Acta anatomica* **1980**, *106* (1), 141-9.
214. Campos, S. A. R.; Sanada, L. S.; Sato, K. L.; Fazan, V. P. S., Morphometry of saphenous nerve in young rats. *Journal of Neuroscience Methods* **2008**, *168* (1), 8-14.
215. Zimmermann, K.; Hein, A.; Hager, U.; Kaczmarek, J. S.; Turnquist, B. P.; Clapham, D. E.; Reeh, P. W., Phenotyping sensory nerve endings in vitro in the mouse. *Nature protocols* **2009**, *4* (2), 174-96.
216. (a) Kress, M.; Koltzenburg, M.; Reeh, P. W.; Handwerker, H. O., Responsiveness and functional attributes of electrically localized terminals of cutaneous C-fibers in vivo and in vitro. *Journal of neurophysiology* **1992**, *68* (2), 581-95; (b) Kerstein, P. C.; del Camino, D.; Moran, M. M.; Stucky, C. L., Pharmacological blockade of TRPA1 inhibits mechanical firing in nociceptors. *Molecular Pain* **2009**, *5*, 19-19.
217. Farrag, K. J.; Costa, S. K.; Docherty, R. J., Differential sensitivity to tetrodotoxin and lack of effect of prostaglandin E2 on the pharmacology and physiology of propagated action potentials. *British journal of pharmacology* **2002**, *135* (6), 1449-56.
218. Sawynok, J., Topical and Peripherally Acting Analgesics. *Pharmacological Reviews* **2003**, *55* (1), 1-20.
219. Cousins, M. J.; Bridenbaugh, P. O.; Carr, D. B.; Horlocker, T. T., *Cousins and Bridenbaugh's Neural Blockade in Clinical Anesthesia and Pain Medicine*. Lippincott Williams & Wilkins: 2009.
220. Huang, J. H.; Thalhammer, J. G.; Raymond, S. A.; Strichartz, G. R., Susceptibility to lidocaine of impulses in different somatosensory afferent fibers of rat sciatic nerve. *The Journal of pharmacology and experimental therapeutics* **1997**, *282* (2), 802-11.
221. Fink, B. R.; Cairns, A. M., Differential peripheral axon block with lidocaine: unit studies in the cervical vagus nerve. *Anesthesiology* **1983**, *59* (3), 182-6.
222. Fink, B. R.; Cairns, A. M., Differential slowing and block of conduction by lidocaine in individual afferent myelinated and unmyelinated axons. *Anesthesiology* **1984**, *60* (2), 111-20.
223. Gokin, A. P.; Philip, B.; Strichartz, G. R., Preferential block of small myelinated sensory and motor fibers by lidocaine: in vivo electrophysiology in the rat sciatic nerve. *Anesthesiology* **2001**, *95* (6), 1441-54.
224. Korsten, H. H.; Ackerman, E. W.; Grouls, R. J.; van Zundert, A. A.; Boon, W. F.; Bal, F.; Crommelin, M. A.; Ribot, J. G.; Hoefsloot, F.; Slooff, J. L., Long-lasting epidural sensory blockade by n-butyl-p-aminobenzoate in the terminally ill intractable cancer pain patient. *Anesthesiology* **1991**, *75* (6), 950-60.
225. Grouls, P. R. J. E.; Meert, M. D. P. T. F.; Korsten, M. D. P. H. H. M.; Hellebrekers, D. V. M. P. L. J.; Breimer, P. D. D., Epidural and Intrathecal n-Butyl-p-Aminobenzoate Solution in the Rat Comparison with Bupivacaine. *The Journal of the American Society of Anesthesiologists* **1997**, *86* (1), 181-187.
226. Theriault, O.; Poulin, H.; Sculptoreanu, A.; de Groat, W. C.; O'Leary, M. E.; Chahine, M., Modulation of peripheral Na(+) channels and neuronal firing by n-butyl-p-aminobenzoate. *European journal of pharmacology* **2014**, *727*, 158-66.
227. Nelsen, J.; Holland, M.; Dougherty, M.; Bernad, J.; Stork, C.; Marraffa, J., Severe central nervous system and cardiovascular toxicity in a pediatric patient after ingestion of an over-the-counter local anesthetic. *Pediatric emergency care* **2009**, *25* (10), 670-3.
-



- 
228. Kang, C.; Shin, S. C., Preparation and evaluation of bioadhesive dibucaine gels for enhanced local anesthetic action. *Archives of pharmacal research* **2010**, *33* (8), 1277-83.
229. Douglas, H. A.; Callaway, J. K.; Sword, J.; Kirov, S. A.; Andrew, R. D., Potent inhibition of anoxic depolarization by the sodium channel blocker dibucaine. *Journal of neurophysiology* **2011**, *105* (4), 1482-94.
230. Ukrainets, I., *Creation of New Local Anesthetics Based on Quinoline Derivatives and Related Heterocycles*. INTECH Open Access Publisher: 2012.
231. Baird, D. C., *Experimentation: An Introduction to Measurement Theory and Experiment Design*. Prentice-Hall: 1962.
232. Meurant, G., *Profiles of Drug Substances, Excipients and Related Methodology*. Elsevier Science: 1986.
233. Fielden, M. R.; Kolaja, K. L., The role of early in vivo toxicity testing in drug discovery toxicology. *Expert opinion on drug safety* **2008**, *7* (2), 107-10.
234. Hughes, J. P.; Rees, S.; Kalindjian, S. B.; Philpott, K. L., Principles of early drug discovery. *British journal of pharmacology* **2011**, *162* (6), 1239-1249.
235. Gupta, N.; Price, P. M.; Aboagye, E. O., PET for in vivo pharmacokinetic and pharmacodynamic measurements. *European journal of cancer (Oxford, England : 1990)* **2002**, *38* (16), 2094-107.
236. Piel, M.; Vernaleken, I.; Rösch, F., Positron Emission Tomography in CNS Drug Discovery and Drug Monitoring. *Journal of medicinal chemistry* **2014**.
237. DePass, L. R., Alternative approaches in median lethality (LD50) and acute toxicity testing. *Toxicology letters* **1989**, *49* (2-3), 159-70.
238. Sass, N., Humane endpoints and acute toxicity testing. *ILAR journal / National Research Council, Institute of Laboratory Animal Resources* **2000**, *41* (2), 114-23.
239. Lipnick, R. L.; Cotruvo, J. A.; Hill, R. N.; Bruce, R. D.; Stitzel, K. A.; Walker, A. P.; Chu, I.; Goddard, M.; Segal, L.; Springer, J. A.; Myers, R. C., Comparison of the up-and-down, conventional LD50, and fixed-dose acute toxicity procedures. *Food and Chemical Toxicology* **1995**, *33* (3), 223-231.
240. Dixon, W. J., Staircase bioassay: the up-and-down method. *Neuroscience and biobehavioral reviews* **1991**, *15* (1), 47-50.
241. Bruce, R. D., An up-and-down procedure for acute toxicity testing. *Fundamental and applied toxicology : official journal of the Society of Toxicology* **1985**, *5* (1), 151-7.
242. Lichtman, A. H., The up-and-down method substantially reduces the number of animals required to determine antinociceptive ED50 values. *Journal of Pharmacological and Toxicological Methods* **1998**, *40* (2), 81-85.
243. Mather, L. E.; Copeland, S. E.; Ladd, L. A., Acute toxicity of local anesthetics: underlying pharmacokinetic and pharmacodynamic concepts. *Regional anesthesia and pain medicine* **2005**, *30* (6), 553-66.
244. Mather, L. E., The acute toxicity of local anesthetics. *Expert Opinion on Drug Metabolism & Toxicology* **2010**, *6* (11), 1313-1332.
245. Munson, E. S.; Tucker, W. K.; Ausinsch, B.; Malagodi, M. H., Etidocaine, bupivacaine, and lidocaine seizure thresholds in monkeys. *Anesthesiology* **1975**, *42* (4), 471-8.
246. Liu, P. L.; Feldman, H. S.; Giasi, R.; Patterson, M. K.; Covino, B. G., Comparative CNS toxicity of lidocaine, etidocaine, bupivacaine, and tetracaine in awake dogs following rapid intravenous administration. *Anesthesia and analgesia* **1983**, *62* (4), 375-9.
247. Berberian, D. A.; Freele, H., Chemotherapeutic Effect of Antischistosomal Drugs in Experimentally Induced *Schistosoma mansoni* Infections in Swiss Mice and Syrian Hamsters. *The Journal of Parasitology* **1964**, *50* (3), 435-440.
248. Dray, A., Neuropathic pain: emerging treatments. *British Journal of Anaesthesia* **2008**, *101* (1), 48-58.
-